Copper(I) polypyridine complexes: the sensitizers of the future for dye-sensitized solar cells (DSSCs)

Inauguraldissertation

zur

Erlangung der Würde eines Doktors der Philosophie

vorgelegt der

Philosophisch-Naturwissenschaftlichen Fakultät

der Universität Basel

von

Ana Hernández Redondo

aus Oñate, Spanien

Basel, 2009

Genehmigt von der Philosophisch-Naturwissenschaftlichen Fakultät auf Antrag von

Prof. Dr. Edwin C. Constable   Prof. Dr. Wolfgang P. Meier

Basel, den 26. 05. 2009

                                    Prof. Dr. Eberhard Parlow

                                    Dekan

creative commons

Namensnennung-Keine kommerzielle Nutzung-Keine Bearbeitung 2.5 Schweiz

---

Sie dürfen:

das Werk vervielfältigen, verbreiten und öffentlich zugänglich machen

Zu den folgenden Bedingungen:

Namensnennung. Sie müssen den Namen des Autors/Rechteinhabers in der von ihm festgelegten Weise nennen (wodurch aber nicht der Eindruck entstehen darf, Sie oder die Nutzung des Werkes durch Sie würden entlohnt).

Keine kommerzielle Nutzung. Dieses Werk darf nicht für kommerzielle Zwecke verwendet werden.

Keine Bearbeitung. Dieses Werk darf nicht bearbeitet oder in anderer Weise verändert werden.

- Im Falle einer Verbreitung müssen Sie anderen die Lizenzbedingungen, unter welche dieses Werk fällt, mitteilen. Am Einfachsten ist es, einen Link auf diese Seite einzubinden.

- Jede der vorgenannten Bedingungen kann aufgehoben werden, sofern Sie die Einwilligung des Rechteinhabers dazu erhalten.

- Diese Lizenz lässt die Urheberpersönlichkeitsrechte unberührt.

Quelle: http://creativecommons.org/licenses/by-nc-nd/2.5/ch/   Datum: 3.4.2009

A mis padres, Mateo y Pilar.

To my parents, Mateo and Pilar.

Acknowledgements

First of all, I would like to thank my supervisors Prof. Dr. Edwin C. Constable and Prof. Dr. Catherine E. Housecroft for helping, advising and supporting me during the last three years. Since the very beginning they encouraged me to work and transmitted me their passion for chemistry, for what I am very grateful. Ed, as the direct supervisor of my project, has led me through the PhD giving me a lot of freedom, and I would say that he has also vibrated with the amazing and to some point unexpected results that we have had. Catherine has always been there for anything that I have needed during the time I was working in the laboratory, and also while I was writing at home. I really appreciate her patience any time I would "skype" her with a question and her invaluable corrections.

I also want to thank Prof. Wolfgang P. Meier and Prof. Dr. Michael Grätzel for being the co-referee and external expert on my PhD-defense.

Prof. Michael Grätzel also has to be acknowledged together with Dr. Md. Khaja Nazeeruddin and Dr. Takeru Bessho for the measurements that were performed in their laboratories, at the EPFL in Lausanne. The results obtained with my copper compounds in collaboration with them allowed us to publish our work very successfully and attracted the attention of the scientific community.

Next, I would also like to say thank you to all the past and present members of the Constable/Housecroft group. During my PhD, I have always feel comfortable working in the laboratory and in the practical courses with the students, and have always find help to any problems/doubts that I could have. Not to forget the good times spent in the kitchen and the good friendships that I have started here. I am not going to mention all these people by name because I am afraid I could forget someone, but thank you to you all!!! I am also very grateful for those that have run MALDI, ESI and NMR experiments for me, and of course to Stefan Graber, who has always repaired any computer problem that I could have (and I can have lots of them in a short time!) and has been patient enough to explain me anything I should know about them.

And last but not least, I want to thank Jorge for his love and help before, during and hopefully after (!) my PhD studies. I still remember my first days here, when I was lost and didn't know what to do; he supported and helped me "see the light". You always see the good things in me and help me see them. Before and especially after my operation, you have been the best partner I could have ever dreamed of, and hope you will keep being it now that we have a common, and I would say, the most important project of our lives coming.

<div align="right">

Ana Hernández Redondo

Basel, 29th June 2009

</div>

iv

Contents

Abreviations

- **General**

A	Ampere
Å	Angstrom
bipy	2,2´-bipyridine
dmbpy	6,6´-dimethyl-2,2´-bipyridine
CH_3CN	Acetonitrile
DMSO	Dimethylsulfoxide
ff	Fill factor
FTO	Fluorine doped SnO_2
HOMO	Highest occupied molecular orbital
Hz	Hertz
IPCE	Incident photon to current conversion efficiency
LUMO	Lowest occupied molecular orbital
phen	1,10-phenanthroline
ppm	Parts per million
THF	Tetrahydrofuran
TMS	Tetramethylsilane
TFA	Trifluoroacetic acid
V	Volt

- **Experimental methods**

Nuclear Magnetic Resonance Spectroscopy (NMR)

^{1}H NMR	Proton nuclear magnetic resonance spectroscopy
^{13}C NMR	Carbon nuclear magnetic resonance spectroscopy
^{31}P NMR	Phosphorus nuclear magnetic resonance spectroscopy
COSY	Correlated spectroscopy

HMBC	Heteronuclear multiple bond correlation
HMQC	Heteronuclear multiple quantum correlation
NOESY	Nuclear overhauser effect spectroscopy
δ	Chemical shift, ppm
J	Coupling constant in Hz
s	Singlet
d	Doublet
t	Triplet
q	Quartet
dd	Doublet of doublets
dt	Doublet of triplets
m	Multiplet
br	Broad

Mass Spectrometry (MS)

EI	Electron impact
ESI	Electrospray ionisation
FAB	Fast-atom bombardment
M	Parent ion
m/z	Mass to charge ratio
MALDI	Matrix assisted laser desorption ionisation

Ultra-Violet Visible (UV-VIS) Spectroscopy

MLCT	Metal-to-ligand charge transfer
λ_{max}	Wavelength at which maximum absorption occurs in nm
ε	Extinction coefficient in M^{-1} cm^{-1}

Infrared (IR) Spectroscopy

w	Weak
m	Medium
s	Strong
br	Broad
υ	Wavenumber

Elemental analysis

Calc.	Calculated

General experimental

^{1}H, ^{13}C and ^{31}P spectra were recorded at room temperature on Bruker AM250 (250 MHz), Bruker DRX400 (400 MHz), Bruker Avance DRX500 (500 MHz) and DRX600 (600 MHz) spectrometers. Chemical shifts for ^{1}H and ^{13}C are relative to residual solvent peaks with TMS δ 0 ppm. ^{31}P spectra are referenced with respect to 85% aqueous H_3PO_4 (δ 0 ppm).

Infrared spectra were recorded on a Shimadzu FTIR-8400S spectrophotometer with solid samples on a Golden Gate diamond ATR accessory.

Electron impact (EI), electrospray ionization (ESI), and MALDI-TOF mass spectra were recorded using Finnigan MAT95 and MAT LCQ and PerSeptive Biosystems Voyager mass spectrometers, respectively.

Electronic absorption spectra were recorded on a Varian-Cary 5000 spectrophotometer.

Electrochemical measurements were performed with an Eco Chemie Autolab PGSTAT 20 system using glassy carbon working and platinum auxiliary electrodes with a silver wire as pseudo-reference electrode. Solvents (see experimental section) were purified and 0.1M [^{n}Bu$_4$N][PF$_6$] was used as supporting electrolyte. Ferrocene (Fc) was added at the end of each experiment as an internal reference. For Na$_3$[Cu(**L17**)$_2$], the supporting electrolyte was 0.1M NaClO$_4$ and measurements were made relative to Ag/AgCl, then corrected to be with respect to Fc/Fc$^+$.

Photoelectrochemical measurements at the University of Basel were performed with a CHI-900B potentiostat connected to the cells. The light source was a 300 W halogen lamp (ELH, General electrics) with a UV-filter to block light with wavelengths under 400 nm. The solar cells were mounted at a distance where the light intensity was 100 mW/cm^2 (measured with an optical power meter head, Thorlabs), the equivalent of one sun at air mass 1.5. Masking tape was added around the cells to prevent reflected light disturbing the measurement.

The elemental analyses were performed with a Leco CHN-900 microanalyser by W. Kirsch.

I   Introduction

Now, more than ever before, energy is what makes our world continuously work. World energy annual consumption is *ca.* 4.7×10^{20} J and is expected to grow about 2% each year for the next 25 years [1]. The World's conventional energy supplies (oil, natural gas and coal) have a finite lifetime as our major source of energy, and current forecasts suggest that alternatives must make a major contribution in the near future, also because mankind cannot afford to continue to progress by relying on sources of energy that release greenhouse gases. Though nuclear power was once regarded as a solution for increasing energy demand and the depletion of fossil fuels, concerns about the storage of nuclear waste led scientists to explore alternative and renewable sources of energy.

Most renewable energy options must rely on a net input of energy into the Earth and since the Sun is our only external energy source, using its energy, which is clean and infinite, is the main objective of all alternative energy strategies. It is remarkable that a mere 10 minutes of solar irradiation onto the Earth's surface is equal to the total annual human energy consumption [2]. However, nowadays renewable sources comprise about 13% of all energy production and photovoltaics (PV) (from photons to electrons) only account for no more than 0.04%, and, most probably, only in 2030 will that figure reach 1% [3]. Solar PV energy costs are not yet competitive and continued PV growth is mainly based on government support, as is easily perceived by analyzing three major consumers: Germany, Japan and the USA. Nevertheless, PV solar cells are clearly very elegant and attractive devices for producing energy: cells are free from chemical and noise pollution; their power output is flexible; production can be done *in situ*, it is not dependent on the electrical grid, which makes them uniquely portable; they do not rely on reserves located abroad in geopolitically unstable countries and, of course, their source of energy, the Sun, as already said, is free and inexhaustible for the next few million years.

The first modern PV solar cells, silicon (Si) p/n, were developed by Chapin *et* al. at Bell Laboratories in 1954 [4], and a few years later they were already used in space exploration. Crystalline silicon (c-Si) solar cells have dominated the terrestrial PV market so far for various

reasons: besides silicon's natural abundance (Si is the most abundant element in the Earth's surface apart from oxygen), low toxicity and a well-established processing technology, manufacturers have been supplied with rejected material from the high-tech semiconductor industry. However, silicon is far from being the ideal material of choice for PV conversion [5], because besides the unwanted dependency to the electronic Si industry, only sustainable if it continues to grow at least at the same rate as the PV industry, which is not the case, the purity level of Si supplied to the PV industry as "by-product" is a fairly expensive feedstock due to two costly purifying processes.

The operating principle of c-Si PV solar cells is quite simple. The cell is made up of three layers: the n-type, the p-type and the pn-junction (the connection formed between the previous two). The n-type layer is doped with elements from group V, normally phosphorus, because it has extra electrons and works as the donor (anode); the p-type layer, on the other hand, is doped with group 13 elements, commonly boron, that has a lack of electrons and therefore creates "holes" and, consequently, becomes the receptor (cathode). Light reception occurs in the pn-junction. Each photon generates an electron-hole pair by exciting electrons from the junction valence band to the conduction band (electrons are driven to the negative layer while "holes" are left as positive). This mechanism leads to different potentials in the anode and cathode, inducing an electron flow, and in doing so generates an electrical current.

However, the dominance of the PV field by inorganic solid-state junction devices is now being challenged by the emergence of another generation of cells based on nanocrystalline and conducting polymers films, which offer the prospective of very low cost fabrication and present attractive features that facilitate market entry. It is now possible to depart completely from the classical solid-state cells, which are replaced by devices based on interpenetrating network junctions where the contacting phase to the semiconductor has been replaced by an electrolyte (liquid, gel or solid) thereby forming a photo-electrochemical cell. The prototype of this family of devices is the dye-sensitized solar cell (DSSC), which performs the optical absorption and the charge separation processes by the association of a sensitizer as light-absorbing material with a wide band gap semiconductor of mesoporous or nanocrystalline morphology [5-7]. It is an analogous situation to that of the photosynthetic process in which chlorophyll absorbs photons

but does not participate in charge transfer [8]. This is contrary to conventional PV cells where a semiconductor assumes both functions.

Photosensitization of semiconductors has a long history, being pioneered in the photographic process by Vogel in Berlin in 1873 [9], and for semiconductors by Moser in Vienna in 1887 [2]. However, it was not until one century later that sensitization started to be used for photo-electrochemical purposes [10]. A US patent submitted in 1977 included almost all the major characteristics of today's DSSCs and is entitled *Dye-sensitized solar cells*. By 1980 ruthenium-based dyes had been identified by the Dare-Edwards group in England [11] and this represented a starting point for DSSCs. However, it was not until the publication of an article by Grätzel in 1991 [6] that the interest in this kind of solar cells took off; indeed, this interest is still increasing every year (see figure 1).
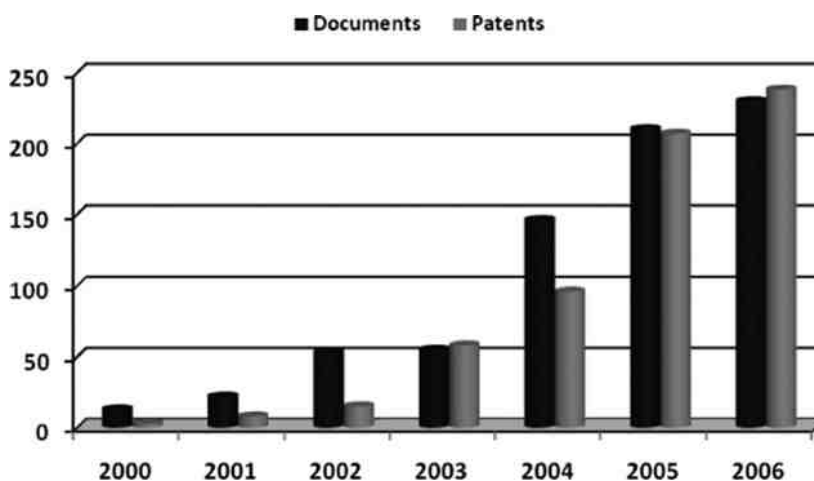
Fig. 1. Number of published documents about DSSCs (articles, conference papers and reviews).

A typical DSSC is composed of two sheets of glass coated with a transparent conductive oxide layer (TCO). One of the glass plates, the working electrode, is covered with a film of small dye-sensitized semiconductor particles; the other glass plate, the counter electrode, is coated with a catalyst. Both plates are sandwiched together and the electrolyte, commonly a redox couple in an organic solvent, fills the gap between them. Upon light irradiation, dye molecules are photo-excited and inject an electron into the conduction band of the oxide. The electron then migrates

through the semiconductor reaching the collector (TCO). Afterwards, the electron goes through an outer circuit to reach the other TCO layer (at the counter electrode), performing electrical work on the way. The electron is then transferred to the electrolyte where it reduces the oxidant species; subsequently, the original state of the dye is restored by electron donation from the reduced specie in the electrolyte, completing the circuit. Overall the device generates electric power from light without suffering any permanent chemical transformation. However, there are undesirable reactions, which are that the injected electrons may recombine either with oxidized sensitizer or with the oxidized redox couple at the TiO_2 surface, resulting in losses in the cell efficiency (dark current – see chapter V). In the next figure a schematic representation of the DSSC is shown:
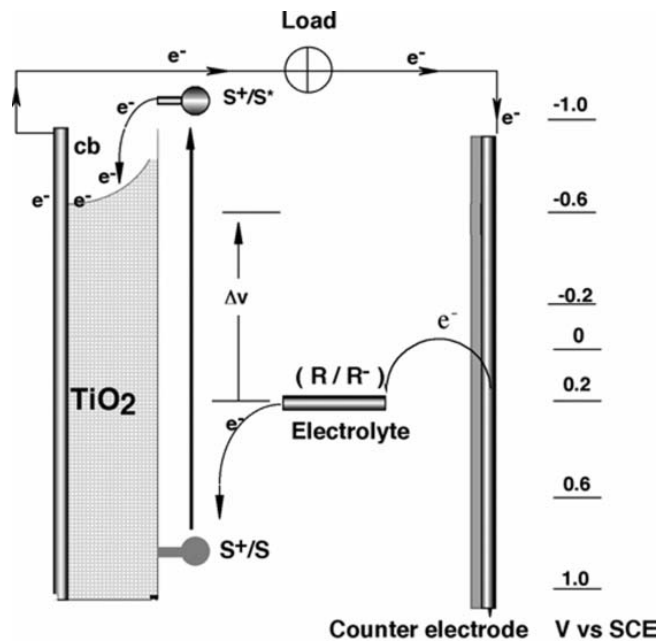
Fig. 2. Principle of operation and energy level diagram of the DSSC. $S/S^+/S^*$ = Sensitizer in the ground, oxidized and excited state, respectively. R/R+ = Redox mediator [12].

I. 1 Different parts of the dye-sensitized solar cell (DSSC)

I. 1. 1 Semiconductor

Those semiconductors with band gaps narrow enough for efficient absorption of visible light are unstable against photo-corrosion. Semiconductors stable under illumination, typically oxides of metals such as titanium or niobium, have a wide band gap, an absorption edge towards the ultraviolet and consequently are insensitive to the visible spectrum. For this reason a chromophoric compound, the sensitizer, is adsorbed onto the semiconductor's surface expanding the absorption spectrum range, and thus increasing light harvesting efficiency [13].

A monolayer of dye on a flat surface absorbs at most a few percent of light because it occupies an area that is much larger than its optical cross section. For this reason, in the first laboratory embodiment of the DSSC which dates back to 1988 [14], the photo-anode was a titanium sheet covered with a high surface area "fractal" TiO_2 film that had a roughness factor of about 150. Years later, in 1991 Grätzel reported a breakthrough, with an efficiency of around 7% achieved by the innovative use of a nanoscopic TiO_2 particle layer that produces a junction of huge contact area. The semiconductor's surface is thus enlarged over 1000 times allowing for efficient harvesting of sunlight by the adsorbed monolayer of sensitizer.
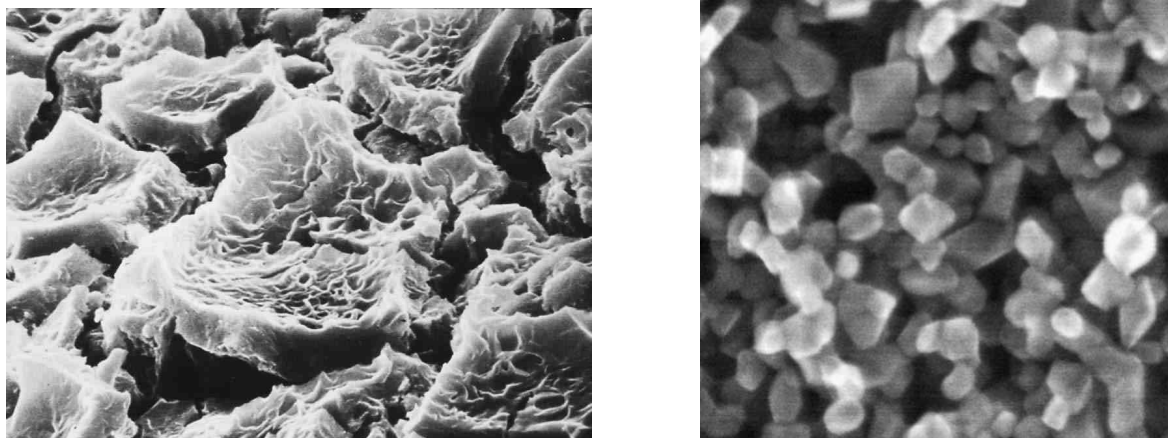
Fig. 3. On the left: scanning electron microscope picture of the fractal TiO$_2$ film used in the first embodiment of the DSSC in 1988. On the right: scanning electron micrograph of a TiO$_2$ anatase colloid film [15].

Another dilemma faced by this kind of PV conversion system is the need for compact oxide semiconductor films to be n-doped to conduct electrons. However, the presence of conduction band electrons is undesirable as they can quench the excited sensitizer by energy transfer, which will inevitably reduce the photovoltaic conversion efficiency. In contrast to these compact oxide layers, the present designs of DSSCs contain a network of undoped (insulating) wide band gap oxide nanocrystallites that, upon injection of one single electron from the surface adsorbed sensitizer, turn the oxides from an insulating to a conductive state, thus solving the problem.

Since research began, TiO$_2$ has been the preferred semiconductor in DSSCs, despite some promising properties offered by other metal oxides such as ZnO [16], SnO$_2$ and Nb$_2$O$_5$ [17]. TiO$_2$, a white pigment, meets the requirements of the present era of ecological and environmental consciousness, where preferences are for inert, non-toxic compounds. As a cheap, readily available material, TiO$_2$ serves as an attractive candidate for many industrial applications (paints, paper, coatings, plastics, etc.). Rutile, anatase and brookite are the three common crystalline polymorphs of TiO$_2$ [18]. Anatase has been widely used because it has a high band gap energy (3.2 eV, and absorbs only below 388 nm) making it invisible to most of the solar spectrum, reducing the recombination rate of photo-injected electrons. Additionally, it has good thermal stability, is chemically inert, non-toxic and relatively cheap [18]. Rutile can also be employed;

however, it has a smaller band gap (3.0 eV) and so is less effective, since photon excitation within the band gap generates holes that act as oxidants making it less chemically stable [19].

As already pointed out, the TiO_2 film morphology is of major importance in the performance of DSSCs. Ideally, the semiconductor layer should have a nanostructured mesoscopic morphology crucial for a high specific surface area, in order to obtain the maximum area available for dye adsorption using the minimum quantity of TiO_2. Initially, it was thought that these mesoporous films could promote charge carrier loss by recombination, however, unexpectedly this does not happen, since the injected electron and the positive charge find themselves within picoseconds after light excitation of the dye on opposite sides of the liquid-solid interface [20]. It has been observed that, in some cases, electron injection is at least eight orders of magnitude faster than any other competing channels of excited state deactivation, including those leading to chemical transformation of the dye [21]. However, because the injected electron has to be transported across a large number of colloidal particles and grain boundaries, there will be an increased probability of recombination with increased film thickness. Thus, there exists an optimal thickness to obtain maximum photocurrent. In addition, Zhu *et al.* observed that recombination occurs close to the glass coated with a TCO layer and not throughout the entire titania matrix. For this reason, present researchers use a compact [22] or nanocrystalline [23] TiO_2 "blocking layer". The use of a light-scattering layer is also quite common; it consists of larger titania particles that work as a photo-trapping system [24]. The two deposition techniques generally used to deposit the semiconductor onto the glass substrate are screen-printing and doctor-blading. Typical film thicknesses are 5-20 μm, with TiO_2 mass of about 1-4 mg cm^{-2}, film porosity 50-65%, average pore size 15 nm and particle diameters of 15-20 nm.

A relatively new and exciting research field in semiconductor morphology is the use of nanostructures, namely nanotubes, nanowires, nanorods and inverse opals [25-27].

I. 1. 2   Dye

As stated before, the dye is the photoreceptor sensitizing the semiconductor, and so several requirements must be fulfilled. Obviously one would like to use a dye that absorbs nearly all the sunlight incident on earth, like a black-body absorber. The solar spectrum has its maximal intensity in the IR region (ca. 1200 nm) and so it is desirable to shift the absorption peak of the dye to as low energy as possible. However, the energy content of the photon decreases as one moves further into the IR region, so 920 nm has been chosen as the threshold wavelength below which the sensitizer should absorb [18].

In addition, it must also carry groups to attach the dye to the surface, for example carboxylate [28, 29] or phosphonate [30, 31] groups, being these the most employed ones. Other groups, like boronic acid [32], salicylate [18], silanes [33], amides [34], ethers [35] or hydroxamic acid groups [36] can also be employed to attach photo-and redox-active molecules to metal oxide surfaces. The anchoring group is an important parameter to consider in the design of efficient sensitizers because it may affect both the stability of the linkage and the electronic coupling between the dye and the semiconductor [31]. Upon excitation it should inject electrons into the solid with a quantum yield of unity, and this is best done when the electronic coupling of the donor levels of the dye and the acceptor levels of the semiconductor are well matched.

The energy level of the excited state of the dye should be well matched to the lower level of the conduction band of the oxide to minimize energetic losses during the electron transfer reaction. And not only that, the redox potential of the sensitizer should be sufficiently positive that it can be regenerated via electron donation from the redox mediator [7]. Given these requirements, it is logical to go, if possible, for systematic design of a mixed ligand complex or organic dye with different constituent groups each for a specific task. Many mixed ligand complexes synthesized so far and reported in the literature as efficient photo-sensitizers are the result of this type of molecular engineering of the composition of the complex [37]. For these studies it was taken into consideration that numerous spectro- and electrochemical studies of polypyridine complexes have clearly established that the first oxidation and reduction potentials are good indicators of the electronic levels of the donor and acceptor molecular orbitals (MOs) [18].

15

Finally, the sensitizer should be stable enough to sustain about 10^8 turnover cycles corresponding to about 20 years of exposure to natural light [15]. In order to stabilize the sensitizer, one has to make sure that the electron injection and the recovery of the oxidized form by the redox couple are fast enough to suppress side reactions like degradation (e.g., loss of ligand), desorption or aggregation.

Much of the research in dye chemistry is devoted to the identification and synthesis of dyes matching these requirements, while retaining stability in the photo-electrochemical environment. To date, the best photovoltaic performance both in terms of conversion yield and long-term stability has been achieved with polypyridyl complexes of ruthenium(II) and osmium(II) [15]. The ruthenium complex *cis*-[RuL$_2$(NCS)$_2$] (where L stands for 2,2´-bipyridyl-4,4´-dicarboxylic acid), known as N3, was the first high-performance dye of this kind of ruthenium complexes. It was first reported by Nazeeruddin *et al.* in 1993 [38] and it was not until 5 years later that its results were surpassed by another ruthenium complex, the so-called "black dye" [RuL´(NCS)$_3$] (where L´ stands for 2,2´:6´,2´´-terpyridyl-4,4´,4´´-tricarboxylic acid) [39]. In 2001 the "black dye" achieved a record 10.4% (air mass 1.5 – see chapter V) solar to power conversion efficiency in full sunlight [40]. Two years later, however, N3 returned to the top ranking position with a new record efficiency of 10.6% thanks to its combination with guanidiunium thiocyanate, a self-assembly facilitating additive allowing one to substantially increase the open circuit voltage (V_{oc}) due to a reduction in dark current (see chapter V) [15, 21]. Thus, N3 has become the paradigm of ruthenium based sensitizers, being its performance better than those of compounds having comparable ground- and excited-state properties [41]. It has been suggested that a peculiar molecular level property of the N3 complex could affect one of the key processes of the cell mechanism leading to an increase in the spectral response [42].
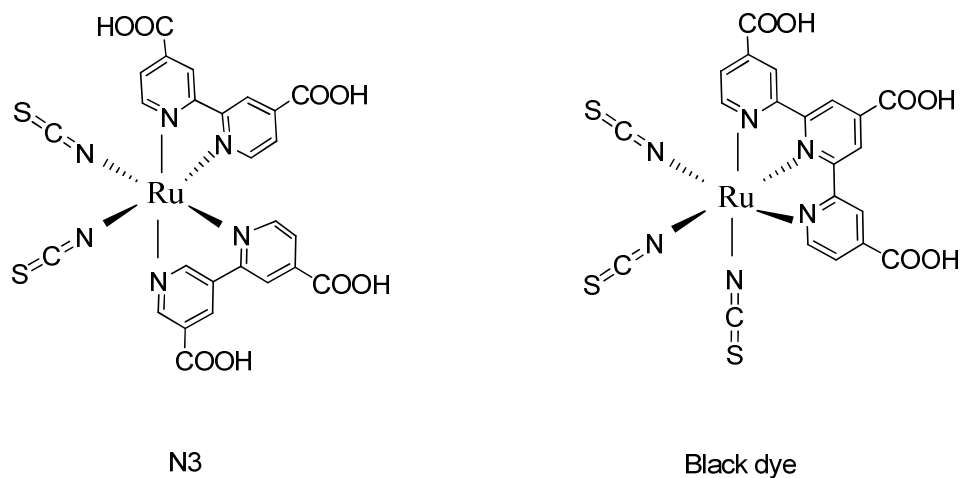
Fig. 4. Chemical structures of N3 and "black dye" ruthenium complexes used as charge transfer sensitizers in DSSCs.

One of the main differences between N3 and the "black dye" is shown in figure 5, which compares the spectral response of the photocurrent observed with the two sensitizers. In that graphic the incident photon to current conversion efficiency (IPCE) of the DSSCs sensitized with the mentioned complexes is plotted as a function of excitation wavelength. The IPCE is defined as the number of electrons generated by light in the external circuit divided by the number of incident photos, so it gives a measure of the conversion of incident photos to electric current [43].

Both chromophores show very high IPCE values in the visible range. However, the response of the black dye extends 100 nm further into the IR than that of N3. The photocurrent onset is close to 920 nm, i.e. near the optimal threshold for single junction converters, as mentioned above. From there on, the IPCE rises gradually until at 700 nm it reaches a plateau of over 80%. And if one accounts for reflection and absorption losses in the conducting glass, the conversion of incident photons to electric current is practically quantitative over the whole visible domain.
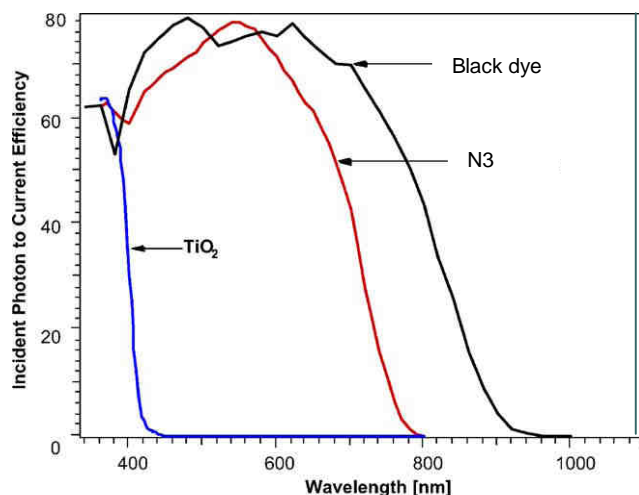
Fig. 5. Photocurrent action spectra obtained with N3 and "black dye" as sensitizer. The photocurrent response of a bare TiO$_2$ film is also shown for comparison [15]. Detailed experimental conditions are given in [44].

Apart from these two sensitizers, hundreds of other ruthenium based complexes have been synthesized for DSSC applications [21, 45-47], and to date these complexes are the most successful dyes and the only ones so far to achieve over 10% efficiency under standard conditions. Recent research has focused on accomplishing a suitable balance of improved molar absorptivity and stability under thermal stress and light soaking by extending the π-conjugation of the hydrophobic ligands [48]. One example of this is the recently reported C104 dye, *cis*-RuLL′(NCS)$_2$ (where L stands for 4,4′-bis(5-octylthieno[3,2-*b*]thiophen-2-yl)-2,2′-bipyridine, and L′ for 4,4′-dicarboxyl-2,2′-bipyridine), which presents a noteworthy efficiency of 10.5% [49].

Besides mononuclear Ru(II) complexes, multinuclear compounds [45, 50], as well as chromophore-acceptor or chromophore-donor dyads made of Ru(II) species and organic quenchers, have been used as sensitizers with the aims of: 1) increasing the absorption properties of the (multicomponent) sensitizer, by using systems featuring the antenna effect, with the energy trap of the antenna being the Ru(II) unit directly connected to the semiconductor; 2) spatially separating the injected electron and the hole on the sensitizer, so decreasing losses due to charge recombination [42].

18

Most of the work in DSSCs has focused on Ru(II) polypyridine complexes, as already mentioned, mainly because of their intense charge transfer absorption across the whole visible range, moderately intense emission with fairly long lifetimes in fluid solutions at ambient temperatures, high quantum yields for the formation of the lowest CT excited state, and redox reactivity and ease of tunability of redox properties. However, research has also been extended to other charge transfer d^6 complexes such as Os(II) [51, 52], Fe(II) [53, 54] and Re(I) [55], and also other metals like Cu(I) [56, 57] and Pt(II) [58, 59].

Ruthenium trisbipyridine complexes have been extensively investigated as photo-sensitizers because their lowest excited states are long-lived MLCT states that can participate in electron- and energy-transfer reactions. However, in DSSCs, electron transfer from the excited states of the sensitizer to the conduction band of TiO_2 occurs within hundreds of femtoseconds [20]. This time scale of electron injection, and its near unity quantum efficiency, imply that the electron transfer occurs from initially populated, non-relaxed excited states. Previous notions that electron transfer occurs exclusively from the lowest excited-state directed the choice of sensitizing molecules on the basis of emissive properties. However, for electron transfer occurring from initially populated states, as in the DSSC, it may be the absorptive properties that matter most [54]. This changed the entire perspective of what makes a "good" sensitizer, and opened up new research directions. Ferrere [54] and Sauvé [51] investigated polypyridyl complexes of Fe(II) and Os(II), respectively, as alternatives to the analogous ruthenium complexes.

Iron, ruthenium and osmium are in the same triad of the periodic table. As a first row transition metal, iron has the weakest ligand field and osmium, a third row metal, has the strongest one (t_{2g}-e_g* splitting). Assuming a regular octahedral structure with O_h symmetry, for osmium and ruthenium the e_g* metal orbitals are substantially higher than the π* molecular orbital from the polypyridine ligand, whereas for iron, the e_g* metal orbitals are lower in energy and comprise the lowest excited state orbitals (see figure 6). As a consequence, not only are the MLCT lifetimes of the iron complexes shortened, but also the population of the e_g* metal orbitals spatially removes the excited electron from the bipyridyl ligand (which in most cases is proximal to the acceptor – the π* orbitals of the polypyridyl ligand are electronically coupled to the Ti(3d)-orbital manifold of the semiconductor through the anchoring group [45]) and can render the complex unstable

since the e_g* metal orbitals are antibonding [54]. All in all, it has been demonstrated that the [Fe(dcbH$_2$)$_2$(CN)$_2$] complex (where dcb stands for 4,4´-dicarboxylic acid-2,2´-bipyridine) can sensitize nanocrystalline TiO$_2$ in a DSSC [53], and although the reported photocurrents and photovoltages are much smaller than those with ruthenium complex sensitizers, the iron complex exhibits relatively high quantum yields. Having in mind that the cost of iron is less than 1% of the cost of ruthenium and much more abundant, it is expected that further research can render iron based dyes an economic alternative to ruthenium sensitizers.
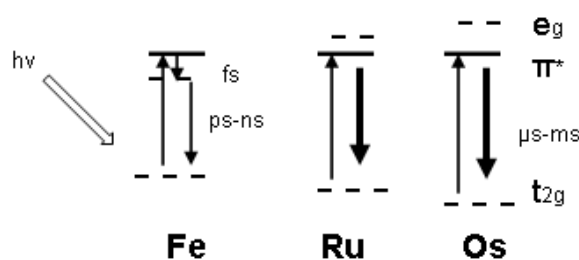
Fig. 6. Comparative excited state orbital ordering in octahedral iron, ruthenium and osmium bipyridyl complexes [54].

In the case of osmium polypyridyl complexes, there is an additional absorption band at longer wavelengths compared to a ruthenium complex having the same ligands, because direct excitation of the triplet state in osmium polypyridyl complexes is less forbidden than in analogous ruthenium complexes. And it has been reported that acting as sensitizers in DSSCs they extend the light absorption and spectral response to longer wavelengths while also providing high external quantum yields for photocurrent flow similar to their analogous ruthenium complexes. Osmium complexes thus seem very promising candidates for further optimization in operating photoeletrochemical cells for solar energy conversion applications.

Islam *et al*. have synthesized square planar platinum(II) diimine dithiolate complexes that can also efficiently sensitize nanocrystalline TiO$_2$ [58, 59]. They reach efficiencies of up to 3%. However, recombination and aggregation problems typical of these platinum (II) complexes [60] seem to stop these sensitizers from being more efficient.

Copper(I) α,α´-diimine complexes have also been employed as sensitizers in DSSCs [56, 57, 61] (see later).

Despite the high performances, especially of the ruthenium dyes, other non-metallic alternatives are currently being pursued [62]. Due to its scarcity, ruthenium is a very expensive metal and hence requires an extra recycling fee. The most promising alternatives are organic dyes, natural or synthetic, which are considerably cheaper, though so far generally less stable and less efficient. However, they have a great potential for this application due to their high absorption coefficients compared to ruthenium sensitizers [63].

When considering organic dye structures, porphyrins [64] and phthalocyanines [65] attract particular attention, the former because of the analogy with natural photosynthetic processes, the latter because of their photochemical and phototherapeutic applications. However, porphyrins cannot compete with the N3 or "black dye" sensitizers due to their lack of red light and near IR absorption. Phthalocyanines do show intense absorption bands in this spectral region. However, problems with aggregation and the unsuitable energetic position of the LUMO level have turned out to be intractable so far [21]. A remarkable advance in the use of organic dyes for DSSCs was made by the group of Hara *et al* [66, 67]. Using coumarine (see figure 7) or polyene type sensitizers, strikingly high solar to electric power conversion efficiencies reaching up to 7.7% in full sunlight have been achieved.
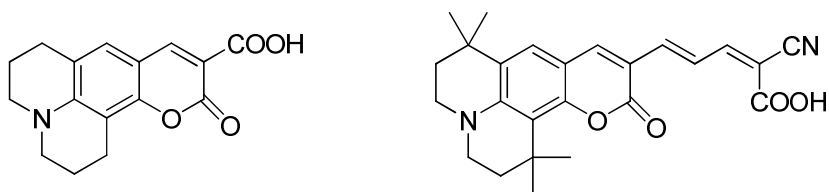

Fig. 7. Molecular structure of coumarine derivatives employed as sensitizers in DSSCs [66].

Another strategy to obtain a broad optical absorption extending throughout the visible and near IR region is to use a combination of two dyes which complement each other in their spectral features [68, 69]. This co-sensitization has the advantage of enhancing photo-absorption in that

the optical effects of the two sensitizers are found to be additive. In particular, there was no negative interference between the co-adsorbed chromophores, opening up the way for testing a multitude of other dye combinations [70].

Semiconductor quantum dots are another attractive option for panchromatic sensitizers [15]. These are II-VI and III-V type semiconductors particles whose size is small enough to produce quantum confinement effects. The absorption spectrum of such quantum dots can be adjusted by changing the particle size. One problem with this approach is the photo-corrosion of the quantum dots, which will almost certainly happen if the junction contact is a liquid redox electrolyte. However, they are expected to display higher stability in the solid-state hetero-junction device [71]. The advantage of these sensitizers over conventional dyes is their very high extinction coefficient allowing the use of thinner films of the mesoporous oxide. This should reduce the dark current increasing V_{oc} and the overall efficiency of the cell.

In addition to all these alternatives, fruits, flowers and/or leaves have been employed as sources of natural photosensitizers and reported as cheaper, low-energy and environmentally friendly alternatives for the production of DSSCs [36].

I. 1. 3   Electrolyte

The electrolyte is a crucial part of all DSSCs. It is responsible for inner charge carrier between electrodes – it is the *hole-transport material*. It regenerates the dye at the photoelectrode with the charge collected at the counter electrode. For stable operation of the solar cell and maximal power output, the oxidized dye must be reduced back to the ground state as rapidly as possible by a suitable electron donor. Since the maximum photovoltage (V_{oc}) obtainable corresponds to the difference between the Fermi level of the electron in the TiO_2 and the redox potential of the electrolyte [15], it is preferable to choose a couple whose potential is as close to the redox potential of the sensitizer as possible. In addition, the choice of the mediator should be such that there is enough driving force for the dye reduction step to have optimal rate. It is also important

for stable performance of the solar cell that the redox couple is fully reversible, without any significant absorption in the visible region and stable in the oxidized and reduced forms [18].

The best results have always been obtained with the triiodide/iodide (I_3^-/I^-) redox couple in an organic matrix, generally acetonitrile. The good performance of this redox mediator is based on the kinectics of the processes: first, the photo-oxidized dye injects an electron into the conduction band of the semiconductor much faster than electron recombination with I_3^-. Secondly, the oxidized dye preferably reacts with I^- than recombines with the injected electron. Finally, the two electron process of I^- regeneration from I_3^- occurs quickly enough at the catalyst-coated counter electrode to be productive. These combined processes lead to coherent I_3^- diffusion towards the counter electrode and I^- diffusion in the opposite direction.

$$2e^- + I_3^- \rightleftharpoons 3I^-$$
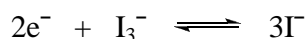
Fig. 8. Triiodide/iodide redox couple.

An issue that has to be taken into consideration when employing this redox couple as electrolyte is its concentration. Obviously, at low concentrations conductivity will be insufficient and rapid reduction will not be ensured. On the other hand, when employed in high concentrations, apart from possible corrosion problems, iodide can substantially suppress cell efficiency by increasing the recombination of I_3^- and injected electrons, and increasing the rate of light absorption by the redox couple. The suppression of the dark current (see below) may be achieved by additives such as tetrabutylammonium hydroxide (TBAOH) [72] and/or methylbenzimidazole [73]. Additionally, these additives also enhance the cell's long-term stability [73].

Other redox couples have also been tested, and theoretically a well designed change in the electrolyte formulation could increase the V_{oc} by up to 300 mV [74]. Some of the couples tested are phenothiazine [75], $(SeCN)_2$/$SeCN^-$ [76], $(SCN)_2$/SCN^- [76] and/or Br_3^-/Br^- [77]. However, probably the most tested and most viable alternative to date is the use of cobalt complexes. Several complexes of Co(II)/Co(III) have been tried [78, 79]. Compared to iodide, their advantage is that they are non-volatile, non-corrosive and have the benefit of being easy for

molecular modifications. However, with present technology the current exchange rate at the counter electrode is much smaller and leads to voltage losses [79].

Regarding the solvents employed for the redox couple, several organic solvents such as methoxypropionitrile [80], butyronitrile [81] and/or methoxyacetonitrile [82] have been used among others. However, acetonitrile is the most used solvent, particularly when one wishes to maximize cell efficiency. Virtually hundreds of chemical compounds can be experimented with as long as they fulfill most of the following requirements: low volatility at the expected cell operating temperature; low viscosity; resistance to decomposition over long periods of time; good redox couple stability; low toxicity and low cost.

The most noteworthy of the non-traditional electrolytes are room temperature ionic liquids, *quasi*-solid state and solid state. These electrolytes are progressively viscous enabling increased stability. They appear to solve problems such as dye desorption, solvent evaporation and sealing degradation, however, until now their performance has been consistently lower. A more viscous electrolyte diminishes regular charge diffusion and, therefore, requires higher concentration of the redox couple to maintain conductivity. Hence, a higher redox couple concentration creates new problems, or makes them meaningful (e.g. corrosion and direct reaction with the semiconductor). Balanced electrolyte development is the missing piece to remove complicated sealing and volatility issues while pursuing long-term high performance.

The development of ionic liquid electrolytes has been one of the most dynamic research areas within DSSCs [83, 84]. Ideally, ionic liquids should have good chemical and thermal stability, negligible vapor pressure, non-flammability, high ionic conductivity and a wide electrochemical window [85]. Molten salts based on imidazolium iodides have revealed very attractive stability features [86, 87]. Despite their high viscosity, linear photocurrent response up to full solar light intensities has been observed. The best results have been obtained with 1,3-dialkylimidazolium iodide compounds [88].

The solid-state DSSC is an alternative that offers itself to confront the sealing problem by the replacement of the volatile redox electrolyte by a solid p-type semiconductor interpenetrating the

nanocrystalline TiO_2 structure, which would permit the charge neutralization of dye molecules after electron injection by its hole transport properties. The main difficulty is optimizing the interface between the sensitized semiconductor and the electrolyte; it is very difficult to achieve an intimate contact, without voids, among particles due to the roughness of the former and the impossibility of high-temperature depositions of the latter. The most successfully employed organic charge transfer material is spiro-MeOTAD. It was initially presented by Grätzel *et al.* in 1998 [89] and presently attains conversion yields above 4% [63].

Finally, there is another important point to think about when trying to have the maximum cell voltage obtainable: dark currents. The oxide layer is an inter-connected network of particles with high porous interior. The dyes can penetrate everywhere and adsorb over a large surface area, but also the redox mediator must penetrate the same domain so as to be present in the immediate vicinity of the photosensitizer. If the redox mediator gets to the back contact, dark currents arise from the reduction of the redox mediator by the collector electrode with the oxide layer. In principle, this charge recombination can occur at surfaces other than that of TiO_2. Due to the porous nature of the TiO_2 film, it can also occur at the back conducting glass (TCO) electrode.

Dark currents can be suppressed by co-adsorption of saturated hydrocarbons with anchoring groups that isolate the uncovered oxide surfaces from interactions with oxidized form of the redox couple, for example chenodeoxycholic acid [18, 90, 91]. Alternatively, exposure of the dye-coated electrode to a solution of a pyridine derivative such as 4-t-butylpyridine has been found to improve dramatically the efficiency of the cell [18]. Another strategy, as mentioned before in this chapter, is to use a compact [22] or nanocrystalline [23] TiO_2 "blocking layer".

I. 1. 4   Conducting substrate

The most commonly used substrates for DSSCs are made of coated glass with a transparent conducting oxide (TCO). Suitable TCO must have high electrical conductivity to efficiently collect all the generated photocurrent, and high transparency. Among a high variety of TCOs, the most widely used is fluorine doped tin dioxide (SnO_2:F or FTO) due to its thermal steadiness and

low cost. Indium tin oxide (In_2O_3:Sn or ITO) has also been used extensively because it has higher specific conductivity. However, it does not remain stable at high temperatures.

These conducting glass electrodes are known to be a poor choice for efficient reduction of I_3^-, therefore a catalyst is needed in the counter electrode to overcome the high activation energy of the two-electron transfer. Platinum is clearly the most widely used material, acting as a catalyst in the redox reaction at the counter electrode and thus avoiding this process becoming rate limiting in the light energy harvesting system. A problem with platinum, however, apart from its high price, is the non-confirmed possibility of corrosion by the iodide solution, which leads to the formation of PtI_4 [92]. Since platinum is very expensive, other cheaper alternatives may take its place like various forms of carbon [93]. Gold, although expensive, is another viable alternative [94] that is consistently used in solid state DSSCs.

Outlook

Understandably in a multi-component device like DSSCs, the overall performance of the cell depends critically on the individual properties of the constituent components and processes. Listed below are some of the major properties that one needs to deal with in the design of solar cells.

- the structure, morphology, optical and electrical properties of the nanoporous oxide layer;
- the chemical, redox, photophysical and photochemical properties of the dye;
- the visco-elastic and electrical properties of the electrolyte carrying the redox couple;
- the redox and optical properties of the redox mediator;
- and the electrical and optical properties of the counter electrode.

Regarding key processes one can cite:

- light absorption of the dye and charge injection from the excited state of the latter;
- regeneration of the oxidized dye;

- electron percolation within the oxide film;
- dark currents;
- and counter electrode performance.

For a photovoltaic device to remain serviceable for 20 years without significant loss of performance, all the aspects mentioned before have to be scrutinized. However, one of the reasons for the outstanding stability of DSSCs is the very rapid deactivation of the excited state of the sensitizer *via* charge injection into the TiO_2, which occurs in the femtosecond time domain (see figure 9). This process is much faster than any other competing channel of excited state deactivation [15].
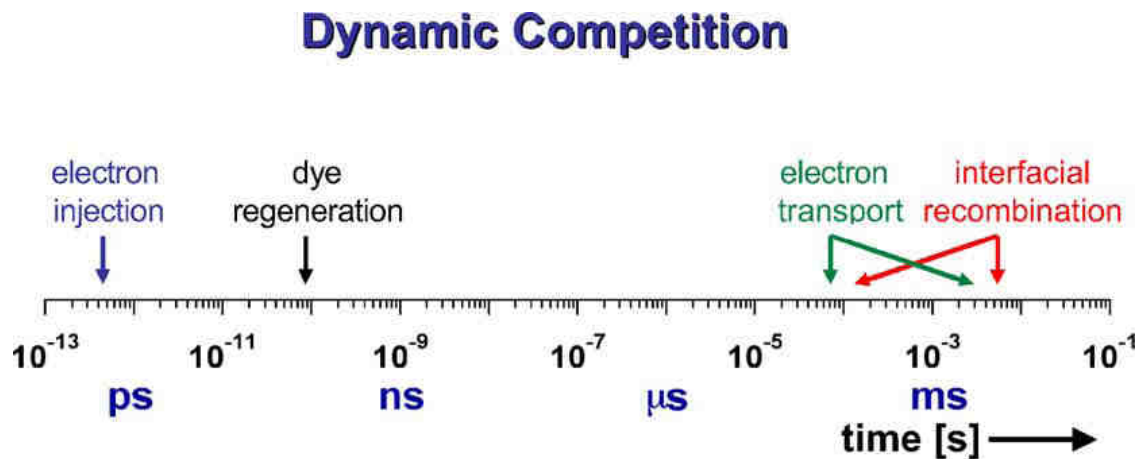
Fig. 9. Dynamics of redox processes involved in the conversion of light to electric power by DSSCs [15].

Optimal performance is obtainable only when one understands the factors that control each of the components and depends on the ability to tune to the required configuration [95]. However, for devices targeted for commercialization, stability and material cost are very important, in addition to efficiency. Several studies have analyzed the components of DSSCs with respect to their stability and how their durability affects the entire system [73] (see figure 10).
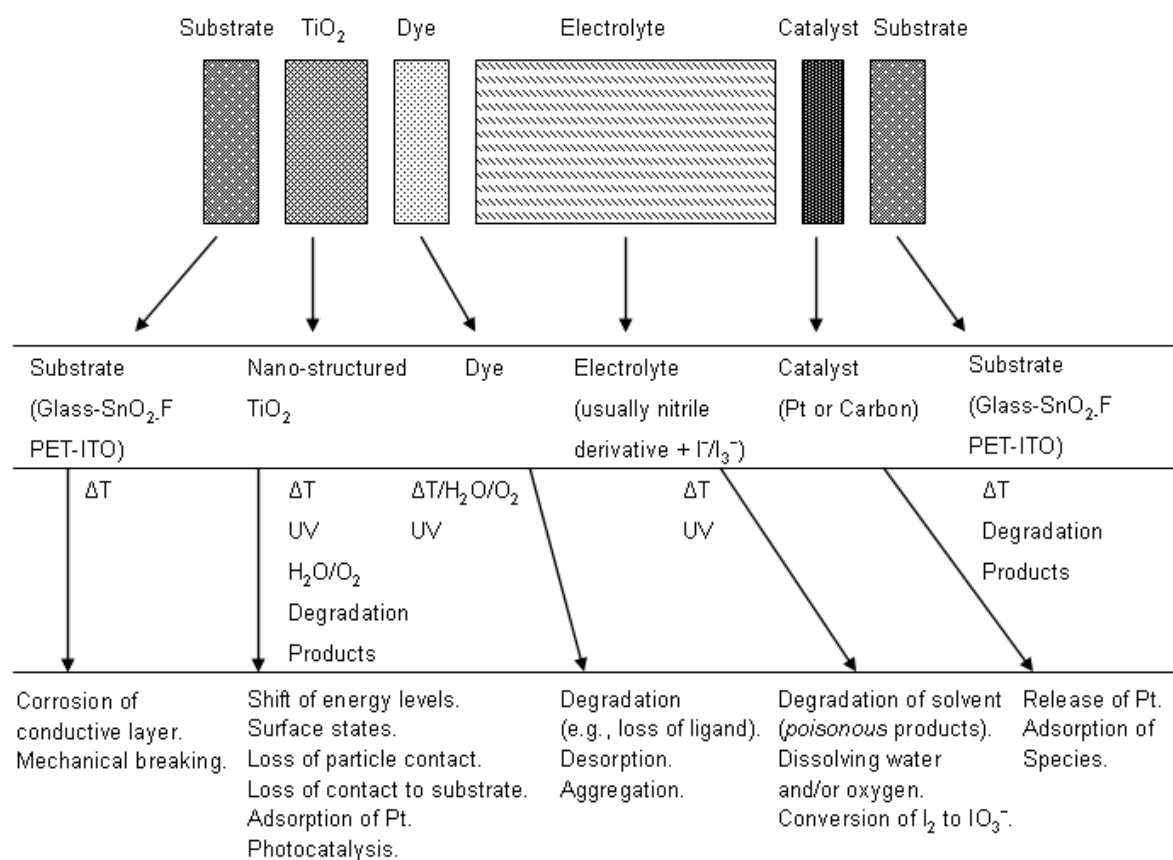
Fig. 10. Degradation mechanisms of the DSSCs – component analysis [73].

I. 2   Ruthenium(II)- vs. copper(I)-polypyridyl complexes for sensitizer applications

Ruthenium(II) is a d^6 system forming octahedral complexes with the usually colourless polypyridine ligands. In order to understand the general properties of Ru(II) polypyridine complexes, it is convenient to refer to the properties of the prototype of this class of compounds, that is, $[Ru(bipy)_3]^{2+}$ (where bipy stands for 2,2´-bipyridine). This complex has certainly been one of the species most extensively studied and widely used in research laboratories during the last 30 years [96].

Regarding copper(I), it has to be noted that its coordination behavior is strictly related to its electronic configuration: d^{10}. The complete filling of d orbitals leads to a symmetric localization of the electronic charge. This situation favors a tetrahedral disposition of the ligands around the metal centre in order to place the coordination sites far from one another and minimize electrostatic repulsions (see figure 11). The most extensively studied $[Cu(NN)_2]^+$ complexes (where NN signifies α,α´-diimine) are copper(I)-bisphenanthroline complexes [97]. The parent compound $[Cu(phen)_2]^+$ (where phen stands for 1,10-phenanthroline) has been scarcely studied, probably due to the lack of long-lived electronic excited states in solution and its instability in air. The most common complexes are those 2,9 or 4,7-disubstituted phenanthrolines [98], due to an easier synthetic accessibility of the related ligands and their stability.
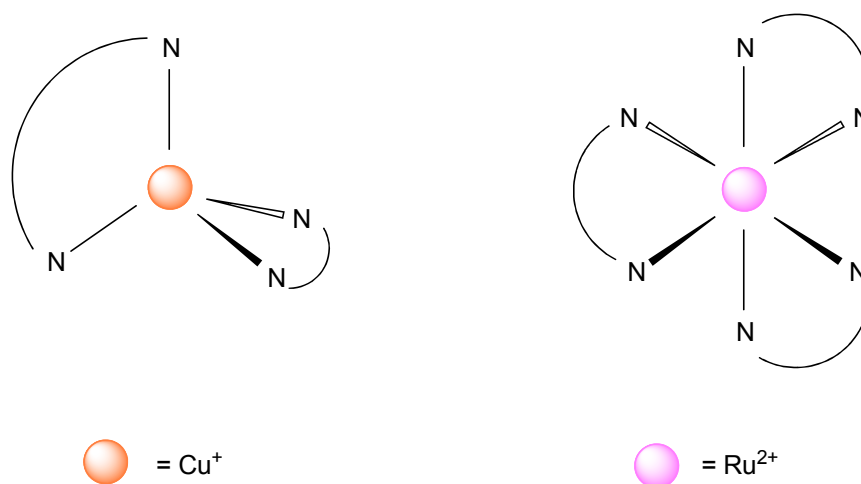
Fig. 11. Different coordination geometries of copper(I)- and ruthenium(II)-polypyridyl complexes.

Copper(I)-polypyridyl complexes show commonly metal-to-ligand charge-transfer (MLCT) transitions, which are also observed for example for Ru(II)-bipyridines. As far as emission is concerned, long-lived luminescent MLCT excited states of d^6 metal complexes, in particular those of Ru(II), can be strongly affected by the presence of upper lying metal-centered (MC) levels. The latter can be partially populated through thermal activation from the MLCT states and prompt non-radiative deactivation pathways and photochemical degradation. Closed shell d^{10} copper(I) complexes cannot suffer these kind of problems, but undesired non-radiative

deactivation channels of their MLCT levels can be favored by other factors. The next orbital diagram illustrates the electronic transitions of Ru(II) and Cu(I) complexes:
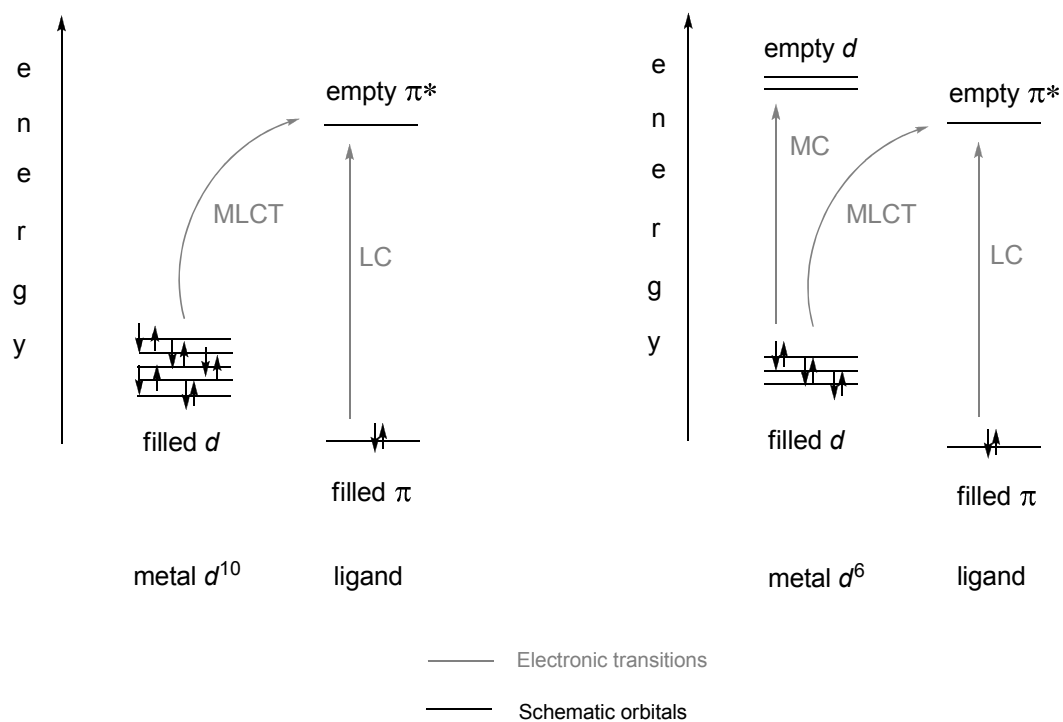
Fig. 12. Qualitative comparison of orbitals and related electronic transitions in metal complexes having d^6 (e.g. Ru(II)) and d^{10} (e.g. Cu(I)) configurations.

In an attempt to compare the absorption, emission and electrochemical properties of copper(I)- and ruthenium(II)-polypyridyl complexes, the photophysical and electrochemical parameters of $[Cu(dpp)_2]^+$ (where dpp stands for 2,9-diphenylphenanthroline) and $[Ru(bipy)_3]^{2+}$ are compared in figure 13:
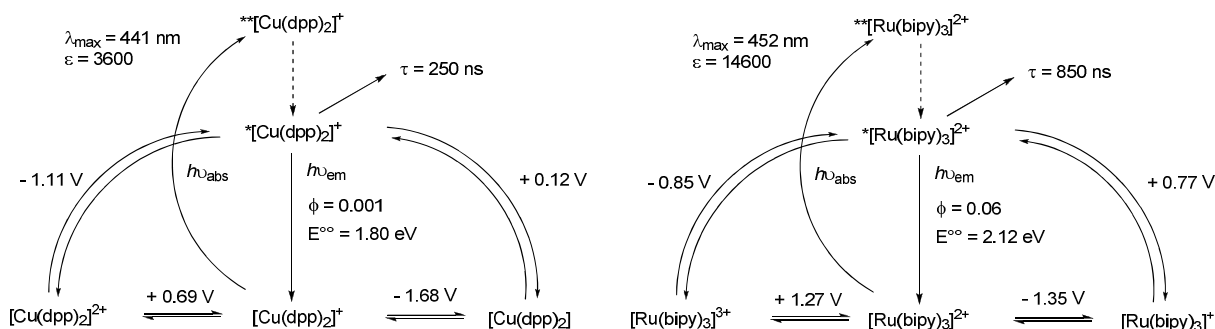
Fig. 13. Comparison between the photophysical and electrochemical properties of $[Cu(dpp)_2]^+$ and $[Ru(bipy)_3]^{2+}$ [97].

As it can be observed, each complex is a better oxidant and reductant in the excited state than in the ground state. Importantly, $*[Cu(dpp)_2]^+$ is a more powerful reductant than $*[Ru(bipy)_3]^{2+}$ (-1.11 vs. -0.85 V, respectively) owing to its more favorable ground state 2+/+ potential (+0.69 *vs.* +1.27 V, respectively), that largely compensates for the lower content of excited state energy (1.80 vs. 2.12 eV). Other parameters seem to disfavor $[Cu(dpp)_2]^+$ *vs.* $[Ru(bipy)_3]^{2+}$. However, iterative studies have shown how to modify NN-type ligands in general, and phenanthrolines in particular, in order to improve their photophysical performances. This progress, together with their similar absorption spectrum [42, 97, 99] suggests that $[Cu(NN)_2]^+$ complexes can be an interesting alternative to Ru(II)-polypyridines for purposes such as sensitizers in DSSCs.

In the literature, a report dating back to 1994 about a copper(I)-phenanthroline derivative sensitizer can be found [56]. However, due to its low efficiency, research has been redirected to copper(I)-bipyridines [61]. In this thesis, mainly copper(I)-bipyridines have been synthesized and studied as sensitizers, with the aim of employing them for DSSCs applications. Further, we have taken advantage of the lability of this metal to form heteroleptic complexes on the surface of the semiconductor (see section V. 4).

II   2,2´-Bipyridine ligands

2,2´-Bipyridine (bipy) is a bidentate chelating ligand, widely used in metallosupramolecular chemistry [100, 101]. It is formed by the coupling of two pyridine rings that have a *trans*-coplanar conformation, which is the energetically most favored geometry.

Upon coordination to a metal centre 2,2´-bipyridine undergoes rotation about the interannular C-C bond to form metal complexes where it acts as a chelating bidentate species with the two nitrogen atoms (see figure 14). In general, a near-planar configuration of the two pyridyl rings is adopted. The C-C distance is relatively independent of the metal ion, whereas the M-L bond distance and the N-M-N angle depend on the metal ion used.
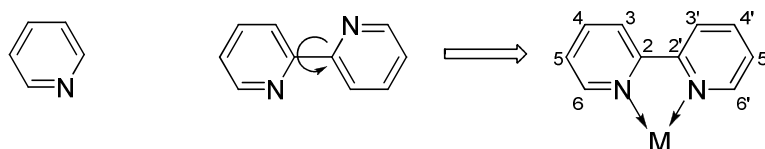
Fig. 14. Chemical structure of pyridine and its derivative 2,2´-bipyridine. The conformational change from the *trans*- to the *cis*-coplanar form upon coordination to a metal together with ligand numeration is shown.

This ligand was first synthesized in 1888 by Fritz Blau by the oxidative coupling of 2-pyridinecarboxylic acids or the oxidation and decarboxylation of 1,10-phenanthroline [102, 103]. But it was not until the 1950s, when large amounts of 2,2´-bipyridine were required for the preparation of Diquat insecticides, that bipyridine chemistry had its renaissance [104]. Since then, thousands of 2,2´-bipyridine derivatives and their complexes have been made and characterized, due to the ability of bipy to coordinate almost all metal in the periodic table [105-107] and also due to the extremely interesting electrochemical, photophysical and photoelectrochemical properties of the complexes. Starting in the area of analytical chemistry, an impressive development utilizing bipyridines as building blocks in supramolecular [108] and macromolecular chemistry [109] as well as nanoscience [110] has been observed, not to mention the interest in the use of bipyridine complexes as photosensitizers [96], catalysts [111], colorimetric reagents [112], neurotoxins [113] or potentiometric indicators [114]. It has to be

noted that 2,2′-bipyridines can also be found in natural products like caerulomycins or collismycins:
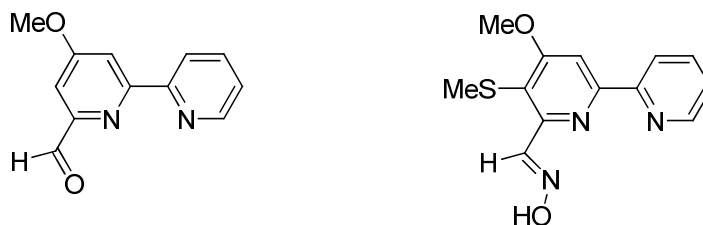
Fig. 15. Structural examples of caerulomycins and collismycins (left and right picture, respectively).

The bonding of the bipyridine moiety can be represented in terms of a delocalized π-system consisting of six overlapping $2p$ orbitals (one from N and five from C atoms). The N atom has five valence electrons, remaining two of them localized outside the ring as a lone pair. Bipyridine is an aromatic compound with a Kekulé-like bonding model.
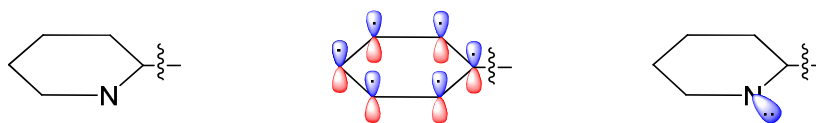
Fig. 16. 6π-Electron system resulting from the overlap of the C and N $2p$ orbitals in the pyridine moiety. The outward-pointing orbital containing the lone pair from the N is shown on the right-hand side diagram.

The two free electron pairs from the nitrogen atoms are used to form the metal-ligand bonds, resulting in a loss of electron density by the ligand and a gain of electron density by the metal. However, it has to be noted that the "real" distribution of electrons between the metal and the ligand is not equal. The sharing of these electron-pairs, in addition to the usual positive charges (+1, +2, etc.) of the metals, have the effect of *polarizing* the ligand and may alter its electronic properties, what is reflected in the properties of the complexes. Associated with this is the presence of filled π and vacant π^* orbitals on the pyridine rings; the precise energies of the π and π^* orbitals depend on the metal ion, and the matching of energies enables bipyridine to act as a π-donor to high oxidation state complexes and a π-acceptor in low oxidation state complexes. It

should also be said here that 2,2′-bipyridine is a strong field ligand that forms relatively stable complexes where the lower oxidation states tend to be favored. However, the bipyridine ligand is associated with a wide range of formal oxidation states ranging from -2 to +7.

So, bipyridines and in general oligopyridines joined through their 2,6-positions have the ability to accommodate different coordination numbers preferred by a particular metal ion and are thus excellent precursors to multimetallic complexes with different coordination geometries. A straightforward example is the case of sexipyridine, which in solution and in the solid state has its pyridine nitrogen atoms arranged in a transoid fashion. Sexipyridine may be considered to consist of three bipyridine or two terpyridine units, and this is recognized by the potential guest. The freedom of choice in the ligand for a particular self-organization induced by the metal's tetrahedral or octahedral coordination number (or other preferred coordination number) is reflected in the assembly of a particular double stranded helix (see figure 17) [115].
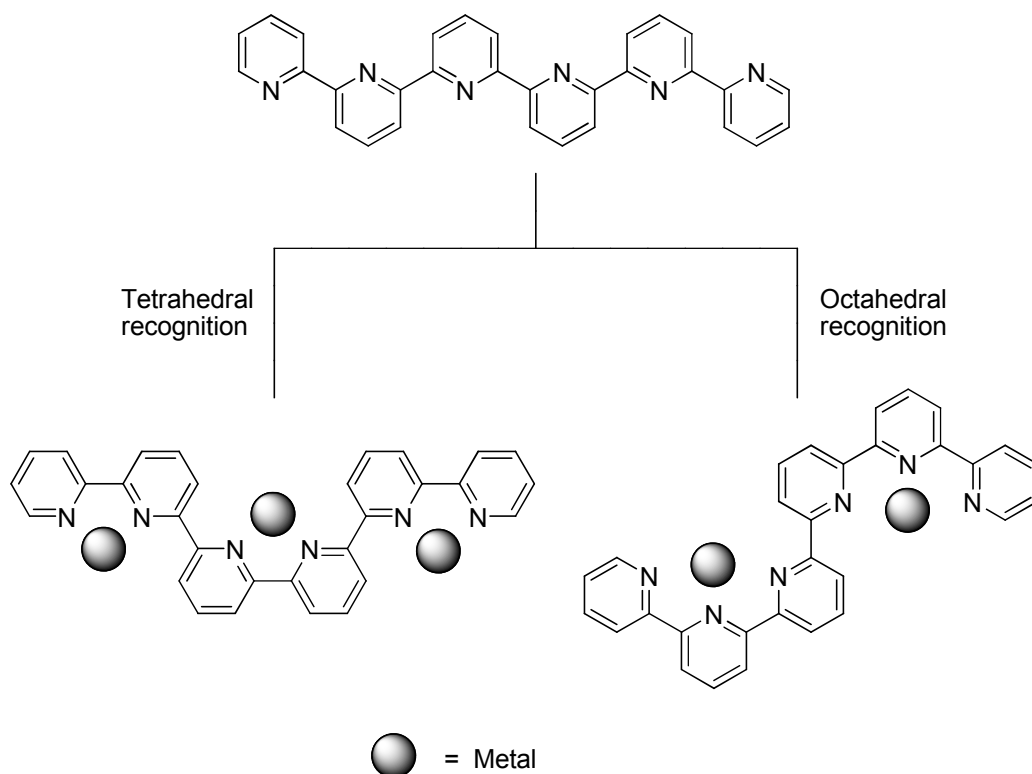

Fig. 17. Tetrahedral and octahedral recognition by sexipyridine. Only half the coordination sphere of each metal centre is shown for clarity.

In this thesis, 2,2´-bipyridine ligands are employed to make complexes with copper(I) metal ions, with the final aim of using these complexes as sensitizers for solar cell applications. For this purpose, the ligands need to fulfill two requirements: i) in order to have stable copper(I) complexes, substituents in the 6 and/or 6´ positions of the 2,2´-bipyridine are required. In this way, one may exclusively impose a tetrahedral coordination geometry and avoid or hinder the oxidation to copper(II) [116]; ii) bear adequate anchoring groups (such as carboxylic or phosphonic acids) to adsorb the complexes to the surface of the semiconductor [36].

Back in 1994, Alonso-Vante *et al.* reported a copper(I) complex of a 1,10-phenanthroline derivative suitable as sensitizer for large band gap semiconductors [56]. The carboxylic acids used for the adsorption to the semiconductors tested (TiO$_2$ and ZnO) were not directly introduced into the 1,10-phenanthroline framework but into the phenyl substituents in the 2 and 9 positions (see figure 18). This study was based on photochemical and spectroscopic properties of some [CuL$_2$]$^+$ complexes with differently substituted ligands, e.g. L = 2,9-diphenyl-1,10-phenanthroline [117, 118]. It was also taken into consideration the previously observed sensitization effect of copper(I) complexes with various phenylated phenanthrolines in photoelectrochemical cells based on semiconducting zinc oxide ceramic electrodes [119]. This was the first report of heterogeneous sensitizers for photoelectrochemical cells based on titanium dioxide colloidal films and a copper(I) complex. An encouraging photopotential of *ca.* 0.6 V was measured. However, the sensitized photocurrent decreased as a function of time, a clear drawback for solar cell applications.
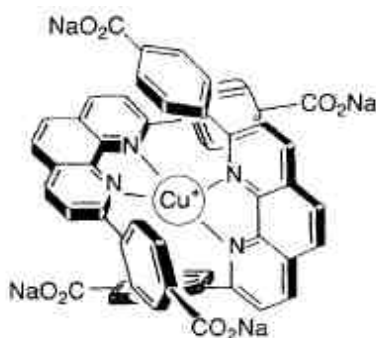

Fig. 18. Bis(2,9-diphenyl-1,10-phenanthroline)copper(I) complex modified at the *para* positions with NaO$_2$C groups used for spectral sensitization of large-band-gap semiconductors by Alonso-Vante *et al*. [56].

35

Years later, in 2002, Sakaki *et al.* went a step further by reporting a copper(I) complex of a 2,2´-bipyridine derivative. When applied to a solar cell with TiO$_2$, it provided successful results: a photocurrent of about 4 mA cm^{-2}, a photovoltage of 630 mV, an energy conversion efficiency of 2.5% and an IPCE value of 30%, under visible light irradiation from a AM 1.5 sunlight simulator (100 mW cm^{-2}) [61]. They achieved these results by introducing the two carboxylic acids directly into the 2,2´-bipyridine framework, more specifically in the 5 and 5´ positions; they claimed that putting a spacer in between them is an unfavorable structure for injection of the excited electron into the conduction band of TiO$_2$ (exactly what Alonso-Vante *et al.* did with their copper(I) 1,10-phenanthroline derivative). Apart from these two carboxylic acid groups, they introduced methyl groups (necessary for a long-lived excited state) at the 4,4´ and 6,6´-positions of 2,2´-bipyridine, the ligand structure is shown in the next figure.
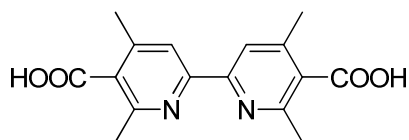
Fig. 19. 4,4´,6,6´-Tetramethyl-2,2´-bipyridine-5,5´-dicarboxylic acid.

As already mentioned before, a critical design feature is the incorporation of an adequate functionality for covalently attaching the dyes to the TiO$_2$ nanoparticles and at the same time for serving as an interlocking group coupling electronically the π* orbitals of the NN-type ligands to the Ti(3d)-orbital manifold of the semiconductor. Most often these groups are carboxylate, phosphonate or borate linkers [32, 36, 43].

With these requirements in mind, five families of 2,2´-bipyridine ligands have been synthesized. An extra family formed by 2,2´-biquinoline ligands has been included in this chapter for being more similar to 2,2´-bipyridine than to 2,2´:6´,2´´-terpyridine. The six families are represented below:

- **Family I:**
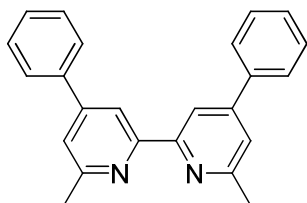
6,6´-Dimethyl-4,4´-diphenyl-2,2´bipyridine **L1**
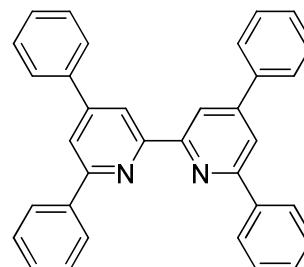
4,4´,6,6´-Tetraphenyl-2,2´bipyridine **L2**

- **Family II:**
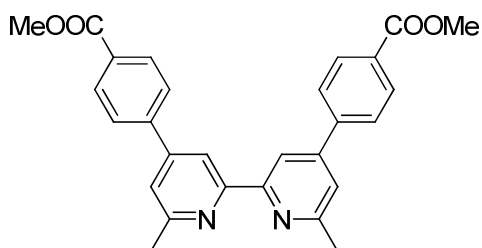
Dimethyl 4,4´-(6,6´-dimethyl-2,2´-bipyridine-4,4´-diyl)-dibenzoate **L3**
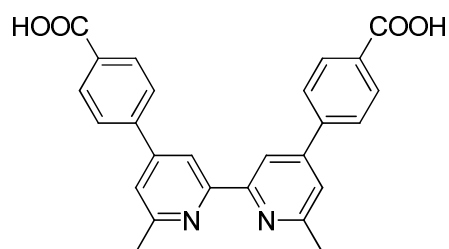
4,4´-(6,6´-Dimethyl-2,2´-bipyridine-4,4´-diyl)-dibenzoic acid H$_2$**L4**
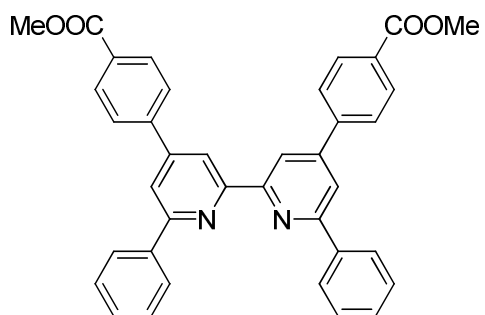
Dimethyl 4,4´-(6,6´-diphenyl-2,2´-bipyridine-4,4´-diyl)-dibenzoate **L5**
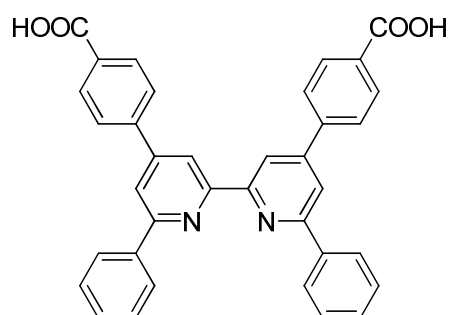
4,4´-(6,6´-Diphenyl-2,2´-bipyridine-4,4´-diyl)-dibenzoic acid H$_2$**L6**

- **Family III:**
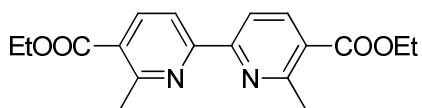
Diethyl 6,6′-dimethyl-2,2′-bipyridine-
5,5′-dicarboxylate **L7**
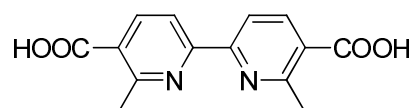
6,6′-Dimethyl-2,2′-bipyridine-
5,5′-dicarboxylic acid H₂**L8**

- **Family IV:**
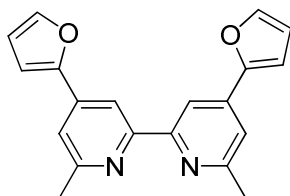
4,4′-Di(furan-2-yl)-6,6′-dimethyl-
2,2′-bipyridine **L9**
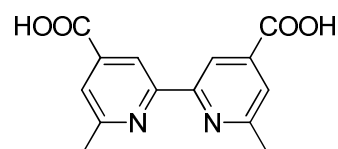
6,6′-Dimethyl-2,2′-bipyridine-
4,4′-dicarboxylic acid H₂**L10**
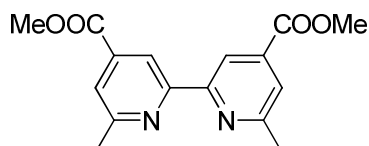
Dimethyl 6,6′-dimethyl-2,2′-bipyridine-
4,4′-dicarboxylate **L11**
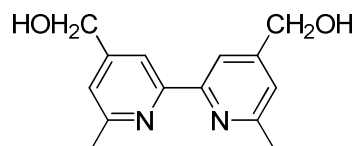
(6,6′-Dimethyl-2,2′-bipyridine-
4,4′-diyl)dimethanol **L12**
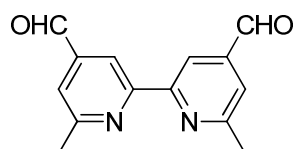
6,6′-Dimethyl-2,2′-bipyridine-
4,4′-dicarbaldehyde **L13**
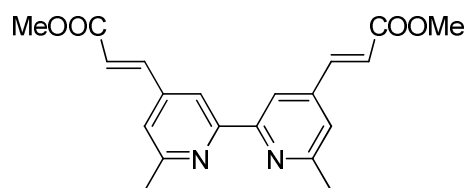
(2E,2′E)-Dimethyl 3,3′-(6,6′-dimethyl
-2,2′-bipyridine-4,4′-diyl)diacrylate **L14**
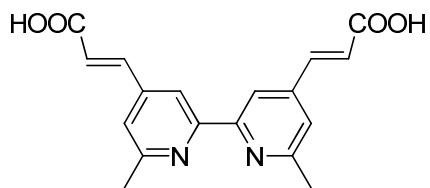
(2*E*,2′*E*)-3,3′-(6,6′-Dimethyl-2,2′-bipyridine-
4,4′-diyl)diacrylic acid H₂**L15**
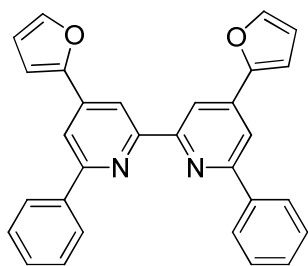
4,4′-Di(furan-2-yl)-6,6′-diphenyl-
2,2′-bipyridine **L16**
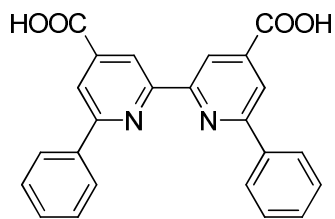
6,6′-Diphenyl-2,2′-bipyridine-
4,4′-dicarboxylic acid H₂**L17**
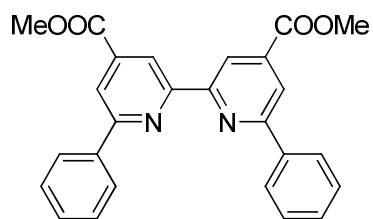
Dimethyl 6,6′-diphenyl-2,2′-bipyridine-
4,4′-dicarboxylate **L18**
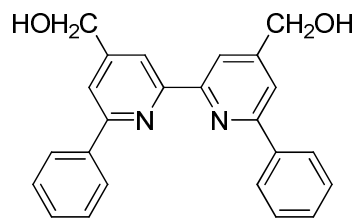
(6,6′-Diphenyl-2,2′-bipyridine-
4,4′-diyl)dimethanol **L19**
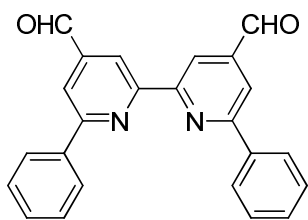
6,6′-Diphenyl-2,2′-bipyridine-
4,4′-dicarbaldehyde **L20**
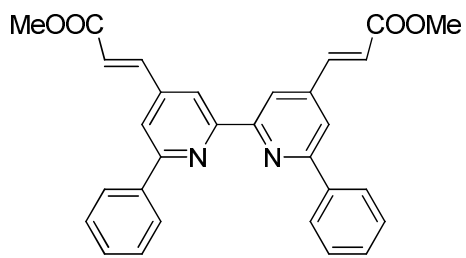
(2*E*,2′*E*)-Dimethyl 3,3′-(6,6′-diphenyl
-2,2′-bipyridine-4,4′-diyl)diacrylate **L21**
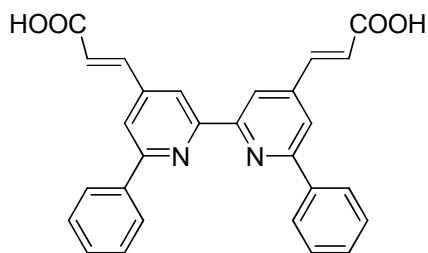
(2*E*,2´*E*)-3,3´-(6,6´-Diphenyl-2,2´-bipyridine-
4,4´-diyl)diacrylic acid H₂**L22**

- **Family V:**
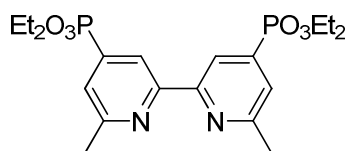
Tetraethyl 6,6´-dimethyl-2,2´-bipyridine-
4,4´-diyldiphosphonate **L23**
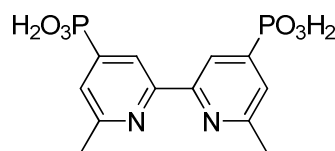
6,6´-Dimethyl-2,2´-bipyridine-
4,4´-diyldiphosphonic acid H₄**L24**

- **Family VI:**
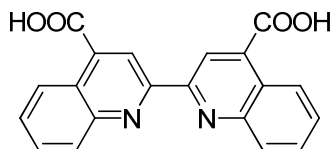
2,2´-Biquinoline-4,4´-dicarboxylic acid H₂**L25**   Dimethyl 2,2´-biquinoline-4,4´-dicarboxylate **L26**
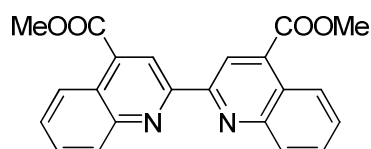
The first family differs from all the others in that members of the group do not contain anchoring groups for solar cell applications. However, these two ligands that differ only in the type of substituent they bear in the 6 and 6' positions (methyl, **L1**; phenyl, **L2**) were of interest to us not only for structural reasons (comparison with other ligands), but also for the *in situ* synthesis of heteroleptic copper(I) complexes. On the contrary, the four ligands of family **II** contain methyl ester or carboxylic acid groups for dye adsorption. These groups are separated from the 2,2´-bipyridine moiety by a phenyl spacer attached to the 4 and 4´ positions of the bipyridine core. The introduction of different functionalities in that position has been explored in this thesis (**L3-**

L6, **L14**, H$_2$**L15**, **L21** and H$_2$**L22**) based on the fact that larger delocalization of the π-electrons from the aromatic part of the molecule normally leads to higher extinction coefficients of the MLCT transitions in their copper(I) complexes [97]. Additionally, other ligands bearing anchoring groups directly attached to the 2,2´-bipyridine moiety, have also been synthesized (**L7**, H$_2$**L8**, H$_2$**L10**, **L11**, H$_2$**L17**, **L18**, **L23**, H$_2$**L24**).

All the ligands and complexes synthesized in this thesis have been characterized by various experimental methods such as nuclear magnetic resonance spectroscopy (NMR), mass spectrometry (MS), ultra-violet visible (UV-VIS) spectroscopy, infrared (IR) spectroscopy, electrochemistry and elemental analysis. In the NMR spectroscopy technique, in order to assign the peaks corresponding to the proton, carbon and phosphorus atoms of the molecules, 1D (^{1}H, ^{13}C, ^{13}C DEPT and ^{31}P) and 2D (COSY, HMQC, HMBC and NOESY) techniques have been employed.

II. 1   Synthesis and characterization of ligands

The synthetic strategy used for the synthesis of ligands **L1**, **L2**, **L3**, **L5**, **L9** and **L16** is based on the methodology of Kröhnke [120], which has been widely used not only for the synthesis of bipyridines [121], but also for the synthesis of functionalized terpyridines [122, 123], quaterpyridines [122, 124], quinquepyridines [122] and sexipyridines [125]. This methodology allows one to prepare a wide range of functionalized oligopyridine derivatives in simple and cheap processes.

First, the cinnamil precursors were synthesized using the methodology described by Sorenson and co-workers for R^1 = Ph, MeOOCC$_6$H$_4$ [126] and Karrer and co-workers for R^1 = furyl (see figure 20) [127]. The cinnamils were prepared as orange crystals from the reaction of 2,3-butanedione with the appropriate aldehyde in methanol or ethanol using piperidium acetate as catalyst. Carbon atoms 1 and 4 of 2,3-butanedione are converted to carbanions by the catalyst, and then each attacks one aldehyde molecule. This intermediate molecule undergoes a condensation that affords the cinnamils in 12-25% yields. The low yields are compensated for by

the inexpensive nature of the starting materials. In the next step, the cinnamils were reacted with the Kröhnke's reagents in the presence of ammonium acetate to produce the desired ligands. This happens through the Michael-addition of the Kröhnke's reagent to the cinnamil, and final cyclisation with ammonium acetate (see figure 21). The Kröhnke's reagents, actually pyridinium salts, were conveniently prepared from the reaction of chloroacetone and/or phenacyl bromide with pyridine following literature procedures [123, 128].
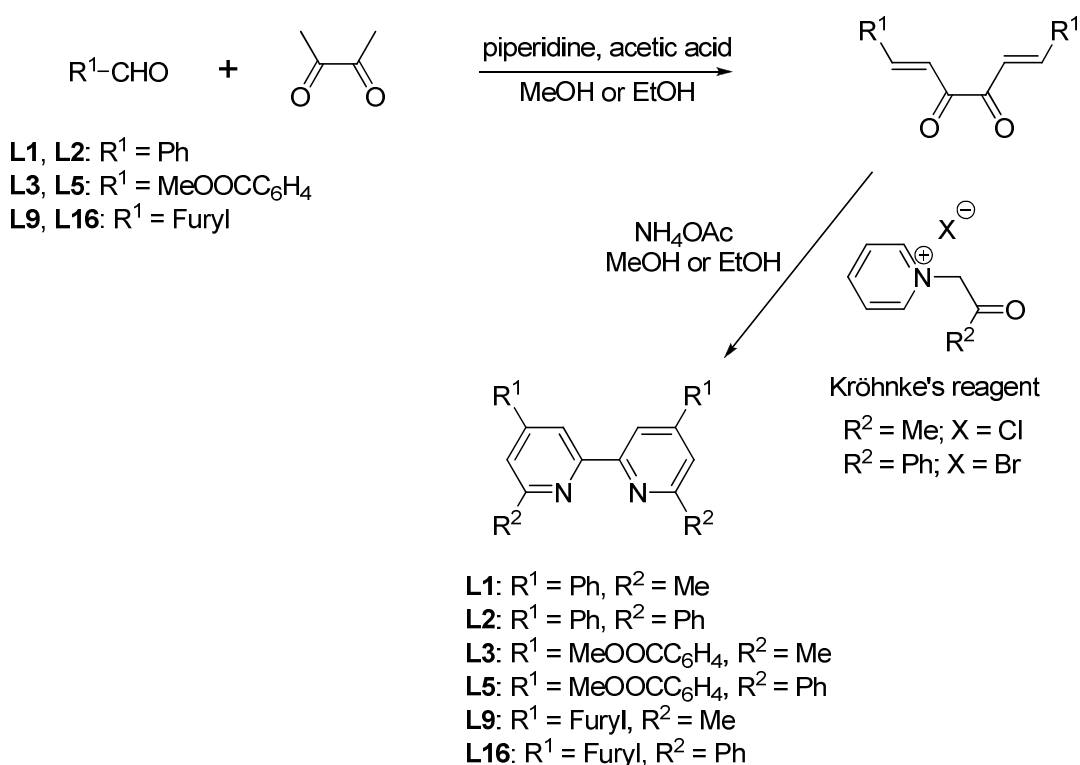
Fig. 20. Synthetic route to ligands **L1**, **L2**, **L3**, **L5**, **L9** and **L16**.
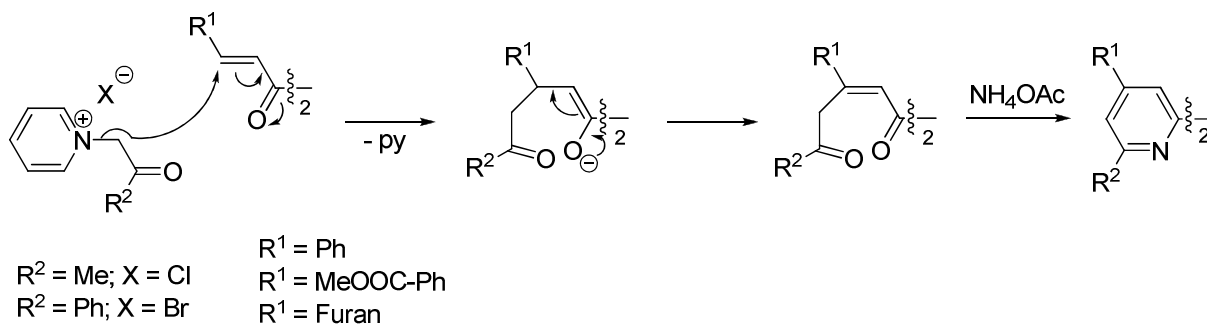
Fig. 21. Reaction mechanism for the synthesis of ligands **L1**, **L2**, **L3**, **L5**, **L9** and **L16**.

In figure 22 the ^{1}H NMR spectra of ligands **L1** and **L2** are shown together with a diagram of the ligands with the number scheme. As normally observed in 2,2´-bipyridines, the signal corresponding to H^{3A} is shifted to higher frequencies than the signal from H^{5A}. This is due to its proximity to the lone electron pair from the nitrogen atom of the second pyridine ring that causes the proton to be more deshielded. This pattern will be observed in all the ^{1}H NMR spectra of the synthesized ligands. The two spectra are readily distinguished by the presence of a signal at δ 2.71 ppm for the methyl groups in **L1** and diagnostic signals for the phenyl substituents (ring C) in the spectrum of **L2**. Apart from that, the signals from H^{3A} and especially H^{5A} are shifted downfield on going from **L1** to **L2**, which is consistent with the deshielding effect of the 6 and 6´ phenyl substituents of ligand **L2**. It is worth saying that in **L2** signals H^{3B} and H^{3C}, and H^{4B} and H^{4C} overlap, leading to a smaller number of resonances than predicted.

L1   L2
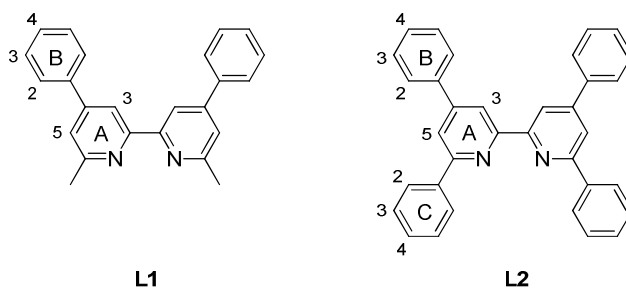
Fig. 22. Diagrams of ligands **L1** and **L2** with number scheme and comparison of their ^{1}H NMR spectra in CDCl$_3$ (*) (500 MHz).

In figure 23 the ^{1}H NMR spectra of ligands **L3** and **L5** are shown. These ligands are similar to **L1** and **L2**, differing only in that they possess a methyl ester group attached to the *para* positions of the rings B (see figure 23 for number scheme). For these ligands, the numeration of the atoms in rings B has been changed, being now 2B and 3B compared to 3B and 2B, respectively, in **L1** and **L2**. A more important consequence of the presence of these functional groups is the strong downfield shift of the signal corresponding to the hydrogen atoms labeled 2B (3B in **L1** and **L2**), due to the electron-withdrawing properties of the methyl ester group. Regarding the rest of the signals, no remarkable shifts are observed in comparison to **L1** and **L2**.

44

Fig. 23. Diagrams of ligands **L3** and **L5** with number scheme and comparison of their ^{1}H NMR spectra in CDCl$_3$ (*) (500 and 250 MHz, respectively).

Ligands **L3** and **L5** were hydrolyzed to their acidic forms by refluxing them with 10 equivalents of LiOH in a H$_2$O:THF 1:10 mixture, to obtain H$_2$**L4** and H$_2$**L6**, respectively. These were obtained as off-white precipitates after the pH of the reaction mixtures is adjusted to 2 with HCl. This methodology was adapted from a reported method [129]. The poor solubility of the ligands brought about the need to employ undesirable solvents like TFA or DMSO for their characterization.

In the next figure the ^{1}H NMR spectra of H$_2$**L4** and H$_2$**L6** dissolved in TFA-d^1 are presented. Once again the deshielding effect of the phenyl groups of H$_2$**L6** on proton H^{5A} is observed. However, the chemical shifts of the signals observed in these spectra cannot be compared with the ones in figure 23 because those were measured in CDCl$_3$ and these in TFA-d^1, due to the low solubility of the ligands. Here it must be taken into consideration that ligands H$_2$**L4** and H$_2$**L6**, after being dissolved in TFA-d^1, have probably undergone protonation at a nitrogen atom and, therefore, they are in a *cis*-conformation, which is the most stable (see figure 25). This may explain why the resonances of H^{3A} and H^{5A} are not so far apart from each other as in **L3** and **L5**.

45
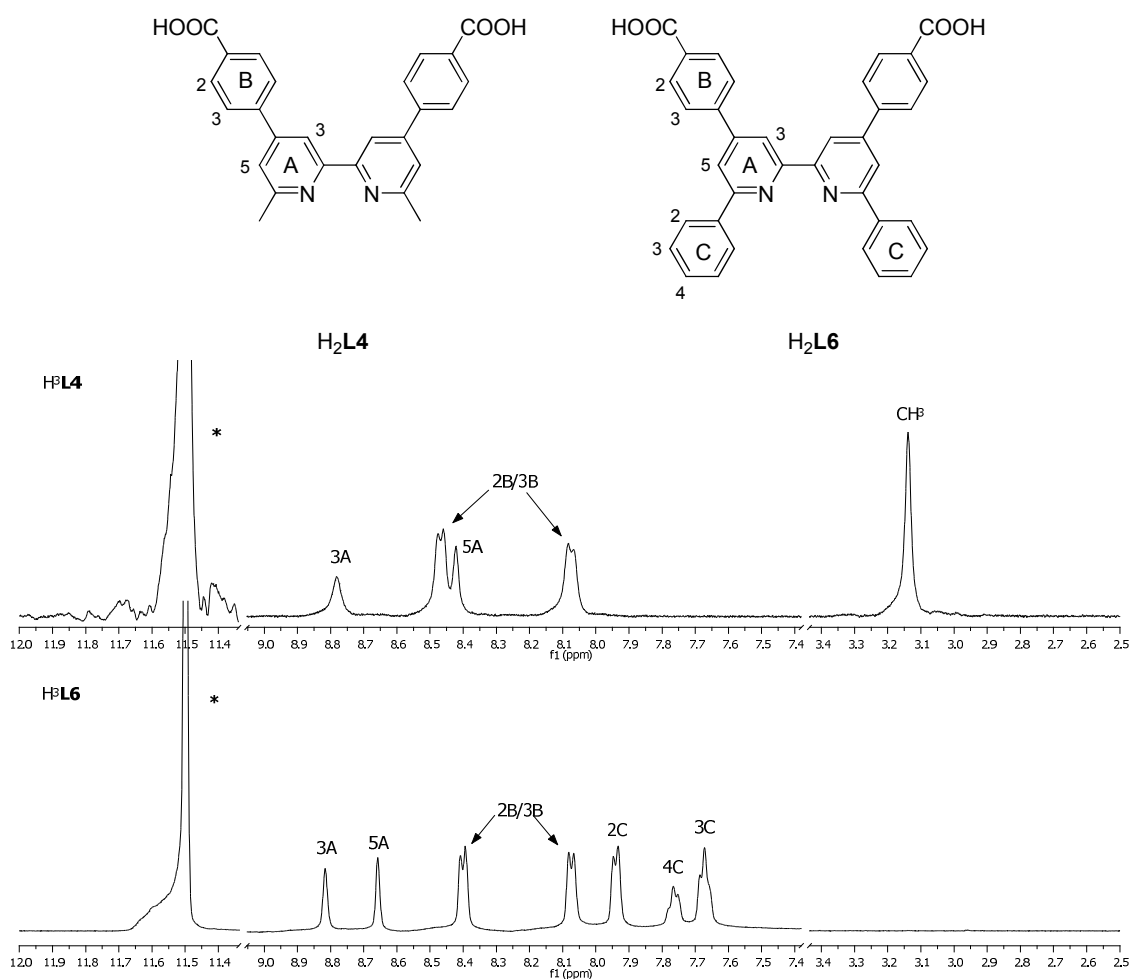
Fig. 24. Diagrams of ligands H$_2$**L4** and H$_2$**L6** with number scheme and comparison of the ^{1}H NMR spectra of H$_3$**L4** and H$_3$**L6** in TFA-d^1 (*) (400 and 500 MHz, respectively).
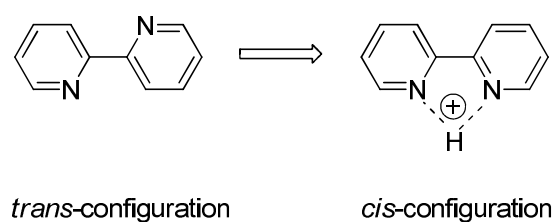
Fig. 25. Upon protonation, 2,2´-bipyridine changes its configuration from transoid to cisoid.

In the case of ligand **L7**, from family III, unlike the previously mentioned ligands (**L1**, **L2**, **L3**, **L5**, **L9** and **L16**), the formation of the pyridine rings does not occur from acyclic precursors, but from the symmetrical coupling of smaller units (see figure 26). The method employed for its

synthesis is based on that reported for the synthesis of diethyl 4,4´,6,6´-tetramethyl-2,2´-bipyridine-5,5´-dicarboxylate, where a Pd/C-catalyzed coupling under reflux and inert atmosphere is employed [130]. Despite the ease of this one-pot-reaction, it has two important disadvantages: the very poor yield of 1.5 % and the 10-days reaction time.
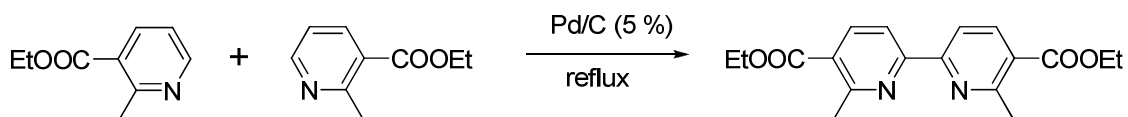
Fig. 26. Synthetic route to ligand **L7**.

In the next step, ligand **L7** was hydrolyzed to its acidic form by refluxing it in a H_2O:EtOH 1:1 mixture with 10 equivalents of KOH. Again, the product, ligand **L8**, is precipitated as an off-white solid by lowering the pH of the solution to 2 with HCl.

The ^1H NMR spectra of ligands **L7** and H_2**L8** were measured in $CDCl_3$ and DMSO-d^6, respectively. There is nothing especially remarkable in them, the resonances being expected. The only interesting thing to mention is that the signals for H^{3A} and H^{4A} (ring A stands for the rings of the 2,2´-bipyridine core) in H_2**L8** overlap, and it is therefore not possible to assign individual signals to these protons. However, it has been possible to assign C^{3A} and C^{4A} by comparison with the ^{13}C spectrum of **L7**.

Moving on to family **IV**, it is worth highlighting that the synthetic route employed for the two groups of ligands which differ only on the substituents in the 6 and 6´ positions is the same.

As mentioned before, ligands **L9** and **L16** were synthesized in two steps starting from the appropriate cinnamil and Kröhnke's reagent, as already described for **L9** [120]. From figure 27 one can appreciate that the ^1H NMR signals from the furan rings (ring B) in **L16** are not influenced by the substituents present in the 6 and 6´ positions of the bipyridine. However, that is not the case for H^{3A} and especially H^{5A}, which are shifted to higher frequencies on going from **L9** to **L16**, in the same way as was described above for related pairs of ligands.
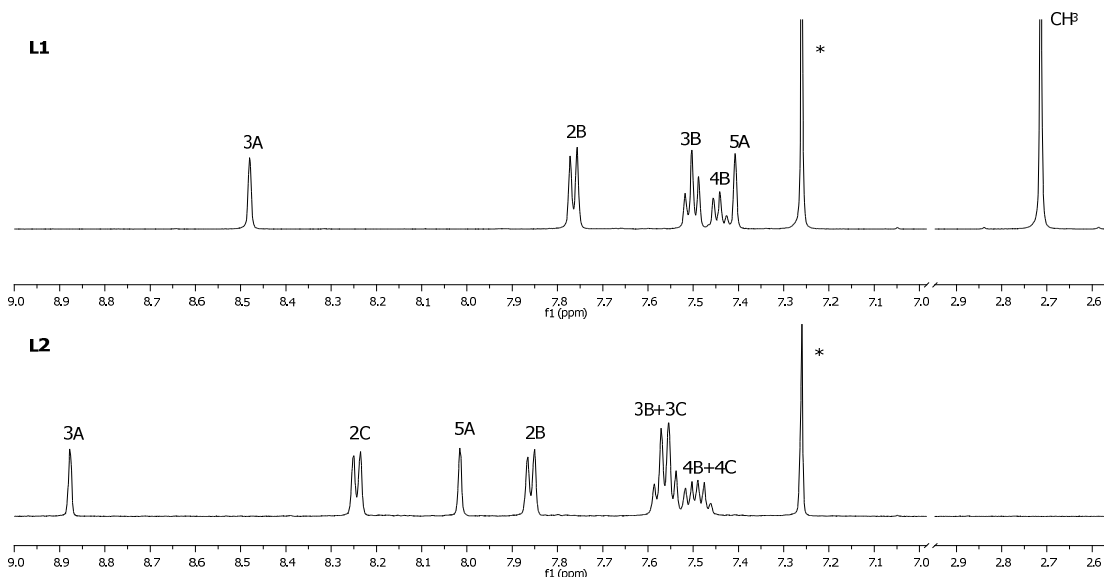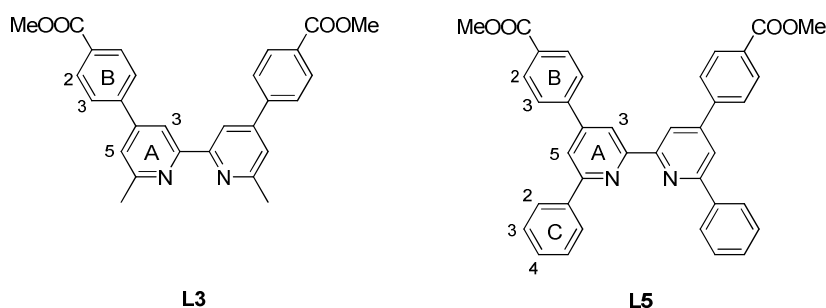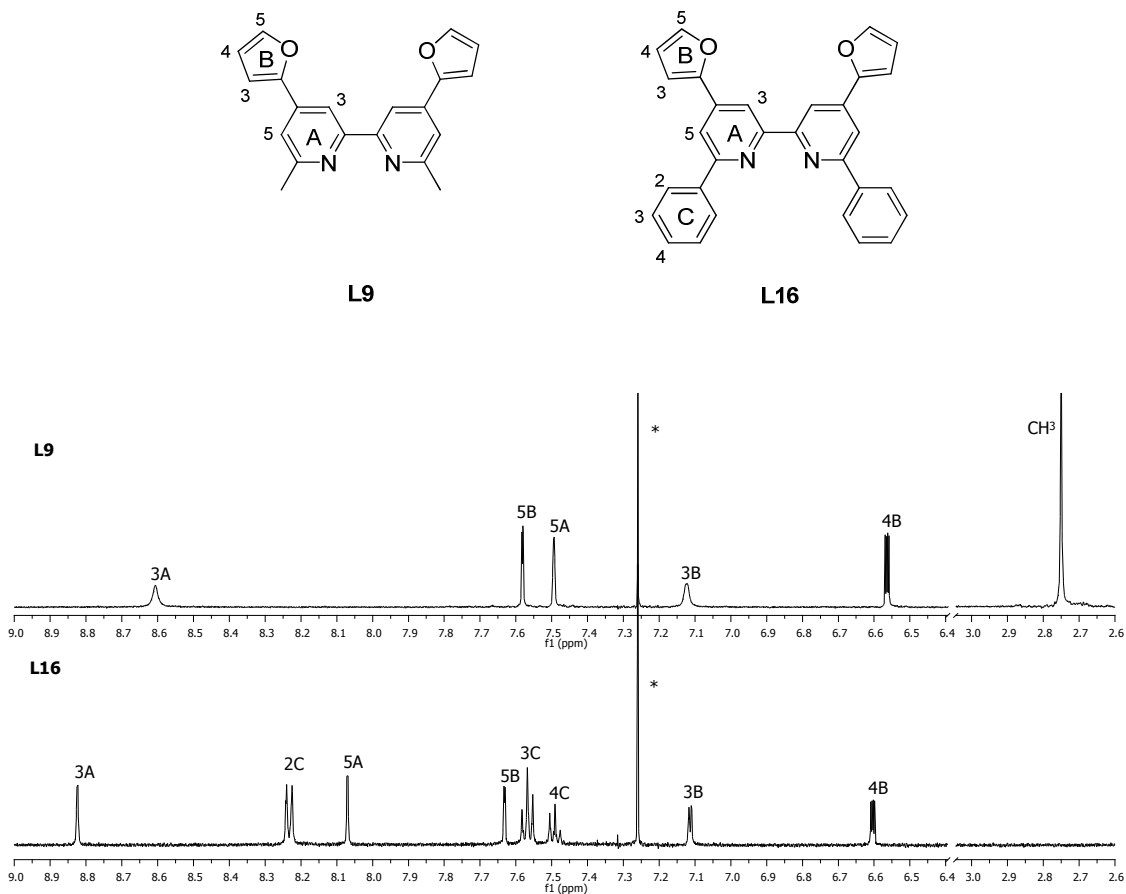
Fig. 27. Diagrams of ligands **L9** and **L16** with number scheme and comparison of their ^{1}H NMR spectra in CDCl$_3$ (*) (500 MHz, respectively).

In the next step, these furyl-substituted compounds were oxidized with KMnO$_4$ in a t-BuOH:H$_2$O solvent mixture to the dicarboxylic acids H$_2$**L10** and H$_2$**L17**. After acidifying the solution mixtures with HCl, the products were obtained as white solids in 36% and 80% yields, respectively, as reported in the literature for H$_2$**L10** [121]. Finally, esterification of ligands H$_2$**L10** and H$_2$**L17** was achieved by refluxing them in an acidic methanolic solution to afford **L11** and **L18** as white solids after neutralizing the solutions with an aq. NaOH solution.

The ^{1}H NMR spectra of H$_2$**L10** and H$_2$**L17** were measured in DMSO-d[6] and TFA-d[1], respectively, due to their low solubility, and their signals appeared as expected. When looking at the ^{1}H NMR spectra of the esterified ligands **L11** and **L18** in figure 28, the absence of the singlet corresponding to the methyl groups and the appearance of the corresponding phenyl signals

48

makes the recognition of the spectra straightforward. The usual downfield shifts of H^{3A} and H^{5A} is observed on going from **L11** to **L18**. However, it is more remarkable that these signals are more deshielded than in ligands **L1**, **L2**, **L3** and **L5**, because in this case, the electron-withdrawing group is directly attached to the bipyridine moiety (see figure 28).
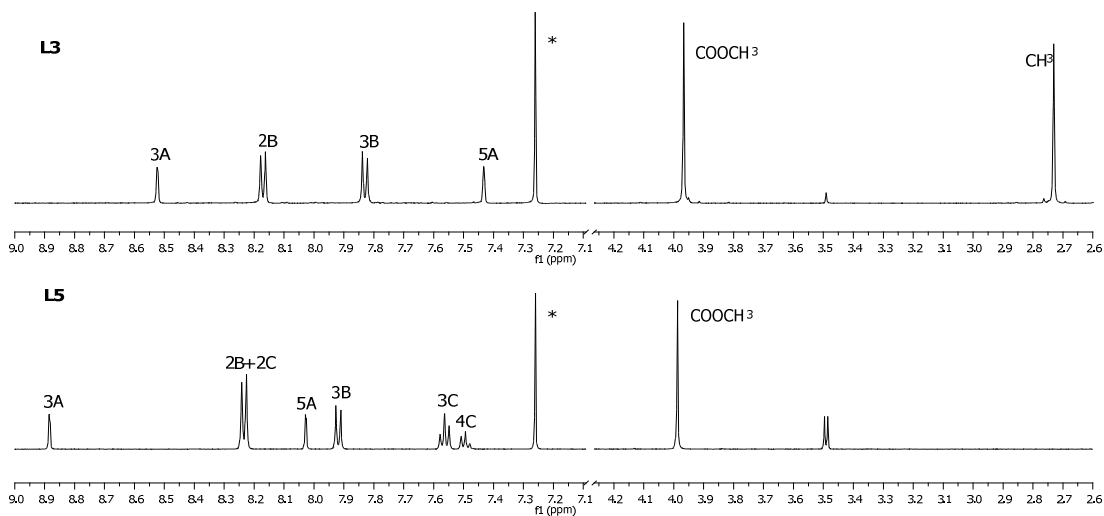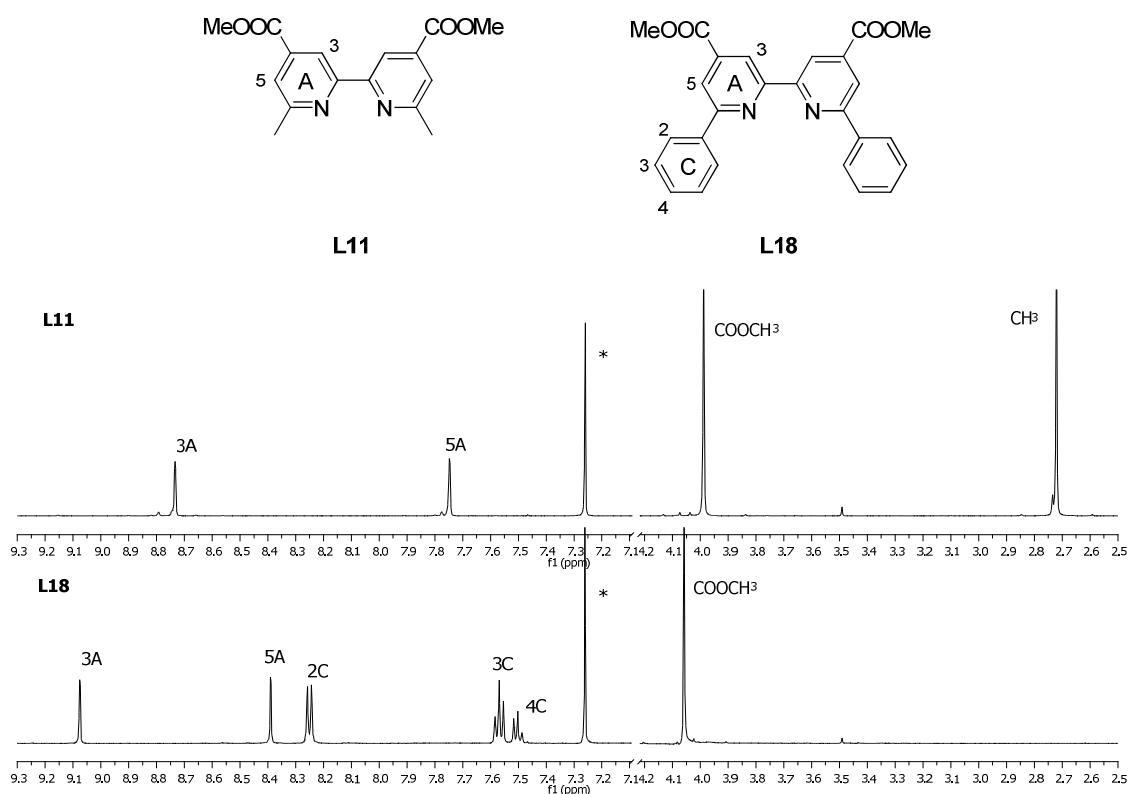

Fig. 28. Diagrams of ligands **L11** and **L18** with number scheme and comparison of their ^{1}H NMR spectra in CDCl$_3$ (*) (500 MHz, respectively).

The methyl esters **L11** and **L18** were reduced to their methoxy forms at low temperature using LiAlH$_4$ as reducing agent, following a method reported in the literature for the synthesis of **L12** [131]. LiAlH$_4$ is an H-nucleophile that transfers hydride-ions to the C-atom of the C=O double bond (see figure 29). This is a reliable way to reduce esters to alcohols, because the aldehydes formed in the reaction react rapidly with a second LiAlH$_4$ molecule to form the alcohols [132]. The products **L12** and **L19** have been obtained as yellow oils after work up in 86% and 89% yields, respectively, and they have been further employed without purification.
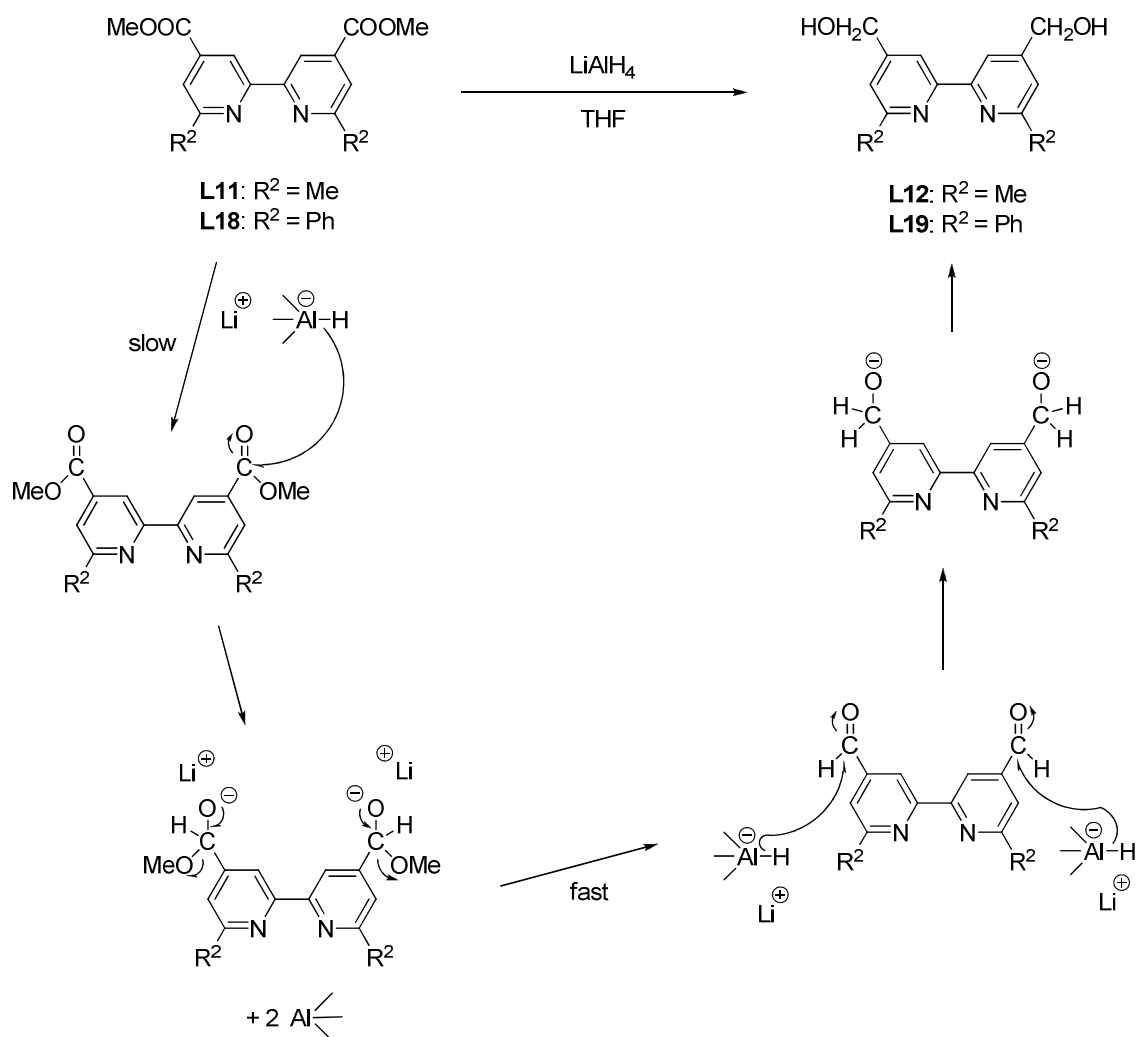
Fig. 29. Reaction mechanism for the reduction of **L11** and **L18** to **L12** and **L19**, respectively [132].

In the next step, the alcohols **L12** and **L19** were oxidized to the aldehydes **L13** and **L20** in 89% and 80% yields, respectively, by a Swern-oxidation employed in the literature for the synthesis of **L13** [131]. In this oxidation dimethylsulfoxide (DMSO) is used as the oxidazing agent in the presence of oxalylchloride and NEt_3. The mechanism of this reaction is known in detail [132] (see figure 30). First an O-atom from DMSO acts as nucleophile in an S_N-reaction and attacts a carbonyl carbon from oxalylchloride, creating "activated DMSO". This molecule can convert into another form of "activated DMSO". Then, any "activated DMSO" form reacts with the alcohol creating a sulfonium salt, which after addition of NEt_3 and temperature increase suffers a ß-elimination to yield the reaction products, the aldehyde and dimethylsulfide, a side-product.

This last product is a very stinking compound, what requires that all the glassware employed during the work up of the reaction has to be thoroughly washed with aqueous $KMnO_4$.
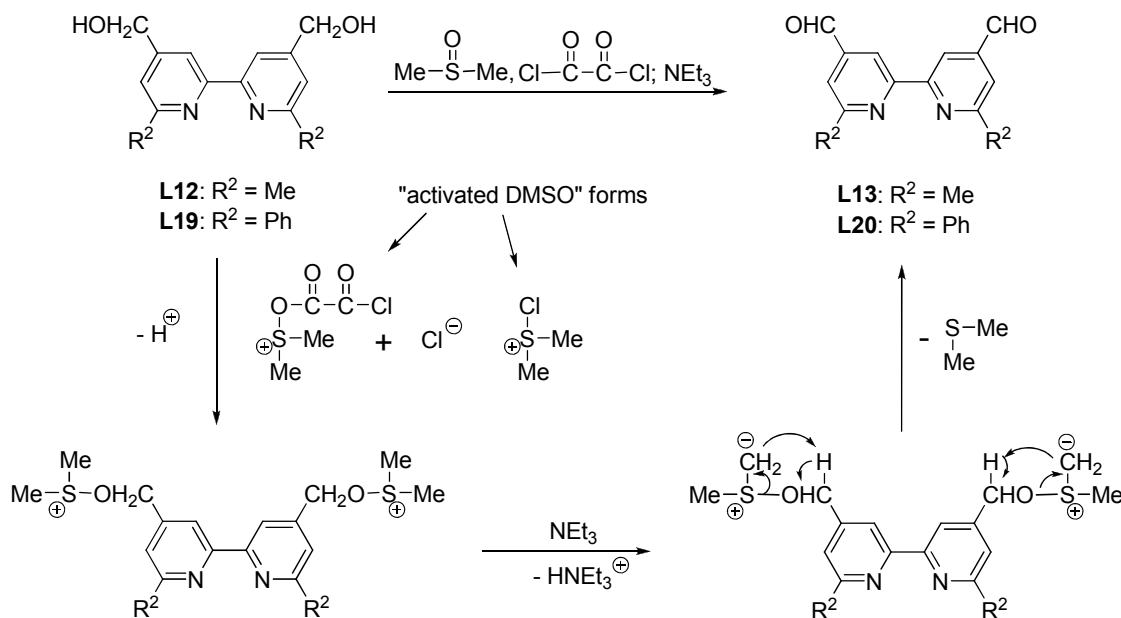
Fig. 30. Reaction mechanism of the Swern-oxidation of alcohols to aldehydes [132].

The aldehydes **L13** and **L20** were converted into **L14** and **L20** in 74% and 41% yield, respectively, by a Wittig-reaction by slight modification of a reported method [129]. The phosphonium-ylide employed for this reaction is methoxycarbonylmethylene-triphenylphosphorane, which allows the formation of the double bond specifically at the location of the original aldehyde by simply refluxing the two reactants in dry toluene for 18 h. Figure 31 shows that the reaction starts by a [2 + 2]-cycloaddition of the ylide to the aldehyde. Then, the heterocycle dissociates in $Ph_3P=O$ and the desired olefin [132]. Once the reaction is finished, one removes the side product of the reaction by column chromatography using alumina as the stationary phase.
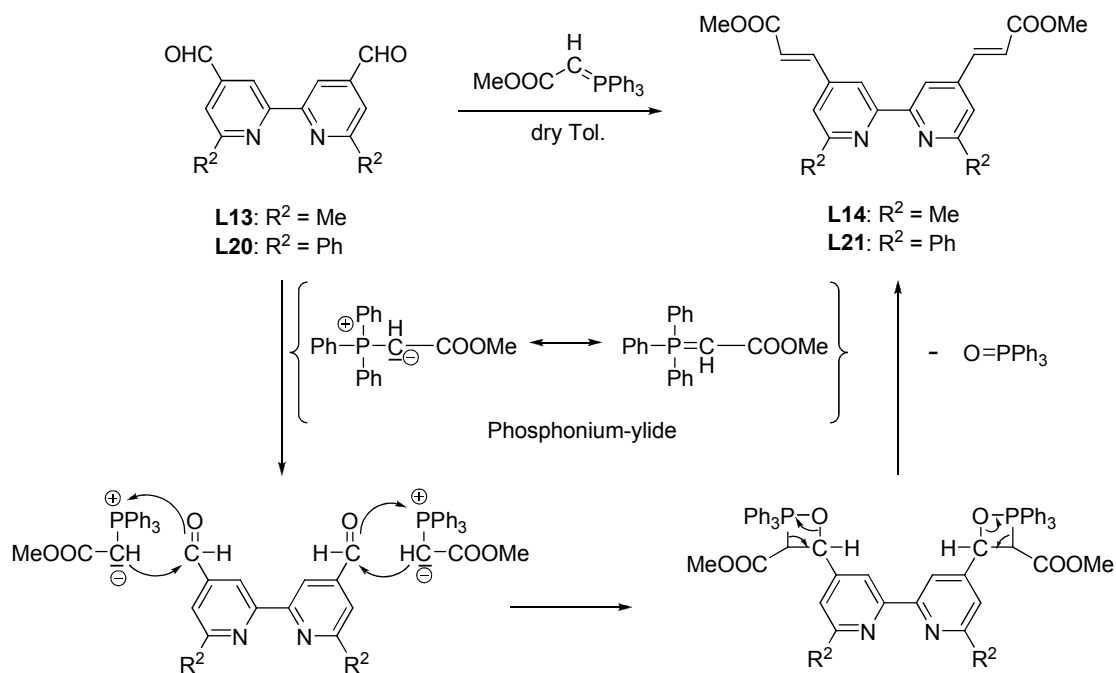
Fig. 31. Reaction mechanism of the Wittig-reaction [132].

In figure 32 the ^{1}H NMR spectra of **L14** and **L21** are shown. The signals from the methyl and phenyl substituents attached to the 6 and 6´ positions in **L14** and **L21**, respectively, appear as expected, as well as the resonances for the protons from the methyl ester groups. As in the spectra discussed above, the deshielding effect suffered by H^{3A} and H^{5A} on going from **L14** to **L21** is observed. The two allyl protons appear as a characteristic doublet with a coupling constant of 16 Hz, the ß proton being strongly shifted to higher frequencies by the electron withdrawing group. Although the α proton is not subjected to this strong resonance effect, it is close enough to the electron-withdrawing carbomethoxy group to be shifted slightly to higher frequency by the inductive effect (see figure 33).

L14

L21
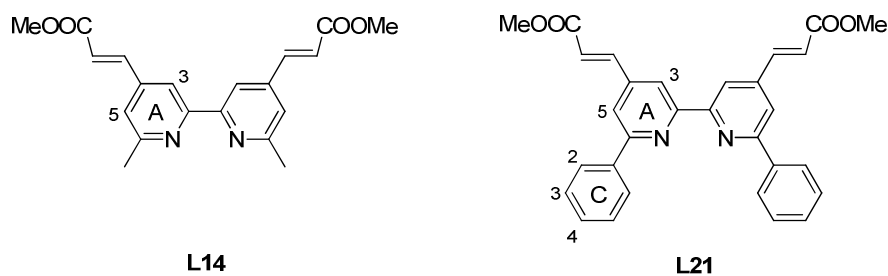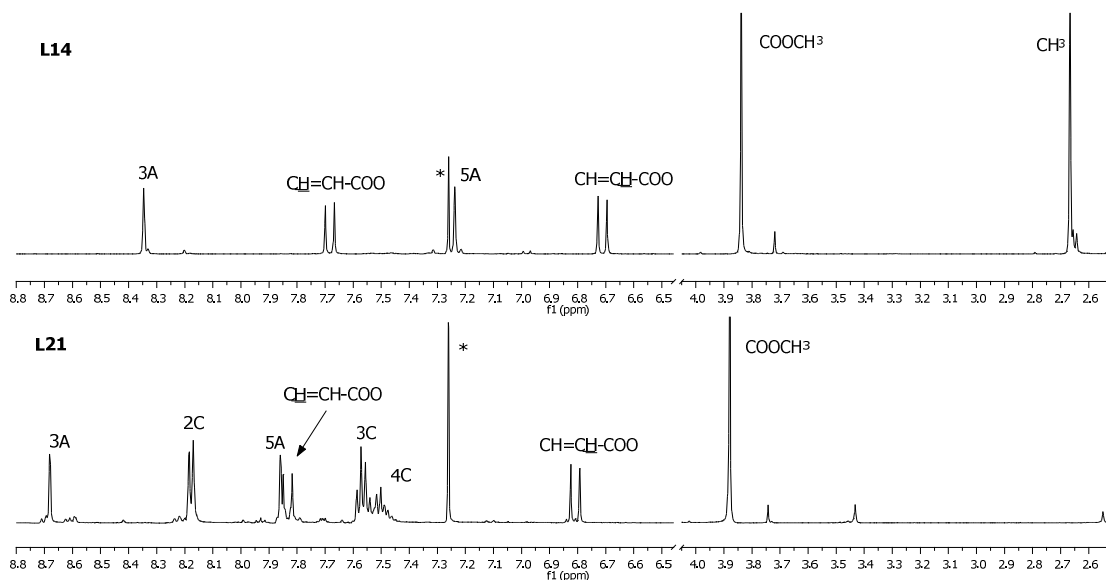
Fig. 32. Diagrams of ligands **L14** and **L21** with number scheme and comparison of their ^{1}H NMR spectra in CDCl$_3$ (*) (500 MHz, respectively).
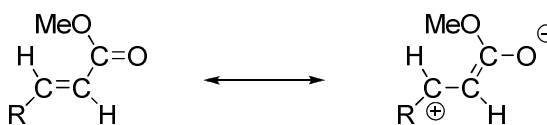
Fig. 33. The two resonance forms of ligands **L14** and **L21**.

Finally, ligands **L14** and **L21** were hydrolyzed to H$_2$**L15** and H$_2$**L22**, respectively, following the same procedure employed for the hydrolysis of ligands **L3** and **L5** to H$_2$**L4** and H$_2$**L6**, respectively [129]. The ^{1}H NMR spectra of these ligands were measured in TFA-d[1], and the resonances appeared at the expected positions, differing from **L14** and **L21** by the absence of the singlet corresponding to the protons from the methyl ester groups.

In the next figure the whole synthetic route from the starting furyl-substituted 2,2´-bipyridines to the final acidic olefins is shown:

53
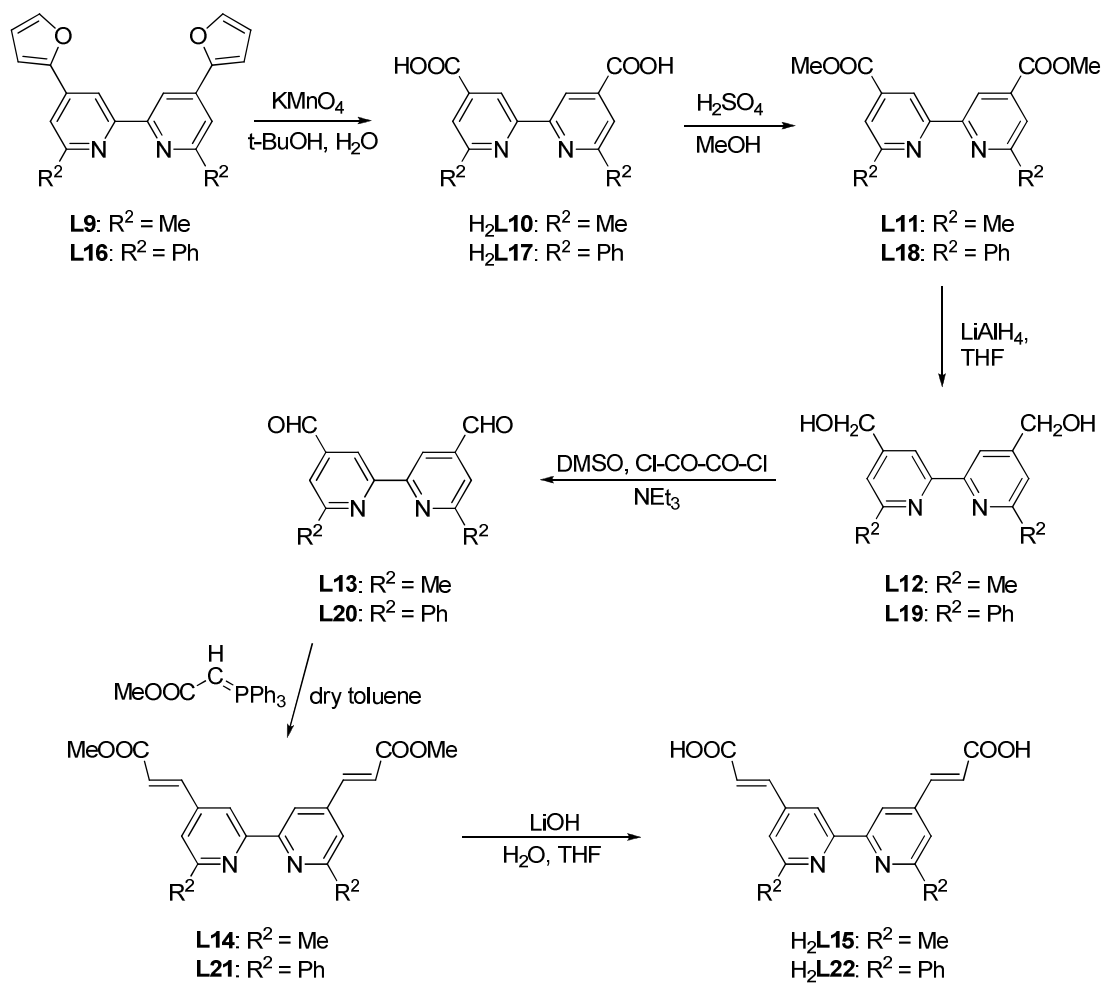
Fig. 34. Synthetic route from ligands **L9** and **L16** to ligands H$_2$**L15** and H$_2$**L22**, respectively.

In this part, the synthetic route used to synthesize the ligands from family **V** will be discussed. The Kröhnke methodology was not employed in this case. Instead, the precursor (4,4′-dibromo-2,2′-bipyridine) for a Suzuki-coupling was synthesized starting from 2,2′-bipyridine.

The starting material for **L23** is the commercially available 2,2′-bipyridine, which was methylated to 6,6′-dimethyl-2,2′-bipyridine using first MeLi and then MnO$_2$ following an already reported method [133]. After, the disubstituted ligand was oxidized and nitrated in the 4 and 4′ positions with H$_2$O$_2$ and H$_2$SO$_4$/HNO$_3$, respectively [134], and then the nitro-groups were substituted by bromide atoms using CH$_3$COBr in acetic acid. Finally, the ligand was reduced

with PBr$_3$ to 4,4´-dibromo-2,2´-bipyridine (see figure 35), the compound used in the Suzuki-coupling to form **L23**.
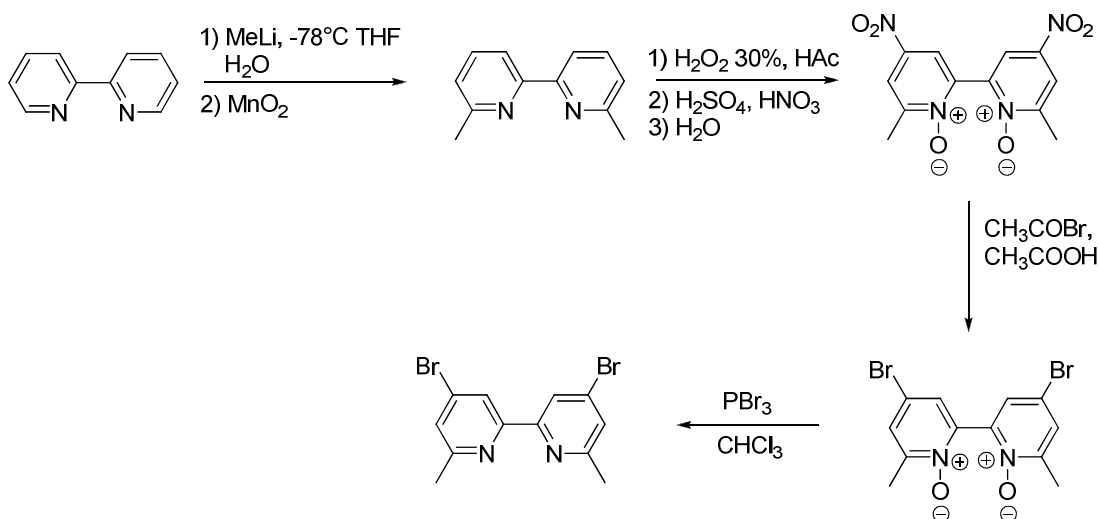
Fig. 35. Synthetic route to 4,4´-dibromo-2,2´-bipyridine.

The Pd(PPh$_3$)$_4$ catalyst employed for the synthesis loses one or two PPh$_3$-ligands in solution yielding electron poor Pd(0)-complexes: Pd(PPh$_3$)$_3$ and/or Pd(PPh$_3$)$_2$. These catalytically active species form a π-complex with the arylbromide in the first step of the reaction mechanism. In the second step, an oxidative addition to the Pd-catalyst occurs, changing its oxidation number from 0 to +2. After this, the –PO$_3$Et$_2$ substitutes the bromide atom, being now bound directly to the Pd-center. Then, the two organic moieties come together in a reductive elimination that forms again a π-complex with the reduced Pd(PPh$_3$)$_2$-complex. Finally, in the fifth step of the catalytic cycle, the Pd(0)-complex dissociates without suffering any change during the cycle, being capable of converting more starting molecules into product (see figure 36) [132].
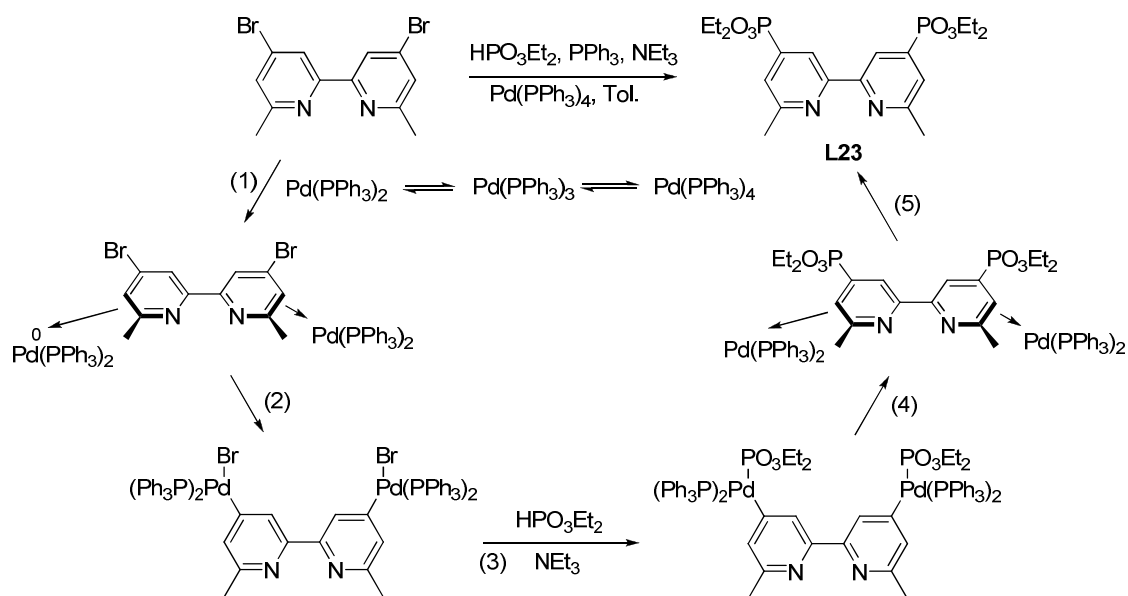
Fig. 36. Reaction mechanism to ligand **L23** [132].

L23 was made by modification of an already reported method [135] where a large excess of triphenylphosphine (10 equivalents) was employed in order to prevent a ligand exchange reaction between the palladium catalyst Pd(PPh$_3$)$_4$ and the chelating 2,2´-bipyridine, what would poison the catalyst. After the reaction is finished, this large amount of triphenylphosphine is easily separated by column chromatography (SiO$_2$, CH$_2$Cl$_2$) and can be almost completely recycled. However, it is very important to work under an inert atmosphere, not only because of the sensitivity of the catalyst, but also because the triphenylphosphine can be oxidized to triphenylphosphine oxide, which is very difficult to separate from the product **L23**. The two compounds are white and crystalline, and run together in either SiO$_2$ or Al$_2$O$_3$ column chromatography. However, it was possible to separate them by recrystallization from hexane.

In the next step of the synthesis, the phosphonate groups of **L23** were hydrolyzed to their acidic forms using McKenna's method to yield ligand H$_4$**L24** [136]. Thus, reacting **L23** in dry dichloromethane with 10 equivalents of bromotrimethylsilane for one day at room temperature resulted in complete trans-esterification into the corresponding silyl esters. These were hydrolyzed in methanol at room temperature to give H$_4$**L24**. Any triphenylphosphine oxide left

over from the previous step can be removed by dissolution in methanol, while H$_4$**L24** precipitates in this solvent.

It is interesting to have a look at the ^{1}H NMR spectra of these ligands (figure 37), because due to the presence of the phosphorus atom (which has a spin quantum number of ½ and a natural abundance of 100%), a coupling between close hydrogen atoms and the ^{31}P nucleus can be observed. The same phenomenon is observed in the ^{13}C NMR spectra, where doublets instead of singlets are seen for carbon atoms that are close to the phosphorus atom. The ^{1}H NMR spectra of **L23** and H$_4$**L24** are shown in figure 37, even if a comparison of the resonance shifts is not possible due to the use of different solvents. The calibration of the ^{31}P NMR spectra was done employing a capillary containing a 85% aq. H$_3$PO$_4$ solution, and the resonance of the ^{31}P moved from δ 16.39 to 6.52 ppm on going from **L23** to H$_4$**L24** (it has to be taken into consideration again that the solvents employed to measure the NMR spectra were not the same).
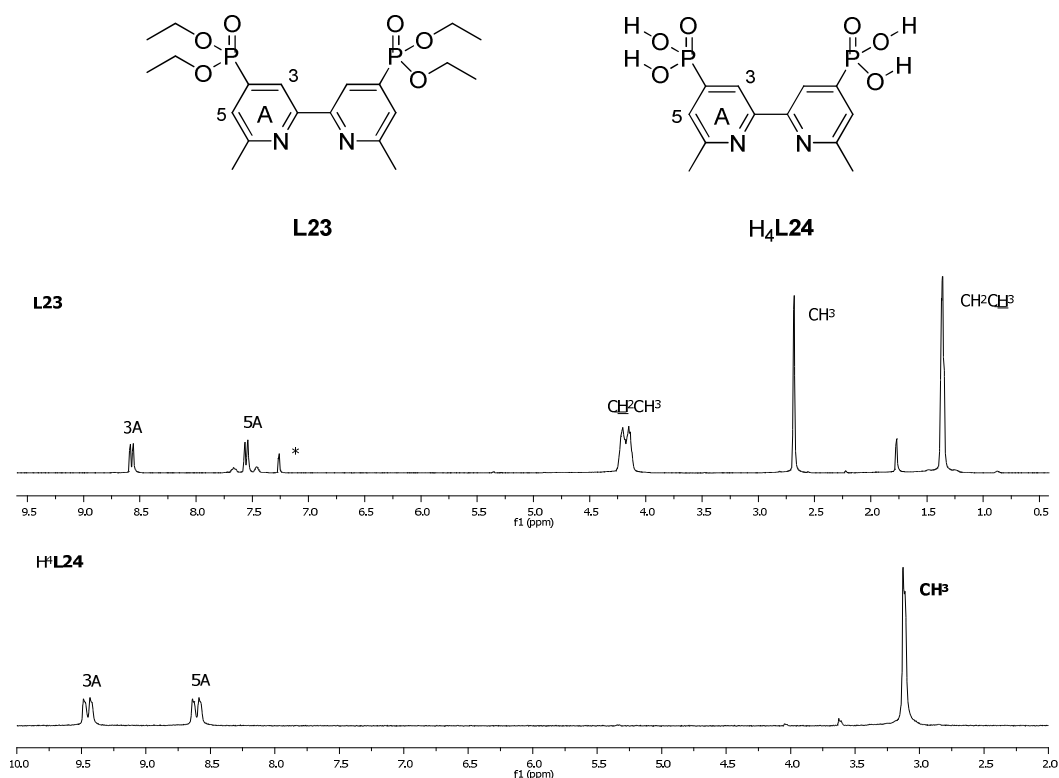
Fig. 37. Diagrams of ligands **L23** and H$_4$**L24** with number scheme and the ^{1}H NMR spectra of **L23** and H$_4$**L24** in CDCl$_3$ (*) and in TFA-d^1, respectively (500 MHz and 250 MHz, respectively).

For the discussion of ligands of family **VI**, H_2**L25** and **L26**, it is important to note that they are not 2,2´-bipyridines, but 2,2´-biquinolines, which are also aromatic compounds, but differ from 2,2´-bipyridines in that they have an arene ring fused to each pyridine ring at carbons 5/5´ and 6/6´. However, both of them have the same coordination environment. The delocalized π-system is formed by ten 2*p*-orbitals (1 from the N atom and 9 from the C atoms) and it is extended through the two fused rings. In the same way as in 2,2´-bipyridine, the two nitrogen atoms have a pair of electrons localized outside the ring that they can use to coordinate metal centres [137, 138]. The employment of these ligands for solar cell applications has its roots in the idea of investigating the influence of the fused rings in the final efficacy of the dyes.
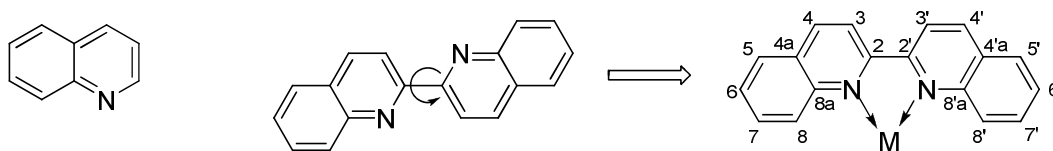
Fig. 38. Chemical structure of quinoline and its derivative 2,2´-biquinoline. The conformational change from the *trans-* to the *cis*-coplanar form upon coordination to a metal, together with ligand numeration is shown.

Ligand H_2**L25** is commercially available from Fluka, so it can be used directly for complexation purposes. This ligand has been used to synthesize **L26** in 56% yield just by a simple esterification reaction in acidic methanol. The ^{1}H NMR spectrum of the white solid dissolved in CDCl$_3$ agreed well with the values reported in the literature [139].

After analyzing the synthetic route and nuclear resonances of the ligands, a brief commentary will be made on the infrared (IR) absorption spectrum of the ligands containing C=O groups. The absorption peak corresponding to this functionality is found in a certain range of the spectrum (1870-1650 cm^{-1}) and depending on the type of compound, the peak is found at higher or lower frequencies in this range, giving thus a direct indication of the presence of the compound. The IR spectra of the ligands which contain ester groups (**L3**, **L5**, **L7**, **L11**, **L14**, **L18**, **L21** and **L26**) exhibit a strong absorption between 1728 and 1641 cm^{-1}. It should be noted that in the case of **L14** and **L21** the wavenumber of the C=O stretching mode is lowered by 30-20 cm^{-1}, due to the conjugation of the carbonyl group with a double bond. In the case of the ligands containing

carboxylic acid groups (H$_2$**L4**, H$_2$**L6**, H$_2$**L8**, H$_2$**L10**, H$_2$**L15**, H$_2$**L17**, H$_2$**L22**) the absorption peaks are found at lower frequencies, between 1705 and 1634 cm^{-1}. Here again one can observe the shift to lower frequencies of the C=O stretching mode in the ligands where this functionality is conjugated to a double bond.

II. 2   Crystal structures of 2,2´-bipyridine ligands

II. 2. 1   (1*E*,5*E*)-1,6-Diphenylhexa-1,5-diene-3,4-dione

X-ray quality crystals of (1*E*,5*E*)-1,6-diphenylhexa-1,5-diene-3,4-dione readily formed from a methanol solution of the compound. The molecule crystallizes in the orthorhombic system, space group *Pbca* (No.61). The asymmetric unit contains half of a molecule, which is fully generated by an inversion centre located at the centre of C1–C1^{-i} (symmetry code i = -1-x, 1-y,-z) bond. The ligand is in an extended conformation (see figure 39). As a consequence of the conjugation of all sp^2 orbitals, the molecule is planar, as also indicated by the presence of the inversion centre. The hydrogen atoms of the double bonds located in between the phenyl rings present a *trans*-configuration, just like the oxygen atoms.
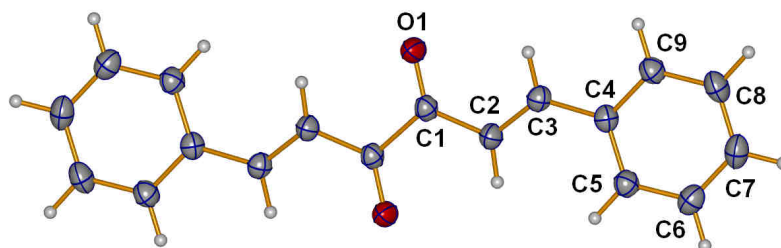
Fig. 39. Structure of (1*E*,5*E*)-1,6-diphenylhexa-1,5-diene-3,4-dione; ellipsoids are plotted at the 50% level.

The molecules along the *a* direction are packed in column-like structures. However, the ring-to-ring distances (centroid to centroid distance: 4.966(4) Å, (symmetry code = -1/2+x, 1-y, 1/2-z)) are relatively large to consider any stabilizing type of π···π stacking in a column. C–H···π

interactions (C7–H7⋯π (centroid) 2.79 Å, (symmetry code = 1/2+x, 1-y, 1/2-z)) are present between aromatic hydrogen atoms from one column and aromatic rings located in the parallel column (see figure 40).
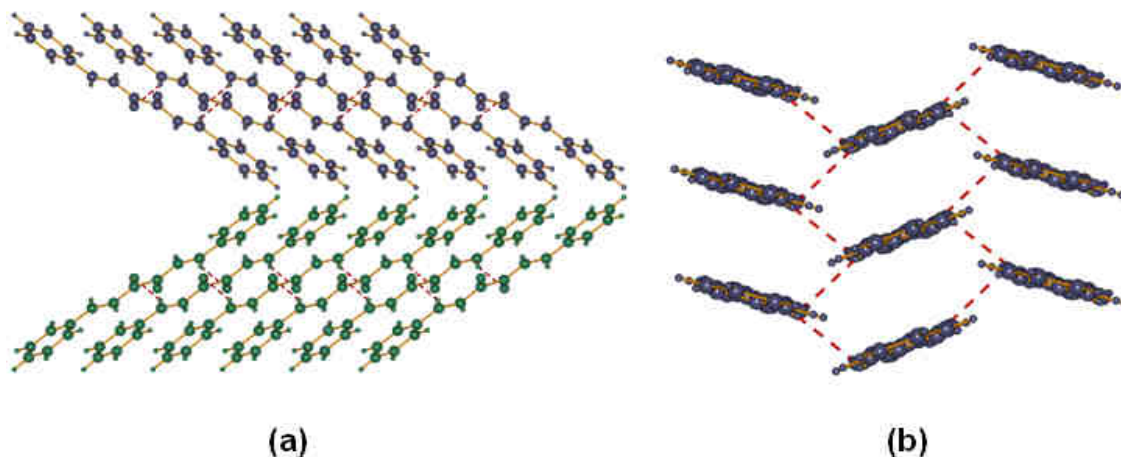
Fig. 40. Crystal packing of (1*E*,5*E*)-1,6-diphenylhexa-1,5-diene-3,4-dione: (a) view along the *b* direction showing the two different packing of the molecules (green and dark blue); hydrogen bonds are represented in red colour; (b) view along the [-6.17, 0.04, -9.41] direction showing individual columns; hydrogen bonds are represented in red.

The presence of oxygen atoms in the molecule allows the formation of hydrogen bonds with the hydrogen atoms of the double bond (C3–H31⋯O1^{ii} 2.59 Å, (symmetry code ii = 1/2+x, 3/2-y, z)) and, less strongly, with hydrogen atoms of the aromatic ring (C5–H51⋯O1^{iii} 2.71 Å, (symmetry code iii = -1/2-x, 1/2+y, -z)). This results in an undulating packing along the *b* direction of the crystal structure, as shown in figure 40 b.

II. 2. 2   (1*E*,5*E*)-1,6-Di(furan-2-yl)hexa-1,5-diene-3,4-dione

X-ray quality crystals of (1*E*,5*E*)-1,6-di(furan-2-yl)hexa-1,5-diene-3,4-dione readily formed from an ethanol solution of the compound, and a search of the CSD revealed that its structure had not previously been reported.

In (1*E*,5*E*)-1,6-di(furan-2-yl)hexa-1,5-diene-3,4-dione the benzene rings have been substituted by furan rings. The molecules crystallize in the monoclinic system, space group *C*2/*c* (No. 15). Unlike in (1*E*,5*E*)-1,6-diphenylhexa-1,5-diene-3,4-dione, two independent half molecules are present in the asymmetric unit, and the centres of symmetry located in the middle of C7–C7^i (symmetry code i = 1-x, 1-y, -z) and the C14–C14^{ii} (symmetry code ii = 1/2-x, 1/2-y, -z) bonds generate the entire molecules (see figure 41). The two independent molecules are located in almost parallel planes, being 0.518(7)° the angle between them.
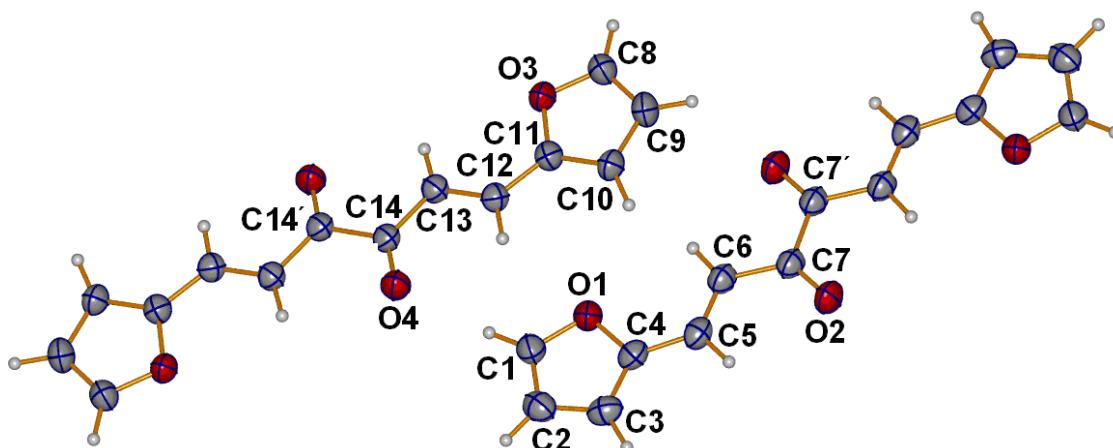
Fig. 41. Structures of two independent molecules of (1*E*,5*E*)-1,6-di(furan-2-yl)hexa-1,5-diene-3,4-dione; ellipsoids are plotted at the 50% level. View along the [-2.78, -3.71, -1.95] plane.

The extended conformation of the molecules allows the formation of columns along the *b* direction through weak π···π stacking interactions between the furan rings (3.774 Å centroid-to-centroid distances), although the molecules are stacked in an offset manner. Carbonyl oxygen atoms form hydrogen bonds with hydrogen atoms located in the furan rings of other adjacent molecules (C8–H81···O2^{iii} 2.66 Å (symmetry code iii = x, -1+y, z); C9–H91···O2^{iv} 2.61 Å

(symmetry code iv = -x, y, 1/2-z) and C2–H21···O4^v 2.63 Å (symmetry code v = 1/2-x, -1/2-y, 1-z); C1–H11···O4^{vi} 2.68 Å (symmetry code vi = x, -y, 1/2+z)). The overall supramolecular assembly is a herring-bone like array, with an angle of 58.4° between the planes of molecules in adjacent stacks.
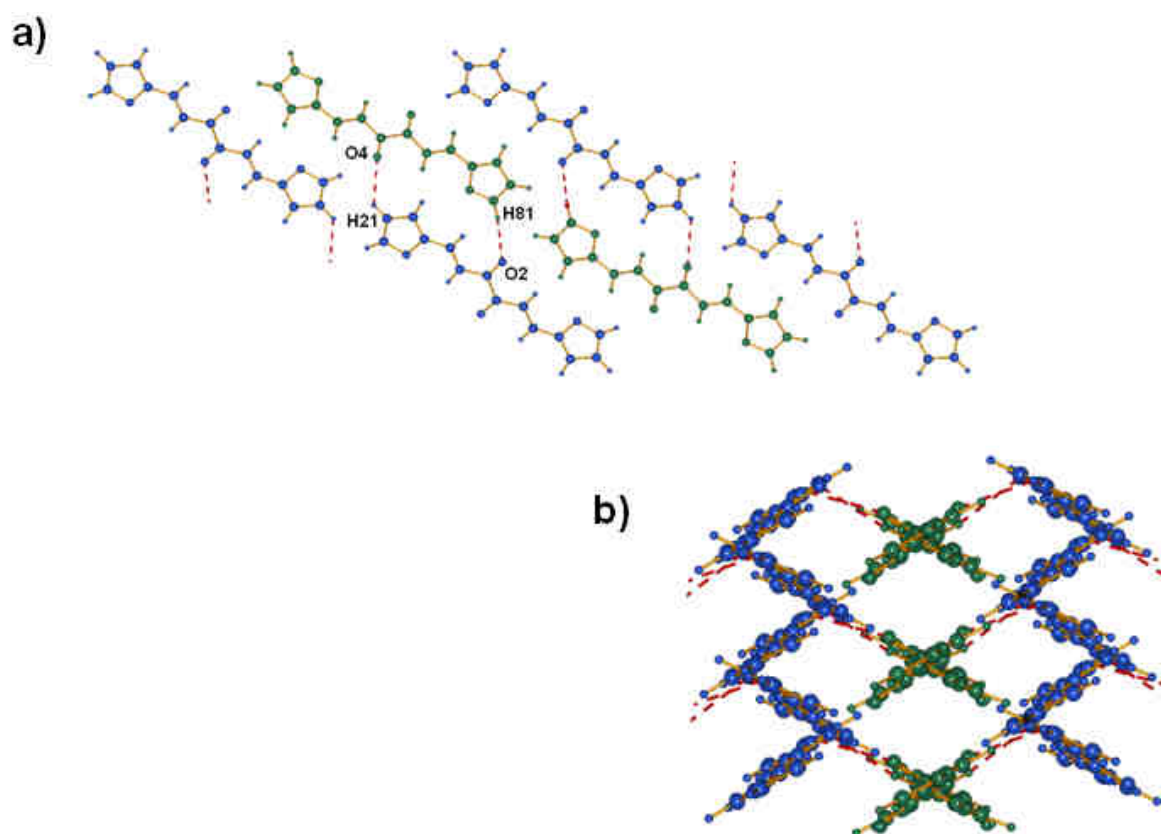
Fig. 42. a) View of the packing along the *b* direction showing hydrogen bonds (in red) between adjacent molecules; b) herring-bone like array observed along the (33.34, -0.01, -0.36) direction.

II. 2. 3   6,6´-Dimethyl-4,4´-diphenyl-2,2´-bipyridine (L1)

Slow evaporation of a chloroform solution of ligand **L1** yielded crystals suitable for X-ray diffraction. **L1** crystallizes in the monoclinic system, space group $P2_1/c$ (No. 14). The molecule is centrosymmetric and consists of two pyridine rings, each of them containing a phenyl group in the *para* position with respect to the nitrogen and a methyl group in the *ortho* position. In the

solid state the pyridine rings are contained in the same plane with the nitrogen atoms pointing in opposite directions, having thus the molecule the typical *trans*-configuration observed in this kind of α,α´-diimine ligands (see figure 43). The phenyl groups are twisted 27.7(9)° (angle between the least square planes formed by the bipyridine moiety and the phenyl rings) with respect to the plane formed by the pyridine rings.
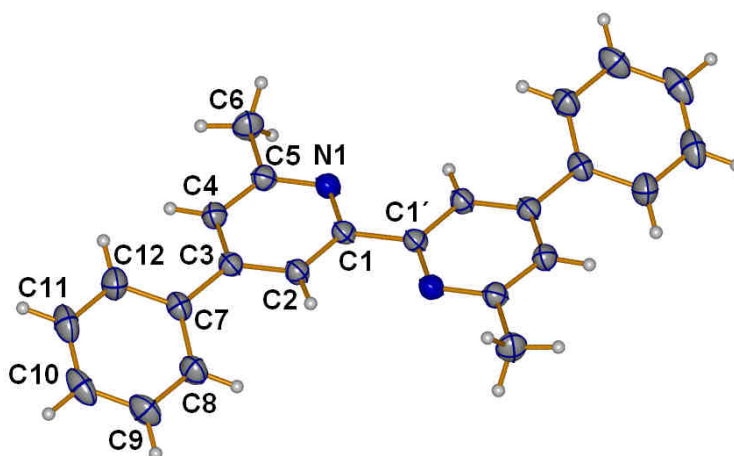
Fig. 43. Structure of 6,6´-dimethyl-4,4´-diphenyl-2,2´-bipyridine (**L1**); ellipsoids are plotted at the 50% level.

Along the *b* direction, the methyl groups are "sandwiched" in between two pyridine groups from other molecules that are positioned in an offset manner (C6–H6A···π^i (centroid) 2.99 Å (symmetry code i = 1-x, 1/2+y, 1/2-z) and C6–H6B···π^{ii} (centroid) 2.99 Å (symmetry code ii = 1-x, -1/2+y, 1/2-z)). The phenyl groups are aligned in columns and are interacting through weak π···π stacking interactions (centroid to centroid distance: 3.8(1) Å, (symmetry code = -x, 2-y, -z)).
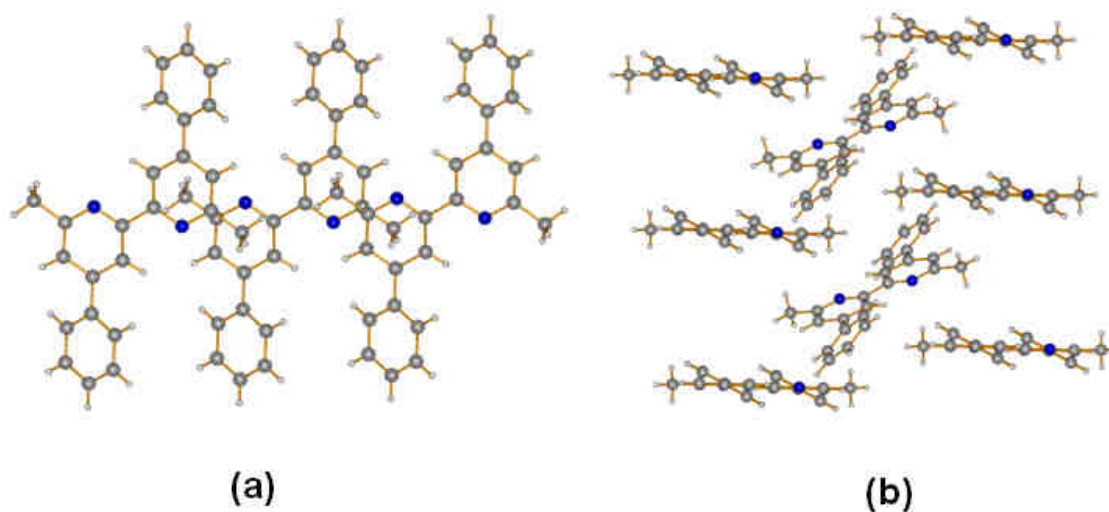
Fig. 44. a) View of the packing along the *b* direction showing the position of the methyl and phenyl groups in the packing; b) view along the [9.40, 1.22, 0.75] direction showing the different packing of the columns in the crystal.

II. 2. 4   4,4´,6,6´-Tetraphenyl-2,2´-bipyridine (L2)

Slow evaporation of a chloroform solution of ligand **L2** yielded crystals suitable for X-ray diffraction. The asymmetric unit of 4,4´,6,6´-tetraphenyl-2,2´-bipyridine (**L2**) contains one molecule of the ligand (triclinic system, space group *P*-1 (No.2)). This ligand is similar to **L1**, a 2,2´-bipyridine core with phenyl group substituents in the 4 and 4´-positions. Unlike **L1**, the substituents attached to the 6 and 6´-positions are phenyl groups (see figure 45), which induce some steric hindrance, causing the pyridine moieties to no longer be co-planar (torsion angle 7.1(7)°, C10–C11–C12–N2). The nitrogen atoms in the bipyridine rings are disordered and occupy two different positions (N1 and C10, N2 and C13, modelled with 50% fractional occupancies) within the crystal structure. The pyridine moieties of different molecules are stacked at more than 5 Å.
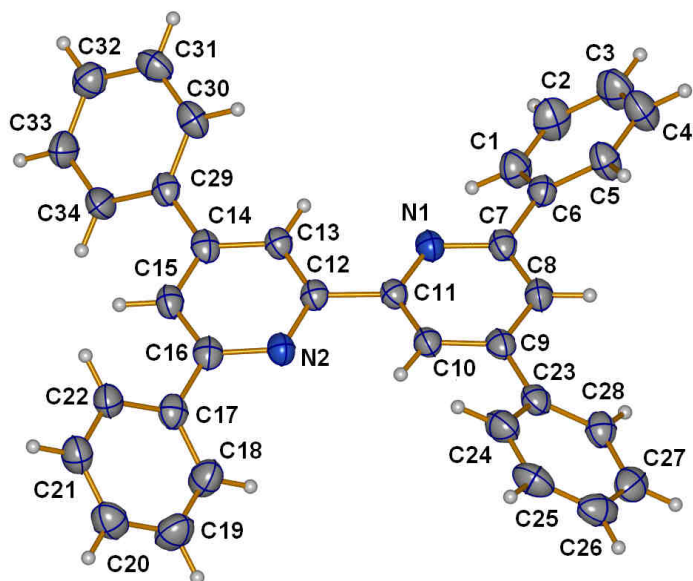
Fig. 45. Structure of 4,4′,6,6′-tetraphenyl-2,2′-bipyridine (**L2**); ellipsoids are plotted at the 50% level.

The phenyl groups are twisted with respect to the pyridine rings: 31.0(5)° (C5–C6–C7–C8); 34.5(8)° (C8–C9–C23–C28); 31.2(2)° (C15–C16–C17–C22) and 34.8(5)° (C15–C14–C29–C34). Even if theoretically a larger number of aromatic rings should promote π···π stacking interactions in these kinds of systems, the molecules here form columns that are stabilized instead by C–H···π interactions between the phenyl groups (C18–H18A···π[i] (centroid) 2.97 Å (symmetry code i = -x, 2-y, -z) and C24–H24A···π[ii] (centroid) 2.99 Å (symmetry code ii = 1-x, 2-y, -z)) when viewed along the *a* direction (see figure 46 c).
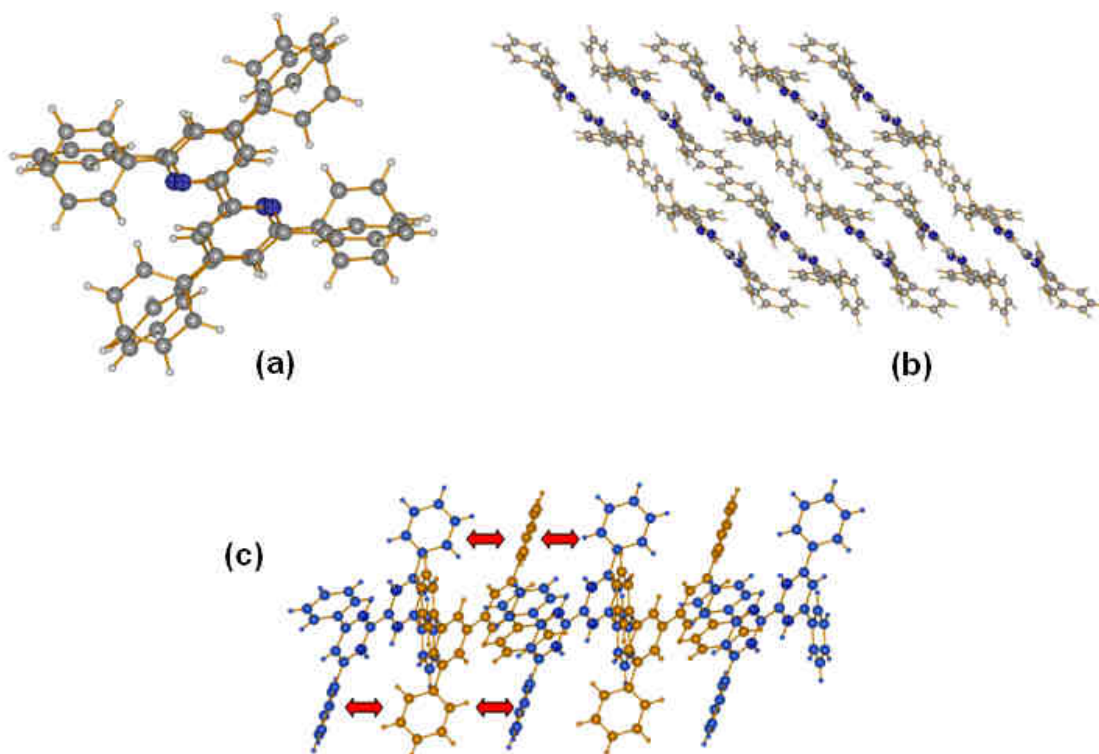
Fig. 46. a) View of the packing of 4,4´,6,6´-tetraphenyl-2,2´-bipyridine (**L2**) molecules along the *b* direction; b) view along the *c* direction; c) view along the [-1.36, 9.76, -5.53] direction showing the C-H···π interactions (red arrows) between the molecules packed along the *b* direction.

A perspective view along the *c* direction shows the formation of compact layers (see figure 46 b), what confirms the good stacking of the molecules in this crystal.

II. 2. 5   Dimethyl 4,4´-(6,6´-dimethyl-2,2´-bipyridine-4,4'-diyl)dibenzoate (L3)

L3 crystallizes in the triclinic system, space group *P*-1 (No.2). The asymmetric unit contains half of the molecule, which can be fully generated by an inversion centre located in the middle of the C1–C1^{i} bond (symmetry code i = 1-x, -y, -z). The bipyridine core is planar and has the pyridine rings in the usual *trans*-configuration.

66

The 6 and 6´-positions of the bipyridine moiety are occupied by methyl groups, being one of the hydrogen atoms of each group almost contained in the plane of the bipyridine rings. In the case of the phenyl groups located in the 4 and 4´-positions, it can be observed that they are twisted 26.6º (torsion angle, C2–C3–C7–C8) with respect to the plane formed by the bipyridine unit. However, the methyl ester functionalities situated in the *para* position with respect to the bipyridine core are co-planar with respect to the phenyl groups (see figure 47).
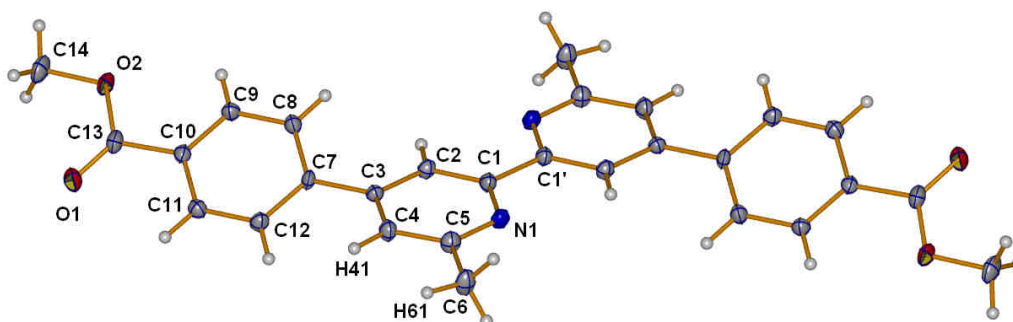
Fig. 47. Structure of dimethyl-4,4´-(6,6´-dimethyl-2,2´-bipyridine-4,4´-diyl)dibenzoate (**L3**); ellipsoids are plotted at the 50% level.

Along the *a* direction the molecules are packed in columns (see figure 48 a). The phenyl and the pyridine rings interact with phenyl and pyridine groups from other molecules, respectively, through π-stacking interactions (3.84(7) Å); the latter are arranged in a head-to-head arrangement.
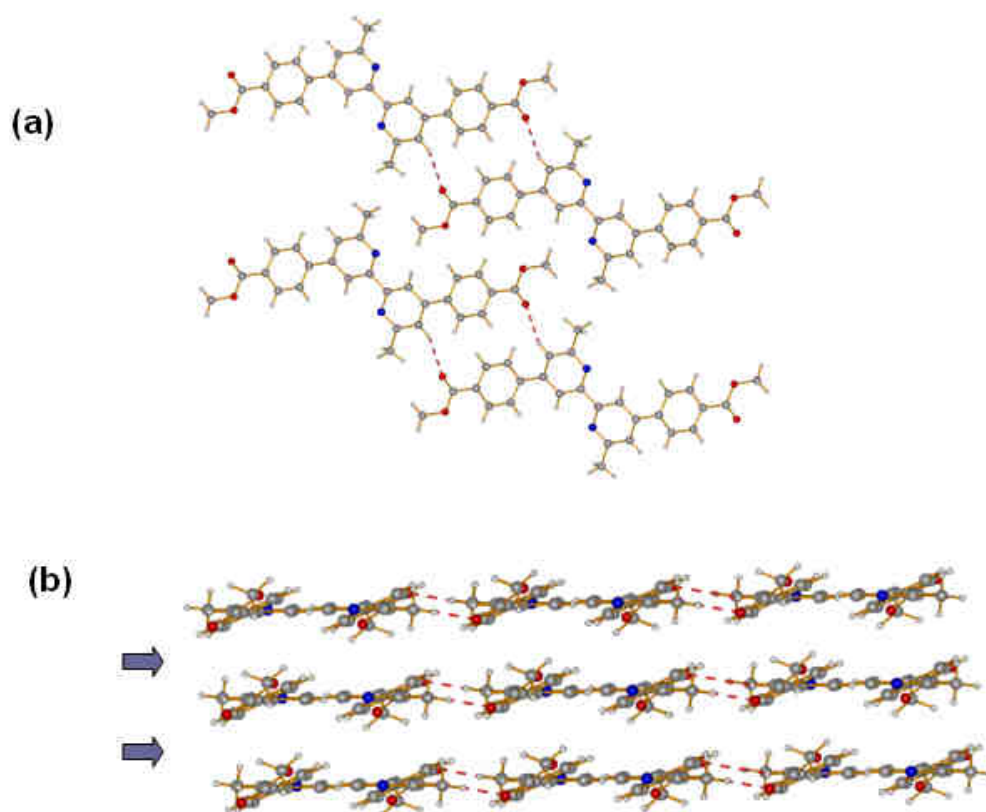
Fig. 48. a) View along the *a* direction showing the packing of dimethyl-4,4´-(6,6´-dimethyl-2,2´-bipyridine-4,4´-diyl)dibenzoate (**L3**) molecules into columns and the formation of hydrogen bonds (represented in red); b) molecules of **L3** on the same plane are related by hydrogen bonds (represented in red) and along the *a* axis through π stacking interactions (blue arrows) forming a 2D motif in the crystal structure.

If the molecules are observed through the [-0.60,5.40,9.09] direction, they form 2D layers that are supported by hydrogen bonds between the carboxylic C=O bond and hydrogen atoms from the pyridine rings (C4-H41···O1[ii] 2.67(3) Å (symmetry code ii = x, -1+y, -1+z)), and hydrogen atoms from the methyl groups present in the 6 and 6´ positions of the bipyridine core (C6-H61···O1[ii] 2.55(3) Å) (see figure 48).

II. 2. 6   4,4´-Di(furan-2-yl)-6,6´-dimethyl-2,2´-bipyridine (L9)

L9 yielded X-ray quality crystals grown by slow evaporation of a chloroform solution of the ligand. The compound crystallizes in the orthorhombic system, space group *Pcab* (No. 61). The ligand is centrosymmetric with an inversion centre located in the middle of the C9–C9´^{i} (symmetry code i = 2-x, -y, 1-z) bond. The molecule consists of a planar 2,2´-bipyridine system with the expected *trans*-configuration. The 4 and 4´-positions are occupied by furan rings that are not co-planar with the bipyridine system (9.4(3)° is the torsion angle C10–C5–C4–O1), and methyl groups occupy the 6 and 6´ positions (see figure 49).
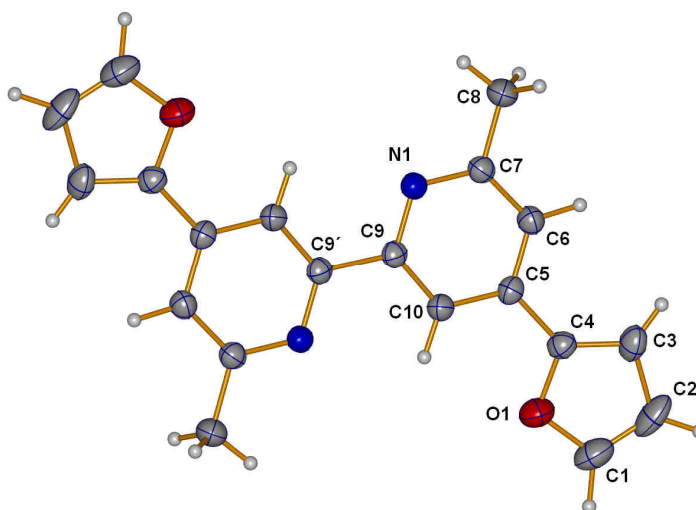
Fig. 49. Structure of 4,4´-di(furan-2-yl)-6,6´-dimethyl-2,2´-bipyridine (**L9**); ellipsoids are plotted at the 50% level.

The principal packing forces are π-stacking interactions between bipyridine units. Pairs of pyridine rings in adjacent molecules are aligned so as to generate an offset stack, the distance between the centroids of the rings containing atoms N1 and N1´ being 3.39 Å (symmetry code ii = 1-x, -y, 1-z). In addition, C6–H61···π^{iii} (centroid) interaction at 2.94 Å (symmetry code iii = 1/2+x, 1/2-y, z) is observed.
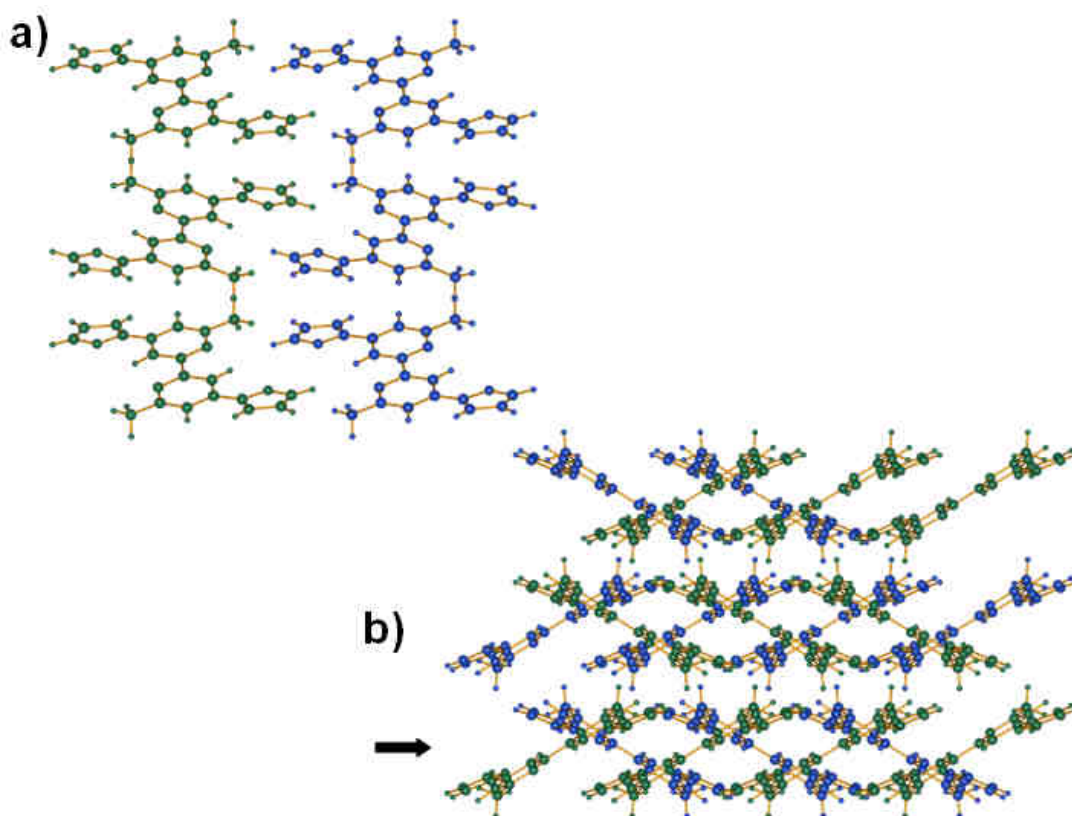
Fig. 50. a) Packing structure of 4,4´-di(furan-2-yl)-6,6´-dimethyl-2,2´-bipyridine (**L9**) along the *a* direction. The molecules, however, are not coplanar as it can be observed from the view along the c direction in (b); b) View along the *c* direction; the black arrow indicates the a direction showed in (a).

II. 2. 7   6,6´-Dimethyl-2,2´-bipyridine-4,4´-dicarboxylic acid (H₂L10)

The oxidation of the furan rings in **L9** affords carboxylic acid groups in the 4 and 4´-position, being now this ligand H₂**L10**. Single crystals of this ligand suitable for X-ray diffraction were grown from a methanol solution of the compound. H₂**L10** crystallizes in the triclinic system, space group *P*-1 (No.2). The unit cell contains half of the molecule, which is planar (maximum deviation of a framework atom from the least squares plane through the molecule is 0.07 Å for C3) and the molecule possesses a *trans*-configuration. The difference in C5-O1 (1.306(3) Å) and C5-O2 (1.234(3) Å) bond distances is consistent with carboxylic acid (rather than carboxylate functionalities). The carboxylic acid groups are almost contained in the plane formed by the bipyridine moiety (2.7(4)°, O2–C5–C4–C6) (see figure 51).
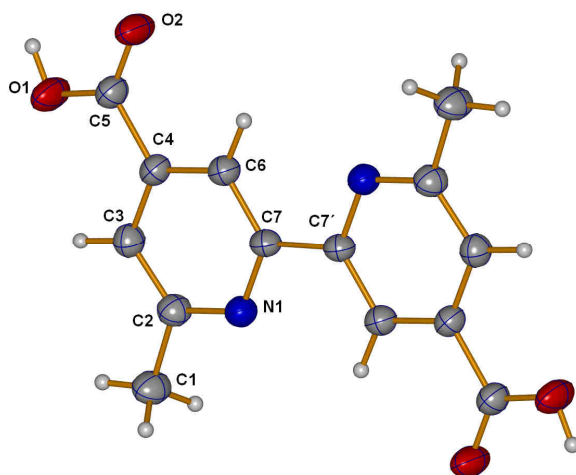
Fig. 51. Structure of 6,6´-dimethyl-2,2´-bipyridine-4,4´-dicarboxylic acid (H$_2$**L10**); ellipsoids are plotted at the 50% level.

The 2,2´-bipyridine units in the crystal lattice form columns along the *a* axis interacting through very weak π···π stacking forces in a head-to-head mode (centroid to centroid distance: 4.102(7) Å (symmetry code i = 1-x, -y, -z)). A view along the *b* axis in the crystal structure shows the formation of infinite polymeric chains in which each molecule is related through its carboxylic acid groups to other molecules located in the same layer (O1–H1···O2^{ii} 1.78 Å (symmetry code ii = 1-x, -1-y, 1-z) and C1–H13···O2^{iii} 2.60 Å (symmetry code iii = -1+x, 1+y, z)) (see figure 52).
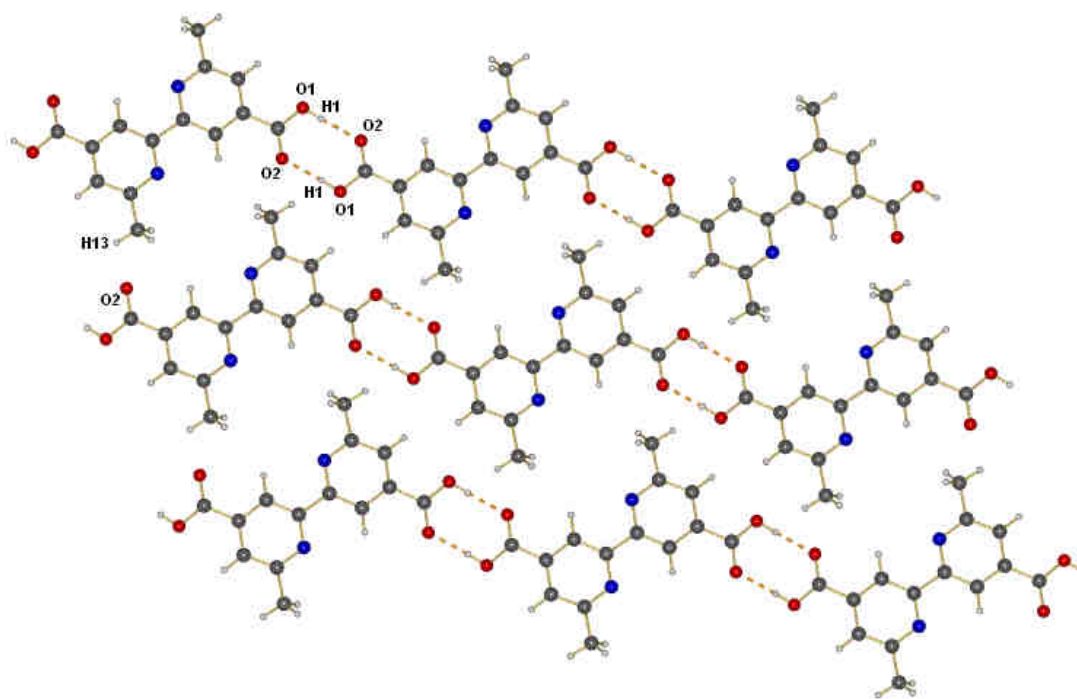
Fig. 52. Adjacent hydrogen-bonded polymeric chains of 6,6´-dimethyl-2,2´-bipyridine-4,4´-dicarboxylic acid (H₂**L10**) assembled into 2D sheets. Hydrogen bonds are represented in red.

II. 2. 8   Dimethyl 6,6´-dimethyl-2,2´-bipyridine-4,4´-dicarboxylate (L11)

L11 yielded X-ray quality crystals grown by slow evaporation of a chloroform solution of the compound. The crystal structure of this ligand is similar to the previously described structure of H₂**L10**, the main structural difference being the substitution of the hydrogen atom from the acid group by a methyl group (see figure 53). The ligand crystallizes in the triclinic system, space group *P*-1 (No.2), and the molecule is centrosymmetric. The asymmetric unit contains half of the molecule with the inversion centre located between the carbon atoms through which the pyridine units are bonded, C1 and C1^i (symmetry code i = -x, -y, -z) in this case.
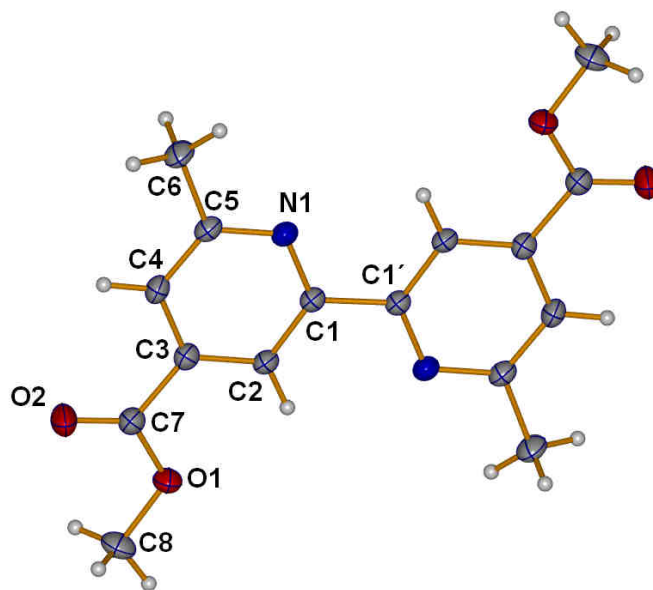
Fig. 53. Structure of dimethyl 6,6´-dimethyl-2,2´-bipyridine-4,4´-dicarboxylate (**L11**); ellipsoids are plotted at the 50% level.

A torsion angle of 2.8(7)° for C2-C3-C7-O1 indicates the *quasi* planarity of the molecule, again the pyridine rings being in a *trans*-conformation. Weak hydrogen bonds are formed between the hydrogen atoms of the methyl groups and the oxygen atoms of the carbonyl groups of vicinal molecules (C6–H6B···O2^{ii} 2.66 Å (symmetry code ii = -1+x, -1+y, -1+z) and C4–H4A···O2^{iii} 2.64 Å (symmetry code iii = -x, 1-y, 1-z)) (see figure 54 a). The molecules are stacked in columns along the *a* direction *via* weak π-π interactions (centroid-to-centroid distance 3.91(4) Å), and are held together by hydrogen bonds (see figure 54 b).
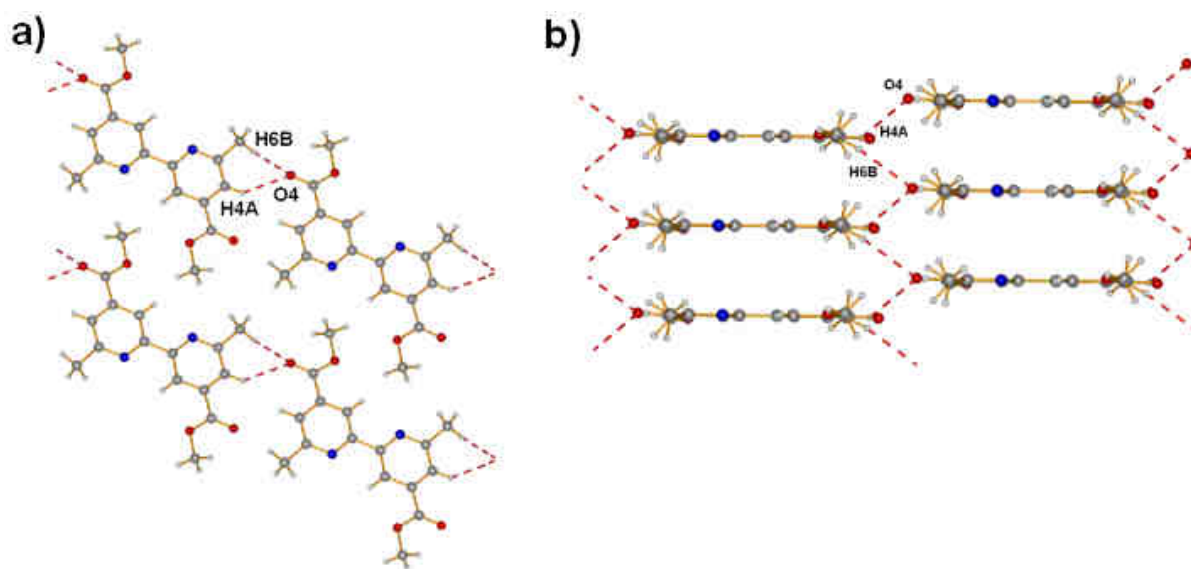
Fig. 54. a) View along the *a* direction showing the hydrogen bonds between vicinal molecules of 6,6´-dimethyl-2,2´-bipyridine-4,4´-dicarboxylate (**L11**); b) view of the stacked molecules along the (1.62, -8.26, 6.61) direction. Hydrogen bonds are represented in red.

II. 2. 9   4,4´-Di(furan-2-yl)-6,6´-diphenyl-2,2´-bipyridine (L16)

L16 yielded X-ray quality crystals grown by slow evaporation of a chloroform solution of the ligand. It consists of a tetrasubstituted 2,2´-bipyridine that contains six aromatic rings in total. Furan rings are located in the 4 and 4´-positions, and phenyl groups are present in the 6 and 6´-positions (see figure 55). The molecule crystallizes in the trigonal system, space group *R*-3 (No.148), and therefore has a high symmetry packing. The asymmetric unit contains half of the molecule, which is fully generated by an inversion centre located at the midpoint of the C11–C11^i (symmetry code i = 1-x, 1-y, 1-z) bond. The two pyridine rings are coplanar with the furan rings. The phenyl substituents, however, are twisted with respect to this plane with a torsion angle of 10.1(8)° (C1–C6–C7–N1).
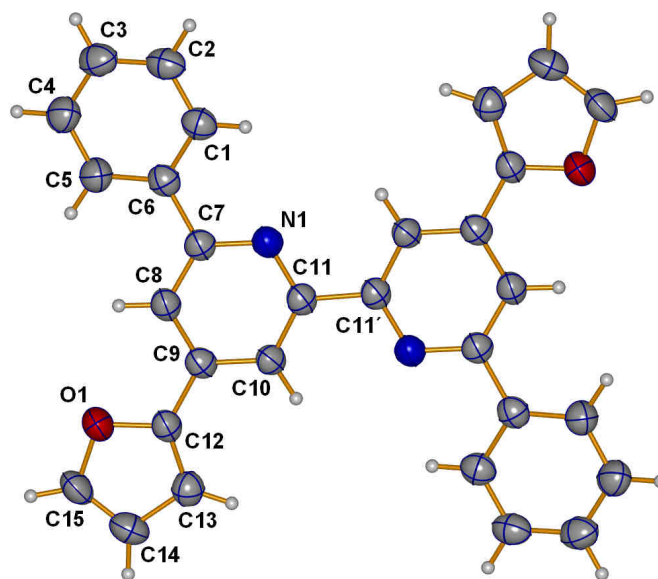
Fig. 55. Structure of 4,4´-di(furan-2-yl)-6,6´-diphenyl-2,2´-bipyridine (**L16**); ellipsoids are plotted at the 50% level.

The molecules are packed along the *c* direction without any remarkable π-π interactions. The dominant attractive forces between molecules of **L16** involve weak edge-to-face π-interactions and weak non-classical hydrogen bonds between the nitrogen atoms from the bipyridine moiety and hydrogen atoms from the furan rings (C15–H151···N1[ii] 2.66 Å (symmetry code ii = y, -x+y, 1-z)) (see figure 56 a), what is in stark contrast to the π-stacking interactions observed in 4,4´-di(furan-2-yl)-6,6´-dimethyl-2,2´-bipyridine, **L9**.
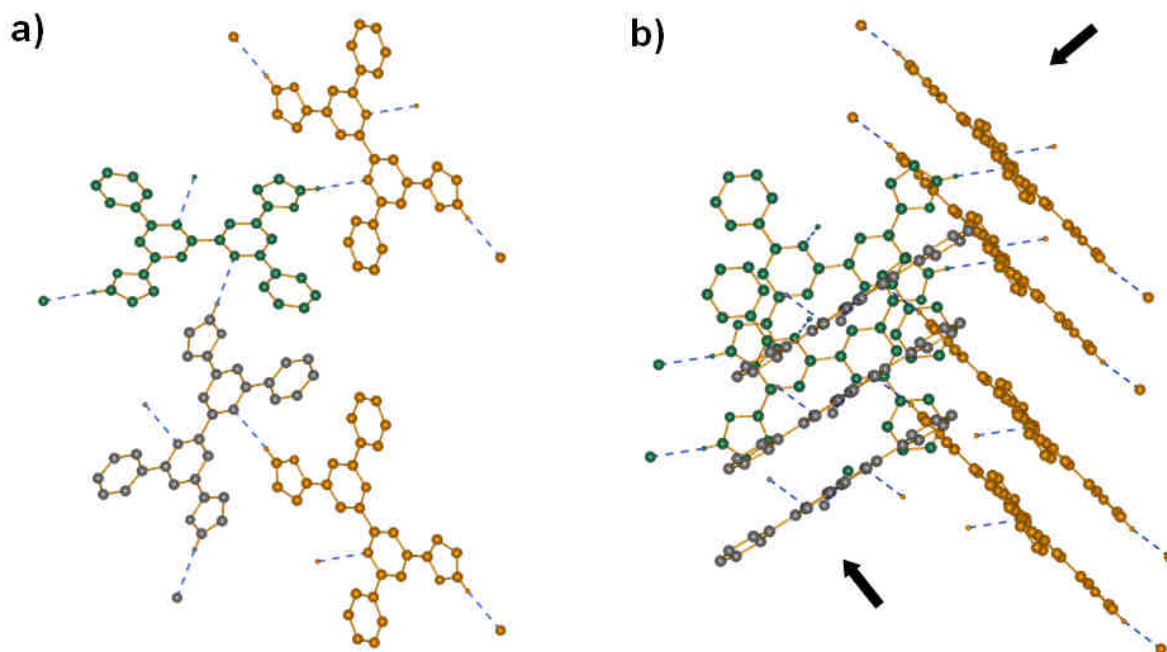
Fig. 56. a) View of 4,4´-di(furan-2-yl)-6,6´-diphenyl-2,2´-bipyridine (**L16**) molecules along the *c* direction showing the non-classical hydrogen bonds between nitrogen atoms from bipyridine and hydrogen atoms from furan rings. b) View along the [-3.38, -22.71, 2] direction showing the three different packing modes of the molecules in the crystal structure. Hydrogen bonds are represented in blue.

II. 2. 10 [H₃L17][CF₃COO]·2CF₃COOH

Crystals of [H₃**L17**][CF₃COO]·2CF₃COOH were grown over a period of two days by dissolving the ligand H₂**L17** in CF₃COOH and placing the vial containing the solution into a sample bottle containing a small amount of water. The asymmetric unit contains the protonated ligand, as a consequence of the acidic conditions used in the crystallization process, a trifluoroacetate counterion and two molecules of trifluoroacetic acid. The molecules crystallize in the triclinic system, space group *P*-1 (No.2). The bipyridine unit adopts a *cis*-conformation, consistent with protonation at one of the nitrogen atoms and the formation of an N1-H1···N2 hydrogen bond (2.185(2) Å). The two pyridine rings are almost coplanar, and only the carbonyl group O1–C11=O2 can be found in this plane as well. The second carboxylic acid group is slightly twisted 6.5(9)° (C9–C8–C12–O3), and so is one of the phenyl groups found in the *ortho* position with respect to the nitrogen 7.3(4)° (N2–C10–C19–C20). The second phenyl group, on the contrary,

presents a considerable twist with respect to the bipyridine core: 31.4(7)° (N1–C1–C13–C18). The difference between the two C-O bond distances in each carboxylic acid group (C11-O1 1.304(3) Å, C11-O2 1.203(3) Å, C12-O3 1.307(3) Å, C12-O4 1.204(3) Å) confirms the protonation state. The fluorine atoms of the –CF$_3$ group in the counterion are disordered, occupying two different crystallographic positions each (modeled with F7 (65%) and F17 (35%), F8 (65%) and F18 (35%), and finally F9 (65%) and F19 (35%)). These two positions can be generated after rotating the –CF$_3$ group *ca*. 30°. Two other molecules of trifluoroacetic acid co-crystallize as solvent, one of them being disordered (modeled with F1 and F11 and F2 and F12, the occupancy factor is 70% for F1 and F2, whereas for F11 and F12 is 30%) (see figure 57).
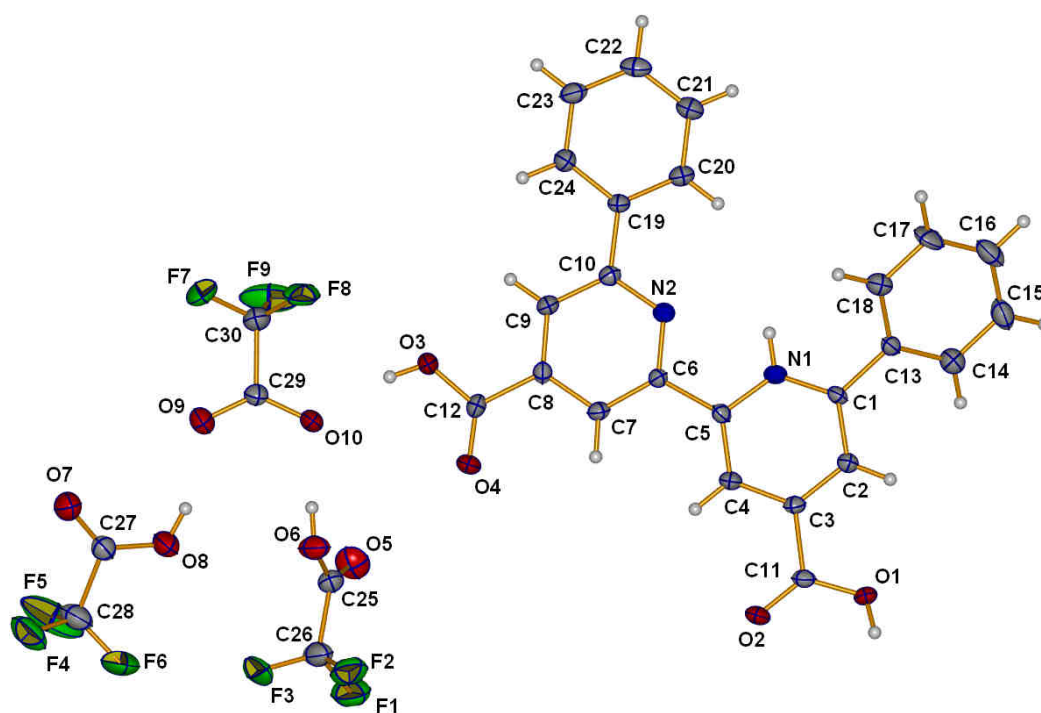
Fig. 57. Structure of the protonated ligand, [H$_3$**L17**]$^+$, a trifluoroacetate counterion and two molecules of trifluoroacetic acid. The ellipsoids are plotted at the 50% level. As a consequence of the disorder in the solvent and counterion molecules, only the fluorine atoms with higher occupancy factor are showed.

The ligand and solvent molecules and the counterion are packed forming layers, having hydrogen bonds bridging the molecules together (see figure 58). These hydrogen bonds are formed between the trifluoroacetic acid molecules (O3–H3⋯O10 1.82(7) Å; O6–H4⋯O10

1.79(1) Å; O8–H5···O9 1.81(5) Å) and the carboxylic acid moieties (O1–H2···O4^i 1.92(3) Å (symmetry code i = -x, 1-y, 1-z)). The layers interact between each other through hydrogen bonds stabilizing the supramolecular array (C18–H181···O7^{ii} 2.43(8) Å (symmetry code ii = 1-x, -y, 1-z) and N1–H1···O5^{iii} 2.33(7) Å (symmetry code iii= 1-x, 1-y, 1-z)) (see figure 59).
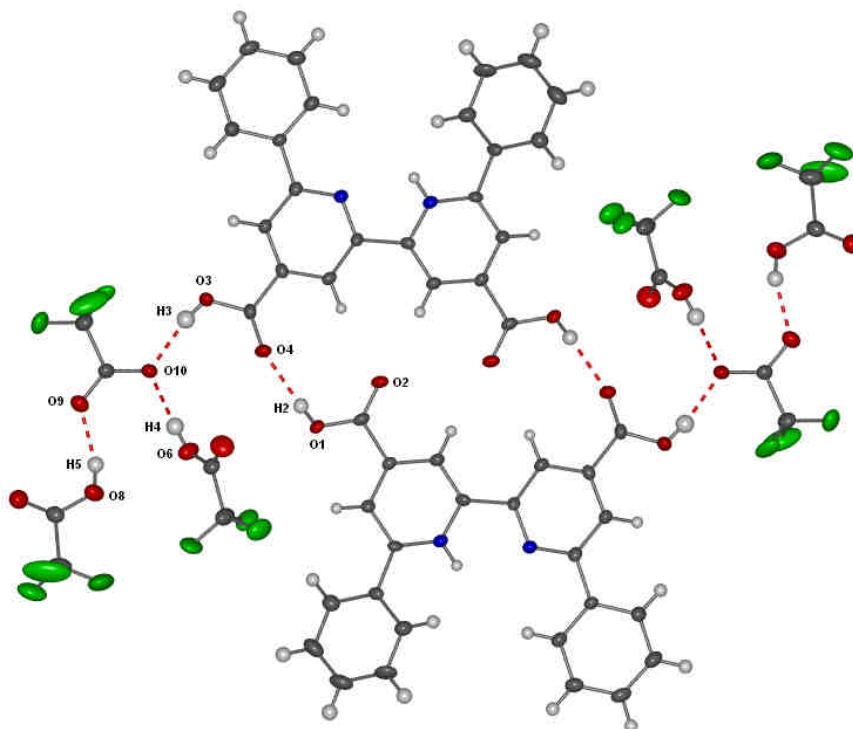
Fig. 58. Hydrogen bonds between cations, anions and solvate molecules in [H$_3$**L17**][CF$_3$CO$_2$]·2CF$_3$CO$_2$H.
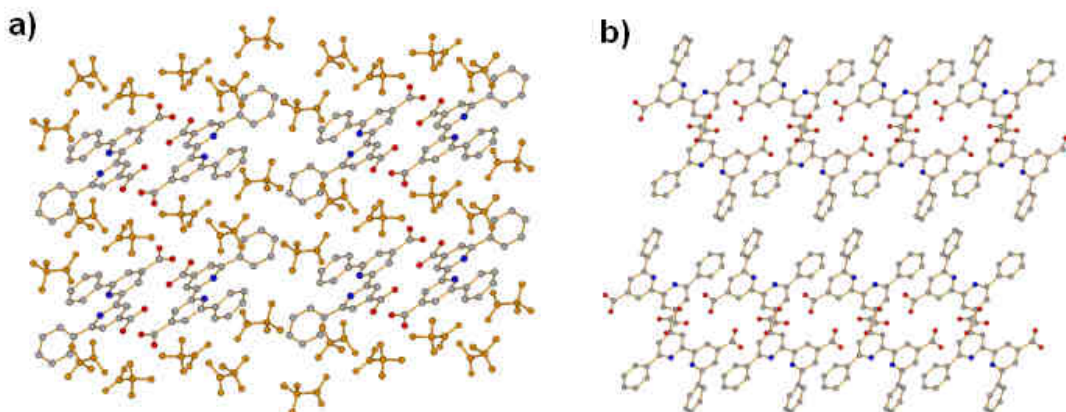
Fig. 59. Two different packing modes of the crystal structure; solvent and counterion molecules are represented in orange colour. a) View along *a* direction; b) view along the *b* direction. Solvent and counterion occupy the empty spaces in the crystal structure and have not been represented for clarity reasons.

II. 2. 11 Dimethyl 6,6´-diphenyl-2,2´-bipyridine-4,4´-dicarboxylate (L18)

L18 yielded X-ray quality crystals grown by slow evaporation of a chloroform solution of the compound. Ligand **L18** crystallizes in the monoclinic system, space group $P2_1/n$ (No. 14). The molecule is centrosymmetric with the inversion centre located in the C1–C1$^{\cdot i}$ bond (symmetry code i = 1-x, -y, -z). The bipyridine system and the phenyl groups located in the 6 and 6´-positions are almost coplanar (the angle between the least square planes of the bipy moiety and the phenyl ring is 3.6(6)°). This ligand differs from the previously described one in that the carboxylic acid groups of the 4 and 4´-positions have been replaced by methyl ester groups. These are slightly twisted with respect to the bipyridine unit by 4.5(2)° (torsion angle C2–C3–C12–O2). The molecules are stacked in columns along the *a* axis, but without π···π stacking interactions (the closest distance between ring centroids is 4.18(9) Å). One hydrogen atom from a phenyl group is oriented towards a vicinal π system in a T-mode (C7–H7A···π^{ii} (centroid) 2.99 Å (symmetry code ii = 3/2-x, 1/2+y, 1/2-z)), however, no classical hydrogen bonds are found in the crystal (see figure 60).

79
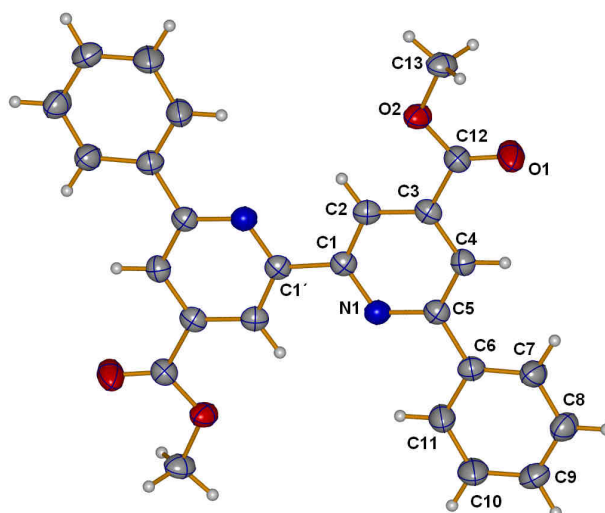
Fig. 60. Structure of dimethyl 6,6´-diphenyl-2,2´-bipyridine-4,4´-dicarboxylate (**L18**); ellipsoids are plotted at the 50% level.

Whereas the views along the *a* and *b* directions show that the molecules seem to be quite well packed in columns ((see figure 61 a)), a view along the *c* direction shows a fish-bone-like motif (see figure 61 b) similar to the one found in **L9**.
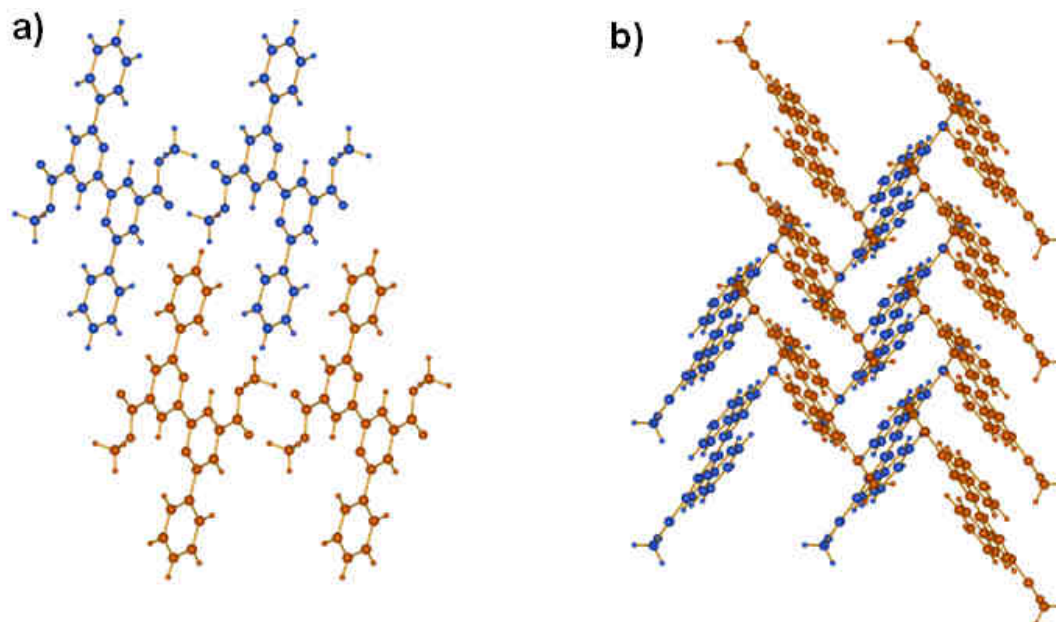
Fig. 61. a) View along *b* direction of the packing of 6,6´-diphenyl-2,2´-bipyridine-4,4´-dicarboxylate (**L18**); b) view along *c* direction showing the fish-bone-like motif.

II. 2. 12   Tetraethyl 6,6´-dimethyl-2,2´-bipyridine-4,4´-diyldiphosphonate (L23)

X-ray quality crystals of tetraethyl 6,6´-dimetyl-2,2´-bipyridine-4,4´-diyldiphosphonate grew after recrystalization of the compound from hexane. Ligand **L23** bears diethylphosphine oxide substituents in the 4 and 4´-positions and methyl groups in the 6 and 6´-positions of 2,2´-bipyridine (see figure 62). The molecule crystallizes, like **L18**, in the monoclinic system, space group $P2_1/n$ (No.14). As a centrosymmetric molecule, only half of the ligand is present in the asymmetric unit. The P=O bond is twisted with respect to the plane formed by the bipyridine unit (torsion angle 23.8(2)° C2–C3–P1–O1).
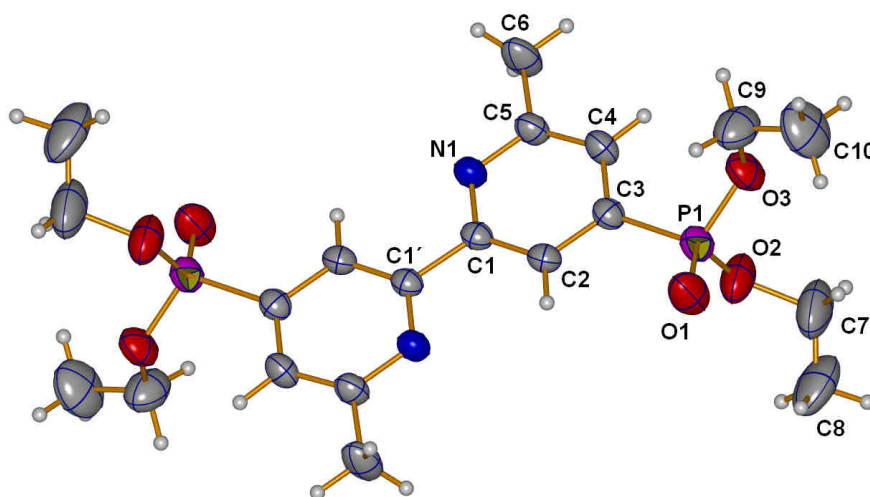
Fig. 62. Structure of tetraethyl 6,6´-dimethyl-2,2´-bipyridine-4,4´-diyldiphosphonate (**L23**); ellipsoids are plotted at the 30% level.

π-Stacking interactions are not a feature of this structure, and instead, hydrogen bonds dominate in the packing. These are formed between the carbonyl oxygen atom and a hydrogen atom from a vicinal aromatic group (C4–H4A···O1[i] 2.53(1) Å (symmetry code i = 1/2+x, 1/2-y, 1/2+z)), and are responsible for the undulating infinite 2D motif in the [-4.56, 0.01, -7.14] direction (see figure 63 b).
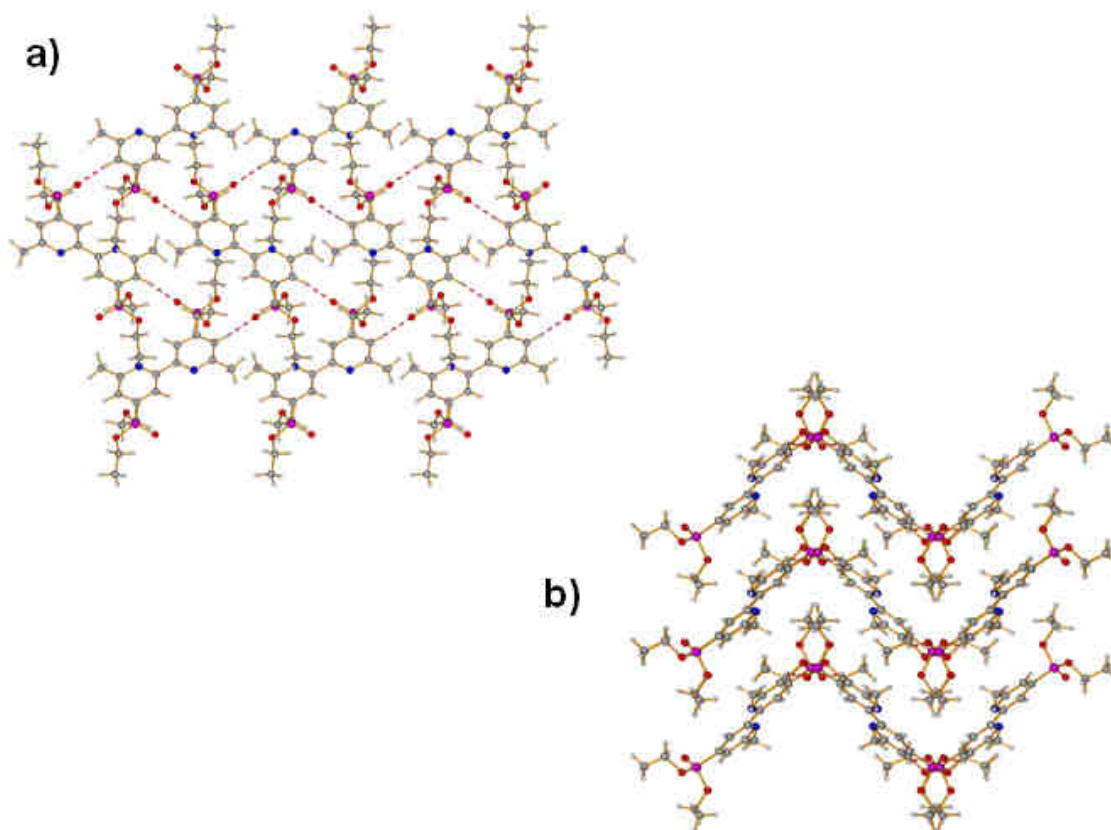
Fig. 63. a) View along *b* direction; b) undulating infinite 2D structure formed by the packing of tetraethyl 6,6´-dimethyl-2,2´-bipyridine-4,4´-diyldiphosphonate (**L23**) molecules. View along the [-4.59, 0.05, -7.11] direction.

III   2,2´:6´,2´´-Terpyridine ligands

2,2´:6´,2´´-Terpyridine is a tridentate ligand formed from three pyridine units, which upon coordination to a metal change their conformation from *trans,trans* to *cis,cis* (see figure 64), occupying its near-planar N_3 donor set three *meridional* sites in an octahedral complex. However, mono- and bidentate bonding modes are now also well established [140]. It forms stable complexes by chelating a broad variety of transition metal ions, and it has the advantage with respect to 2,2´-bipyridine that simple achiral bis-terpyridine complexes can be obtained with octahedrally coordinating metal ions, as opposed to the racemic mixtures derived from the use of bipyridine as coordinating ligand. Exhaustive research has been done on 2,2´:6´,2´´-terpyridines functionalized in their 4´-positions [141, 142], because despite chemical

modification in this position, the terpyridine complexes retain their achirality, being arranged in a *trans* configuration along a C_2 axis. However, it is possible to create and isolate chiral species either by introducing chiral auxiliaries or by forming helical structures, i.e. dicoper(I) and/or disilver(I) helicates, as shown in the literature [143].
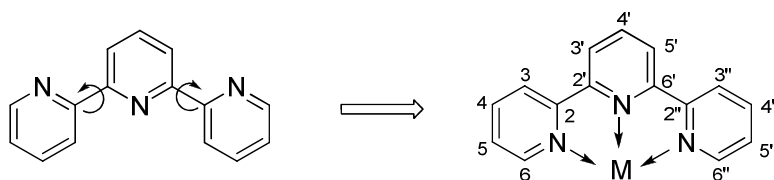
Fig. 64. Chemical structure of 2,2´:6´,2´´-terpyridine. The conformational change from the *trans,trans* to the *cis,cis* coplanar form upon coordination to a metal together with ligand numeration is shown.

The chemistry of 2,2´:6´,2´´-terpyridine is much younger than that of bipyridines. Terpyridine was first isolated by Morgan and Burstall in the 1930s [144, 145]. Since then, hundreds of terpyridine derivatives have been synthesized for different purposes including supramolecular chemistry [146], analytical chemistry [147], biological applications [148], solar cells [40], or synthesis of dendrimers [149].

In this thesis, tetrasubstituted symmetrical 2,2´:6´,2´´-terpyridines have been synthesized using Kröhnke's methodology [120]. This method has been employed to make some of the 2,2´-bipyridine ligands discussed in the previous chapter, and more specifically it has been often used in the literature to synthesize 2,2´:6´,2´´-terpyridines similar to the ones presented here [122, 123, 150]. The ligands discussed in this chapter have been created with the aim of employing them together with copper(I) for solar cell applications; for this reason, they possess ester or acid groups, for dye adsorption, and substituents in the 6 and 6´´-positions, in order to stabilize the system with respect to oxidation to copper(II) complexes [151, 152].

III. 1   Synthesis and characterization of 2,2´:6´,2´´-terpyridine ligands

To make **L27** and **L29**, the bis-enone shown in figure 65 was synthesized first. This was achieved by refluxing 2,6-diacetylpyridine with two equivalents of methyl 4-formylbenzoate and diethyl amine in 1-propanol, a procedure slightly different to the already reported one [153]. This novel bis-chalcone was isolated as a beige-solid in 42% yield and fully characterized by standard spectroscopic and analytical techniques.
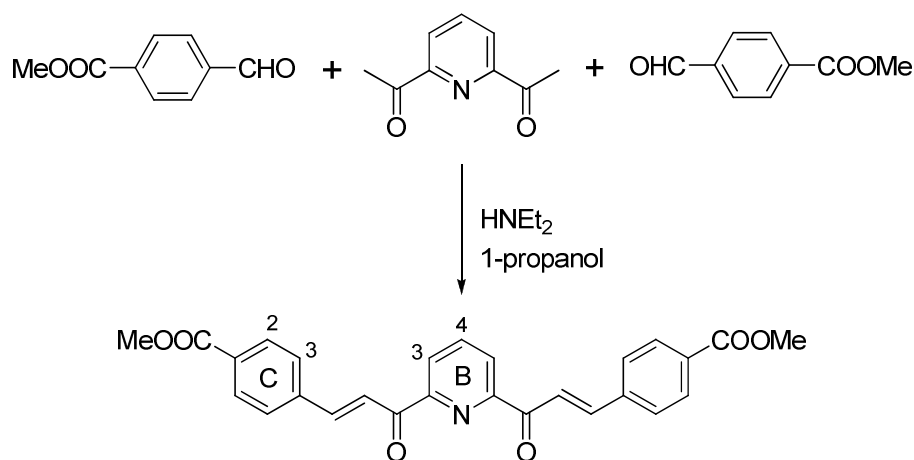
Fig. 65. Synthetic route to the bis-enone dimethyl 4,4´-(1*E*,1´*E*)-3,3´-(pyridine-2,6-diyl)bis(3-oxoprop-1-ene-3,1-diyl)dibenzoate and its numeration.

From the ^{1}H NMR spectrum of the bis-enone in figure 66 (see figure 65 for ring name assignment and numeration), it is clear that the most deshielded proton of the molecule is the ß proton with respect to the carbonyl group, and this is due to the charge distribution of the two resonance forms, as it was illustrated in figure 33 in the previous chapter. The resonances of the allyl protons present a coupling constant of 16 Hz, as expected for this type of protons. Apart from that, it should be noted that the characteristic triplet coming from H^{4B} is hidden under the doublet of one of the allyl protons.
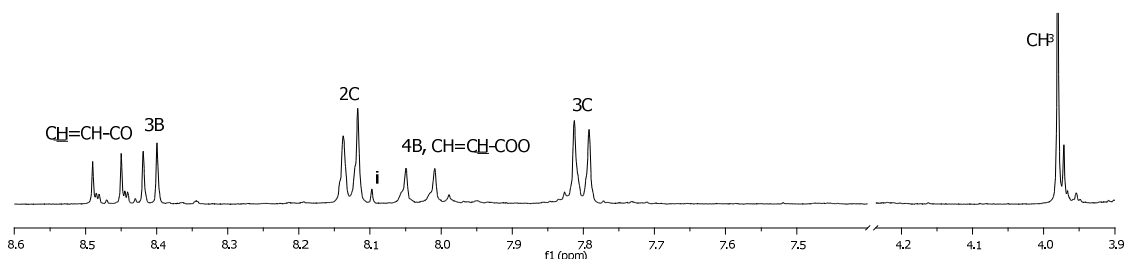
Fig. 66. ^{1}H NMR spectrum of dimethyl 4,4´-(1E,1´E)-3,3´-(pyridine-2,6-diyl)bis(3-oxoprop-1-ene-3,1-diyl)dibenzoate in CDCl$_3$ (i = impurity) (400 MHz).

Then, the reaction of the bis-chalcone with the appropriate Kröhnke's reagent in the presence of ammonium acetate afforded the desired ligands as white solids after purification by column chromatography (see figure 67). A similar method has been reported previously [153].
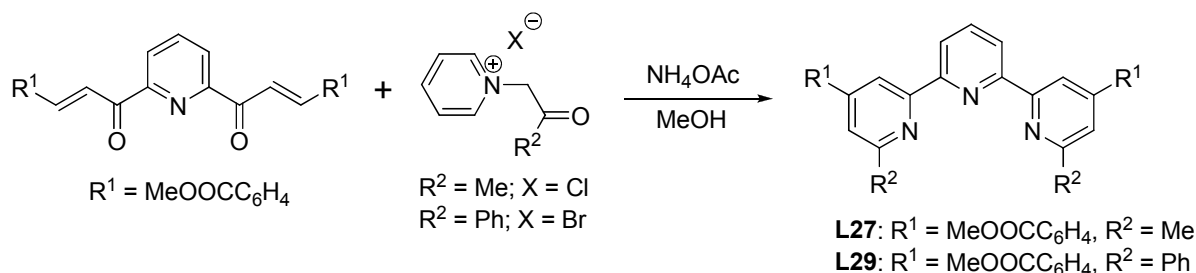
Fig. 67. Synthetic route to ligands **L27** and **L29**.

In figure 68 the ^{1}H NMR spectra of ligands **L27** and **L29** in CDCl$_3$ are shown. They are easily distinguished by the presence of a signal at δ 2.74 ppm for the methyl groups in **L27** and diagnostic signals for the phenyl groups (ring D) attached to the 6 and 6´´-positions in **L29** (see figure 68 for number scheme). The signals corresponding to ring A, especially H^{5A}, and H^{3B} are shifted downfield as a consequence of the introduction of the phenyl groups in **L29**, a phenomenon also observed in the previous chapter. In contrast, the resonances corresponding to H^{4B} and ring C, as well as the methyl ester group, are not considerably shifted (not even in comparison with the starting material), so it can be concluded that the introduction of phenyl groups does not have much influence on them.

85
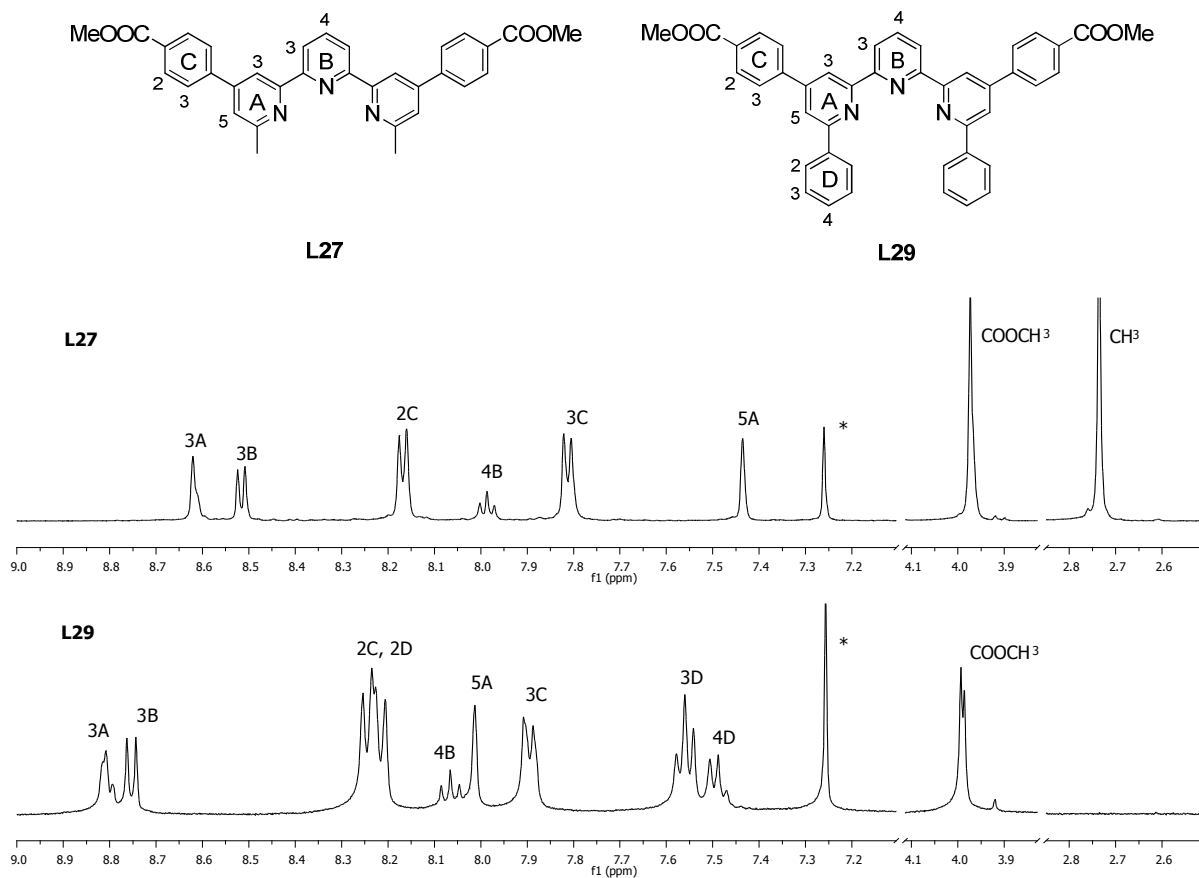
Fig. 68. Diagrams of ligands **L27** and **L29** with number scheme and comparison of their ^{1}H NMR spectra in CDCl$_3$ (*) (400 MHz).

Finally, **L27** was hydrolyzed to H$_2$**L28**, its acidic form, using the methodology already employed to hydrolyze some of the 2,2´-bipyridine ligands (**L3**, **L5**, **L14** and **L21**) described in the previous chapter [129]. **L27** was refluxed for 12 h with 10 equivalents of LiOH in a H$_2$O:THF 1:10 mixture. Finally, the pH of the reaction mixture was adjusted to 2 with HCl, what caused the precipitation of an off-white ligand, H$_2$**L28**, in 65 % yield. Its poor solubility brings about the need to use TFA-d^1 to run the ^{1}H NMR spectrum shown below (the number scheme used is the same as for **L27** and **L29**):
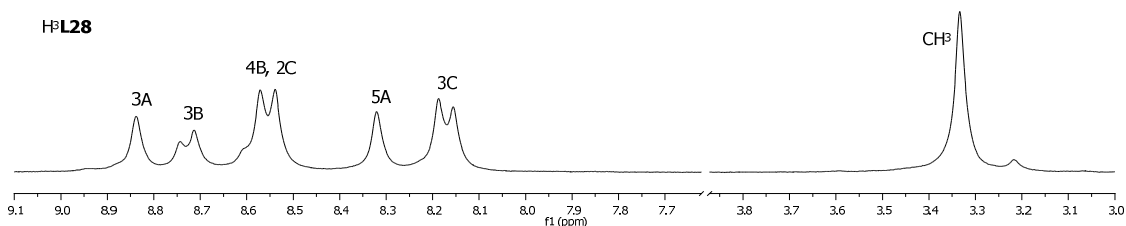
Fig. 69. ^{1}H NMR spectrum of H_3**L28** in TFA-d[1] (250 MHz).

A quick look at the spectrum shows that the resonance corresponding to the methyl ester groups is missing; there is only one singlet at δ 3.33 ppm assigned to the methyl groups from the 6 and 6´´-positions. This signal appears at higher frequencies than the resonances of the methyl groups attached to the 6 and 6´-positions in H_3**L4** (δ 3.14 ppm), H_3**L15** (δ 3.06 ppm) and H_3**L24** (δ 3.10 ppm), probably due to structural differences between 2,2´-bipyridine and 2,2´:6´,2´´-terpyridine. The rest of the spectrum shows the expected pattern of signals, the signal of H[4B] again overlapping with the one for H[2C].

IV   Copper(I) complexes

Copper (Cu) is in the *d* block (ground state electronic configuration: $[Ar]4s^13d^{10}$) and occupies the same group of the periodic table (11) as silver (Ag) and gold (Au). Although they have the same (except for principal quantum number) electronic configuration, Cu oxidation states are primarily +1 and +2, Ag is usually +1, and Au is typically +1 or +3. Among the many distinct isotopes that copper has, two of these, [63]Cu and [65]Cu, are stable and occur naturally, with the first one comprising approximately 69% of naturally occurring copper. The old names for copper(II) and copper(I) of *cupric* and *cuprous*, respectively, are still sometimes used.

Copper has played an important role in the history of mankind, which has used the easily accessible metal for thousands of years. In the Roman era, copper was principally mined on Cyprus, hence the origin of the name of the metal as Cyprium, "metal of Cyprus", later shortened to Cuprum. Nowadays, Chile is the top mine producer of copper with at least one-third world

share followed by the USA, Indonesia and Peru, and the main copper ore for traditional mining is chalcopyrite ($CuFeS_2$). The recovery of copper from scrap metal is an essential part of copper-based industries, e.g. in 2005 in the USA, recycled metal constituted *ca.* 30% of the copper supply. This recycling of the metal is important not only for environmental reasons, but also because copper, like fossil fuels, is a finite resource which supplies are estimated to be getting tight.

Copper is an essential trace metal present in plants and humans, having a biological role in electron transfer systems (blue copper proteins), O_2 storage and transport (haemocyanin) and Cu transport proteins (ceruloplasmin). Apart from that, it is used as an electrical conductor, in architecture due its resistance to corrosion and as a component of coins, among other applications.

An interesting property inherent to copper coordination compounds is the structural difference between the Cu(I) and the Cu(II) oxidation states: Cu(I) has a d^{10} configuration and generally prefers to be four-coordinate with a nearly tetrahedral or "pseudotetrahedral" geometry, tending towards planarity [154-156], while Cu(II) has a d^9 configuration and adopts a Jahn-Teller distorted geometry that is usually 5- or 6-coordinate [157], although it is also possible to prepare tetracoordinated Cu(II) complexes under some conditions (weakly coordinating solvents with weakly coordinating anions or substituents that inhibit higher coordination numbers) [116]. The copper complexes synthesized in this thesis (they will be referred to as $[Cu(NN)_2]^+$ where NN signifies an α,α'-diimine) are all in the oxidation state +1. When adsorbed onto the semiconductor in solar cells, they inject an electron into the conduction band of TiO_2, and thus the copper centre must be oxidizable. However, as mentioned before, copper in oxidation state +1 has a strong preference for a particular coordination environment, i.e. "pseudotetrahedral", so the ligand design must be precise. The most important observation comes from the classical work of Williams [116] who demonstrated that i) copper(I) complexes of 6,6´-disubstituted bipyridine (bipy) or 2,9-disubstituted phenanthroline (phen) ligands did not disproportionate in aqueous conditions, and ii) the introduction of these substituents dramatically stabilized the copper(I) complexes with respect to copper(II) whereas $[Cu(bipy)_2]^+$ undergoes an autooxidation reaction with O_2 [158].

Fig. 70. Structure and numeration of 2,2´-bipyridine and 1,10-phenanthroline.

James and Williams proposed that substituents in the 2- and 9-positions of 1,10-phenanthroline, when coordinated to copper(I), would interact in a destabilizing manner with the 2- and 9-substituents on the opposite ligand in the cupric state, arguing that this interaction would dramatically stabilize the cuprous state (see figure 71) (this example can be extended to complexes with bipy ligands) [116]. They also found that the electrochemical properties of the complexes were quite sensitive to the extent of "encapsulation" of the metal center, in that it is over 400 mV easier to oxidize $[Cu(phen)_2]^+$ than $[Cu(dmp)_2]^+$ (dmp = 2,9-dimethylphenanthroline) in aqueous electrolyte. Furthermore, it has been established that even with only one substituent, the copper(I) centre is enough "encapsulated" to be stabilized from oxidation to copper(II) [155]. It should be noted here that the chelating bipyridine fragment, on the contrary to the phenanthroline one, can sustain a substantial dihedral twist between the aromatic rings and still remain coordinated, so it is possible that bipy-based and phen-based complexes may have significantly different coordination geometries; however, the general characteristics of $[Cu(NN)_2]^+$ complexes given here, are extended to both families of compounds.

$Cu^I(dmp)_2^+$ $\qquad$ $Cu^{II}(dmp)_2^{2+}$
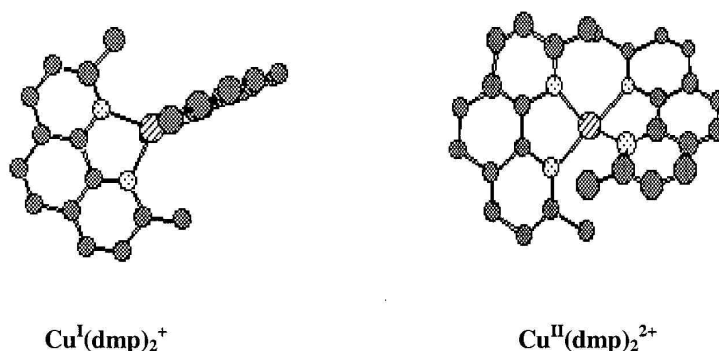
Fig. 71. Schematic representation of the steric effects that hinder the achievement of a high degree of planarity by the ligands in the cupric state [99].

89

A less well appreciated aspect of Cu(II/I) redox chemistry is the solvent dependence. Examining the cyclic voltammetry of $[Cu(dmp)_2][PF_6]$ (see figure 72) one observes that the measured half-wave potential, $E_{1/2}$, assigned to the Cu(II/I) couple is surprisingly sensitive to the solvent used (this can be extended to $[Cu(NN)_2]^+$ complexes), while the peak-to-peak separations measured are typically 100-200 mV and essentially independent of it [159, 160]. The reason for this half-wave potential dependence is based on the addition of a solvent molecule to the oxidized complex standing from the oxidation of Cu(I) at the electrode surface. It is assumed that solvent coordination is fast and reversible with respect to the cyclic voltammogram time scale and that concentration of the five-coordinate compound is negligibly small.
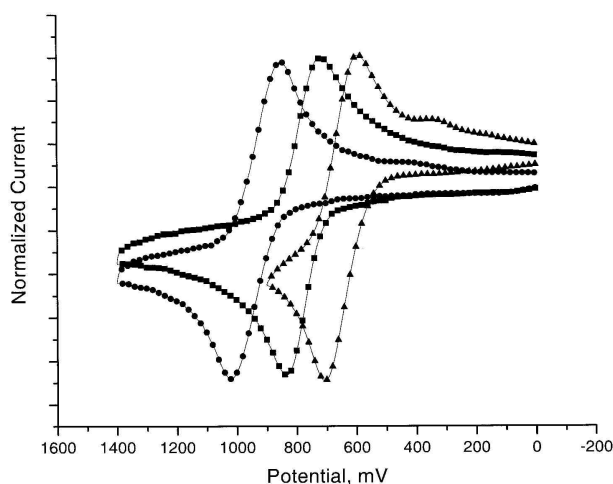
Fig. 72. Cyclic voltammograms of $[Cu(dmp)_2]^+$ in CH_2Cl_2 (circles), CH_3CN (squares) and DMSO (triangles) measured at 200 mV s^{-1} with 0.1 M tetrabutylammonium hexafluorophosphate, a Ag wire reference electrode, a Pt gauze auxiliary electrode and a glassy carbon working electrode. The potentials are measured vs. SCE [160].

Another consequence of this geometry modification is found when the luminescence behavior of Cu(I)-phenanthrolines is examined [97]. Upon light excitation, the lowest ^{3}MLCT excited state is populated, thus the metal centre changes its formal oxidation state from Cu(I) to Cu(II); the latter tends to assume a more flattened coordination geometry [161]. In this "open" structure a fifth coordination site is made available for the newly formed d^9 ion (see figure 73), that can be attacked by nucleophilic species such as solvent molecules and counterions, leading to pentacoordinated excited complexes (exciplexes). These can deactivate via non-emissive

deactivation paths, thereby shortening the lifetime of the excited state and quenching the luminescence. Direct spectroscopic evidence for these five-coordinate compound formation is still lacking, however convincing clues for their formation have been given by McMillin *et al.* in a variety of investigations where the effect of the solvent and of the counterion in several $[Cu(NN)_2]^+$ complexes was examined [162].
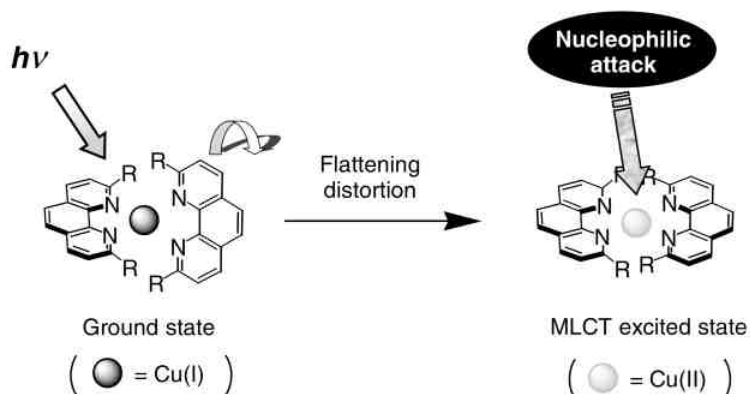
Fig. 73. Flattening distortion and subsequent nucleophilic attack by solvent, counterion or other molecules following light excitation in Cu(I)-phenanthrolines. The size of the R substituents is of paramount importance in determining both the extent of the distortion and the protection of the newly formed Cu(II) ion from nucleophiles [97].

However, examining the visible absorption spectra of $[Cu(dmp)_2]^+$, it has been noted that these are, within experimental error, the same in all solvents employed, with only small changes in the extinction coefficients. This is expected since light absorption is a vertical process in the Franck-Condon sense and, unlike cyclic voltammetry, it is not influenced by processes that occur after charge transfer. At the same time, the absorption and emission energies of the $[Cu(NN)_2]^+$ compounds are almost independent of half-wave potential, $E_{1/2}$. As a consequence, the expected correlations between optical energy gaps (E_{abs}, E_{em}) and metal based reduction potentials ($\Delta E_{1/2}$) that exist for $(d\pi)^6$ polypyridyl transition metal compounds (e.g. Ru(II) and Os(II) complexes [163]) are not observed for copper(I) $(d\pi)^{10}$ complexes [163, 164]. This is significant in that it points to a fundamental difference between Cu(I) and Ru(II) chromophores. Typically, the $Ru^{III/II}$ and $L^{0/-}$ (L = ligand) redox couples approach electrochemical and chemical reversibility at the electrode surface. This is not true for $[Cu(NN)_2]^+$ complexes, where there are significant inner-sphere geometric changes associated with the oxidation of Cu(I) to Cu(II), as already mentioned,

and the redox process is not strictly reversible. Therefore, incorporated within $\Delta E_{1/2}$ values for $[Cu(NN)_2]^+$ systems are the energetics associated with torsional distortion and coordination number changes that are not relevant to light absorption.

Regarding the absorption spectra of these $[Cu(NN)_2]^+$ complexes, it should be pointed out that no matter what the nature of the ligand is, bipy or phen, these are dominated by intense, broad absorption bands maximizing at a wavelength in the range 440-470 nm [165], and a weak shoulder at longer wavelengths [165, 166]. The former absorption was originally assigned by Irving and Williams [167] as a metal-to-ligand charge-transfer (MLCT) transition where an electron is promoted from a $3d$ orbital of copper to a low-lying π^* orbital of the ligands, and the orbital parentage of the dominant charge-transfer absorption has since been established [166, 168]. Analyses suggest that a static or dynamic flattening distortion of the D_{2d} structure accounts for the weak but non-negligible intensity and the polarization of the low-energy shoulder [165], as also suggested by Ichinaga et al. [168]. In other words, the low energy shoulder observed in the ground state absorption spectra of $[Cu(NN)_2]^+$ complexes is thought to reflect the degree of distortion away from D_{2d} symmetry.

Still another characteristic of Cu(I) complexes is the difficulty to prepare heteroleptic compounds due to the lability of first-row transition metals in general, and copper in particular. Ligand exchange in fluid solution can be facile. For example, immediately after mixing $[Cu(dmp)_2]^+$ and another Cu(I) complex with a different phen ligand, the ^{1}H-NMR spectra revealed the presence of the mixed chelate [160], also observed for 6,6´-disubstituted bipyridines. The replacement of 2,2´-biquinoline ligands coordinated to Cu(I) by dmp also occurs in fluid solution [169]. This property of Cu(I) complexes (not shown by Ru(II) or Os(II) complexes) may be an impediment for some applications. However, it will be shown in section V. 4 that one can take advantage of it in order to make heteroleptic Cu(I) complexes on the surface of TiO_2. Finally, it should be mentioned that some novel approaches have been described recently to synthesize heteroleptic copper(I) complexes in solution and that they have been reported in the literature [170].

IV. 1   Synthesis and characterization of copper(I) complexes

Two synthetic methods to copper(I) complexes have been employed depending on whether the ligand contained acid groups or not. In the case where these groups are missing, the complexes have been synthesized by simply mixing together a solution containing two equivalents of the ligand with another solution containing one equivalent of $[Cu(CH_3CN)_4][PF_6]$. Immediately a colour change is observed, a direct indication that a complex has been formed. After stirring the mixture for *ca*. 15-30 min, the $[Cu(NN)_2]^+$ complexes were precipitated as their hexafluorophosphate salts by simply adding ether or in some cases hexane to the solution mixtures.

When the ligands contain carboxylic acid or phosphonic acid groups, a different procedure has been used, mainly because of the insolubility of these ligands. [61] The standard synthetic procedure implies the suspension of two equivalents of the ligand in water and heating the mixture up to *ca*. 70 °C before addition of some drops of a 1M NaOH solution, that deprotonate the ligand and solubilize them in water. Then, one equivalent of copper(II) sulfate dissolved in water is added, followed by further addition of some drops of a 1M NaOH solution. After, ascorbic acid dissolved in water is added to the solution mixture in order to reduce the Cu(II) to Cu(I), what entails a colour change. Finally, the pH of the solution is adjusted to 2 by addition of 1M HCl, and the $[Cu(NN)_2]^+$ complexes are precipitated as their chloride salts.

The complexes that will be described in this work have been classified in two different groups for an easier comparison. The first group contains complexes with 6,6´-dimethyl substituted ligands, whereas the second group encloses those complexes containing 6,6´-diphenyl substituted ligands and two more complexes with biquinoline ligands (they have been placed in this group for their bigger similarity with 6,6´-diphenyl-2,2´-bipyridine than with 6,6´-dimethyl-2,2´-bipyridine).

The mass spectra of the complexes synthesized show in all cases the $[Cu(NN)_2]^+$ ion, direct evidence of the presence of the complex, with the characteristic pattern of the naturally occurring copper isotopes. However, in order to establish the nature of the counter ion, especially in the

complexes with acid groups, elemental analysis is necessary. These data show that a chloride ion is the counter ion in all these cases, whereas in the complexes without acid groups, a hexafluorophosphate ion is present.

In order to summarize the ^{1}H NMR spectra of the complexes, one example is shown for each group comparing the ligand and the complex ^{1}H NMR spectra. This will illustrate the resonance shifts that occur upon coordination of the ligands to the Cu(I) metal centre. In almost all of them, as Constable pointed out in 1989 [104], the signal from H^{3A} is the lowest field resonance, and this is interpreted in terms of van der Waals deshielding of H^{3A}, associated with the close H^{3A}-$H^{3'A}$ contacts.

In figure 74, the ^{1}H NMR spectra of ligand **L3** and its copper(I) complex are shown. The signal shifts observed here are also seen in the rest of the complexes of this group, where the ligands have methyl substituents in the 6 and 6´-positions. From the spectra, it is straightforward that the signals of the protons that are far away from the metal coordination environment (H^{2B}, H^{3B} and $H^{COOC\underline{H}3}$), do not suffer significant shifts upon coordination to copper(I). On the contrary, the signals corresponding to the protons close to the metal centre (H^{3A}, H^{5A} and $C^{C\underline{H}3}$) are shifted, and also their resonance signals are broadened in comparison to the free ligand. The shift of the signal of the methyl groups attached to the 6 and 6´-positions of the bipyridine moiety is a consequence of the shielding resulting from each methyl substituent lying over the π-cloud of a bipy domain of the second ligand, whereas the deshielding observed for the signal of H^{5A} is probably caused by a ring strain from the other ligand of the complex. The broadening of these three signals is most likely related to the restricted movement (C_{py}-C_{phenyl}) of the protons in the complex. As mentioned before, the same pattern is observed in the other complexes of this group.
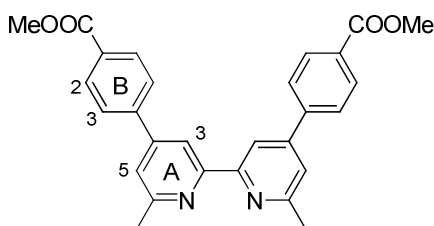
L3
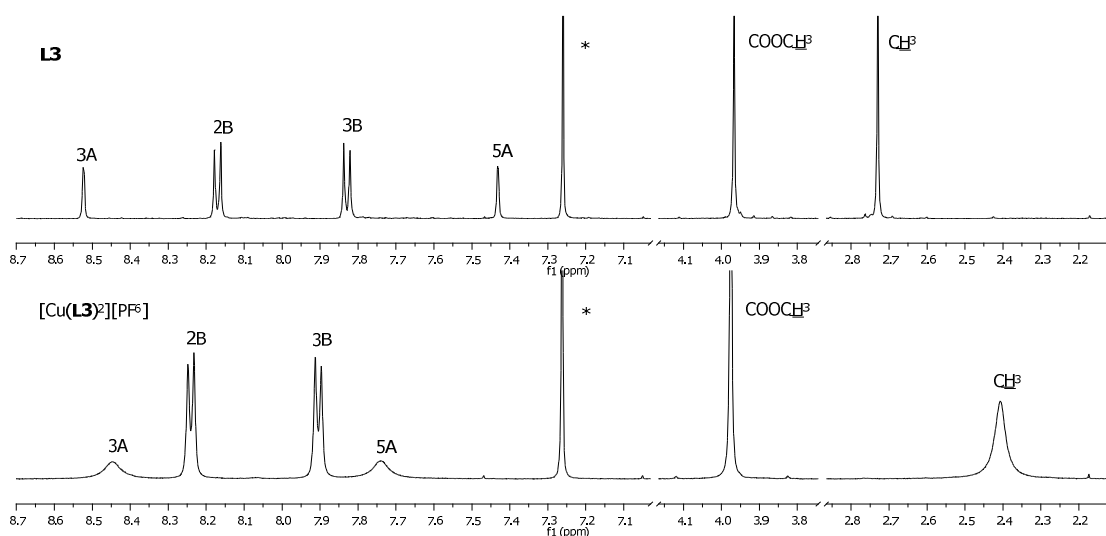
Fig. 74. Diagram of ligand **L3** with number scheme and ^{1}H NMR spectra of **L3** and [Cu(**L3**)$_2$][PF$_6$] in CDCl$_3$ (*) (500 MHz).

The ^{1}H NMR spectra of ligand **L5** and its complex are shown in figure 75. This example is representative for the second group of complexes discussed above, the ones with ligands bearing phenyl substituents in the 6 and 6´-positions. Again, the signals of the protons situated far away from the metal centre (H^{2B}, H^{3B} and H^{COOCH3}) are not significantly shifted, so it can be concluded that upon complexation, no remarkable changes in their electronic environment are noticeable. However, the protons closer to the copper(I) centre (H^{3A}, H^{5A}, H^{2C}, H^{3C} and H^{4C}) have resonances considerably shifted with respect to the ones from the free ligand. All these signals are shifted to lower frequencies; in the case of H^{3A} and H^{5A} this is probably due to a ring in the adjacent pyridine and the other ligand, respectively, that have a shielding effect. In the case of the signals assigned to the protons of the pendant phenyl groups, they are shielded upon coordination to copper(I), for the same reason explained in the previous example in the case of the methyl groups.

95
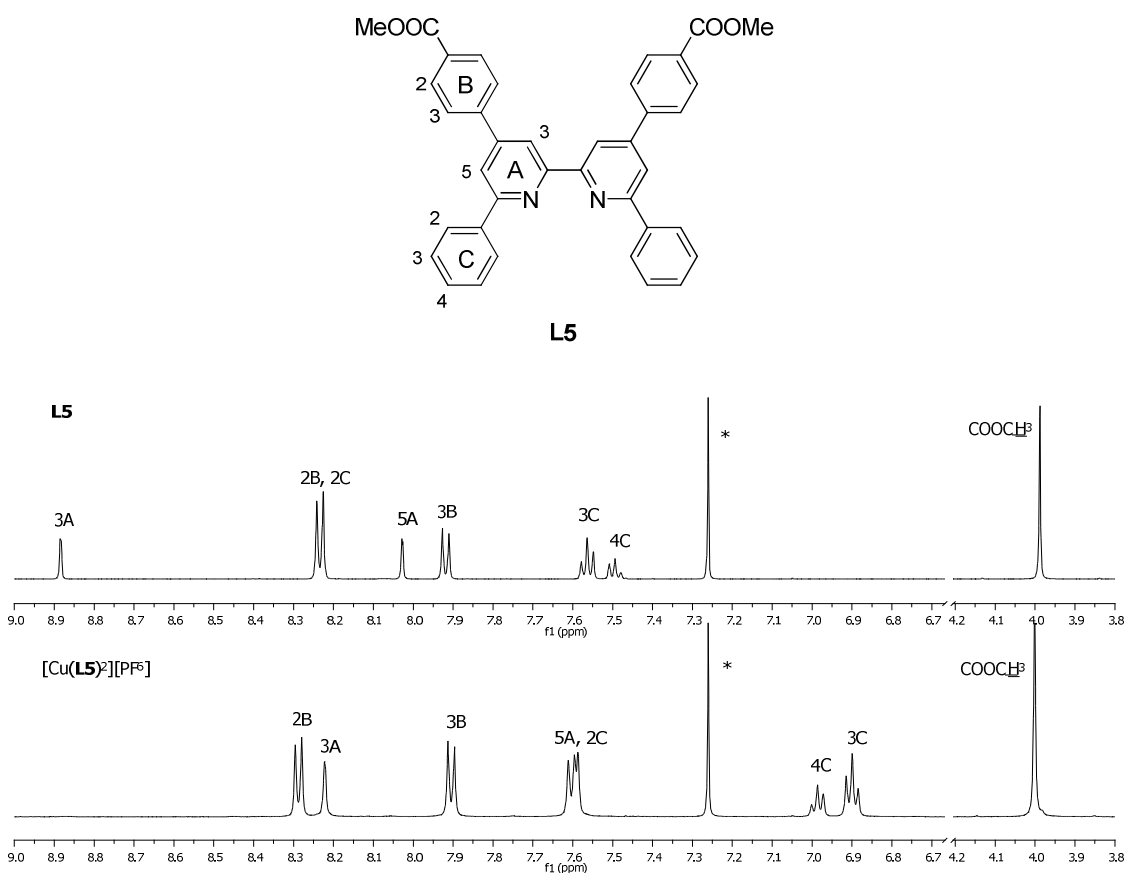
Fig. 75. Diagram of ligand **L5** with number scheme and ^{1}H NMR spectra of **L5** and [Cu(**L5**)$_2$][PF$_6$] in CDCl$_3$ (*) (500 MHz).

At this point, the geometrical distortion suffered by some of the complexes of the second group will be discussed. This [Cu(NN)$_2$]$^+$-type of complexes is prone to structural distortion on crystallization arising from intermolecular crystal packing forces. And even if solid-state structural studies are of limited value in understanding solution properties, it is worth having a look at them, since some intramolecular interactions which control the coordination geometry, such as aromatic π-π stacking interactions between ligand fragments, may persist in solution and so their crystallographic study may be of value in understanding their physical properties in solution. The distortion away from ideal D$_{2d}$ symmetry is expressed by θ (the dihedral angle), the angle of intersection of the two CuN$_2$ planes of each chelate ring. In D$_{2d}$ symmetry, with the ligands mutually perpendicular, θ = 90°; in a square planar geometry, θ = 0°. In copper(I)

complexes of substituted bipyridines and phenanthrolines, θ is typically 70-80° [154, 155, 171-173].

Considering the parent compounds of the two series of complexes of this thesis in more detail, it should be noted that $[Cu(dmbipy)_2]^+$ (where dmbipy is 6,6′-dimethyl-2,2′-bipyridine) has a θ of 81° [154], whereas $[Cu(dpbipy)_2]^+$ (where dpbipy is 6,6′-diphenyl-2,2′-bipyridine) has a θ of 83° [156], which is a somewhat smaller distortion than often observed when bulky substituents are attached to the ligands [174, 175]. However, examining the crystal structures of some of the phenyl substituted complexes synthesized in this thesis (see section IV. 2), the following dihedral angles are observed: $[Cu(L2)_2]^+$, θ = 73.4(2)°; $[Cu(L5)_2]^+$, θ = 69.0(1)°; $[Cu(L17)_2]^{3-}$ (see below and IV. 2. 7.), θ = 72.9(2)°; $[Cu(L18)_2]^+$, θ = 70.8(2)°. From these values, especially the second one, it is clear that the distortion suffered by the complexes of this group is bigger than that observed in the parent complex ion, and this flattening distortion is probably responsible for the slow precipitation of complexes $[Cu(H_2L6)_2]Cl$, $[Cu(H_2L17)_2]Cl$ and $[Cu(H_2L22)_2]Cl$ observed in DMSO solution and responsible for the unsuccessful ^1H NMR measurements in that solvent. Initially, the restricted bond rotation around the C_{py}-C_{phenyl} bond was thought to be responsible for the broadening of the signals seen in the ^1H NMR measurements, however, these did not sharpen upon increasing the temperature of the solution. Instead, the coordination ability of DMSO seems to take advantage of the flattened distortion of the complex to bind to the copper, in that the five-coordinate paramagnetic copper(II) species is probably formed hindering the measurement of the ^1H NMR spectrum. In the case of $[Cu(H_2L17)_2]Cl$, crystals of the complex were grown by leaving the crude reaction mixture (still containing excess of NaOH) to stand for several days, and single crystals of $Na_3[Cu(L17)_2]$ were obtained. This compound was soluble in water, so a ^1H NMR spectrum with sharp signals could be obtained in D_2O.

In the case of complexes $[Cu(L16)_2][PF_6]$ and $[Cu(L21)_2][PF_6]$, their ^1H NMR spectra were run in CD_2Cl_2 and $CDCl_3$, respectively, but decomposition of the compounds was observed, in this case due to the acidity of the solvents. This was proved by adding an excess of a base, K_2CO_3, to the solvent in which $[Cu(L16)_2][PF_6]$ was dissolved. The base neutralized the acid and consequently resulted in a well resolved spectrum, even after 16 hours (see figure 76).
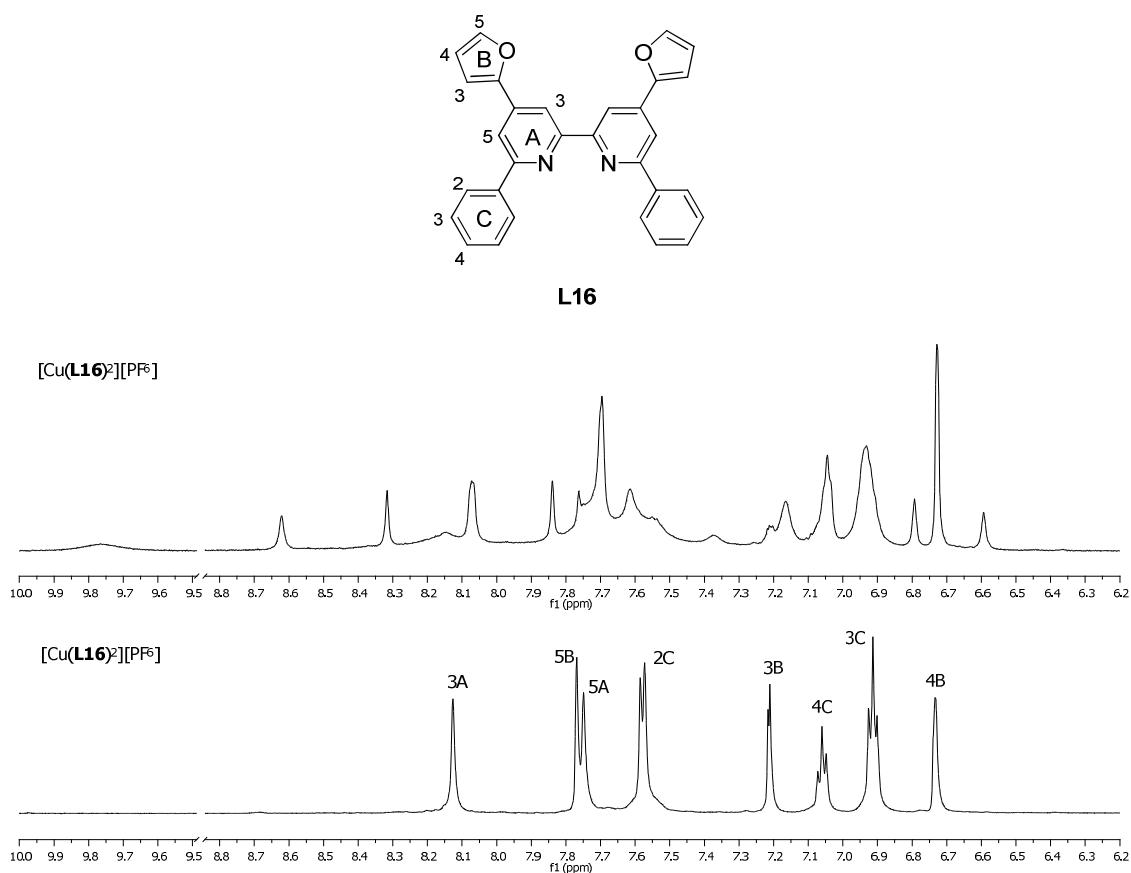
Fig. 76. Diagram of ligand **L16** with number scheme and ^{1}H NMR spectra of [Cu(**L16**)$_2$][PF$_6$] in CD$_2$Cl$_2$ (above) and [Cu(**L16**)$_2$][PF$_6$] in K$_2$CO$_3$/CD$_2$Cl$_2$ (below) (600 MHz).

Absorption of UV (200-400 nm) or visible (400-700 nm) light occurs only when the energy of incident radiation is the same as that of a possible electronic transition in the molecules studied. Such absorption of energy is termed *electronic excitation* and is typically associated with moving a single electron from an occupied to an unoccupied molecular orbital. The UV-VIS spectrum typically represents the absorption of light as a plot of energy (usually reported as wavelength, λ) *vs.* the intensity of absorption (as absorbance, A, or molar extinction coefficient, ε, where ε is a rough measure of the transition probability). The wavelength at maximum absorbance (A_{max}) for each electronic transition is termed λ_{max}. In order to calculate the molar extinction coefficient of the bands observed in the UV-VIS spectra, the laws of Lambert, Bouger and Beer, or more simply, Beer's law, have been used:

$$A = \varepsilon \cdot l \cdot c$$

where ε is the molar extinction coefficient with units of M^{-1} cm^{-1} and constant for each species; l is the cell pathlength (usually 1 cm) and c is the concentration of the sample studied with units of M (molarity, mol dm^{-3}).

In this thesis, solutions of the complexes with different, but known, concentrations have been prepared, and after measurement of the UV-VIS absorption spectra, the molar extinction coefficients of the maximum absorbances have been calculated. Studying these electronic spectra, one can obtain information about structure and bonding of metal complexes, although interpretation of these is not always straightforward. A characteristic feature of many *d*-block metal complexes is their colours, which arise because they absorb light in the visible region; but apart from these absorptions, there are also some in the near UV-region (190-400 nm). The last ones arise from ligand centered $\pi^* \leftarrow \pi$ transitions, whereas the former ones come from transitions between metal- and ligand-centered molecular orbitals which transfer charge from metal to ligand or ligand to metal (MLCT or LMCT, CT signifies charge transfer bands). So, in this part of the thesis, transitions in the visible part of the spectrum will be discussed. These are much weaker than those in the UV, and are assigned to MLCT electronic transitions. [176] An MLCT transition occurs when a ligand that is easily reduced, like for example bipy, which has a vacant, low-lying π^*-orbital, is bound to a metal centre that is readily oxidized, like copper(I).

In tables 1 and 2, the wavelength together with the extinction coefficient at the absorption maxima of all the complexes are shown. The solvent employed in each measurement is also given in these tables, because although it has no influence in the absorption spectra, as already said before, it will have to be taken into consideration in some cases where the solvent seems to make the copper complex precipitate in solution.

The complexes which absorption data are shown in table 1 form the group of complexes that have ligands with methyl substituents in the 6 and 6´-positions. Their MLCT absorption bands are located between 481 and 515 nm, and each complex therefore appears red. In contrast, the second group of complexes, those that have ligands bearing phenyl groups in the 6 and 6´-

positions and/or biquinoline ligands, are green and purple, respectively, because their MLCT absorption bands are shifted to lower energies or longer wavelengths, due to a strongly distorted tetrahedral geometry (D_2) under which the transition corresponding to this band is allowed. This flattening distortion comes from the π-π stacking interactions between the pendant phenyl groups of one ligand and the bipyridine moiety of the other ligand, as also occurs in the Cu(I) complex with 2,9-diaryl substituted phenanthrolines [97].

	λ_{max} / nm ($\varepsilon \cdot 10^{-3}$ / M^{-1} cm^{-1})	Solvent
[Cu(**L1**)$_2$][PF$_6$]	274 (1.0), 310 (0.5), 352 (sh), 481 (0.15)	CHCl$_3$
[Cu(**L3**)$_2$][PF$_6$]	271 (50.0), 323 (25.0), 488 (4.3)	CHCl$_3$
[Cu(H$_2$**L4**)$_2$]Cl	-	-
[Cu(H$_2$**L8**)$_2$]Cl	214 (74.4), 274 (47.0), 314 (60.0), 482 (8.0)	MeOH
[Cu(**L9**)$_2$][PF$_6$]	274 (sh), 289 (71.0), 493 (4.1)	CH$_3$CN
[Cu(H$_2$**L10**)$_2$]Cl	202 (34.3), 252 (27.2), 268 (sh), 319 (35.4), 483 (9.9)	MeOH
[Cu(**L11**)$_2$][PF$_6$]	204 (90.0), 241 (sh), 308 (27.0), 317 (sh), 495 (0.5)	CH$_3$CN
[Cu(**L14**)$_2$][PF$_6$]	255 (94.0), 324 (24.0), 508 (4.0)	CH$_3$CN
[Cu(H$_2$**L15**)$_2$]Cl	260 (75.0), 331 (24.0), 515 (6.7)	DMSO
[Cu(**L23**)$_2$][PF$_6$]	254 (16.0), 273 (16.0), 317 (30.0), 490 (5.7)	CHCl$_3$
[Cu(H$_4$**L24**)$_2$]Cl	271 (1.8), 313 (2.1), 324 (2.0), 478 (0.8), 558 (sh)	DMSO

Table 1. Charge transfer absorption data of the Cu(I) complexes with 6,6´-dimethyl substituted ligands.

	λ_{max} / nm ($\varepsilon \cdot 10^3$ / M^{-1} cm^{-1})	Solvent
[Cu(**L2**)$_2$][PF$_6$]	261 (48.0), 289 (sh), 332 (16.0), 421 (3.3), 572 (2.2)	CHCl$_3$
[Cu(**L5**)$_2$][PF$_6$]	271 (100.0), 337 (27.0), 434 (6.0), 589 (4.3)	CHCl$_3$

[Cu(H$_2$**L6**)$_2$]Cl *	271 (192.0), 325 (37.0), 435 (1.5), 590 (0.9)	DMSO
[Cu(**L16**)$_2$][PF$_6$]	244 (35.0), 282 (sh), 313 (48.0), 432 (4.0), 587 (2.4)	CHCl$_3$
Na$_3$[Cu(**L17**)$_2$]	296 (10.0), 343 (11.0), 437 (2.0), 608 (1.17)	H$_2$O
[Cu(**L18**)$_2$][PF$_6$]	300 (12.0), 350 (16.0), 441 (3.0), 610 (2.0)	CH$_2$Cl$_2$
[Cu(**L21**)$_2$][PF$_6$]	244 (88.0), 348 (23.0), 420 (10.0), 615 (4.0)	CH$_2$Cl$_2$
[Cu(H$_2$**L22**)$_2$]Cl *	261 (100.0), 339 (20.0), 462 (1.7), 630 (1.0)	DMSO
[Cu(H$_2$**L25**)$_2$]Cl	268 (57.0), 344 (24.0), 358 (sh), 553 (4.0)	MeOH :DMSO 9 :1
[Cu(**L26**)$_2$][PF$_6$]	272 (50.0), 343 (26.0), 581 (1.1)	DMSO

Table 2. Charge transfer absorption data of the Cu(I) complexes with 6,6´-diphenyl substituted ligands. The * signifies that the complex is not stable over the time in the solvent used for the measurement.

The chemical nature, size and position of the substituents is also important when looking at the spectral intensities. These are strictly related to the symmetry of the complex that, in its turn, is affected by the distortion from the tetrahedral geometry. As a general trend, it can be deduced from tables 1 and 2 that the extended delocalization of the π-electrons of the bipyridine moiety by the introduction of phenyl rings in the 6 and 6´-positions or as spacers in the 4 and 4´-positions, and a double bond as well as spacer in the 4 and 4´-positions, increases the extinction coefficients of the MLCT bands. This phenomenon is summarised in figure 77:

λ_{max} / nm (ε / M^{-1} cm^{-1})

L11 — 495 (500)

L18 — 441 (3000), 610 (2000)

L3 — 488 (4300)

L5 — 434 (6000), 589 (4300)

L14 — 508 (4000)

L21 — 420 (10000), 615 (4000)
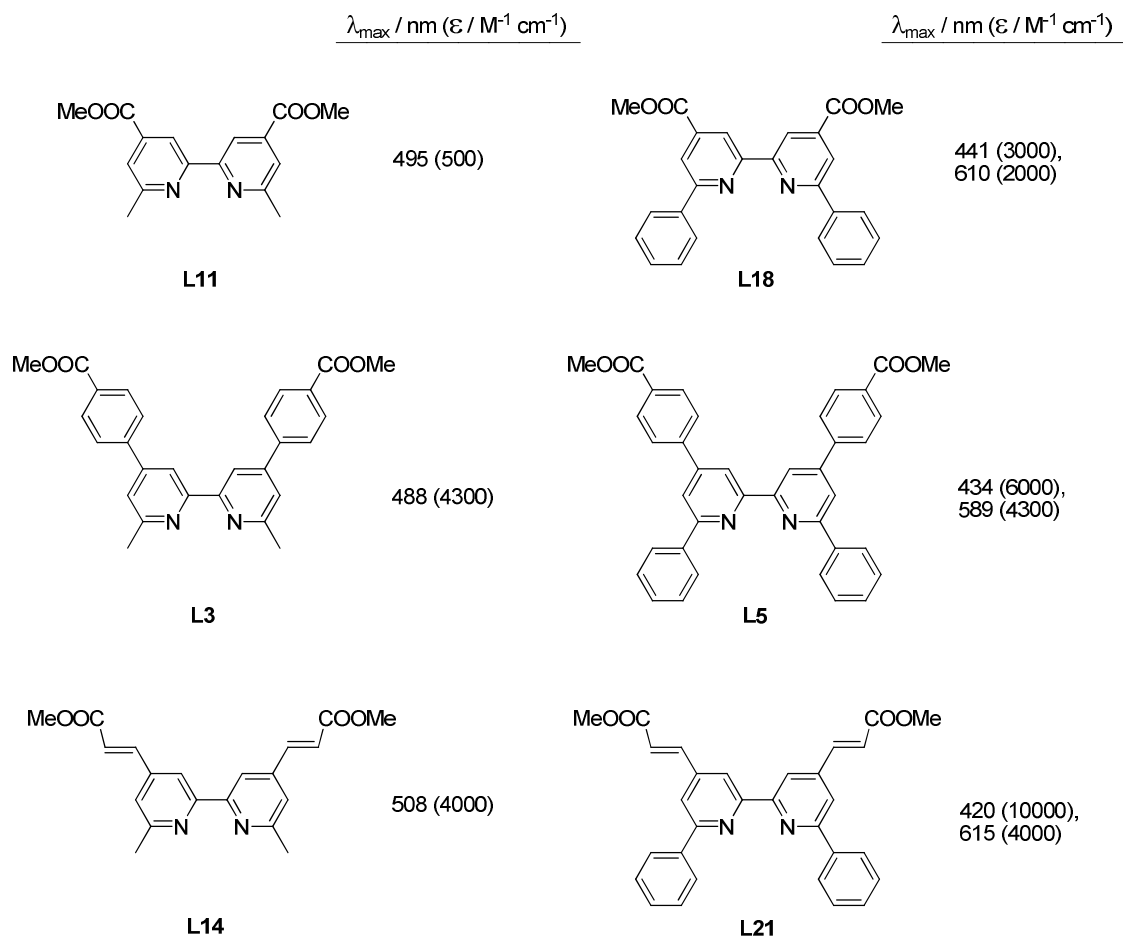
Fig. 77. Selected ligands with MLCT absorption maxima and molar absorption coefficients (ε) of the corresponding Cu(I) complexes.

The electrochemical properties of the complexes were explored by cyclic voltammetry and differential pulse voltammetry. In tables 3 and 4, the $Cu^{2+/+}$ reduction potentials of the two groups of complexes are shown, respectively.

As already mentioned in this chapter, substituent groups in the ortho positions with respect to the nitrogen atoms in the ligands have an important impact on the stability of the copper systems. For example, the presence of alkyl substituents, even though their electron donating tendency, elevate the $Cu^{2+/+}$ reduction potential of the complexes [116, 177]. Thus, it is easier (> 400 mV) to oxidize $[Cu(phen)_2]^+$ than $[Cu(dmphen)_2]^+$ in aqueous electrolyte [178]. The increased oxidation potential observed for the complexes with substituted ligands cannot be explained by

inductive substituent effects of the ligands. Rather, it is a result of steric interactions between the two chelating moieties.

A range of values for the $Cu^{2+/+}$ reduction potentials between 0.07 and 0.59 V vs. Fc/Fc^+ is observed, corresponding these values to measurements where CH_2Cl_2, MeOH or CH_3CN were used as solvents. In the cases where DMSO was employed, mostly in complexes with ligands bearing acid groups, the $Cu^{2+/+}$ reduction potentials appear at negative values with respect to Fc/Fc^+, probably due to solvent coordination to the oxidized complex. In complexes $[Cu(H_2L4)_2]Cl$ and $[Cu(H_2L15)_2]Cl$ the peak-to-peak separation, ΔE_p, is 147 and 186 mV, respectively, which are within the range of 100-200 mV observed in systems where there are no pronounced structural changes during the Cu(I)/Cu(II) redox process [160, 175]. However, in the complexes that are not stable in DMSO solution, $[Cu(H_2L6)_2]Cl$, $[Cu(H_2L17)_2]Cl$ and $[Cu(H_2L22)_2]Cl$, the ΔE_p values are bigger, being 434 mV for $[Cu(H_2L22)_2]Cl$, so this probably gives a measure of the structural reorganization that takes place, before and during the electrochemical conversion processes.

	$E°/V$ Cu^{II}/Cu^{I}	Solvent
$[Cu(L1)_2][PF_6]$	+ 0.07 (rev.)	CH_2Cl_2
$[Cu(L3)_2][PF_6]$	+ 0.45 (rev.)	CH_2Cl_2
$[Cu(H_2L4)_2]Cl$	– 0.14 (rev.)	DMSO
$[Cu(H_2L8)_2]Cl$	+ 0.53 (quasirev.)	MeOH
$[Cu(L9)_2][PF_6]$	+ 0.29 (rev.)	CH_3CN
$[Cu(H_2L10)_2]Cl$	+ 0.42 (quasirev.)	MeOH
$[Cu(L11)_2][PF_6]$	+ 0.59 (quasirev.)	CH_2Cl_2
$[Cu(L14)_2][PF_6]$	+ 0.33 (rev.)	CH_3CN
$[Cu(H_2L15)_2]Cl$	– 0.12 (rev.)	DMSO
$[Cu(L23)_2][PF_6]$	-	-

	E°/V Cu^{II}/Cu^{I}	Solvent
[Cu(**H$_4$L24**)$_2$]Cl	-	-

Table 3. Half-wave potentials of the Cu(II)/Cu(I) couples in the complexes with 6,6´-dimethyl substituted ligands. These potentials are given vs. ferrocene-ferrocenium.

	E°/V Cu^{II}/Cu^{I}	Solvent
[Cu(**L2**)$_2$][PF$_6$]	+ 0.36 (rev.)	CH$_2$Cl$_2$
[Cu(**L5**)$_2$][PF$_6$]	+ 0.40 (rev.)	CH$_2$Cl$_2$
[Cu(**H$_2$L6**)$_2$]Cl	– 0.05 (quasirev.)	DMSO
[Cu(**L16**)$_2$][PF$_6$]	+ 0.27 (rev.)	CH$_3$CN
Na$_3$[Cu(**L17**)$_2$]	0.00 (rev.)	H$_2$O
[Cu(**L18**)$_2$][PF$_6$]	+ 0.59 (rev.)	CH$_2$Cl$_2$
[Cu(**L21**)$_2$][PF$_6$]	+ 0.44 (rev.)	CH$_2$Cl$_2$
[Cu(**H$_2$L22**)$_2$]Cl	– 0.10 (quasirev.)	DMSO
[Cu(**H$_2$L25**)$_2$]Cl	– 0.18 (rev.)	DMSO
[Cu(**L26**)$_2$][PF$_6$]	– 0.38 (rev.)	DMSO

Table 4. Half-wave potentials of the Cu(II)/Cu(I) couples in the complexes with 6,6´-diphenyl substituted ligands. These potentials are given vs. ferrocene-ferrocenium.

IV. 2   Crystal structures of copper(I) 2,2´-bipyridine complexes

IV. 2. 1   [Cu(L1)$_2$][PF$_6$]·2CHCl$_3$

X-ray quality crystals of [Cu(**L1**)$_2$][PF$_6$]·2CHCl$_3$ readily formed from a chloroform solution of the compound. [Cu(**L1**)$_2$][PF$_6$]·2CHCl$_3$ crystallizes in the monoclinic system, space group *C*2/*c* (No.15). The asymmetric unit contains a copper(I) cation coordinated by two ligand moieties, a

PF_6^- counterion and two chloroform molecules. The latter are disordered; one of the chloroform molecules may be described as two half molecules with a factor of occupancy of 0.5 each, while the second molecule is best modelled by assuming that in the asymmetric unit there are 4 crystallographic positions available for 3 chlorine atoms.

The homoleptic Cu(I)-bisbipyridine unit presents an almost ideal tetrahedral geometry being the dihedral angle, θ (defined by the planes formed between each set of bipyridyl nitrogens and the copper centre) 84.8(4)°. The structure of the ligand, **L1**, was already discussed in section II. 2. 3, however, in contrast to the free ligand, a cisoid conformation is observed here, due to coordination to copper(I) (see figure 78). The 2,2´-bipyridine is tetrasubstituted, having phenyl groups attached to the 4 and 4´- positions and methyl groups at the 6 and 6´-positions. The Cu-N bond lengths have values of: N1–Cu1, 2.011(2) Å; N2–Cu1, 2.053(2) Å; N3–Cu1, 2.040(3) Å and N4–Cu1, 2.011(2) Å. From these distances one can observe that the Cu-N distances for the two nitrogen atoms of the same ligand are not equal, a phenomenon also observed in the crystal structure of the parent [Cu(dmbpy)$_2$][BF$_4$] (dmbpy stands for 6,6´-dimethyl-2,2´-bipyridine), where the Cu-N distances vary between 2.018 and 2.052 Å [154].
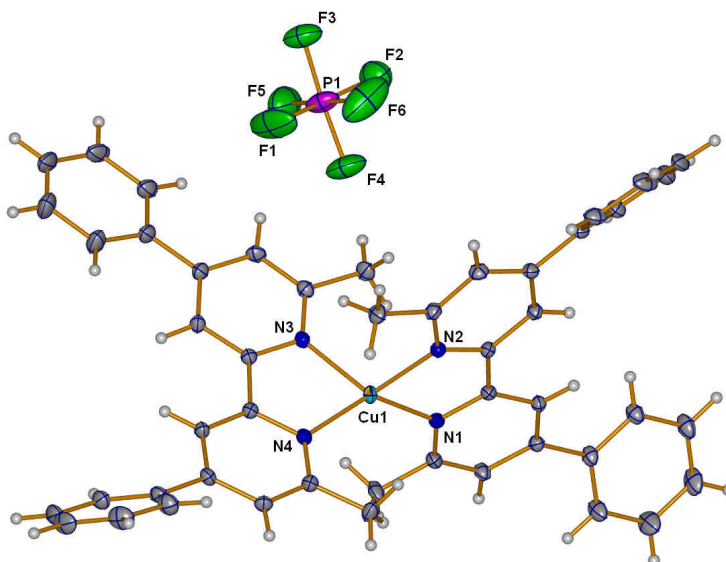
Fig. 78. View of [Cu(**L1**)$_2$][PF$_6$] in the asymmetric unit. Disordered solvent molecules are not shown for clarity. Ellipsoids are plotted at the 30% level.

105

The phenyl groups are not co-planar with the bipy system: the torsion angles in py-N1 and py-N2 are 26.4(5)º (C10–C5–C4–C11) and 35.4(8)º (C21–C16–C15–C22), respectively, and in py-N3 and py-N4 the values of the torsion angles are 16.2(9)º (C30–C29–C28–C27) and 43.5(8)º (C45–C40–C39–C46), respectively.

Aromatic interactions are formed between bipy moieties of two different complexes (centroid to centroid distance: 3.851(2) Å (symmetry code i = 1-x, 1-y, 1-z)) and between phenyl and pyridine groups from different complexes as well (centroid to centroid distance: 3.912(2) Å (symmetry code ii = 1/2-x, 1/2-y, 1-z)) (see figure 79). Assuming that π⋯π interactions held the molecules together, the overall motif in this crystal structure may be described as 1D chains in the [280, -24, -60] plane. At the same time, these chains are connected by weak hydrogen bonds formed between fluorine atoms of the counterion molecules and hydrogen atoms available from the aromatic rings and from one methyl group (C27–H271⋯F1 2.43 Å; C30–H301⋯F1 2.51 Å; C48–H481⋯F6[iii] 2.46 Å, (symmetry code iii = x, 1-y, -1/2+z) and C49–H491⋯F4 2.33 Å).
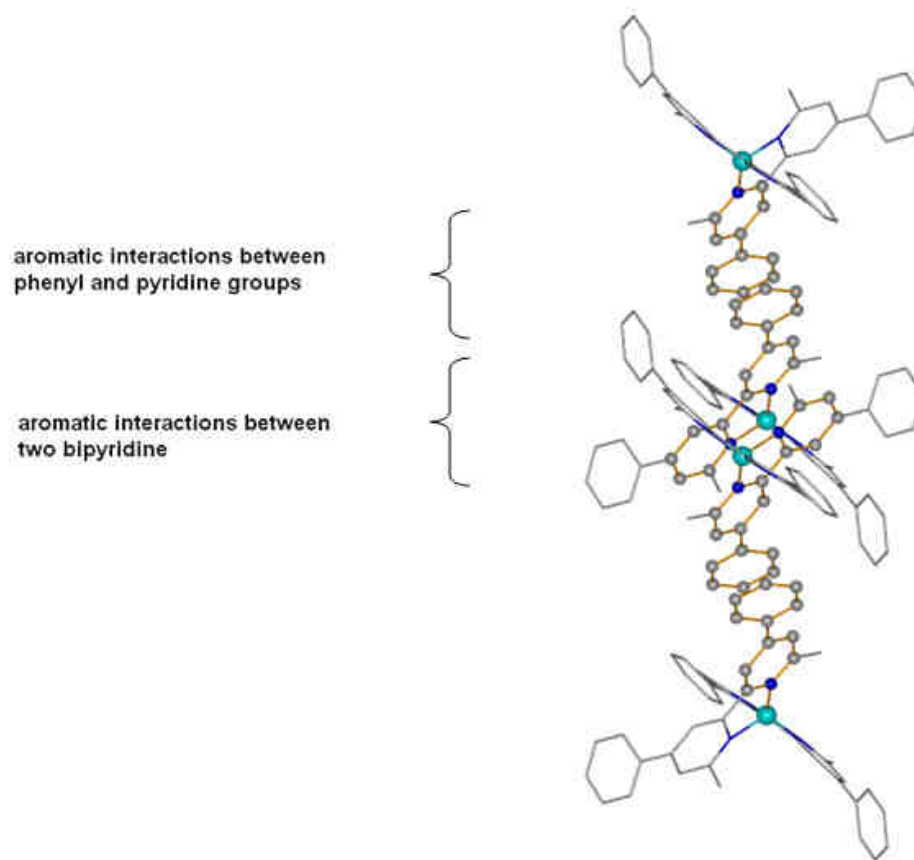
Fig. 79. View of $[Cu(\textbf{L1})_2]^+$ units along the *a* direction. Aromatic interactions are symbolized using ball and stick representation.

IV. 2. 2   2{[Cu(L2)₂][PF₆]}·Et₂O

Single crystals suitable for X-ray diffraction were obtained after slow diffusion of Et_2O into a $CHCl_3$ solution of $[Cu(\textbf{L2})_2][PF_6]$. $2\{[Cu(\textbf{L2})_2][PF_6]\}\cdot Et_2O$ crystallizes in the triclinic system, space group *P*-1 (No.2). The asymmetric unit contains two molecules of **L2** coordinating the Cu(I) atom in a bidentate mode through their nitrogen atoms. Two counterion units are present, one of them with a noticeable disorder (the $P1F_6$ counterion molecule lies in a crystallographic special position x/a, y/b, z/c; 0.28185(16), 0.46848(14), 0.99985(11)). The second counterion unit possesses atoms heavily disordered with occupancy factors of 50% (P1); 30% (P3, F21, F22, F23, F24, F25 and F26) and 20% (F11, F13 and F15). A molecule of Et_2O co-crystallizes in the

asymmetric unit as well and lies in a crystallographic special position (x/a, y/b, z/c; 0.5641(6), 0.0122(7), 0.8433(5)).

The Cu-N bond distances are: N1–Cu1 2.015(2) Å, N2–Cu1 2.034(2) Å, N3–Cu1 2.008(2) Å and N4–Cu1 2.041(2) Å. These bond lengths are contained in a much smaller range than the Cu-N bonds in the parent complex [Cu(dpbpy)$_2$][BF$_4$] (dpbpy stands for 6,6´-diphenyl-2,2´-bipyridine) (2.001-2.187 Å) [156]. The dihedral angle, θ, has a value of 73.4(2)°, so the planes formed by each bipy system with the Cu(I) atom are far from being orthogonal. However, this value is contained in the typically observed θ range of 70-80° in copper complexes of substituted bipyridines and phenanthrolines [154, 155, 171-173]. The pyridine rings are slightly twisted one with respect to the other in both bipy systems, being this twist more obvious in the unit containing the N3 and N4 atoms than in the system containing the N1 and N2 atoms: torsion angles 13.9(2)° for N3–C45–C46–N4 and 11.0(0)° for N1–C11–C12–N2.

L2, as already discussed in section II. 2. 4, bears phenyl substituents in the 4, 4´, 6 and 6´-positions, although in the structure discussed here the bipyridine moiety is found in its *cis*-configuration (see figure 80). These aromatic substituents are twisted out of the planes formed by each pyridine ring, being the extent of this bend different in all cases: py-N1: 35.4(2)° C1–C6–C7–N1 and 37.0(3)° C8–C9–C23–C24; py-N2: 50.0(3)° C18–C17–C16–N2 and 42.3(4)° C13–C14–C29–C30; py-N3: 37.6(8)° N3–C41–C40–C39 and 38.1(2)° C42–C43–C57–C62; and finally py-N4: 49.4(3)° N4–C50–C51–C52 and 36.8(3)° C49–C48–C63–C64.
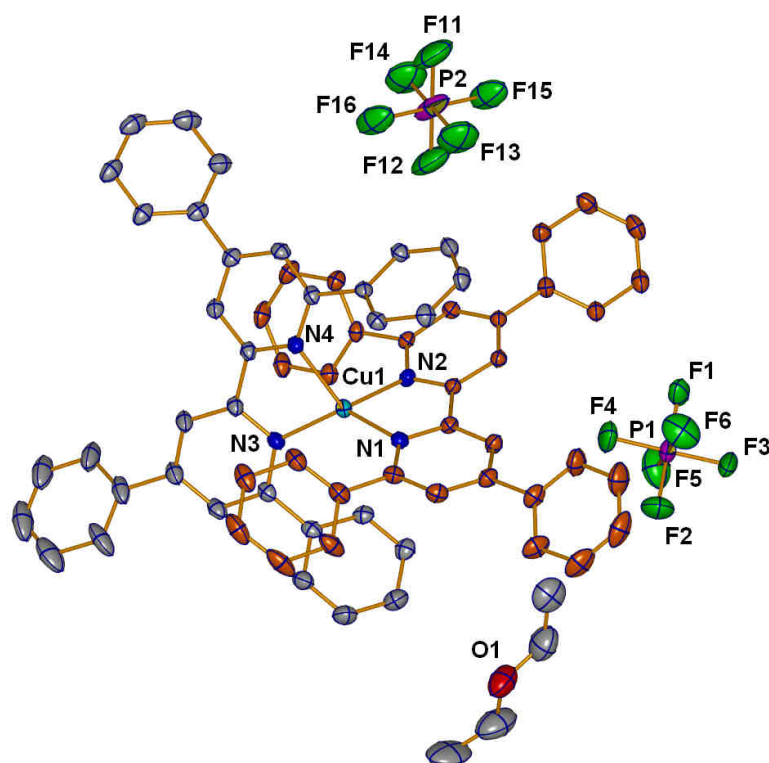
Fig. 80. Asymmetric unit of [Cu(**L2**)$_2$][PF$_6$]·Et$_2$O. The two ligand molecules are represented in different colours (grey and orange) for a clearer view. The copper atom (light blue) is tetracoordinated by nitrogen atoms (blue). A diethylether molecule is present as well as the counterion, which may occupy two different crystallographic positions, being disordered in one of them. Hydrogen atoms have been omitted for clarity.

The reason for these different twist values may be explained by the multiple weak intramolecular π···π interactions present in the structure, which stabilize the complex in the solid state (centroid to centroid distances: ring 1, 3.609(2) Å; ring 2, 3.691(2) Å and ring 3, 4.130(3) Å) (see figure 81). Further π···π interactions favour the packing of molecules in the *a* direction.
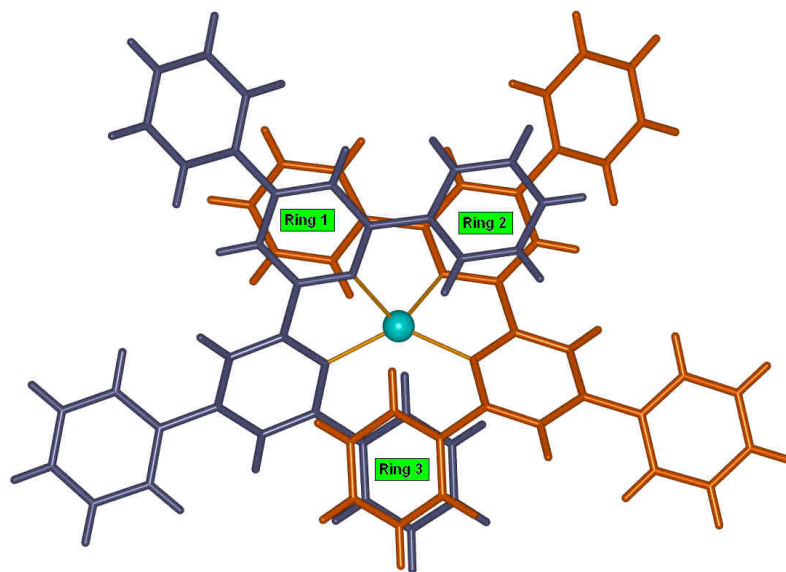
Fig. 81. Schematic representation of the intramolecular $\pi\cdots\pi$ stacking interactions present in $[Cu(\mathbf{L2})_2]^+$.

Along the same direction, the formation of voids in the crystalline structure allows to distinguish some important aspects of the overall supramolecular structure: 1) the molecules are arranged in 2D layers separated by the solvent molecules and the disordered counterion molecules; 2) these layers are forming well defined voids where other counterions are trapped. The formation of these cavities is achieved by the packing of the complexes through aromatic interactions between the rings of the ligands (fig 82).
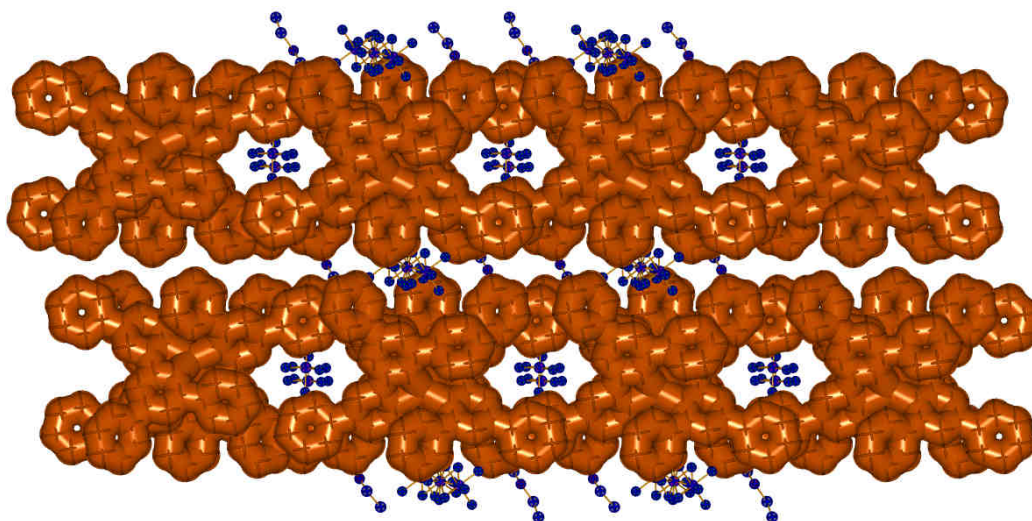
Fig. 82. Schematic representation of the packing structure formed by $[Cu(\textbf{L2})_2][PF_6]\cdot CH_3CH_2OCH_2CH_3$. Some counterion molecules are contained in the voids; disordered counterion molecules and solvent molecules are located between the 2D layers.

The presence of a flexible polyaromatic system in the ligand affords another type of interaction in the solid state, C–H···π (centroid) interactions: C1–H11···π 2.62 Å; C2–H21···π^i 2.83 Å (symmetry code i = -x, 1-y, -z); C31–H311···π^{ii} 2.79 Å; C38–H381···π^{ii} 2.78 Å (symmetry code ii = 1-x, 1-y, 1-z); C39–H391···π 2.72 Å and C67–H671···π^i 2.90 Å.

There are weak hydrogen bonds formed by some of the hydrogen atoms of the aromatic moieties, and they may be classified into two different types of H-bonds: 1) hydrogen bonds that do not extend the dimensionality of the supramolecular array, like for example: C37–H371···O1 2.47 Å; and 2) hydrogen bonds that may increase this dimensionality from 0D to 1D chains, like for example: C10–H101···F4 2.31 Å, C44–H441···F3 2.26 Å and C47–H471···F3 2.51 Å.

IV. 2. 3   2{[Cu(L5)$_2$][PF$_6$]}·2Et$_2$O·CHCl$_3$

Single crystals suitable for X-ray diffraction were grown after slow diffusion of Et$_2$O into a CHCl$_3$ solution of $[Cu(\textbf{L5})_2][PF_6]$. The asymmetric unit of this structure (triclinic system, space

group *P*-1 (No.2)) contains two copper atoms which are tetrahedrally coordinated by two 2,2´-bipyridine derivatives. The ligands contain phenyl groups attached to the 6 and 6´-positions. In the 4 and 4´-positions, however, phenylene spacers separate the bipyridine core from methyl ester groups located in the *para* position of the phenylene ring. As expected, the hexafluorophosphate counterions remain non-coordinating towards the metal cation. Two diethylether molecules co-crystallize together with a chloroform molecule, the latter being structurally disordered.
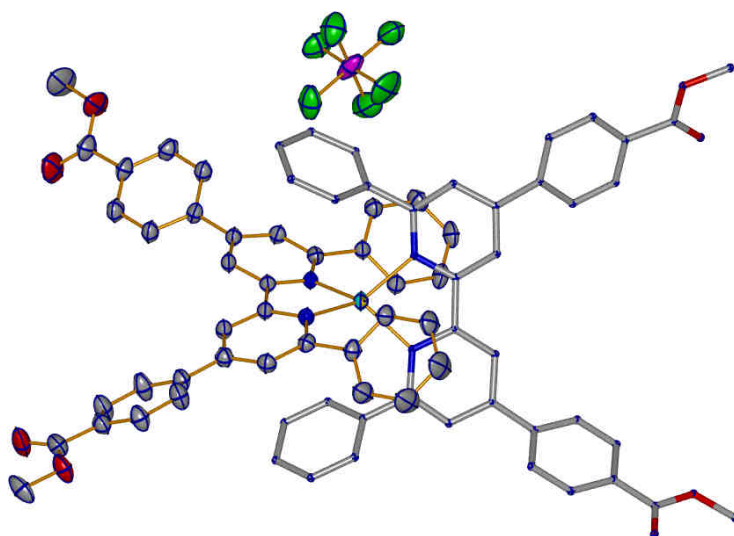
Fig. 83. The two ligands in complex [Cu(**L5**)$_2$][PF$_6$] are represented using different models. The copper atom is represented in light blue and is coordinated by four nitrogen atoms. The counterion remains non-coordinating. Solvent molecules and hydrogen atoms have been omitted for clarity.

The dihedral angles, θ, are 69.0(2)° and 71.4(6)° for the complexes bearing the Cu1 and the Cu2 atoms, respectively. These values are far from the ideal perpendicular value, and are out or in the edge of the typically observed 70-80°, respectively.

N–Cu distances are: N1–Cu1 2.028(2) Å; and N2–Cu1 2.0302(19) Å, N3–Cu1 2.0276(19) Å and N4–Cu1 2.036(2) Å, and N5-Cu2 2.0393(19) Å, N6-Cu2 2.031(2) Å, N7-Cu(2) 2.032(2) Å and N8-Cu2 2.023(2) Å. The Cu-N bond lengths are similar, in contrast to the observations discussed for [Cu(**L2**)$_2$][PF$_6$]. The molecule is thus, regarding the N-C bond distances, more symmetrical. The first consequence of this fact is that the packing structure is now more suitable for

intramolecular $\pi\cdots\pi$ interactions. Whereas in complex $[Cu(\mathbf{L2})_2][PF_6]$ three rings of each ligand are involved in this kind of interactions, in complex $[Cu(\mathbf{L5})_2][PF_6]$ all four aromatic rings around the copper atom (two from the bipy core and the two phenyl substituents in the 6 and 6´-positions) are involved in aromatic interactions (see figure 84), what might be the reason for the strong deviation of the complexes from the ideal tetrahedral geometry.
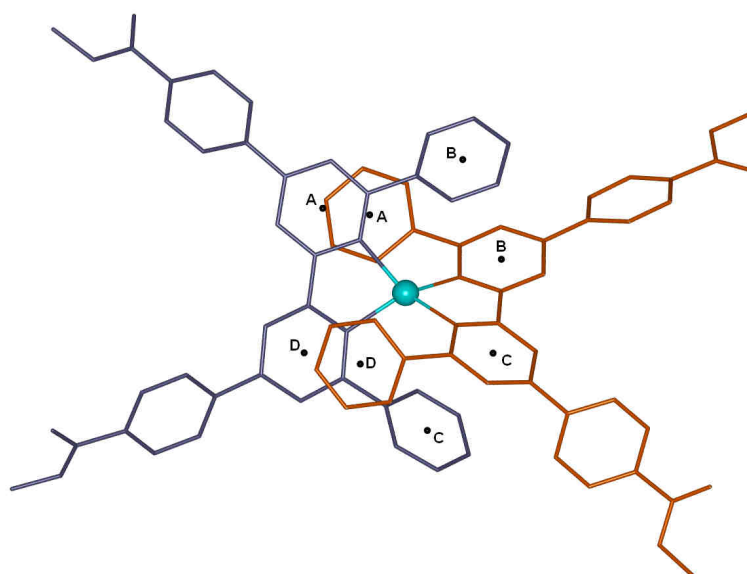
Fig. 84. Schematic representation of the four intra- $\pi\cdots\pi$ stacking interactions present in $[Cu(\mathbf{L5})_2]^+$ (centroid to centroid distances: A$\cdots$A 3.655 Å, B$\cdots$B 3.656 Å, C$\cdots$C 3.729 Å and D$\cdots$D 3.728 Å).

Further $\pi\cdots\pi$ and C–H$\cdots\pi$ interactions are present in the crystal and they are responsible for the stacked packing between different molecules observed along the *c* axis. The potential formation of hydrogen bonds is increased through the presence of the PF_6^- counterions and oxygen atoms from the ester groups (see table 5). These weak interactions increase the dimensionality from 2D to 3D in the final supramolecular array.

Donor–H⋯Aceptor	H⋯A (Å)	D–H⋯A (°)
C107–H1071⋯O8 $^{x,1+y,z}$	3.349(3)	166
C109–H1091⋯F2 $^{1-x,1-y,1-z}$	3.470(5)	175
C124–H1241⋯F26	3.407(3)	176
C136–H1361⋯O97 $^{1-x,1-y,1-z}$	3.377(12)	170
C4–H41⋯O14 $^{x,-1+y,z}$	3.356(3)	177
C45–H451⋯O12 $^{x,1+y,z}$	3.267(3)	167
C56–H561⋯F24	3.420(3)	177
C74–H741⋯O83 $^{x,-1+y,z}$	3.281(4)	174
C75–H751⋯Cl93 $^{-x,1-y,2-z}$	3.752(5)	163

Table 5. Hydrogen bond lengths and direction in the packing structure of [Cu(**L5**)$_2$][PF$_6$] molecules.

IV. 2. 4   4[Cu(H$_2$**L8**)(H**L8**)]·3H$_2$O

Crystals of 4[Cu(H$_2$**L8**)(H**L8**)]·3H$_2$O (monoclinic system, space group *C*2/*c* (No.15)) grew from a methanol solution of [Cu(H$_2$**L8**)$_2$]Cl that had been standing at room temperature for several weeks. The copper(I) centre is in the expected pseudo-tetrahedral environment, the angle between the least squares planes of the two bpy units being 84.49(7)°. N–Cu distances are slightly larger than in the previous structures: N1–Cu1 2.036(2) Å, N2–Cu1 2.049(2) Å, N3–Cu1 2.0552 Å and N4–Cu1 2.043(2) Å. The molecular structure is shown in figure 85.
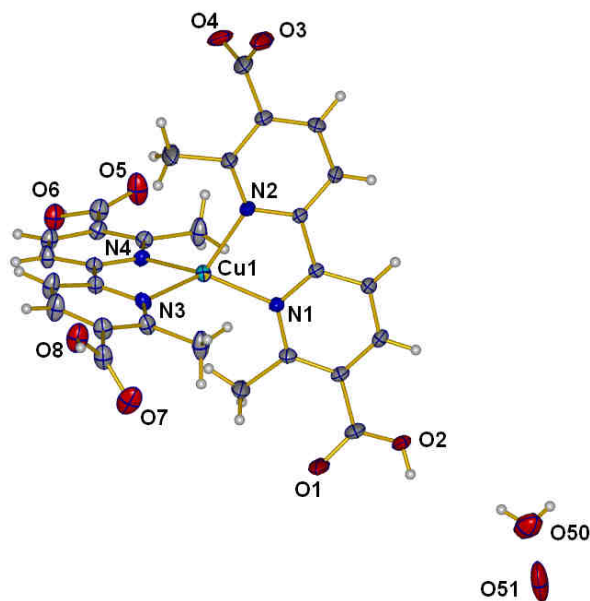
Fig. 85. Asymmetric unit of [Cu(H$_2$**L8**)(H**L8**)]. Ellipsoids are plotted at the 30% level.

The disordering leads to large esds, but the bond distances are consistent with the protonation states shown in the figure. The fully protonated ligand is ordered, while the CO$_2$H and CO$_2$ units of the second ligand are disordered and have been modelled (each with the CO$_2$ units constrained to being planar) over two sites, each with equal occupancy (50%).

The compound crystallizes as a hydrate, and one water molecule resides on a two-fold axis. The packing of [Cu(H$_2$**L8**)(H**L8**)] molecules is worthy of note and involves both π-stacking between bipy domains (see figure 86 *Domain 1*) and extensive hydrogen bonding between carboxylate and carboxylic acid groups (see figure 86 *Domain 2*). The bipy unit containing N1 and N2 stacks over that containing N3 and N4 of an adjacent molecule (*x*, 1–*y*, 1/2+*z*) (see figure 86 *Domain 1*). The stacking is not ideal, and while the bipy units overlap effectively, their planes are not parallel. The distance from the centroids of the rings containing N1 and N2 to the least squares plane through the adjacent bipy unit with N3 and N4 are 3.24 and 3.47 Å, respectively. In contrast, for the N3/N4 bipy unit, only the ring containing N3 is involved in significant π-stacking. The π-stacked interactions operate in orthogonal directions to produce a network that is reinforced by hydrogen bonding between carboxylates and carboxylic acids (see figure 86 *Domain 2*). Every CO$_2$ – and/or CO$_2$H group is involved, as well as the water molecules,

resulting in a rigid network (O2–H2···O7^i 1.64 Å (symmetry code i = -1/2+x, 1/2-y, -1/2+z); O6–H6···O8^{ii} 1.80 Å; O8–H8···O6^{ii} 1.77 Å (symmetry code ii = -1/2+x, 1/2+y, z); O50–H50···O5^{iii} 2.10 Å (symmetry code iii = x, 1-y, -1/2+z) and C1–H284···O40^{iv} 2.24 Å (symmetry code iv = 1/2-x, -1/2+y, 3/2-z)).
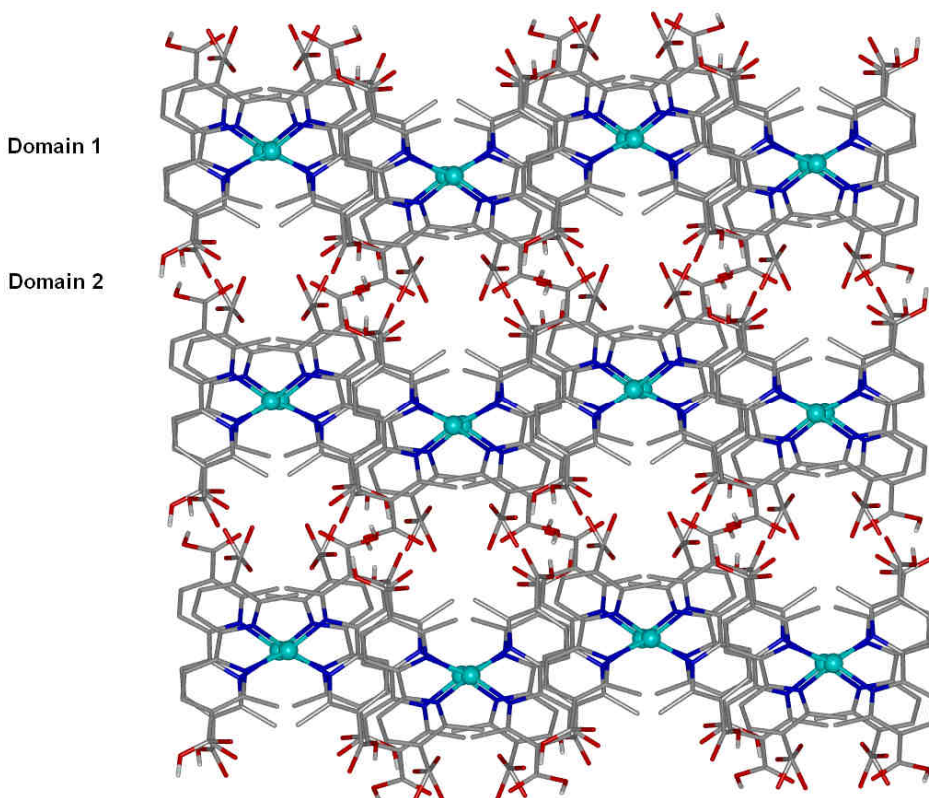
Fig. 86. Wireframe model representation of [Cu(H$_2$**L8**)(H**L8**)]. View along the *a* axis. Solvent molecules have been omitted for clarity.

IV. 2. 5 [Cu(L9)$_2$][PF$_6$]

Crystals of [Cu(**L9**)$_2$][PF$_6$] suitable for X-ray analysis were grown by slow diffusion of Et$_2$O into a CHCl$_3$ solution of the complex. The complex crystallizes in the triclinic system, space group *P*-1 (No.2). The cation consists of a copper(I) atom coordinated by two **L9** ligands that, as discussed in II. 2. 6, consist of a 2,2´-bipyridine ligand with furan rings in the 4 and 4´-positions and methyl groups attached to the 6 and 6´-positions. As usual when coordinating a metal, the bipy unit is found in a *cis*-configuration (see figure 87). The dihedral angle, θ, of the complex is

82.4(4)°, and the cation therefore has a pseudotetrahedral geometry. The C-N bond lengths are: N1–Cu1 2.0241(16); N2–Cu1 2.0113(15) Å; N3–Cu1 1.9995(15) Å and N4–Cu1 2.0256(14) Å. The furan groups are co-planar with the pyridine rings with the exception of the furan-py-N2 system, where the furan ring is slightly twisted 14.1(3)° (C10–C9–C29–O2). The furan rings in the py-N3 and py-N4 system are disordered by rotation at 180°.
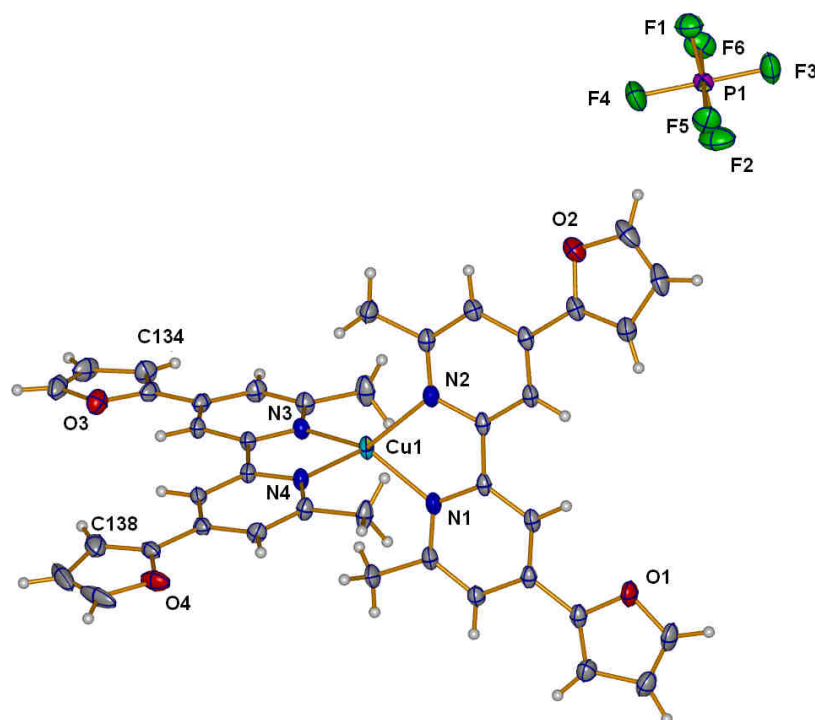
Fig. 87. Asymmetric unit of [Cu(**L9**)$_2$][PF$_6$]. The oxygen atoms O3 and O4 share a 50% occupancy factor with the carbon atoms C134 and C138, respectively. Ellipsoids are plotted at the 30% level.

The packing along the *a* direction allows the molecules to interact through a variety of aromatic-aromatic interactions like furan···furan and furan···pyridine (centroid to centroid distances: 3.8030(14) Å (symmetry code i = 1-x, -y, 1-z), 3.7117(16) Å (symmetry code ii = 1+x, y, z), 3.7209(13) Å (symmetry code iii = 2-x, -y, -z), 3.7118(16) Å (symmetry code iv = -1+x, y, z), 3.5923(15) Å (symmetry code v = 1-x, 1-y, -z) and 3.7209(13) Å (symmetry code iii = 2-x, -y, -z)) (see figure 88).
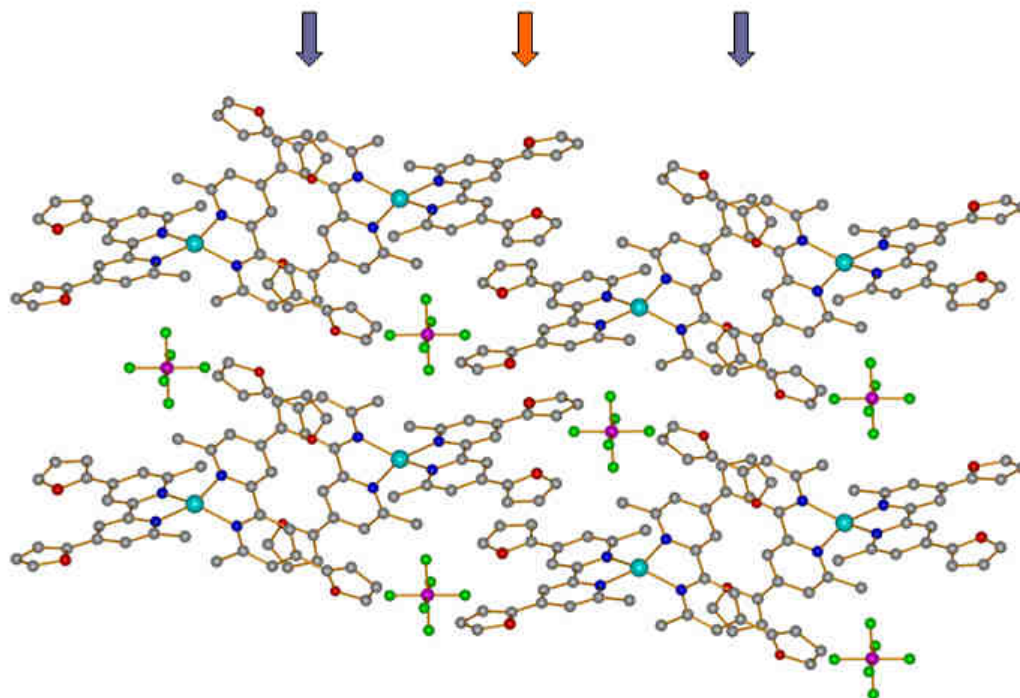
Fig. 88. View along the *a* axis showing the aromatic interactions present in the crystal structure of [Cu(**L9**)$_2$][PF$_6$]. Blue arrows indicate pyridine-furan stacking, while furan-furan stacking interactions are indicated by an orange arrow. Hydrogen atoms have not been represented for clarity.

Other interactions like C–H⋯π (centroid) (C24–H242⋯π^{vi} 2.95 Å (symmetry code vi = x, y, z)) and hydrogen bonds are present (C24–H241⋯F1^{vii} 2.44 Å (symmetry code vii = 1-x, 1-y, 1-z); C26–H261⋯F4^i 2.43 (symmetry code i = 1-x, -y, 1-z)) and stabilize the crystal structure.

IV. 2. 6   [Cu(L11)$_2$][PF$_6$]

Single crystals suitable for X-ray diffraction were grown after slow diffusion of Et$_2$O into a CHCl$_3$ solution of [Cu(**L11**)$_2$][PF$_6$]. Complex [Cu(**L11**)$_2$][PF$_6$] crystallizes in the monoclinic system, space group *P*2$_1$/*c* (No. 14). The asymmetric unit contains two molecules of the ligand **L11** coordinating a copper(I) cation, and a hexafluorophosphate counterion.

One of the nitrogen atoms of each ligand appears to coordinate a little more strongly to the cation than the other nitrogen atom, as can be seen by looking at the C-N bond lengths: N1–Cu1

2.009(2) Å, N2–Cu1 2.016(2) Å and N4–Cu1 2.039(2) Å, N5–Cu1 2.002(3) Å. The dihedral angle, θ, is 87.1(5)°, so it is very close to the ideal value of 90°. Each bipy unit, as already seen in section II. 2. 8, has two methyl ester and two methyl groups in the 4 and 4´- and in the 6 and 6´-positions, respectively (see figure 89). The ester groups are all co-planar with the aromatic system with exception of the py-N1 system (O1–C5–C4–C3 16.5(0)°).
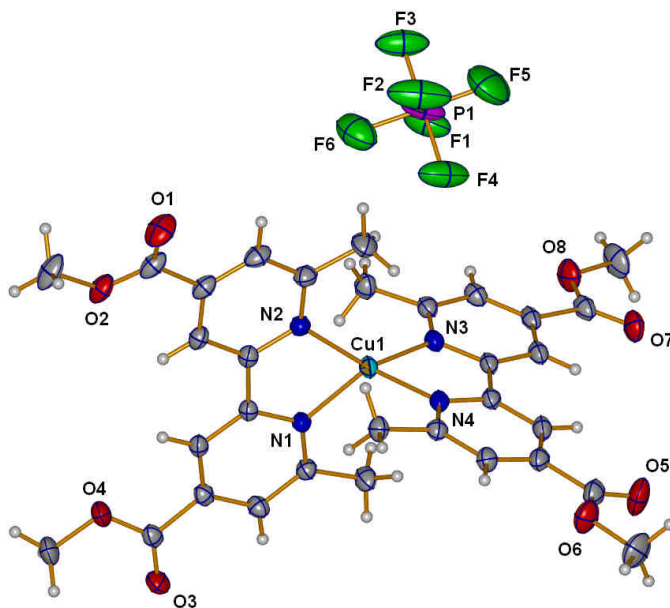
Fig. 89. View of complex [Cu(**L11**)₂][PF₆] in the asymmetric unit. Ellipsoids are plotted at the 30% level.

In this structure, along the *c* axis, the molecules are stacked forming columns stabilized through weak aromatic interactions (centroid-to-centroid distances are: 3.9850(18) Å (symmetry code i = x, 1/2-y, 1/2+z); 4.1484(18) Å (symmetry code i = x, 1/2-y, 1/2+z)). These head-to-tail π··π interactions form a 1D motif, and this motif forms channels were the counterions are located (see figure 90).
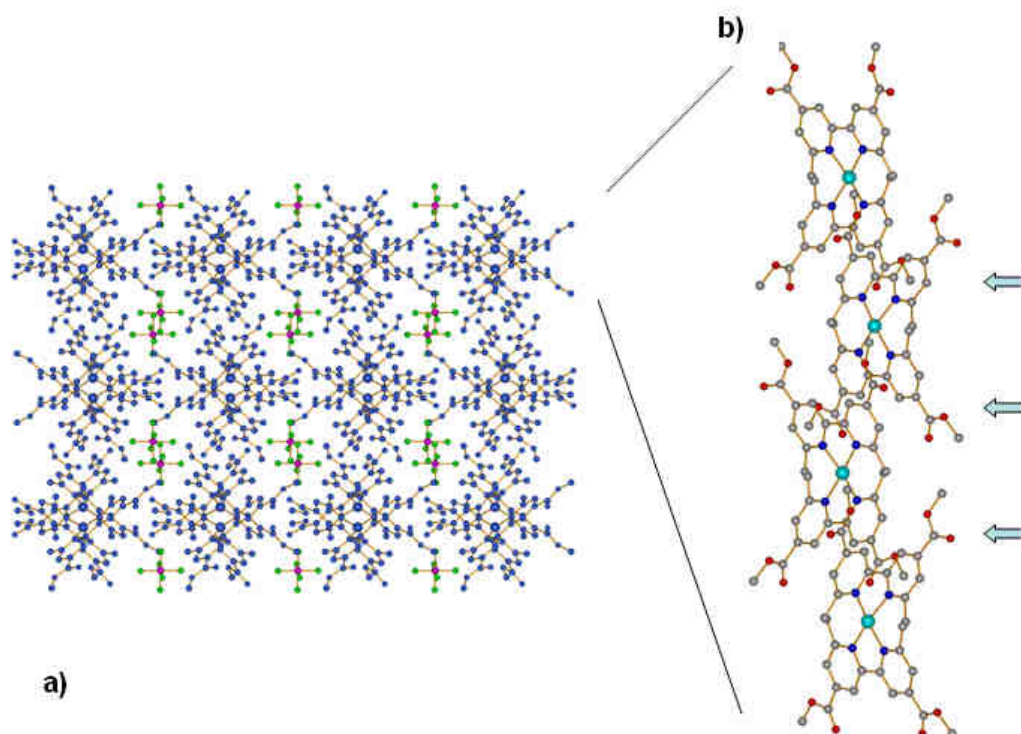
Fig. 90. a) View along the *c* direction showing the channels where the counterion molecules are located; b) view along the *a* axis showing the aromatic interactions between different molecules (arrows). Hydrogen atoms have been omitted for clarity.

The counterion molecules form weak hydrogen bonds with hydrogen atoms of the ligands (C1–H11···F1 2.39 Å; C1–H11···F6 2.39 Å; C13–H131···O5[ii] 2.32 Å (symmetry code ii = x, y, 1+z); C16–H161···F1[iii] 2.45 Å (symmetry code iii = 1-x, -1/2+y, 1/2-z); C17–H171···F3[iv] 2.44 Å (symmetry code iv = 2-x, -1/2+y, 1/2-z); C17–H173···O3[v] 2.45 Å (symmetry code v = 1-x, -y, 1-z); C29–H292···F5[vi] 2.42 Å (symmetry code vi = 1-x, 1-y, -z)). Other kind of interactions such as C–H···π (centroid) are present (C16–H163···π[vii] 2.81 Å and C17–H173···π[vii] 2.97 Å (symmetry code vii = x, y, z)) and stabilize further the structure.

IV. 2. 7   Na$_3$[Cu(L17)$_2$]

An attempt to grow crystals of [Cu(H$_2$**L17**)$_2$]Cl by leaving the crude reaction mixture (still containing an excess of NaOH) to stand for several days afforded crystals of medium quality. The system crystallizes in the triclinic system, space group *P*-1 (No.2). The asymmetric unit

shows the presence of $[Cu(\mathbf{L17})_2]^{3-}$ anions (see figure 91) were the carboxylate groups of the ligands are coordinated to sodium cations, some of which are disordered over several positions, and water molecules.
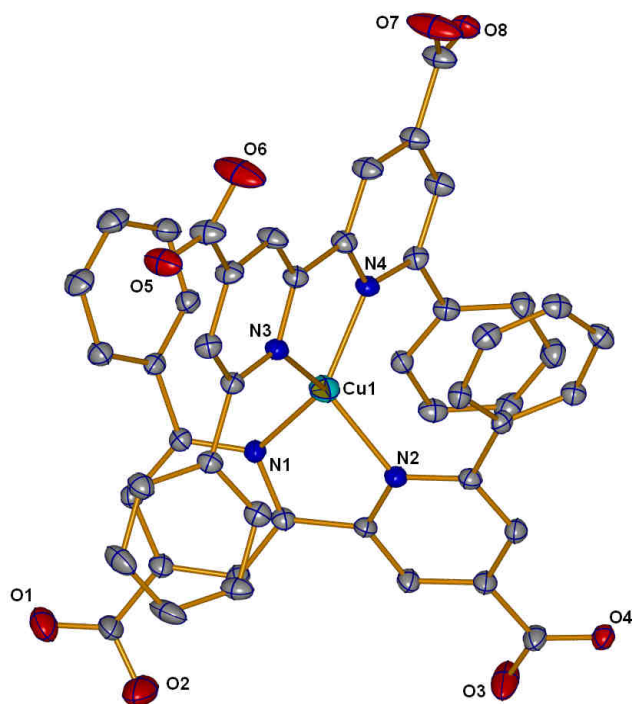
Fig. 91. View of the $[Cu(\mathbf{L17})_2]^{3-}$ anion. Hydrogen, sodium and remaining oxygen atoms from the solvent have been omitted for clarity. Ellipsoids are plotted at the 30% level.

Each ligand possesses carboxylate groups in the 4 and 4'-positions and phenyl groups in the 6 and 6'-positions. The C-N bond distances are: N1–Cu1 2.005(3) Å; N2–Cu1 2.059(3) Å; N3–Cu1 2.062(3) Å and N4–Cu1 1.999(3) Å. The dihedral angle of 72.9(2)° between the N1–Cu1–N2 and the N3–Cu1–N4 planes shows that the structure is strongly deviated from the ideal value of 90° of the tetrahedral geometry. The phenyl groups are twisted with respect to the pyridine rings: 52.5(6)° (C1–C6–C7–N1), 32.9(2)° (C24–C19–C18–N2), 35.1(5)° (C29–C30–C31–N3) and 41.3(6)° (C48–C43–C42–N4). This twisting favors the π-stacking interactions discussed below.

Four very weak π···π interactions are present in each molecule between each pyridine ring and a phenyl substituent of the other ligand (perpendicular distances from centroids to plane: 2.3891(13) Å; 3.3662(14) Å; 3.8399(13) Å and 3.4271(13) Å) (see fig 92 a). The packing along the *b* direction allows further aromatic interactions between different anionic molecules (perpendicular distances from centroid to ring: 3.3213(11) Å and 2.6196(12) Å) (see figure 92 b).
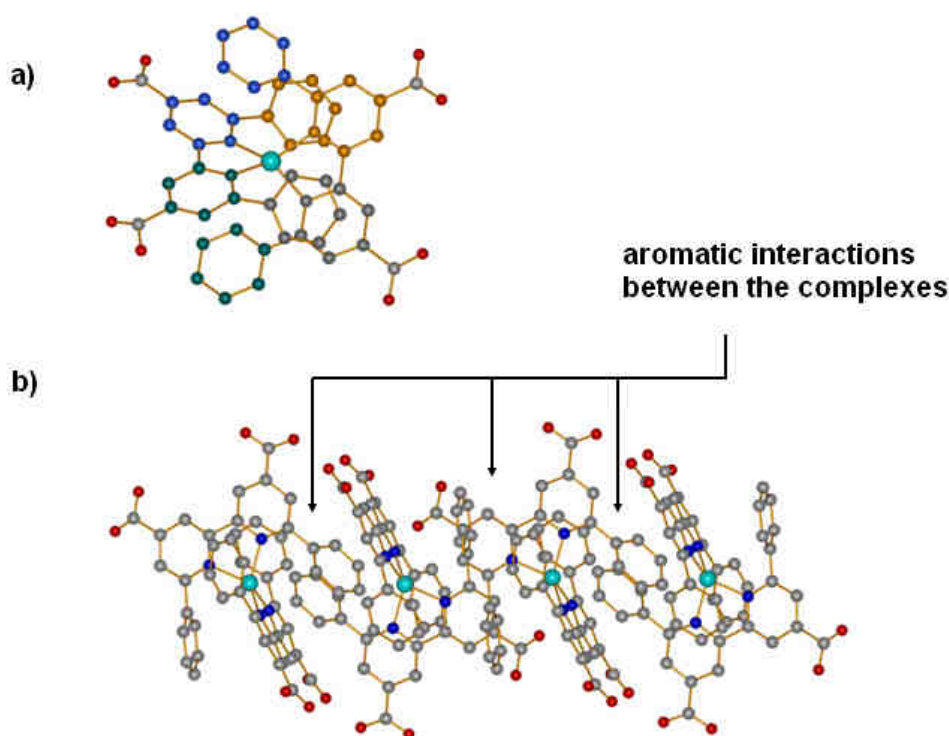
Fig. 92. *a)* Intra-aromatic interactions in $[Cu(\textbf{L17})_2]^{3-}$. The rings with the same colour interact with each other (centroid-to-centroid distances: blue 3.758(2) Å, green 3.938(2) Å, grey 3.944(2) Å and orange 4.063(2) Å); *b)* view along the *a* direction showing the inter-aromatic interactions.

Along the *b* direction, channels are formed, and some oxygen atoms (solvent molecules) are contained in them. Regarding the remaining electronic density found in the structure, it is worth mentioning that five maxima which are located at a distance between 2.2 and 2.5 Å from the oxygen atom of the carboxylate groups were assigned to disordered sodium atoms. The occupancy factors were calculated to afford a value of 1 between the sum of all of them. Other

electronic densities located between 2.2-2.5 Å of these sodium atoms were assigned to coordinated oxygen atoms from the solvent.

Complex anions are further related by hydrogen bonds. These are formed between the oxygen atom from the carboxylate group in the py-N4 moiety and the hydrogen atom from the phenyl group attached to the py-N2 moiety of a close complex (C20–H201⋯O8[i] 2.58 Å (symmetry code i = 1-x, 1-y, 1-z)).

The following atoms are disordered in the crystal structure: O20, Na51, Na52, Na61, Na62, Na63, O2, O51, O52, O53, O60, O61, O62, O91, O92, O93, C51, C52.

Any attempts to grow better quality crystals were unsuccessful.

IV. 2. 8   [Cu(L18)$_2$][PF$_6$]

Single crystals suitable for X-ray diffraction were grown after slow diffusion of Et$_2$O into a CHCl$_3$ solution of [Cu(**L18**)$_2$][PF$_6$]. The complex crystallizes in the monoclinic system, space group $P2_1$ (No.4). The asymmetric unit contains a copper(I) cation coordinated by two ligands **L18**, and a counterion that is disordered.

The ligands that coordinate the metal atom, as already discussed in II. 2. 11, are 2,2´-bipyridines that have methyl ester groups in the 4 and 4´-positions and phenyl groups in the 6 and 6´-positions, presenting the bipy moiety in this structure the typical *cis*-configuration adopted upon coordinating to a metal centre (see figure 93). The nitrogen atoms of the pyridine rings coordinate the copper(I) atom at 2.049(4), 2.034(4), 2.032(2) and 2.029(4) Å (N1–Cu1, N2–Cu1, N3–Cu1 and N4–Cu1, respectively). The geometry of the complex deviates severely from the ideal 90° of the tetrahedral geometry, as the value of the dihedral angle shows: 70.8(2)°. The phenyl groups are all twisted with respect to the pyridine rings to which they are connected (39.6(9)° N1–C1–C11–C12, 39.8(3)° N2–C10–C21–C26, 34.7(5)° N3–C31–C41–C42 and 39.5(3)° N4–C40–C51–C56). The principal reason for this twisting might be the aromatic interactions present in the molecule between phenyl and pyridine groups (perpendicular distance

from centroid to plane: 3.6159(17), 2.9262(15), 2.6595(13) and 3.5137(18) Å). These interactions may also be responsible for the distorted geometry of the complex. C–H···π interactions, although weak, can also be found, occurring between adjacent molecules, (C12–H121···π (centroid) 2.79 Å; C26–H261···π 2.86 Å; C42–H421···π 2.72 Å; C48–H481···π[i] 2.93 Å, (symmetry code i = 1+x, y, 1+z) and C56–H561···π 2.98 Å).
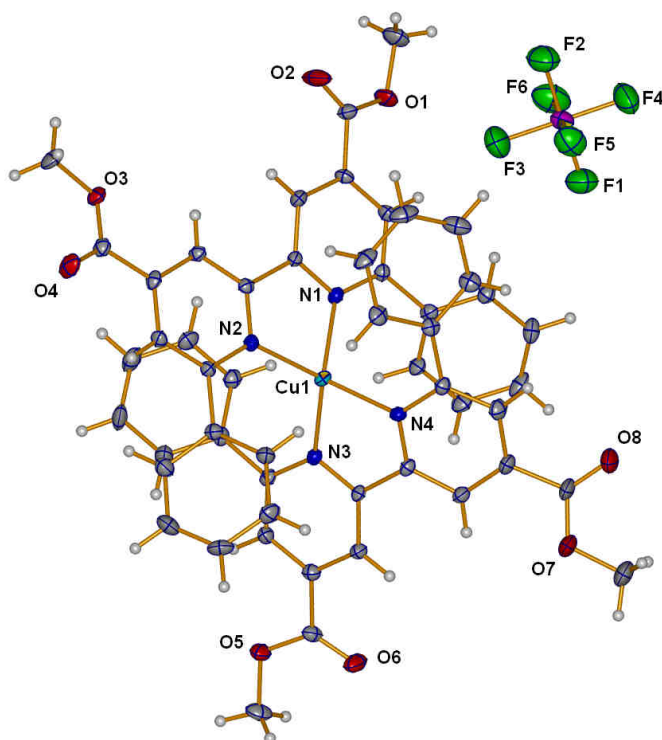
Fig. 93. Asymmetric unit of complex [Cu(**L18**)$_2$][PF$_6$]. Atoms F13, F14, F15 and F16 have not been represented in the picture. Ellipsoids are plotted at the 30% level.

The four ester groups are slightly twisted with respect to the pyridine system to which they are attached (py-N1: 9.9(7)º O2–C17–C3–C4; py-N2: 11.8(9)º O4–C19–C8–C9; py-N3: 15.0(5)º O6–C47–C33–C34 and py-N4: 18.3(5)º O8–C49–C38–C39).
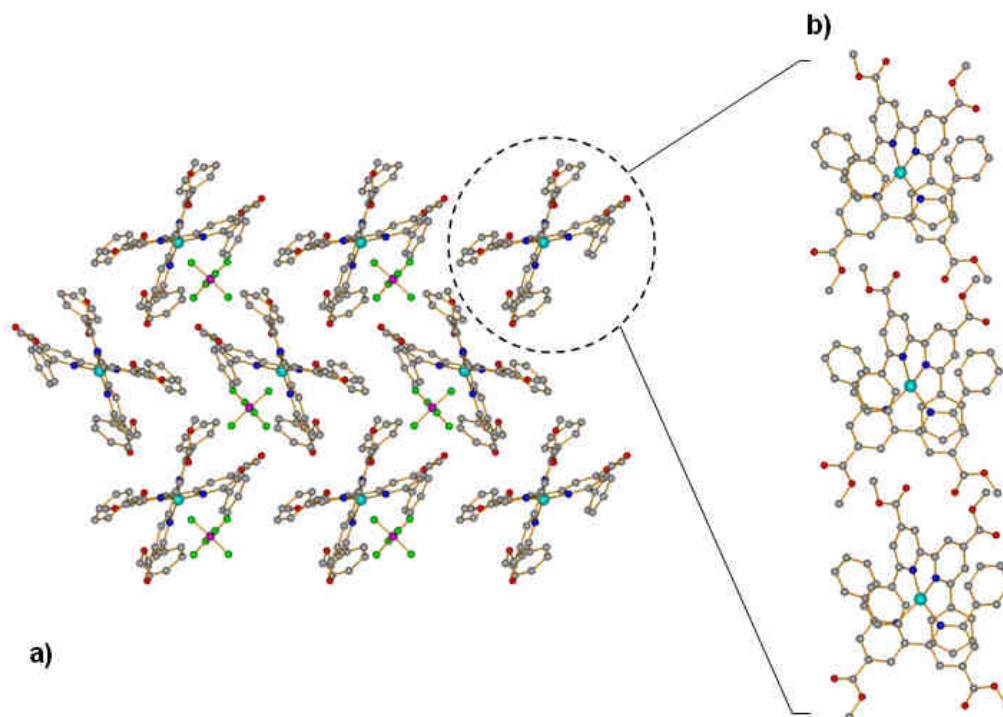
Fig. 94. a) View along the *c* direction showing the packing of the [Cu(**L18**)$_2$]$^+$ cations and the position of the counterion molecules. The latter form hydrogen bonds with close standing molecules; b) view along the [-10.35, 6.95, 0] direction. Inter-aromatic interactions are present in each molecule. Hydrogen atoms have been omitted for clarity.

Hydrogen bonds are formed between: 1) the carbonyl oxygen atom O2 and the hydrogen atom H371 of the py-N4; 2) the carbonyl oxygen atom O6 and the hydrogen atom H71 of the py-N2; and 3) the fluorine atom F2 from the counterion and the hydrogen atom H502 from the methyl group ester group attached to py-N4 (C7–H71···O6^{ii} 2.58 Å (symmetry code ii = x, y, -1+z); C37–H371···O2^{iii} 2.50 Å and C50–H502···F2^{iii} 2.39 Å (symmetry code iii= x, y, 1+z), respectively).

Atoms F3, F4, F5, F6, F13, F14, F15 and F16 are disordered.

IV. 2. 9   Na$_3$[Cu(H$_2$L24)$_2$]·15O

Single crystals were obtained from slow diffusion of ethanol into an aqueous solution of the unpurified complex [Cu(H$_4$**L24**)$_2$]Cl. Complex Na$_3$[Cu(H$_2$**L24**)$_2$] crystallizes in the monoclinic system, space group $P2_1/c$ (No.14). The asymmetric unit contains a copper(I) cation tetrahedrally coordinated by two ligands H$_2$**L24**, both of them doubly deprotonated. The N-C bond distances are: N1–Cu1 2.024(3) Å, N2–Cu1 2.0322 Å, N3–Cu1 2.0213 Å and N4–Cu1 2.024(3) Å. The dihedral angle formed by the N1–Cu1–N2 and N3–Cu1–N4 planes is 86.8(0)º, very close to the ideal value of 90° in tetrahedral geometries. The ligands forming this complex have methyl groups in the 6 and 6´-positions and deprotonated phosphonic acid groups in the 4 and 4´-positions (see figure 95). By looking at the following table, the P–O distances may constitute a piece of evidence that at least one oxygen atom in each group may be deprotonated:

py-N1	py-N2	py-N3	py-N4
P1-O10 1.576(3) Å	P2-O20 1.491(3) Å	P3-O30 1.490(2) Å	P4-O40 1.569(3) Å
P1-O11 1.494(3) Å	P2-O21 1.515(3) Å	P3-O31 1.500(3) Å	P4-O41 1.501(2) Å
P1-O12 1.496(3) Å	P2-O22 1.566(3) Å	P3-O32 1.580(2) Å	P4-O42 1.508(3) Å

Table 6. P-O bond distances in Na$_3$[Cu(H$_2$**L24**)$_2$].

Based on the distances given in table 6, the protonated oxygen atoms are probably O10, O22, O32 and O40 as their longer bond lengths to the respective phosphor atom show. The remaining negative charge on the complex (3-) is neutralized by the presence of sodium atoms in the crystal structure, where some solvent molecules co-crystallize as well.
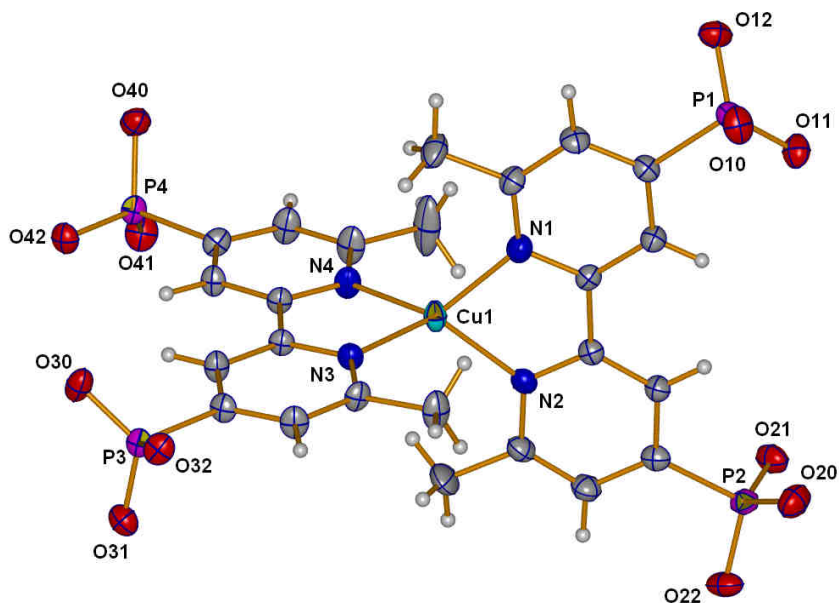
Fig. 95. Crystal structure of the $[Cu(H_2\mathbf{L24})_2]^{3-}$ anion. Na and O atoms, and H atoms from the phosphoric acid groups have been omitted for clarity.

The molecules are packed along the *c* axis. The presence of oxygen atoms in the lattice from the solvent allows the formation of hydrogen bonds with the hydrogen atoms from the pyridine rings (C8–H8A···O81 2.58 Å and C17–H17A···O61 2.46 Å).

The solvent and the sodium cations are forming a 2D-layer-like structure into where the molecules of the complexes are "sandwiched" (see figure 96).
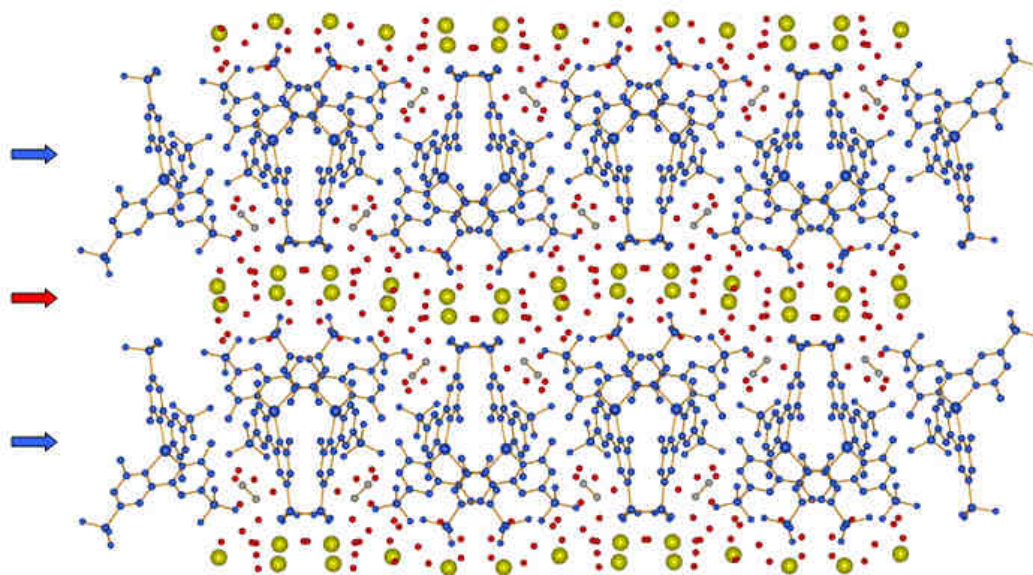
Fig. 96. View along the *c* direction showing the formation of a 2D layer structure between molecules of the complex and sodium and oxygen atoms. The molecules of the complexes are represented in blue, sodium atoms in yellow, oxygen atoms in red and carbon atoms from solvent molecules in grey.

Aromatic interactions are not present in this crystal structure (the closest distance between ring centroids is 4.832(2) Å).

V   Building dye sensitized solar cells (DSSCs)

V. 1   Characteristic parameters of DSSCs

The DSSC technology contains broadly four components: a semiconductor (see section I. 1. 1), a dye or sensitizer (see section I. 1. 2), an electrolyte (see section I. 1. 3) and a conducting substrate (see section I. 1. 4). The total efficiency of the DSSC depends on the optimization and compatibility of each of these constituents.

The solar cell can take the place of a battery in a simple electric circuit (see figure 97). In the dark, the cell in circuit A does nothing. When it is switched on by light it develops a voltage, or electromotive force (e.m.f.), analogous to the e.m.f. of the battery in circuit B. The voltage developed when the terminals are isolated (infinite load resistance) is called the *open circuit voltage* (V_{oc}) [179]. Power output from DSSCs requires the generation of a photovoltage corresponding to the free energy difference between the working and counter electrodes. In the dark at equilibrium, the Fermi energy of the TiO_2 electrode (corresponding to the free energy of electrons in this film after thermalization) equilibrates with the midpoint potential of the redox couple, resulting in zero output voltage. Under these conditions, the TiO_2 Fermi level lies deep within the band gap of the semiconductor, and the film is effectively insulating, with a negligible electron density in the TiO_2 conduction band. Photoexcitation results in electron injection into the TiO_2 conduction band and the concomitant hole injection into the redox electrolyte. The high concentrations of oxidized and reduced redox couple present in the electrolyte in the dark mean that this photoxidation process does not result in a significant change in chemical potential of the electrolyte, which remains effectively fixed at its dark, resting value. In contrast, electron injection into the TiO_2 conduction band results in a dramatic increase in electron density, raising the TiO_2 Fermi level towards the conduction band edge, and allowing the film to become conducting. This shift of the TiO_2 Fermi level under irradiation increases the free energy of injected electrons and is responsible for the generation of the photovoltage in the external circuit [43]. Thus in DSSCs, V_{oc} is determined by the energy difference between the Fermi level of the solid under illumination and the potential of the redox couple in the electrolyte (see figure 2). However, the experimentally observed open-circuit potential, V_{oc}, for various sensitizers is smaller than the difference between the conduction band edge and the redox couple, probably due to the competition between electron transfer and charge recombination pathways.
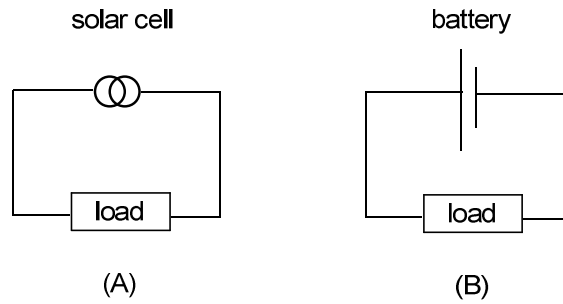
Fig. 97. Schematic representation of a solar cell and a battery [179].

The current drawn when the terminals are connected together under illumination in figure 97 in circuit A is the *short circuit current* I_{sc}, and is dependent on the incident light. The current is roughly proportional to the illuminated area, and the short circuit current density, J_{sc}, is the useful quantity for comparison [179]. To relate the photocurrent density, J_{sc}, to the incident spectrum, we need the cell's conversion efficiency or IPCE, that shows the probability that an incident photon of energy E will deliver one electron to the external circuit. It can be calculated in two ways:

$$\text{IPCE [\%]} = \frac{[(1.24 \times 10^3) \times \text{photocurrent density } [\mu\text{A/cm}^2]]}{[\text{wavelength [nm]} \times \text{photon flux } [\text{W/m}^2]]} \qquad \text{or} \qquad \text{IPCE} = \text{LHE} \cdot \phi_{inj} \cdot \eta_c$$

LHE is the light harvesting efficiency, Φinj is the quantum yield of the charge injection and η_c is the efficiency of collecting the injected electrons in the external circuit. The IPCE is a key quantity in describing solar cell performance under different conditions, and it can be given as a function of either photon energy or wavelength, λ (see figure 5). From the overlap integral of the curves of IPCE vs. λ with the solar emission spectrum, one can predict the short circuit photocurrent of a sensitizer; these values are normally in agreement with experimental observations [15].

For any intermediate load resistance R_L, the cell develops a voltage V between 0 and V_{oc} and delivers a current I such that $V = I \cdot R_L$, and $I(V)$ is determined by the current-voltage characteristics of the cell under that illumination, as described above. However, when a load is

130

present, a potential difference develops between the terminals of the cell, and this potential difference generates a current which acts in the opposite direction to the photocurrent, and the net current is reduced from its short circuit value. This reverse current is usually called the *dark current* in analogy with the current which flows across the device under an applied voltage *V* in the dark. Most solar cells behave like a diode in the dark, admitting a much larger current under forward bias (V > 0) than under reverse bias (V < 0). This rectifying behavior is a feature of photovoltaic devices, since an asymmetric junction is needed to achieve charge separation. The overall current voltage response of the cell, its current-voltage characteristics, can be approximated as the sum of the short circuit photocurrent and the dark current [179].

The cell power density is given by the equation:

$$P = J \cdot V$$

The power density of the cell reaches a maximum at the cell's operating point or *maximum power point*. This occurs at some voltage V_p with a corresponding current density J_p, as shown in figure 98. The fill factor (ff) is defined as the ratio shown below, and describes the "squareness" of the *J-V* curve.

$$ff = \frac{J_p \cdot V_p}{J_{sc} \cdot V_{oc}}$$

Graphically, the maximum power density or fill factor is given by the area of the rectangle formed by $J_p \cdot V_p$ (see figure 98). The outer rectangle has an area $J_{sc} \cdot V_{oc}$. If the fill factor was equal to 1, the current voltage curve would follow the outer rectangle.
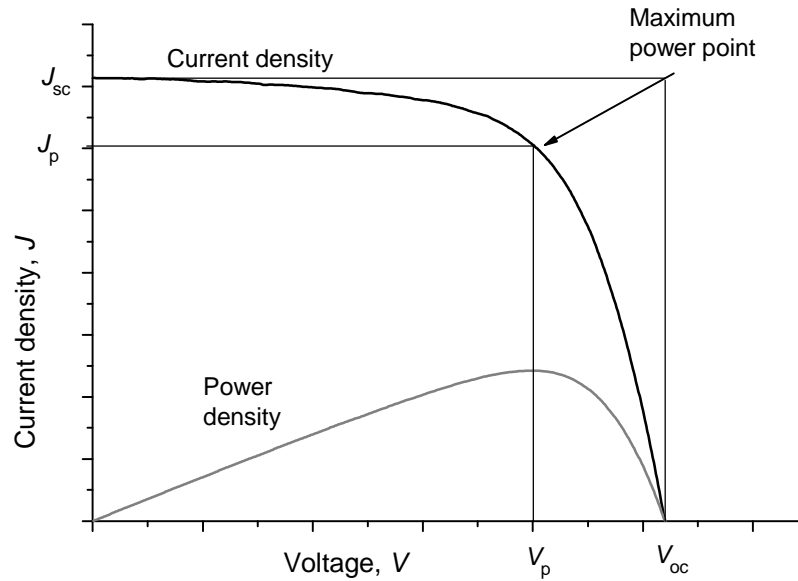
Fig. 98. The current voltage (black) and power-voltage (grey) characteristics of a solar cell.

The *global efficiency*, η_{global}, of the cell is the power density delivered at operating point as a fraction of the incident light power density, I_s, and is related to J_{sc} and V_{oc} using the ff:

$$\eta_{global} = \frac{J_p \cdot V_p}{I_s} \qquad \text{or} \qquad \eta_{global} = \frac{J_{sc} \cdot V_{oc} \cdot ff}{I_s}$$

These four quantities: J_{sc}, V_{oc}, ff and η_{global} are the key performance characteristics of a solar cell. All of these should be defined for particular illumination conditions. The Standard Test Condition (STC) for solar cells is the Air Mass (AM) 1.5 spectrum (see below), an incident power density of 1000 W·m^{-2} (1 sun) and a temperature of 25°C [179].

On passing through the atmosphere, solar light is absorbed and scattered by various atmospheric constituents, so that the spectrum reaching the Earth's surface is both attenuated and changed in shape from the "original" solar spectrum. Attenuation by the atmosphere is quantified by the "Air Mass" factor, n_{AM}, which is defined as the ratio between the optical path length to the Sun and the optical path length if the Sun is directly overhead. In other words, is the cosec of the

angle of elevation of the sun, γ_s, as shown in figure 99. The standard spectrum for temperature latitudes is Air Mass 1.5, or AM 1.5, corresponding to the sun being at an angle of elevation of 42° [179].
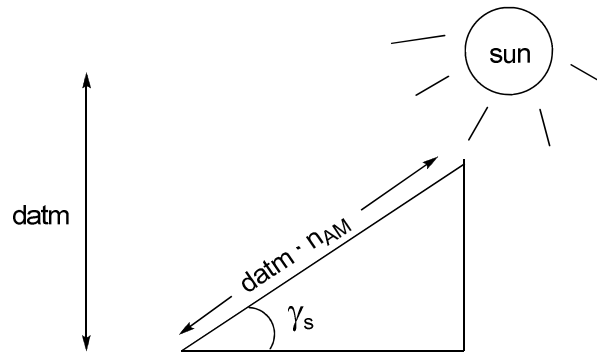
Fig. 99. If the atmosphere has a thickness d_{atm}, then when the sun is at an angle of elevation γ_s, light from the sun has to travel through a distance $d_{atm} \cdot \text{cosec } \gamma_s$ through the atmosphere to an observer on the Earth's surface [179].

V. 2 Preparation of dye-coated nanocrystalline TiO$_2$ electrodes

Nanocrystalline oxide electrodes for photoelectrochemical studies carried out in our laboratories in the University of Basel were prepared by spreading (doctor blading) a colloidal TiO$_2$ paste (Solaronix Nanooxide-T, colloidal anatase) on a conductive transparent surface of a glass piece (F-doped SnO$_2$, FTO, Hartford glass company, Tec 8, 8Ω/cm^2) that had been cut to 0.9 x 2.0 cm and cleaned with water and ethanol. The FTO-coated glass was covered with two layers of parallel adhesive tape 0.5 cm apart to control the thickness and the area of the TiO$_2$ film (0.9 x 0.5 cm). The colloidal paste was applied between the tapes on the FTO-coated glass by rolling a glass rod on the surface. The film thickness, which was measured with a profilometer (Dektak), was 6.0 $\pm$0.5 μm, even if often, for the best cells, around 10-12 μm thick films are employed as it can be seen from the next figure:
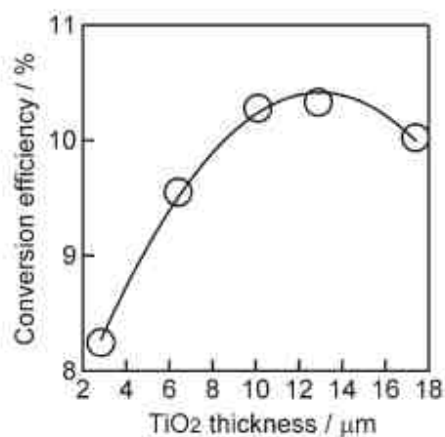
Fig. 100. Photoconversion efficiency as a function of nanocrystalline TiO$_2$ layer thickness. Illuminated-TiO$_2$ and aperture areas of cells are 0.16 cm^2 and 0.25 cm^2, respectively [180].

After air drying the TiO$_2$ nanocrystalline electrode for *ca*. 20 min., it was heated on a plate at *ca*. 450°C for 30 min. The heating enables contaminations (such as added polymer in the colloidal paste) to be burnt off and reduces the resistivity of the film. In addition, the surface is dehydroxylated during this process, leaving reactive Ti^{3+} centers available for reaction with the anchoring groups of the sensitizers. To minimize rehydration of the TiO$_2$ surface from moisture at ambient air (which causes dye desorption), the electrodes, while still warm (80-100°C) from annealing, were immersed into a solution of dye for several hours depending on the experiment that was carried out (see later). The porous oxide layer acts like a sponge and there is efficient uptake of the dye, leading to intense coloration of the film.

FTO glass pieces of the same dimensions as the ones used for the TiO$_2$ nanocrystalline electrode were used as cathode electrodes. A few drops of a 5mM H$_2$[PtCl$_6$] isopropanol solution were spread onto their surface, letting the solvent to evaporate in air. Then the counter electrodes were heated at *ca*. 380°C for 15 min. to deposit a platinum coating that acts as catalyst reducing the oxidated form of the electrolyte (see section I. 1. 4.).

The photo-anode (rinsed with an appropriate solvent after taken out of the sensitizing solution) and the counter electrode were assembled together using Surlyn (Dupont) plastic between the electrodes and heating it to 110-120°C while pressing them together. The construction of the

134

sandwich type cell was finished by depositing a drop of electrolyte (see later) on the surface between the two electrodes and so that it penetrated the space between the electrodes by capillarity and also inside the TiO_2.

N719 (see figure 101) (Solaronix) has been used as a standard dye for comparison during the measurements. It is widely recognized as one of the best dyes for DSSCs and has a reported efficiency of 10% [38, 181].
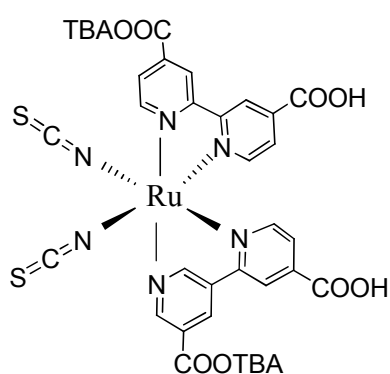
N719

Fig. 101. Chemical structure of the ruthenium dye N719.

The electrolytes that have been used are:

Standard 1: 0.5 M LiI, 0.05 M I_2 and 0.5 M MBI in 3-MPN.
Standard 2: 0.5 M LiI, 0.05 M I_2, 0.5 M MBI and 0.6 M MBII in 3-MPN.

The main components of the electrolytes are LiI and I_2, which form the redox couple I^-/I_3^-. MBI (1-methylbenzimidazole) is added as an additive in order to increase V_{oc}. To replace some of the LiI, an ionic salt of iodide, MBII (1-buthyl-3-methylimidazolium iodide), is added. 3-MPN stands for 3-methoxypropionitrile.

The efficiency of some of the dyes (homoleptic [57] and heteroleptic) synthesized in this thesis was measured at the *Ecole Polytechnique Federale de Lausanne* (EPFL) by Takeru Bessho from the group of Prof. Grätzel. The solar cells were constructed using a standard protocol optimized for the production of ruthenium-sensitized dye-cells [182] and evaluated using a standard procedure [180]. The electrolytes employed were A7172 (for the measurements of homoleptic complexes) and Z960 (for the measurement of heteroleptic complexes). It is worth pointing out here that the cells made in the EPFL were completely sealed, thereby avoiding leaking or evaporation of the electrolyte and/or rehydration of the TiO_2 surface.
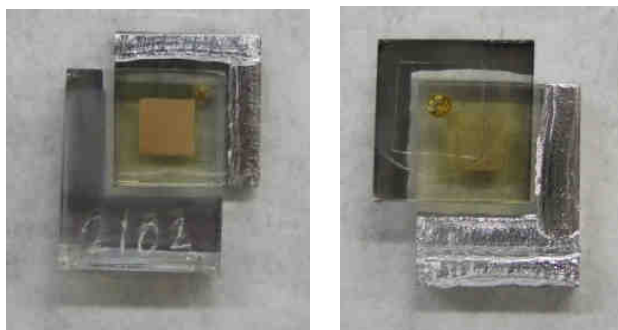
Fig. 102. Front (left) and back (right) view of a DSSC made at the EPFL in Lausanne.

The electrolytes used for the measurements done in Lausanne were:

A7172: 0.6 M *N*-methyl-*N*-butylimidazolium iodide, 0.03 M I_2, 0.1 M guanidinium thiocyanate and 0.5 M *tert*-butylpyridine in 15:85 (v/v) valeronitrile-acetonitrile.
Z960: 1.0 M *N,N´*-dimethylimidiazolium iodide (DMII), 50 mM LiI, 30 mM I_2, 0.5 M tert-butylpyridine and 0.1 M guanidinium thiocyanate in 15:85 (v/v) valeronitrile-acetonitrile.

In order to estimate the coverage or amount of dye adsorbed onto the surface of TiO_2, the extinction coefficient of the complexes adsorbed to TiO_2 is assumed to be the same as it is in solution (see tables 1 and 2). A rearranged form of the Beer-Lambert law for the TiO_2 films allows one to calculate the number of moles of dye adsorbed per 1 cm^2 on the TiO_2 surface:

$$OD = \varepsilon \cdot 1 \cdot C \qquad\qquad (1)$$

$$OD = \varepsilon \cdot (t \cdot 10^{-4}) \cdot [x / (t \cdot 10^{-4})] \qquad (2)$$

Where OD is the optical density or absorption, ε is the molar extinction coefficient of the dye in solution ($M^{-1} \cdot cm^{-1}$), l is the path length (cm) and C is the concentration of the sample solution (M) in equation 1. In equation 2, t represents the thickness of the sample films (µm) and x is the number of dyes in the cube of 1 cm $\cdot$ 1 cm $\cdot$ t µm of film (mol). Consequently, x is the number of moles of dye per 1 cm^2 on the surface of the TiO_2 film and it can be easily calculated using equation 3:

$$x = OD / (\varepsilon \cdot 10^3) \qquad (3)$$

V. 3 DSSCs with homoleptic copper(I) complexes as sensitizers

In this section, the results of the investigation on the photoelectrochemical properties of the synthesized Cu(I) complexes is reported. In table 7 the characteristic parameters describing the efficiency of the mentioned complexes when employed as sensitizers in DSSCs are presented. The cells were made as described above and measured in our laboratories at the University of Basel.

	J_{sc} (mA/cm^2)	V_{oc} (V)	ff	η_{global} (%)	λ_{max} solut.	λ_{max} dye
[Cu(H$_2$**L4**)$_2$]Cl[a]	0.15	0.44	0.50	0.03	-	-
[Cu(H$_2$**L6**)$_2$]Cl[a]	2.12	0.58	0.62	0.76	435, 590	446, 592
[Cu(H$_2$**L8**)$_2$]Cl[b]	1.21	0.57	0.65	0.45	482	480
[Cu(H$_2$**L10**)$_2$]Cl[b]	1.15	0.53	0.68	0.41	483	492
[Cu(**L11**)$_2$][PF$_6$][c]	1.77	0.49	0.60	0.52	495	496
[Cu(**L14**)$_2$][PF$_6$][c]	0.15	0.43	0.64	0.04	508	504
[Cu(H$_2$**L15**)$_2$]Cl[d]	2.54	0.54	0.64	0.87	515	504

[Cu(H$_2$**L17**)$_2$]Cl[a]	0.69	0.484	0.63	0.21	437, 608	494, 604
[Cu(**L18**)$_2$][PF$_6$][e]	0.23	0.495	0.70	0.08	441, 610	445, 612
[Cu(**L21**)$_2$][PF$_6$][e]	0.03	0.278	0.39	0.03	420, 615	468, 618
[Cu(H$_2$**L22**)$_2$]Cl[a]	1.91	0.52	0.68	0.67	462, 630	481, 619
[Cu(**L23**)$_2$][PF$_6$][f]	0.04	0.31	0.40	0.005	490	486
[Cu(H$_4$**L24**)$_2$]Cl[a]	-	-	-	-	-	-
[Cu(H$_2$**L25**)$_2$]Cl[a]	0.10	0.34	0.50	0.02	553	563
N719[f]	11.3	0.75	0.67	5.0	534 [38]	392, 530

Table 7. Current-voltage characteristics data derivatized with copper(I) complexes and a comparison with the ruthenium dye N719. The dye solution were 1 mM in *a* DMSO, *b* MeOH, *c* CHCl$_3$, *d* 1:9 DMF:CHCl$_3$, *e* CH$_2$Cl$_2$ and *f* CH$_3$CN. Electrolyte: Standard 2.

The best results were obtained with complexes [Cu(H$_2$**L15**)$_2$]Cl, [Cu(H$_2$**L6**)$_2$]Cl and [Cu(H$_2$**L22**)$_2$]Cl, that presented efficiencies of 0.87, 0.76 and 0.68%, respectively. These three dyes, all of them anchored to the semiconductor through carboxylic acid groups, have very similar open-circuit potentials, V_{oc}, and Cu$^{2+/+}$ reduction potentials; however, they differ in their short-circuit photocurrents, J_{sc}. For the best sensitizer, [Cu(H$_2$**L15**)$_2$]Cl, J_{sc} is 2.54 mA/cm^2, and for the other two J_{sc} is reduced to 2.12 and 1.91 mA/cm^2 for [Cu(H$_2$**L6**)$_2$]Cl and [Cu(H$_2$**L22**)$_2$]Cl, respectively. Regarding the UV-VIS absorption spectra of the dyes bound to the TiO$_2$, while for the adsorbed complex [Cu(H$_2$**L6**)$_2$]Cl the MLCT absorption maxima are red shifted if compared to the solution spectrum, in complex [Cu(H$_2$**L15**)$_2$]Cl the opposite effect is observed, being thus the $\Delta E_{HOMO-LUMO}$ in the latter dye increased on attachment of the complex to the semiconductor. In the case of complex [Cu(H$_2$**L22**)$_2$]Cl, the high-energy MLCT band is red shifted from 462 to 481 nm, while the low-energy MLCT band is blue shifted from 630 to 619 nm upon binding to TiO$_2$.

Another relatively efficient sensitizer tested in our laboratories is [Cu(**L11**)$_2$][PF$_6$], with an efficiency of 0.52%. Surprisingly, [Cu(**L11**)$_2$][PF$_6$] has methyl ester instead of carboxylic acid

groups as anchoring units. However, it showed good dye-modified surfaces, as it can be observed from figure 103, and we attribute this to *in situ* hydrolysis of the ester groups. In contrast, [Cu(**L14**)$_2$][PF$_6$], a complex also containing methyl ester groups, did not bind significantly to the TiO$_2$ nanoparticles (see figure 103), and this is reflected in a very poor efficiency of 0.04%. In figure 103, one can observe the different binding behavior of these methyl ester containing complexes and compare it with the analogous complexes with carboxylic acid groups, which, as expected, bind strongly to the TiO$_2$ surface.
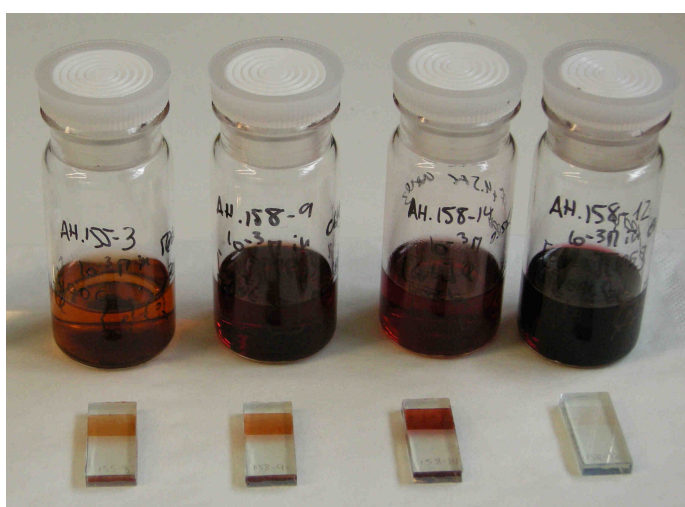
Fig. 103. Binding to TiO$_2$ of 1mM [Cu**L**$_2$]$^+$ complexes with (from left to right) [Cu(H$_2$**L10**)$_2$]Cl, [Cu(**L11**)$_2$][PF$_6$], [Cu(H$_2$**L15**)$_2$]Cl and [Cu(**L14**)$_2$][PF$_6$]. The FTO conducting glass slides were coated with 6-7 μm TiO$_2$ nanoparticles and then immersed in solution (MeOH for [Cu(H$_2$**L10**)$_2$]Cl, CHCl$_3$ for [Cu(**L11**)$_2$][PF$_6$] and [Cu(**L14**)$_2$][PF$_6$], and 1:9 DMF-CHCl$_3$ for [Cu(H$_2$**L15**)$_2$]Cl) for a period of 12 h.

It is curious, however, that complexes [Cu(H$_2$**L17**)$_2$]Cl, [Cu(**L18**)$_2$][PF$_6$], [Cu(**L21**)$_2$][PF$_6$] and [Cu(H$_2$**L22**)$_2$]Cl, that differ from the complexes in figure 103 in that they have phenyl substituents attached to the 6 and 6´-positions of bipyridine, present different binding behavior (see figure 104).

Fig. 104. Binding to TiO$_2$ of 1mM [Cu**L**$_2$]$^+$ complexes with (from left to right) [Cu(**L18**)$_2$][PF$_6$], [Cu(H$_2$**L17**)$_2$]Cl, [Cu(**L21**)$_2$][PF$_6$] and [Cu(H$_2$**L22**)$_2$]Cl. The FTO conducting glass slides were coated with 6-7 μm TiO$_2$ nanoparticles and then immersed in solution (CH$_2$Cl$_2$ for [Cu(**L18**)$_2$][PF$_6$] and [Cu(**L21**)$_2$][PF$_6$], and DMSO for [Cu(H$_2$**L17**)$_2$]Cl and [Cu(H$_2$**L22**)$_2$]Cl) for a period of 12 h.

In this case, not only the carboxylic acid containing complexes, but also the complexes with methyl ester groups ([Cu(**L18**)$_2$][PF$_6$] and [Cu(**L21**)$_2$][PF$_6$]) produced good dye-modified TiO$_2$ surfaces, as it can be observed by the green colour of the semiconductor's surface in figure 104. However, these methyl ester containing complexes turned out to exhibit poor efficiencies in contrast to complexes [Cu(H$_2$**L17**)$_2$]Cl and [Cu(H$_2$**L22**)$_2$]Cl, which showed efficiencies of 0.21 and 0.68%, respectively.

It has to be noted at this point, that even if complexes [Cu(H$_2$**L17**)$_2$]Cl and [Cu(H$_2$**L22**)$_2$]Cl were not particularly stable in DMSO, they seem to attach rapidly enough to the TiO$_2$ surface and result in not negligible efficiencies. However, it would be worth, in the future, to find another solvent to make the solutions, as this may increase the surface coverage of the semiconductor.

As pointed out before in this thesis, the dyes used for sensitization of the semiconductor in solar cells, need to have positive redox potentials to ensure rapid donor oxidation. However, sensitizers with positive metal-based oxidation potential have the disadvantage of exhibiting high energy absorption bands which only harvest a fraction of visible light [164, 183]. Argazzi *et al.*, in an attempt to extend the spectral sensitivity of dye molecules towards the red, designed ruthenium based complexes based on the ligand 2,2′-bipyridine-5,5′-dicarboxylic acid, which has π* accepting orbitals at lower energy than the corresponding 2,2′-bipyridine-4,4′-dicarboxylic acid ligand, and investigated the surface attachment and photoelectrochemical properties of ruthenium complexes made with these ligands [183]. Effectively they observed an enhanced spectral sensitivity from Ru(II) polypyridyl photovoltaic devices with 2,2′-bipyridine-

5,5´-dicarboxylic acid ligands. However, the enhanced response at longer wavelengths was counteracted by the low photocurrent efficiency measured with 5,5´-based sensitizers, in part due to a lower quantum yield for electron injection.

In this thesis, the position of the anchoring group in the bipyridine ligand was also studied. Complexes $[Cu(H_2\mathbf{L8})_2]Cl$ and $[Cu(H_2\mathbf{L10})_2]Cl$ differ in that they bear carboxylic acid groups on the 5,5´- and in the 4,4´-positions, respectively. Indeed, the former has a more positive $Cu^{II/I}$ oxidation potential than the latter (see table 3). However, the MLCT band of $[Cu(H_2\mathbf{L8})_2]Cl$, in solution, is not red shifted with respect to $[Cu(H_2\mathbf{L10})_2]Cl$ (see table 1 or 7), as observed by Argazzi *et al.* with the Ru(II) complexes [183]. The explanation for this difference could have its roots on the effect exerted by the modulating ligands present in the Ru(II) complexes (Cl, CN and NCS).

Our preliminary studies showed that the two sensitizers had very similar I-V characteristics and efficiencies of 0.45 and 0.41% for $[Cu(H_2\mathbf{L8})_2]Cl$ and $[Cu(H_2\mathbf{L10})_2]Cl$, respectively. This is a little bit surprising, since in various papers in the literature, the highest yields are obtained with the bipyridine ligands bearing the anchoring groups on the 4,4´-positions [30, 31, 54]. This result has been rationalized by a difference in the magnitude of the electronic coupling between the sensitizer and the TiO_2 conduction band.

During this work, the substitution of the carboxylic acid by phosphonic acid groups was also studied in DSSCs, as it has also been made in the literature [30, 184, 185]. $[Cu(\mathbf{L23})_2][PF_6]$ and $[Cu(H_4\mathbf{L24})_2]Cl$ have phosphonic ester and phosphonic acid groups, respectively, attached to the 4,4´-positions of 2,2´-bipyridine, and methyl groups at the 6,6´-positions. A solution of $[Cu(\mathbf{L23})_2][PF_6]$ in CH_3CN was used to prepare the TiO_2 modified electrode, and although the dye seemed to adsorb to the semiconductor surface, the coverage, as it can be directly seen from figure 105, was too small to yield considerable efficiencies.

Fig. 105. Binding to TiO$_2$ of 1mM [Cu(**L23**)$_2$][PF$_6$] in CH$_3$CN. The FTO conducting glass slides were coated with 6-7 μm TiO$_2$ nanoparticles and then immersed in solution for a period of 12 h.

Complex [Cu(H$_4$**L24**)$_2$]Cl containing phosphonic acid groups gave no better efficiencies. The main reason for this is its insolubility in organic solvents. As observed from its crystal structure (see section IV. 2. 9), the unpurified complex is actually a sodium salt, and it is therefore soluble in water. However, this solvent is not appropriate for solar cell preparation, so DMSO was used instead although the complex is poorly soluble in it. No dye adsorption to the TiO$_2$ surface could be observed, and consequently no photocurrent was measured. It is possible that another solvent other than DMSO could considerably increase the attachment of the dye to the TiO$_2$ and consequently its efficiency as a sensitizer. It is a pity that this experiment was unsuccessful, since no comparison between the two different anchoring groups, carboxylic and phosphonic acid, could be made.

Finally, the effect of the introduction of a fused phenyl ring to the bipyridine core on the current-voltage characteristics of the dye was studied. For this, complexes [Cu(H$_2$**L25**)$_2$]Cl and [Cu(**L26**)$_2$][PF$_6$] were synthesized, where biquinolines are the ligands coordinating the copper(I) centre. The latter complex, bearing methyl ester groups, did not bind significantly to the TiO$_2$ nanoparticles. In contrast, [Cu(H$_2$**L25**)$_2$]Cl showed good dye-modified purple surfaces thanks to its carboxylic acid groups (see figure 106), but the regenerative DSSC made with it yielded a very poor efficiency of 0.02%. This is probably due to the low J_{sc} and ff exhibited by the cell.

Fig. 106. Binding to TiO$_2$ of 1mM [Cu**L**$_2$]$^+$ complexes in DMSO with (from left to right) [Cu(H$_2$**L26**)$_2$][PF$_6$] and [Cu(H$_2$**L25**)$_2$]Cl. The FTO conducting glass slides were coated with 6-7 μm TiO$_2$ nanoparticles and then immersed in solution for a period of 12 h.

Looking at the results obtained in our laboratories, it was decided to test the dye that gave the best results, [Cu(H$_2$**L15**)$_2$]Cl, and its parent compound, [Cu(H$_2$**L10**)$_2$]Cl, with no extended conjugation, at the EPFL in Lausanne. Takeru Bessho, from the group of Prof. Grätzel, prepared and measured the DSSCs. The photovoltaic action spectra and current-voltage characteristics for the devices are shown below:
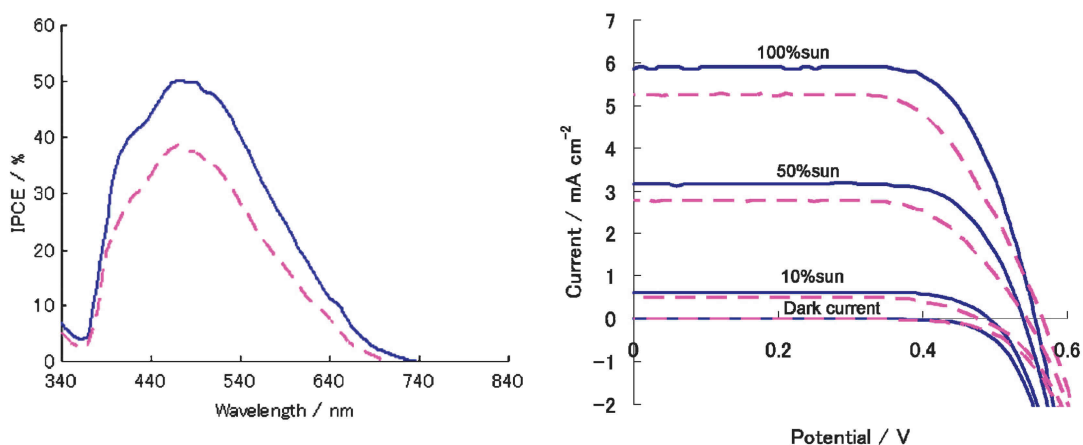
Fig. 107. IPCE (left) and I-V (right) curves for DSSCs prepared with [Cu(H$_2$**L10**)$_2$]Cl (pink broken line) and [Cu(H$_2$**L15**)$_2$]Cl (blue line) at light intensity of 100%, 50% and 10% sun, respectively.

Enhanced IPCE values of 50% with complex [Cu(H$_2$**L15**)$_2$]Cl were observed in comparison to the device containing complex [Cu(H$_2$**L10**)$_2$]Cl, which yielded only 38%. Unfortunately the

143

spectral response of the two sensitizers are almost restricted to the visible range, not extending, as would be ideal, further into the IR region.

The current-voltage curves showed on the right-hand-side of figure 107 were measured under simulated air mass (AM) 1.5 solar illumination at an intensitiy of 1000, 500 and 100 W m^{-2} and in the dark. A slightly enhanced short-current density and a reasonable decrease in the open-circuit voltage for complex [Cu(H$_2$**L15**)$_2$]Cl compared to complex [Cu(H$_2$**L10**)$_2$]Cl was observed, resulting in power conversion efficiencies of 2.3 and 1.9%, respectively. The effect of solvent on dye deposition and the addition of chenodeoxycholic acid (see above) was also tested. The data obtained after deposition from ethanol solution are superior to those from acetonitrile or *tert*-butanol solutions. Adding chenodeoxycholic acid did not improve the efficiency compared to comparable cells without this additive.

Table 8 shows current-voltage characteristics data for solar cells derivatized with copper(I) complexes [Cu(H$_2$**L10**)$_2$]Cl and [Cu(H$_2$**L15**)$_2$]Cl. The data represent the optimized results for cells, measured using 7.4 + 4.4 μm double layer sensitized TiO$_2$ films. In order to reduce scattered light from the edge of the glass electrodes of the dyed TiO$_2$ layer, a light shading mask was used on the DSSCs, so that the active area of the DSSC was fixed at 0.2 cm^2.

	J_{sc} (mA/cm^2)	V_{oc} (V)	ff	η_{global} (%)	IPCE % (max)	nm
[Cu(H$_2$**L10**)$_2$]Cl	5.25	0.566	0.64	1.9	38.6	470
[Cu(H$_2$**L15**)$_2$]Cl	5.9	0.556	0.70	2.3	50.1	470
N719	17.7	0.767	0.71	9.7	87	550

Table 8. Current-voltage characteristics data derivatized with [Cu(H$_2$**L10**)$_2$]Cl and [Cu(H$_2$**L15**)$_2$]Cl and a comparison with the ruthenium dye N719. 7.4 + 4.4 μm double layer sensitized nanocrystalline TiO$_2$ film on FTO conducting glass. Electrolyte: A7172.

The results obtained at the EPFL, and successfully published [57], together with the ones obtained in our laboratories at the University of Basel, show that [Cu**L**$_2$]$^+$ complexes are

surprisingly effective as sensitizers for DSSCs. Although these initial results are not comparable with state of the art ruthenium dyes such as N719, they indicate that with iterative chemical optimization, sensitizers comparable to ruthenium complexes might be prepared. In addition, even though the efficiency of the copper complexes, specifically $[Cu(H_2\textbf{L15})_2]Cl$, is 4 times lower than that of the ruthenium sensitizer N719, the cost is an order of magnitude lower, what means that copper sensitizers less efficient than the actual ruthenium dyes would be economically viable.

In the literature, different studies have been carried out in order to establish the binding mode of the carboxylic acid groups contained in ruthenium(II) complexes to the semiconductor's surface [28, 186], and also kinetic and thermodynamic studies have been done to have an insight into the nature of the binding [187].

Brunschwig *et al.* reported in 2004 that there are different binding modes possible for dyes that use carboxy groups to anchor to TiO_2 [187]. For example, either one (ester linkage) or both (carboxylato linkage) oxygen atoms in the carboxy group can bind to either one or two titanium atoms (see figure 108). If only one carboxy group is attached, the binding is expected to be rather flexible. In contrast, dyes with two carboxy groups binding from the same or from neighboring bipyridine ligands are expected to produce a more robust linkage to the surface.

unidentate (ester)   bidentate   bridging
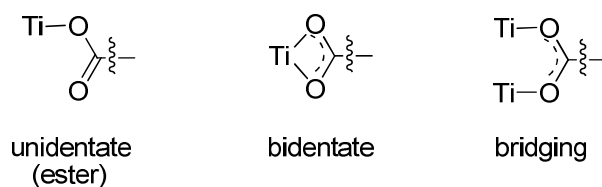
Fig. 108. Different binding modes possible for dyes that use carboxylic acid groups to anchor to TiO_2.

In order to establish the kind of binding presented by the dyes, infrared spectroscopy has been employed in the literature. Unfortunately, in our case, these experiments were unsuccessful and they threw no insight into the binding mode of our copper(I) complexes.

Regarding the thermodynamics and kinetics of the dye bound to the semiconductor, some easy to reproduce experiments have been done in the literature in that the adsorption and desorption kinetics of ruthenium(II) polypyridyl complexes in general, and the N3 dye, in particular, have been carried out [188]. Based on those studies, Fillinger et al. suggested a two-step adsorption mechanism for the binding of N3 to nanocrystalline TiO_2 [188] and could fit the experimental data of both, adsorption and desorption experiments, to Langmuir isotherms.

In our laboratories, the kinetics of the binding of different dyes together with their coverage has also been measured. We observe that the curves obtained could be fitted to an isotherm. First of all a 0.1mM solution of complex $[Cu(H_2L10)_2]Cl$ in DMSO was prepared and the quantity of adsorbed dye was monitored as a function of time (see figure 109) by measuring the increase of the absorption peak of the anchored sensitizer. As mentioned before, in order to calculate the coverage of the TiO_2 by the dye, the extinction coefficient of the complex in solution was used. Then, solar cells were constructed with each electrode and the photocurrent density obtained with them was measured. The results obtained are shown graphically in figure 109.
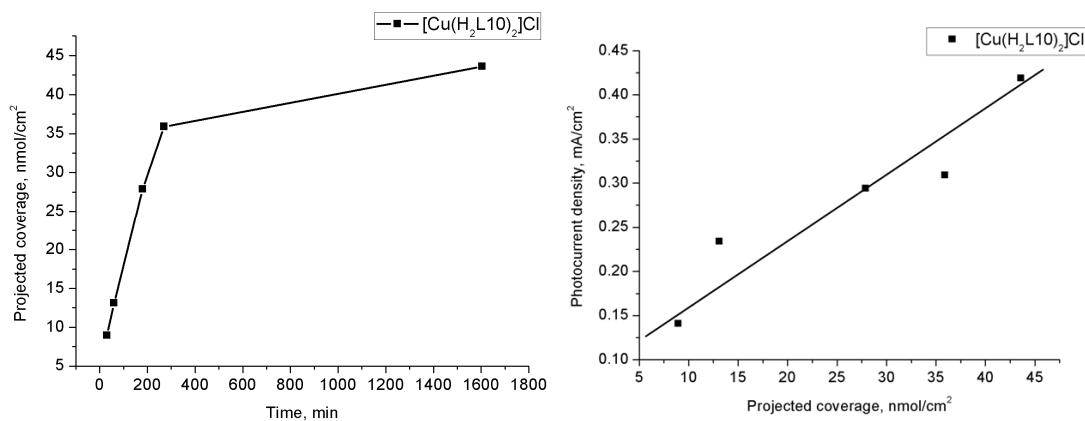
Fig. 109. On the left: binding isotherm of $[Cu(H_2\textbf{L10})_2]Cl$. On the right: linear correlation of the photocurrent density of the solar cell sensitized with $[Cu(H_2\textbf{L10})_2]Cl$ and its projected coverage.

On the left-hand-side of figure 109, the projected coverage obtained with complex $[Cu(H_2\textbf{L10})_2]Cl$ *vs.* time is represented. From the graphic, it is straightforward that during the first 4 h the binding of the dye is much faster than after this time, when the curve reaches slowly

a plateau level. This would mean that after approximately 10 h, the dipping time of the electrode in the dye solution makes no significant difference in the coverage obtained. However, from the graphic on the right-hand-side of figure 109, one can see that it is very important to have the maximum coverage possible, because the photocurrent density obtained grows linearly with the coverage of the film.

In another experiment, the binding properties of complex $[Cu(H_2L17)_2]Cl$ were studied in that different concentration solutions of the complex were prepared and TiO_2 electrodes were dipped in them for 20 h. After this time the absorption spectrum of each derivatized electrode was measured. In figure 110, the coverage of the TiO_2 nanoparticles *vs*. the initial concentration of the solutions is represented.
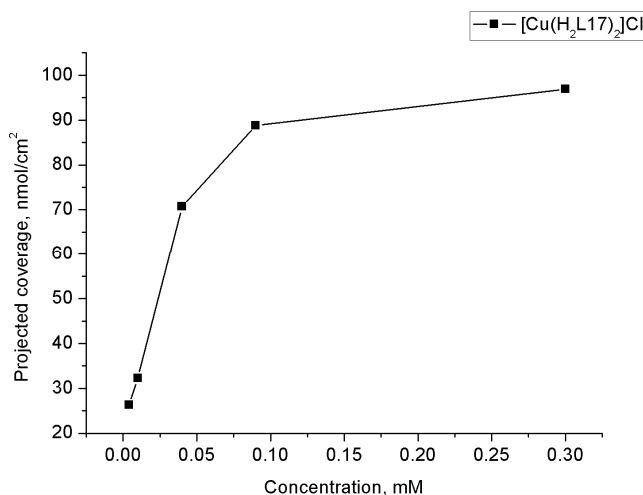
Fig. 110. Binding isotherm of $[Cu(H_2L17)_2]Cl$.

Comparing the binding isotherm obtained with complex $[Cu(H_2L17)_2]Cl$ with binding isotherms of ruthenium(II) complexes [187], one can observe that the coverage obtained with this copper(I) complex is in the same range as the coverage obtained with ruthenium(II) complexes that bear more than one carboxylic acid group. So one could say that the binding behavior of copper(I) complexes is similar to that observed for ruthenium(II) complexes. However, further studies are necessary.

V. 4 DSSCs with heteroleptic copper(I) complexes as sensitizers

In this section, the synthesis of heteroleptic copper(I) complexes made *in situ* on the surface of TiO$_2$ will be described and the results obtained when employing them as sensitizers in DSSCs will be discussed.

Ligand exchange reactions in solution are facile in copper(I) complexes due to the great lability presented by this metal, as already discussed at the end of the introduction in chapter IV. For this reason, it is very difficult to synthesize heteroleptic Cu(I) complexes in solution, and consequently, the number of complexes that one is able to make is restricted. However, the new strategy that we present here, namely the stepwise synthesis of complexes on the semiconductor surface (not easily achieved with kinetically inert ruthenium centres), opens up a new horizon and permits the synthesis of many more complexes. With this method, one can also tune the properties of the complex synthesized by choosing the appropriate ligands.

The first step of the synthesis of these heteroleptic Cu(I) complexes is the functionalisation of the semiconductor surface with a ligand bearing anchoring groups, **L**, (see figure 111 a). This is achieved by immersing a still warm TiO$_2$ nanocrystalline electrode in a ligand solution for 3 h. After this time, the electrode presents no colour. This step is followed by dipping the functionalized electrode overnight in a solution containing a $[Cu(\mathbf{L'})_2]^+$ complex lacking anchoring groups (see figure 111 b). The surface-bound ligand behaves as an N$_2$ donor in exactly the same way as a solution species and equilibrates with the solution $[Cu(\mathbf{L'})_2]^+$ complex through ligand exchange. As the new surface bound complex is removed from the equilibrium, the process proceeds to complete surface coverage with the copper, as shown by the red colour observed at the surface (see figure 111). Naturally, the surface-bound species is now an heteroleptic complex $[Cu(\mathbf{LL'})]^+$, being adsorbed to the semiconductor by the anchoring groups of **L** with the remaining coordination sites occupied by ligand **L'**. Logically, **L'** may be varied at will to optimize absorption or redox characteristics, or to prevent/inhibit water adsorption to TiO$_2$ and retard recombination with I$_3^-$, as happens with the ruthenium dye Z907 due to the presence of aliphatic chains in one of the ligands [189].
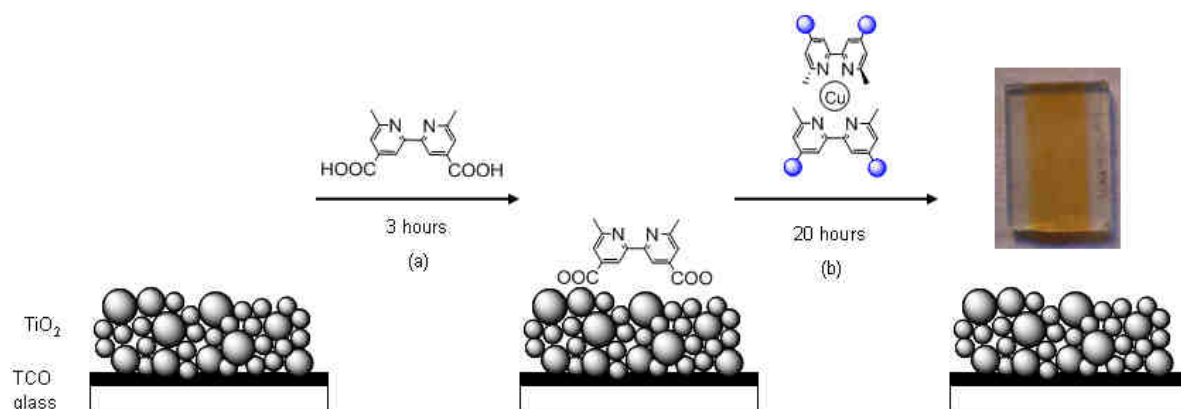
Fig. 111. Schematic representation of a DSSC involving the initial binding of a carboxylic acid containing ligand (in this example **L** = H$_2$**L10**) to the semiconductor surface (a) to give a colourless device, followed by ligand exchange with a [Cu(**L´**)$_2$]$^+$ complex (b) to give a surface-bound red heteroleptic species.

The first attempt done in our laboratories with the aim of testing this stepwise synthesis of heteroleptic Cu(I) complexes involved ligand H$_2$**L10**, as anchoring moiety, and complexes [Cu(dmbipy)$_2$][PF$_6$] and [Cu(CH$_3$CN)$_4$][PF$_6$], which are colourless, for the second step. The red colour observed on the TiO$_2$ surface was a direct proof of the success of the experiment, a direct proof that the heteroleptic complex had been formed, and these are the results obtained:
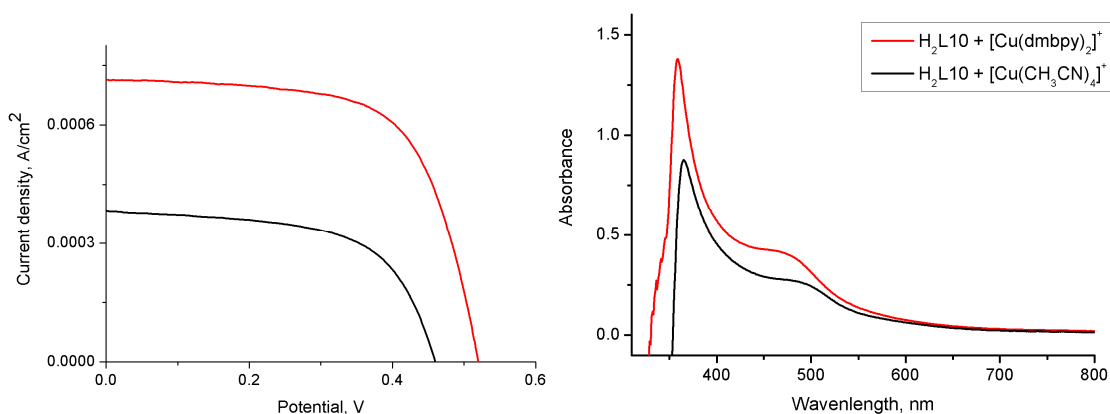
Fig. 112. On the left, the I-V curves of the DSSCs made with H$_2$**L10** and [Cu(dmbipy)$_2$]$^+$, in red, and with H$_2$**L10** and [Cu(CH$_3$CN)$_4$]$^+$, in black, are shown. On the right-hand side, the UV-VIS spectra of the functionalized TiO$_2$ electrodes are shown.

149

	J_{sc} (mA/cm^2)	V_{oc} (V)	ff	η_{global} (%)	λ_{max} dye (nm)
H$_2$**L10** + [Cu(dmbipy)$_2$]$^+$	0.714	0.52	0.66	0.25	474
H$_2$**L10** + [Cu(CH$_3$CN)$_4$]$^+$	0.383	0.46	0.59	0.10	497

Table 9. Current-voltage characteristics data derivatized with heteroleptic copper(I) complexes. The TiO$_2$ containing electrodes were initially immersed for 3 h in a 1mM solution of H$_2$**L10** in MeOH, and then in a 1mM solution of [Cu(dmbipy)$_2$][PF$_6$] and [Cu(CH$_3$CN)$_4$][PF$_6$] in CH$_3$CN, respectively, for 12 h. Electrolyte: Standard 2.

The complex formed between ligand H$_2$**L10** and [Cu(dmbipy)$_2$][PF$_6$] is more effective as sensitizer in DSSCs than the one formed with [Cu(CH$_3$CN)$_4$][PF$_6$], as the higher global efficiency, η_{global}, shows. The absorption maxima of the two *in situ* made complexes are 23 nm far one from another, being the complex formed between ligand H$_2$**L10** and [Cu(CH$_3$CN)$_4$][PF$_6$] the more red shifted one with its MLCT band at 497 nm (see table 9). Regarding this complex, two possible species can be formed in solution: 1) heteroleptic complex with one **L10** ligand and two CH$_3$CN molecules coordinating the copper(I) centre; and 2) homoleptic complex where two anchored **L10** ligands would have displaced the starting CH$_3$CN molecules. By looking at the UV-VIS absorption spectrum of the functionalised TiO$_2$ it can be concluded that only one kind of complex has been formed, because there is only one MLCT absorption band, although it is possible that the two species have similar MLCT absorption maxima. However, comparing the MLCT absorption maxima measured in this experiment with the value obtained for TiO$_2$ sensitized with complex [Cu(H$_2$**L10**)$_2$]Cl (492 nm) (see table 7), one can conclude that the complex formed in this experiment is the homoleptic copper(I) complex, because the MLCT absorption maxima have the same value within experimental error. Even if the aim of the experiment was to synthesize mixed-ligand Cu(I) complexes, this test was successful in that it could be demonstrated that the complexes obtained, no matter if homo- or heteroleptic, had been formed on the surface of the semiconductor.

Ligand H$_2$**L6** was also studied for the stepwise synthesis of heteroleptic Cu(I) complexes. It was stated that this ligand does also bind to the surface of the semiconductor (see colouration of the TiO$_2$ surface after the stepwise synthesis in figure 114), and it was observed that the Cu(I)

species formed *in situ* had red shifted absorption maxima (see figure 113), as also observed for Cu(I) homoleptic complexes bearing phenyl groups attached to the 6 and 6´-positions (see section IV. I).
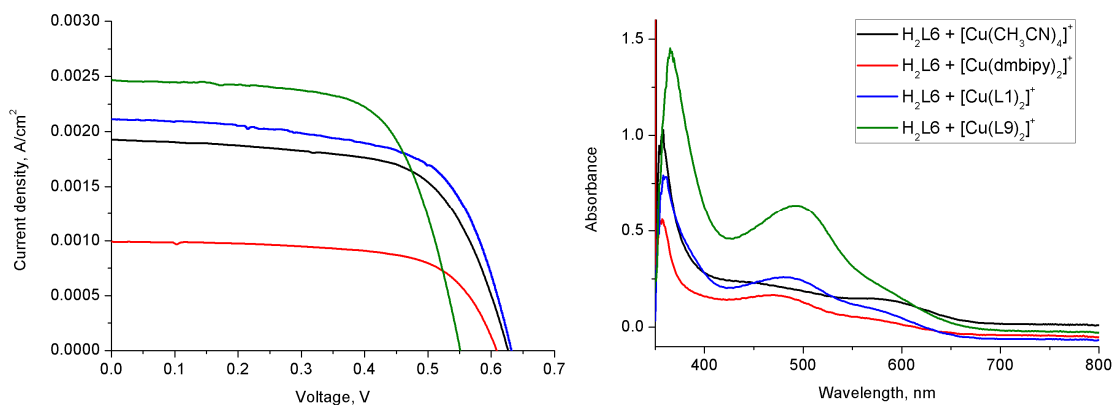
Fig. 113. On the left, the I-V curves of the DSSCs made with H$_2$**L6** and four different washing complexes: [Cu(CH$_3$CN)$_4$][PF$_6$] in black; [Cu(dmbipy)$_2$][PF$_6$] in red; [Cu(**L1**)$_2$][PF$_6$] in blue and [Cu(**L9**)$_2$][PF$_6$] in green. On the right-hand side, the UV-VIS absorption spectra of the functionalized TiO$_2$ electrodes are shown.

Fig. 114 TiO$_2$ functionalised electrodes with H$_2$**L6** and (from left to right) [Cu(CH$_3$CN)$_4$]$^+$, [Cu(dmbipy)$_2$]$^+$, [Cu(**L9**)$_2$]$^+$ and [Cu(**L1**)$_2$]$^+$.

	J_{sc} (mA/cm^2)	V_{oc} (V)	ff	η_{global} (%)	λ_{max} dye (nm)
H$_2$**L6** + [Cu(CH$_3$CN)$_4$]$^+$	1.92	0.63	0.65	0.77	452, 583
H$_2$**L6** + [Cu(dmbipy)$_2$]$^+$	0.99	0.61	0.66	0.37	470, 572
H$_2$**L6** + [Cu(**L1**)$_2$]$^+$	2.11	0.63	0.64	0.84	483, 577
H$_2$**L6** + [Cu(**L9**)$_2$]$^+$	2.47	0.55	0.67	0.67	494, 588

Table 10. The TiO$_2$ nanocrystalline electrodes were dipped for 3 h in a 0.3mM solution of ligand H$_2$**L6** in DMSO. After that time, the electrodes were dipped for 23 h in a 1mM solution of the complexes in CH$_3$CN, for [Cu(CH$_3$CN)$_4$][PF$_6$] and [Cu(dmbipy)$_2$][PF$_6$], and in CHCl$_3$, for[Cu(**L1**)$_2$][PF$_6$] and [Cu(**L9**)$_2$][PF$_6$]. Electrolyte: Standard 2.

From table 10 it is again obvious that the heteroleptic Cu(I) complexes have been formed and that they work as sensitizers in DSSCs. The highest efficiency was measured with the washing complex [Cu(**L1**)$_2$][PF$_6$] which had a global efficiency of 0.84%. In all the species the UV-VIS absorption spectrum shows two MLCT bands, the lowest energy one appearing at wavelengths between 572 and 588 nm.

Another anchoring ligand tested in our laboratories in Basel was H$_4$**L24**, which instead of carboxylic acid groups has phosphonic acid groups to anchor to the semiconductor. Since anchoring the homoleptic Cu(I) complex made with H$_4$**L24** to the TiO$_2$ surface was unsuccessful, it was decided to try to use this ligand to make *in situ* Cu(I) complexes. The two washing complexes employed were [Cu(CH$_3$CN)$_4$][PF$_6$] and [Cu(**L1**)$_2$][PF$_6$]. The results are summarized in figure 115 and table 11.
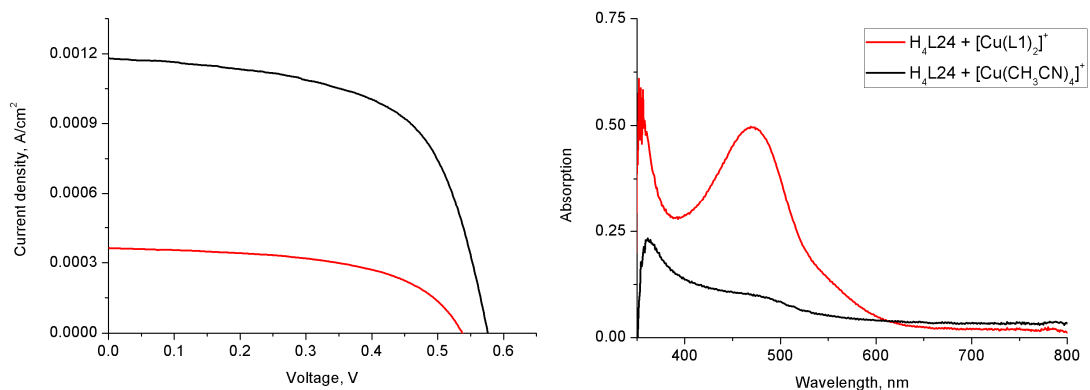
Fig. 115. On the left, the I-V curves of the DSSCs made with H$_4$**L24** and [Cu(**L1**)$_2$]$^+$, in red, and with [Cu(CH$_3$CN)$_4$]$^+$, in black, are shown. On the right-hand side, the UV-VIS absorption spectra of the functionalized TiO$_2$ electrodes are shown.

Fig. 116. TiO$_2$ functionalised electrodes with H$_4$**L24** and [Cu(**L1**)$_2$]$^+$ (on the left) and with H$_4$**L24** and [Cu(CH$_3$CN)$_4$]$^+$ (on the right).

	J_{sc} (mA/cm^2)	V_{oc} (V)	ff	η_{global} (%)	λ_{max} dye (nm)
H$_4$**L24** + [Cu(**L1**)$_2$]$^+$	0.363	0.537	0.56	0.11	470
H$_4$**L24** + [Cu(CH$_3$CN)$_4$]$^+$	1.176	0.575	0.61	0.41	485

Table 11. The TiO$_2$ nanocrystalline electrodes were dipped for 3 h in a 1mM solution of ligand H$_2$**L24** in DMSO. After that time, the electrodes were dipped for 23 h in a 0.3mM solution of [Cu(**L1**)$_2$][PF$_6$] in EtOH and in a 1mM solution of [Cu(CH$_3$CN)$_4$][PF$_6$] in CH$_3$CN, respectively. Electrolyte: Standard 2.

From the results obtained with this experiment, one would say that ligand H_4L24 is a better anchoring ligand for making these kind of heteroleptic Cu(I) complexes, because an efficiency of 0.41% is obtained when employing $[Cu(CH_3CN)_4][PF_6]$ as the washing complex, in comparison to the 0.10% obtained (see table 9) when using ligand H_2L10 with the same complex. It is noteworthy, that despite the good I-V characteristics of the *in situ* made complex between H_4L24 and $[Cu(CH_3CN)_4]^+$, its UV-VIS absorption is considerably lower than the complex formed between H_4L24 and $[Cu(L1)_2]^+$. The reason for this could be the extended conjugation presented by the latter complex due to the phenyl groups of ligand L1.

In this experiment, again, the doubt of the existence of an homo- or heteroleptic Cu(I) complex is presented in the case when $[Cu(CH_3CN)_4][PF_6]$ is used as washing complex. As discussed in the previous section of this chapter, it was not possible to attach the $[Cu(H_4L24)_2]Cl$ complex to the surface of TiO_2 in order to measure its sensitizing characteristics. For this reason, the λ_{max} observed in this experiment will be compared with the one obtained for the adsorbed complex $[Cu(L23)_2][PF_6]$, even if this species bears phosphonic ester groups. These are presumably hydrolyzed before attachmet to the semiconductor. In table 7, one can see that the absorption maxima of complex $[Cu(L23)_2][PF_6]$ attached to the TiO_2 surface is at 486 nm, which is almost the same value found for the MLCT band of the species formed when the TiO_2 modified with H_4L24 is washed with $[Cu(CH_3CN)_4][PF_6]$. Consequently, it can be concluded that the species formed is not the heteroleptic Cu(I) complex, but it is a homoleptic species formed with two anchored H_4L24 ligands. Nevertheless, there is no doubt that this species has been formed on the surface on the semiconductor.

Having proof of the viability of the experiment, it was decided to have this experiment done in the laboratories of Prof. Grätzel at the EPFL in Lausanne. Three different anchoring ligands (H_2L6, H_2L10 and H_2L17) were tested each with two different washing complexes ($[Cu(L1)_2][PF_6]$ and $[Cu(L9)_2][PF_6]$). The TiO_2 nanocrystalline electrodes were dipped for 4 h in a 0.3mM solution of the ligands in DMF. After that time, the electrodes were dipped for 23 h in a 0.3mM solution of $[Cu(L1)_2][PF_6]$ and $[Cu(L9)_2][PF_6]$, in EtOH and CH_3CN:*t*-BuOH 1:1, respectively. These measurements were carried out by Takeru Bessho and the results obtained are summarized in table 12.
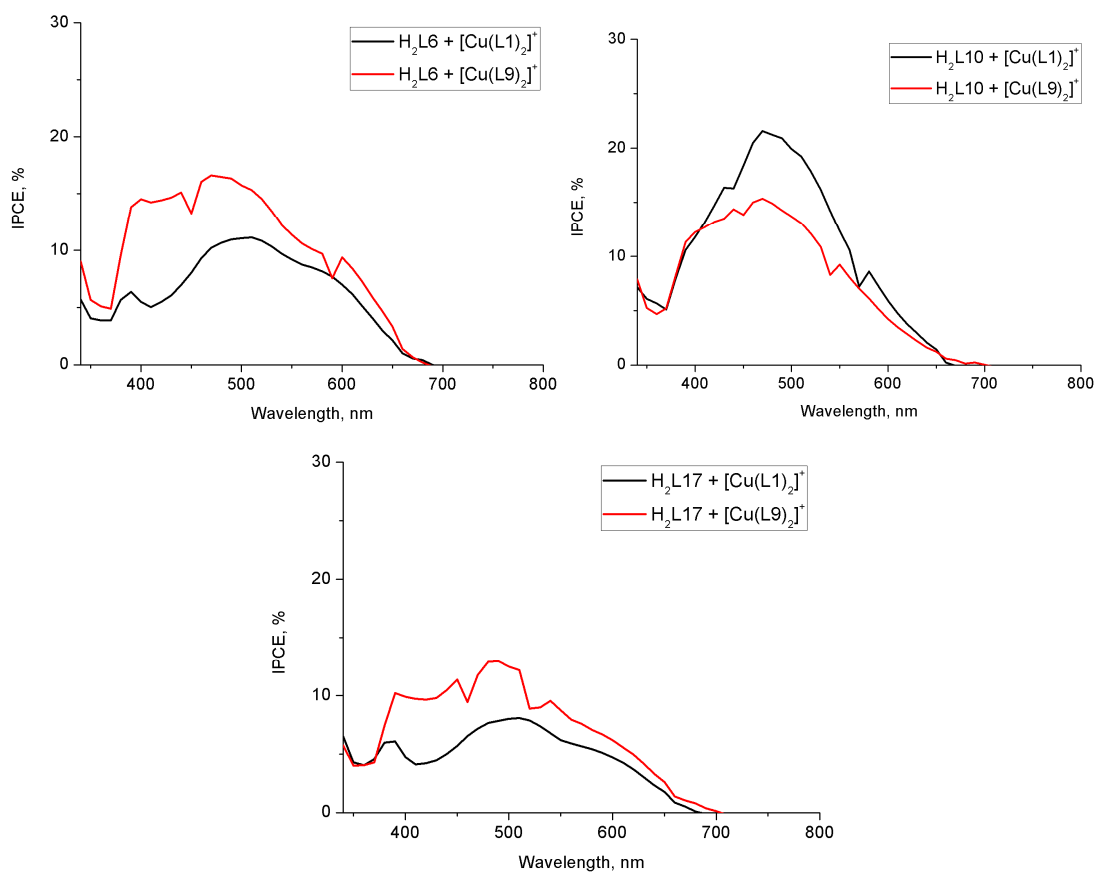
Fig. 117. IPCE curves for DSSCs prepared with anchoring ligands H₂**L6**, H₂**L10** and H₂**L17** with [Cu(**L1**)₂][PF₆] (in black) and [Cu(**L9**)₂][PF₆] (in red) at light intensity of 1 sun.

	J_{sc} (mA/cm^2)	V_{oc} (V)	ff	η_{global} (%)	IPCE % (max)	nm
H$_2$**L6** + [Cu(**L1**)$_2$]$^+$	2.45	0.649	0.72	1.15	16.5	473
H$_2$**L6** + [Cu(**L9**)$_2$]$^+$	2.37	0.544	0.76	0.97	11.1	504
H$_2$**L10** + [Cu(**L1**)$_2$]$^+$	3.30	0.605	0.71	1.41	21.5	471
H$_2$**L10** + [Cu(**L9**)$_2$]$^+$	2.46	0.530	0.74	0.96	15.2	471
H$_2$**L17** + [Cu(**L1**)$_2$]$^+$	1.57	0.574	0.72	0.65	8.1	508
H$_2$**L17** + [Cu(**L9**)$_2$]$^+$	1.85	0.532	0.75	0.74	12.9	486

Table 12. The TiO$_2$ nanocrystalline electrodes were dipped for 4 h in a 0.3mM solution of the ligands in DMF. After that time, the electrodes were dipped for 23 h in a 0.3mM solution of [Cu(**L1**)$_2$][PF$_6$] and [Cu(**L9**)$_2$][PF$_6$] in EtOH and CH$_3$CN:*t*-BuOH 1:1, respectively. Electrolyte: Z960. The results shown in the table correspond to 1 sun intensity.

The IPCE values obtained with these heteroleptic Cu(I) sensitizers are not as good as the ones measured for [Cu(H$_2$**L15**)$_2$]Cl. For anchoring ligands H$_2$**L6** and H$_2$**L17**, the maximum IPCE values are found at longer wavelengths than for ligand H$_2$**L10**, as expected because of the phenyl substituents at the 6 and 6´-positions.

The best global efficiencies were obtained with the sensitizers formed between ligand H$_2$**L10** and complex [Cu(**L1**)$_2$]$^+$ (1.41%) and ligand H$_2$**L6** and complex [Cu(**L1**)$_2$]$^+$ (1.15%). The other dyes studied have efficiencies ranging from 0.65 to 0.97%. These preliminary studies are not discouraging at all, in that these efficiencies are very good for non-optimized first generation DSSCs. It is also remarkable that all the sensitizers tested showed similar fill factors of *ca*. 0.73, which is a good value.

However, long term stability tests of these heteroleptic dyes showed that these complexes formed on the surface of the TiO$_2$ were sensitive to attack by the iodide present in the electrolyte, probably due to their smaller stability because of being anchored only through a single ligand. As a consequence of this, the characteristic red colour of the Cu(I) complexes turned slowly into yellow, as seen in figure 118. In order to establish the redox potential of the newly formed

complex, electrochemistry measurements were carried out with the anchored complex. However, these measurements were unsuccessful and it could not be ascertained if the complex was being oxidized to Cu(II) or simply destroyed by addition of any component from the electrolyte.
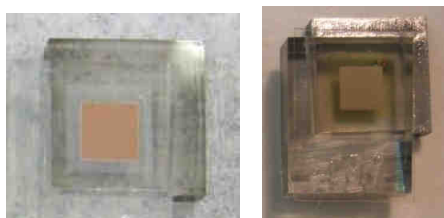
Fig. 118. DSSCs sensitized with an heteroleptic Cu(I) complex before (left) and after (right) electrolyte injection.

After doing these experiments, a test was carried out to see if $[Cu(L1)_2][PF_6]$ and $[Cu(L9)_2][PF_6]$ were capable of anchoring to the TiO_2 surface on their own in order to rule out the possibility of obtaining the surface red colour from the washing complexes instead of from the *in situ* made heteroleptic complexes. To our surprise, $[Cu(L9)_2][PF_6]$ did indeed attach to the surface of the semiconductor as the red colour of the TiO_2 indicated (see figure 119) and did sensitize it effectively as seen in figure 119 and table 12.
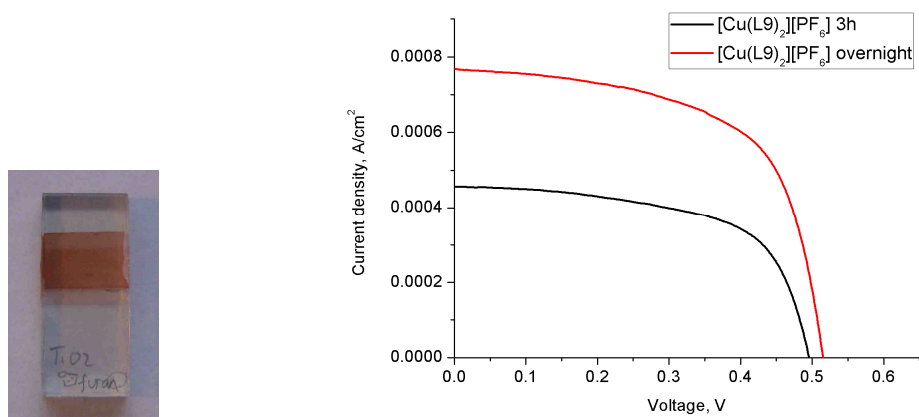
Fig. 119. On the left, the red colour of a TiO_2 electrode functionalized with $[Cu(L9)_2]^+$. On the right, the I-V curves of DSSCs functionalized with that complex are shown (3 h dipping time in black; overnight dipping time in red).

	J_{sc} (mA/cm^2)	V_{oc} (V)	ff	η_{global} (%)	λ_{max} dye (nm)
[Cu(**L9**)$_2$]$^+$ 3 h	0.46	0.49	0.62	0.14	494
[Cu(**L9**)$_2$]$^+$ 20 h	0.76	0.52	0.61	0.24	494

Table 12. The TiO$_2$ nanocrystalline electrodes were dipped for 3 h and 20 h, respectively, in a 1mM solution of [Cu(**L9**)$_2$][PF$_6$] in CHCl$_3$. Electrolyte: Standard 2.

In the same way, a test was carried out to see if complex [Cu(**L16**)$_2$][PF$_6$] was capable of anchoring to the semiconductor's surface. Its ligands also bear furan rings in the 4,4´-positions of 2,2´-bipyridine, but have, in contrast to [Cu(**L9**)$_2$][PF$_6$], phenyl groups at the 6,6´-positions. Effectively, the TiO$_2$ nanoparticles were coloured after the electrode had been immersed in a solution of the complex for 3 h, so it can be concluded that the complex did attach to the semiconductor. Unfortunately, it was not possible to measure the efficiency of this complex as sensitizer, since the cell broke up during the measurement.
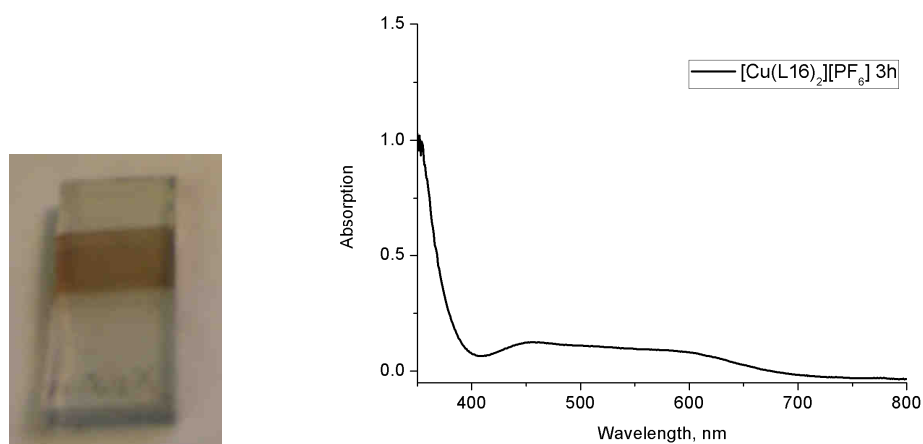
Fig. 120. Coloured TiO$_2$ electrode after being immersed for 3 h in a 0.3mM solution of [Cu(**L16**)$_2$][PF$_6$] in CHCl$_3$.

As far as we know, no dyes have been reported until now using furan rings as anchoring moieties to the semiconductor. This fact is an important discovery, since it offers the possibility to avoid the use of carboxylic and/or phosphonic acid groups, which are difficult to work with due to insolubility problems and the pH dependence of their protonation state.

However, how do complexes bearing furan rings attach to the TiO$_2$ nanoparticles? This is a difficult question to answer, since the IR experiments done in our laboratories were poorly resolved and did not give any insights into the kind of bonds formed. One could think that the oxygen atom of the furan ring binds directly to the titanium atom from the semiconductor; however, the possibility of the furan ring oxidizing and converting into a carboxylic acid group on the surface can not be ruled out.

Looking at the UV-VIS absorption spectra of complexes [Cu(**L9**)$_2$][PF$_6$], [Cu(H$_2$**L10**)$_2$]Cl and [Cu(**L11**)$_2$][PF$_6$] anchored to the TiO$_2$ surface, one can observe that their MLCT absorption maxima appear almost at the same wavelength: 494, 492 and 496 nm, respectively. However, in the case of complexes [Cu(**L16**)$_2$][PF$_6$], [Cu(H$_2$**L17**)$_2$]Cl and [Cu(**L18**)$_2$][PF$_6$] (which have ligands that bear phenyl groups at the 6 and 6´-positions), the MLCT absorption bands differ significantly: 456 and 597, 494 and 604, and 440 and 605 nm. For this reason, it is not possible to establish here how complexes with furan groups anchor to the semiconductor surface, but it is thought that diffuse reflectance infrared spectroscopy could help in this task, as reported in the literature [187].

It was also tested in our laboratories whether methyl ester containing ligands **L23** (tetraethyl 6,6´-dimethyl-2,2´-bipyridine-4,4´-diyldiphosphonate) and **L27** (dimethyl 4,4´-(6,6´´-dimethyl-2,2´:6´,2´´-terpyridine-4,4´´-diyl)dibenzoate) were capable of anchoring to the surface of the semiconductor in order to afterwards form an heteroleptic Cu(I) complex. 1mM solutions of these ligands in CHCl$_3$ were prepared, and two nanocrystalline TiO$_2$ electrodes were dipped into each solution overnight. Then, one of the electrodes from each solution was heated in an oven up to 300°C and dipped overnight in a 0.3mM solution of [Cu(**L1**)$_2$][PF$_6$] in EtOH, for the electrode that had been immersed in a solution of **L23**, and in a 1mM solution of [Cu(CH$_3$CN)$_4$][PF$_6$] in CH$_3$CN, for the electrode that had been immersed in a solution of **L27**. The other electrodes were immersed, without previous heating, also overnight, in a solution of [Cu(**L1**)$_2$][PF$_6$] (for **L23**) and [Cu(CH$_3$CN)$_4$][PF$_6$] (for **L27**) without having been heated.

In both cases, with and without heating, no colouration of the semiconductor surface could be observed, and there was also no UV-VIS absorption. For this reason, it was concluded that

ligands containing methyl ester groups, instead of acid groups, do not bind to the semiconductor surface. This is a little surprising since, as it has been shown in the previous section, some Cu(I) complexes bearing methyl ester functionalities do sensitize TiO_2 effectively and, in some cases, the efficiency obtained with these dyes is comparable with the ones having carboxylic acid groups.

Finally, it was tested if a terpyridine containing carboxylic acid groups was able to form *in situ* Cu(I) heteroleptic complexes. For this experiment, a 1mM solution of H_2**L28** in DMSO was prepared, and a TiO_2 containing electrode was dipped into this solution for 3h. Then, the electrode was immersed overnight into a 1mM solution of $[Cu(CH_3CN)_4][PF_6]$ in CH_3CN. Unfortunately, no colouration of the semiconductor surface could be observed, so again we came to the conclusion that, in contrast to 2,2´-bipyridines, 2,2´:6´,2´´-terpyridine do not form Cu(I) complexes on the surface of the semiconductor.

In the case when terpyridines were employed with the purpose of making this stepwise complexation, $[Cu(CH_3CN)_4][PF_6]$ was used as the washing complex, because it was thought that the ligand could displace three CH_3CN molecules and so form an heteroleptic Cu(I) complex. However, as it has been explained, this did not happen.

VI   Experimental part

6,6´-Dimethyl-2,2´-bipyridine
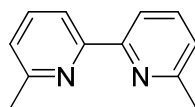
1.6 M Methyl lithium in Et_2O (100 ml, 160.0 mmol) was added through a cannula under nitrogen to a stirring solution of 2,2´-bipyridine (6.24 g, 40.0 mmol) in dry THF (125 ml) cooled to -78 °C. The dark red solution was stirred at this temperature for 30 min an then it was warmed to r.t. After 2 h at this temperature, the mixture was refluxed for 4 h. Then the reaction mixture was

cooled and ice water (50 m) was added very slowly. Following evaporation of THF and extraction of the aqueous phase with CH_2Cl_2 (4 x 70 ml), $MgSO_4$ and MnO_2 (100 g) were added and the mixture was stirred overnight. Then the mixture was filtered over Celite and the solvent was evaporated to afford an orange solid. The solid was passed through a column chromatography (Alox, hexane:acetone 9:1) to yield the product as a white solid (3.55 g, 19.3 mmol, 48 %). Proton NMR agrees well with the values reported in the literature [133].

^{1}H NMR (CDCl$_3$, 250 MHz): δ/ppm 8.17 (d, J = 7.8 Hz, 2H; H^{3A}), 7.68 (t, J = 7.7, 2H; H^{4A}), 7.14 (d, J = 7.6 Hz, 2H; H^{5A}), 2.62 (s, 6H; H$^{\underline{CH3}}$).

4,4´-Dinitro-2,2´-bipyridine-1,1´-dioxide
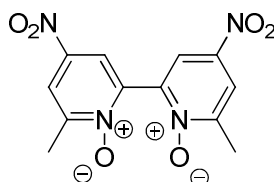
Aqueous 30% H_2O_2 was added to a vigorously stirring solution of 6,6´-dimethyl-2,2´-bipyridine (3.55 g, 19.3 mmol) in acetic acid (15 ml), and the mixture was heated at *ca*. 70 °C overnight. After let it cool down, volatile compounds were removed in vacuo to give a yellow residual oil. The oil was cooled in an ice-salt bath and sulfuric acid (8 ml) was then added. Fumic acid (12 ml) in concentrated sulfuric acid (8 ml) was added to the reaction mixture and it was heated at 100 °C for 2 h. The nitrous gases created during this process were trapped with a 1M K_2CO_3 solution. After cooling the reaction mixture down, it was poured into *ca*. 100 g of ice, and a yellow precipitate formed. Once the ice was melted, the yellow solid was filtered and washed with water (3.86 g, 12.6 mmol, 65 %) and used for the next synthetic step without further purification.

^{1}H NMR (DMSO-d^6, 400 MHz): δ/ppm 8.61 (d, J = 3.4 Hz; 2H), 8.53 (d, J = 3.4 Hz; 2H), 2.48 (s; 6H) [121].

IR: υ /cm^{-1} 3078 (w), 1767 (w), 1736 (w), 1520 (s), 1335 (s), 1281 (s), 1219 (w), 1165 (w), 1095 (w), 1034 (w), 1003 (w), 941 (m), 902 (m), 833 (w), 794 (m), 740 (m), 671 (m), 617 (m).

4,4´-Dibromo-2,2´-bipyridine-1,1´-dioxide
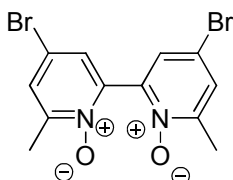
4,4´-Dinitro-2,2´-bipyridine-1,1´-dioxide (3.86 g, 12.6 mmol) was suspended in acetic acid (52 ml). Upon addition of acetyl bromide (30 ml, 0.40 mol), the compound dissolved and the solution was heated at 60 °C for 3 h. The nitrose gases produced during this reaction were trapped with a 1M K_2CO_3 solution with a small current of N_2. Then the reaction was allowed to cool down to r.t. and poured into H_2O (170 mol). The mixture was neutralized with K_2CO_3, and the standing precipitate was filtered and washed with water and ethanol to afford a white solid (2.01 g, 5.39 mmol, 43 %) that was used for the next synthetic step without further purification and/or characterization.

4,4´-Dibromo-2,2´-bipyridine
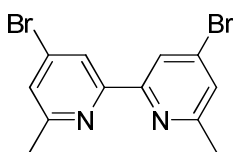
4,4´-Dibromo-2,2´-bipyridine-1,1´-dioxide (2.00 g, 5.37 mmol) was suspended in $CHCl_3$ (35 ml) and cooled down to ca. 0 °C. Upon addition of PBr_3 (2.87 ml, 30.6 mmol), the compound dissolved and the solution was refluxed overnight. After cooling down to room temperature, the yellow mixture was poured into a mixture of ice/H_2O. After the ice melted, the aqueous phase was neutralized with K_2CO_3 and washed with $CHCl_3$ (3 x). The combined organic phases were dried over $MgSO_4$ and the solvent removed in vacuo to afford a beige solid that was purified by

column chromatography (Alox, CHCl$_3$) to yield the product as a white solid (1.59 g, 4.67 mmol, 87 %). The ^{1}H NMR spectrum agrees well with the one given in the literature [121].

^{1}H NMR (CDCl$_3$, 250 MHz): δ/ppm 8.39 (d, J = 1.2 Hz, 2H; H^{3A}), 7.36 (d, J = 1.5 Hz, 2H; H^{5A}), 2.60 (s, 6H; H^{CH3}).

(1E,5E)-1,6-Diphenylhexa-1,5-diene-3,4-dione
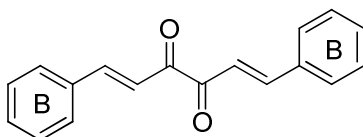
Piperidine (1 ml, 100 mmol) and glacial acetic acid (0.6 ml, 100 mmol) were added to a stirring solution of 2,3-butadione (4.4 ml, 50 mmol) and benzaldehyde (20.3 ml, 200 mmol) in methanol (25 ml). The mixture was heated under reflux for 2 h and then the methanol and unreacted 2,3-butadione were removed in vacuo. The solution was placed in a freezer overnight and the orange crystals that had formed were isolated by filtration (2.14 g, 8.19 mmol, 17 %). [190]

^{1}H NMR (CDCl$_3$, 250 MHz): δ/ppm 7.87 (d, J = 16.2 Hz, 2H; H$^{CH=CH-CO}$), 7.67 (dd, J = 6.6 Hz, 4H; H^{2B}), 7.45 (m, 8H; H$^{CH=CH-CO}$, H^{3B}, H^{4B}).

Anal. Calc. for C$_{18}$H$_{14}$O$_2$: C, 82.42; H, 5.38; found: C, 81.50; H, 5.31 %.

(1E,5E)-1,6-Bis[4-(methoxycarbonyl)phenyl]hexa-1,5-diene-3,4-dione
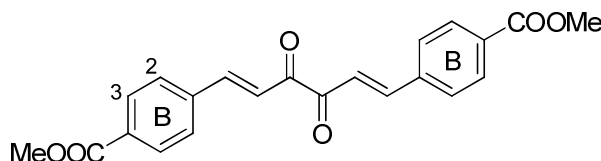
Piperidine (0.5 ml, 5.0 mmol) and acetic acid (0.3 ml, 5.0 mmol) were added to a stirring solution of methyl 4-formylbenzoate (1.55 g, 9.0 mmol) and 2,3-butanedione (0.4 ml, 4.5 mmol) in methanol (15 ml). The mixture was refluxed for 6 h, while bright orange crystals started to

form. After cooling to room temperature, the crystals were filtered and washed with methanol (25 ml) to yield the title compound (0.42 g, 25 %) that was used without further purification. The ^{1}H NMR matched well the one reported in the literature [124].

^{1}H NMR (DMSO-d[6], 200 MHz): δ/ppm 8.03 (d, J = 8.0 Hz, 4H; H[3B]), 7.95 (d, J = 8.0 Hz, 4H; H[2B]), 7.84 (d, J = 16.0 Hz, 2H; H$^{C\underline{H}=CH-CO}$), 7.50 (d, J = 16.0 Hz, 2H; H$^{CH=C\underline{H}-CO}$), 3.88 (s, 6H; H$^{COOC\underline{H}3}$).

(1E,5E)-1,6-Di(furan-2-yl)hexa-1,5-diene-3,4-dione
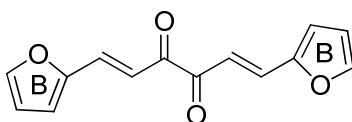
Furfuraldehyde (21.5 ml, 260 mmol) and 2,3-butanedione (11.35 ml, 130 mmol) were stirred in ethanol (20ml) with 4 drops of piperidine at room temperature for 7 days. After this time orange needles were filtered and washed with ethanol (3.677 g, 15.2 mmol, 12 %). This compound was synthetised according to literature, [127] however, ^{1}H and ^{13}C NMR spectra have not been reported before.

^{1}H NMR (CDCl[3], 500 MHz): δ/ppm 7.61 (d, J = 15.9 Hz, 2H; H$^{C\underline{H}=CH-CO}$), 7.57 (dd, J = 0.4 Hz, J = 1.7 Hz, 2H; H[5B]), 7.31 (d, J = 15.9 Hz, 2H; H$^{CH=C\underline{H}-CO}$), 6.80 (d, J = 3.5 Hz, 2H; H[3B]), 6.53 (dd, J = 1.8 Hz, J = 3.5 Hz, 2H; H[4B]).

^{13}C NMR (CDCl[3], 126 MHz): δ/ppm 188.73 (C^{CO}), 151.62 (C[2B]), 146.16 (C[5B]), 133.13 (C$^{CH=CH-CO}$), 117.89 (C[3B]), 117.44 (C$^{CH=\underline{C}H-CO}$), 113.13 (C[4B]).

MS (EI): m/z 242.1 [M]$^+$ (calc. 242.1), 121.0 [M/2]$^+$ (calc. 121.0).

IR: υ /cm^{-1} 3123 (w), 1662 (m), 1585 (m), 1543 (m), 1471 (m), 1388 (w), 1289 (m), 1265 (m), 1200 (m), 1068 (w), 995 (m), 974 (s), 926 (s), 881 (m), 850 (m), 831 (m), 811 (m), 746 (s), 637 (s), 588 (s), 548 (s).

Anal. Calc. for $C_{14}H_{10}O_4$: C, 69.42; H, 4.16; found: C, 69.23; H, 4.20 %.

Dimethyl 4,4´-(1*E*,1´*E*)-3,3´-(pyridine-2,6-diyl)bis(3-oxoprop-1-ene-3,1-diyl)dibenzoate
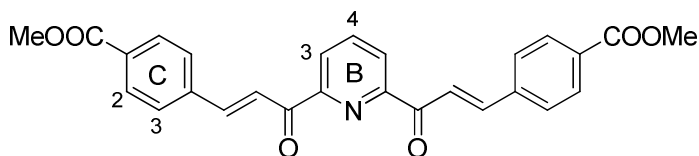
A solution of 2,6-diacetylpyridine (2.00 g, 12.2 mmol) and diethylamine (4 ml) in 1-propanol (40 ml) was heated to reflux. Then a solution of methyl 4-formylbenzoate (4.00 g, 24.5 mmol) dissolved in hot 1-propanol (20 ml) was added to it by means of a dropping funnel. This mixture was refluxed for 12 h. After cooling down to room temperature a beige solid was filtered off and washed with 1-propanol (2.30 g, 5.06 mmol, 42 %). Similar compounds to this one have been reported in the literature [153, 191] .

^{1}H NMR (CDCl$_3$, 400 MHz): δ/ppm 8.47 (d, *J* = 16.1 Hz, 2H; H$^{\underline{CH}=CH-CO}$), 8.41 (d, *J* = 7.8 Hz, 2H; H^{3B}), 8.13 (d, *J* = 8.2 Hz, 4H; H^{2C}), 8.03 (d, *J* = 16.2 Hz, 2H; H$^{CH=\underline{CH}-CO}$), 8.01 (m, 1H; H^{4B}) 7.80 (d, *J* = 8.4 Hz, 4H; H^{3C}), 3.98 (s, 6H; H$^{COOC\underline{H}3}$).

MS (FAB): m/z 455.2 [M]$^+$ (calc. 455.1).

IR: υ /cm^{-1} 2955 (w), 1720 (s), 1674 (m), 1612 (s), 1566 (m), 1435 (m), 1281 (s), 1186 (m), 1103 (s), 1026 (m), 987 (m), 818 (m), 764 (s), 617 (m).

Anal. Calc. for $C_{27}H_{21}NO_6$: C, 71.20; H, 4.65; N, 3.08; found: C, 71.14; H, 4.78; N, 3.17 %.

6,6´-Dimethyl-4,4´-diphenyl-2,2´-bipyridine (L1)
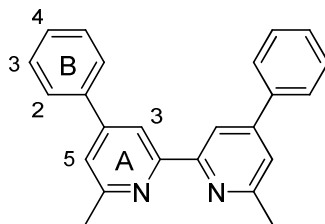
(1*E*,5*E*)-1,6-diphenylhexa-1,5-diene-3,4-dione (0.50 g, 1.9 mmol), 1-acetonylpyridinium chloride (0.65 g, 3.81 mmol) and ammonium acetate (2.00 g) were refluxed in ethanol (20 ml) for 12 h. After letting the solution cool down to room temperature the beige solid that had formed was filtered. After flash column chromatography (Alox, $CHCl_3$) and removal of solvent from the fraction, a white-beige solid was obtained. This was recrystallised from $CHCl_3$/hexane to yield a white crystalline solid (0.41 g, 1.22 mmol, 64 %). ^{1}H NMR spectrum agrees well with the values given in the literature. [121] ^{13}C NMR spectrum has not been reported before.

^{1}H NMR (CDCl$_3$, 500 MHz): δ/ppm 8.48 (s, 2H; H^{3A}), 7.76 (d, *J* = 7.8 Hz, 4H; H^{2B}), 7.50 (t, *J* = 7.5 Hz, 4H; H^{3B}), 7.44 (t, *J* = 7.2 Hz, 2H; H^{4B}), 7.41 (s, 2H; H^{5A}), 2.71 (s, 6H; H$^{\underline{CH3}}$).

^{13}C NMR (CDCl$_3$, 126 MHz): δ/ppm 158.6 (C^{6A}), 156.7 (C^{2A}), 149.7 (C^{4A}), 139.0 (C^{1B}), 129.06 (C^{3B}), 128.91 (C^{4B}), 127.3 (C^{2B}), 121.3 (C^{5A}), 116.8 (C^{3A}), 24.9 (C$^{\underline{CH3}}$).

MS (EI): m/z 336.2 [M]$^+$ (calc. 336.2), 168.1 [M/2]$^+$ (calc. 168.1).

IR: υ/cm^{-1} 3060 (w), 3032 (w), 2984 (w), 2960 (w), 2917 (w), 1745 (w), 1589 (m), 1546 (m), 1493 (w), 1445 (w), 1385 (m), 1366 (w), 1210 (w), 1071 (w), 1027 (w), 998 (w), 898 (w), 869 (m), 762 (s), 740 (m), 692 (s), 620 (s), 601 (m), 502 (m), 444 (s), 424 (s), 414 (s).

UV-VIS (CHCl$_3$): λ$_{max}$/nm (ε/M^{-1} cm^{-1}) 245 (40000), 303 (13500).

Anal. Calc. for $C_{24}H_{20}N_2$: C, 85.68; H, 5.99; N, 8.33; found: C, 84.97; H, 6.03; N, 8.17 %.

4,4´,6,6´-Tetraphenyl-2,2´-bipyridine (L2)
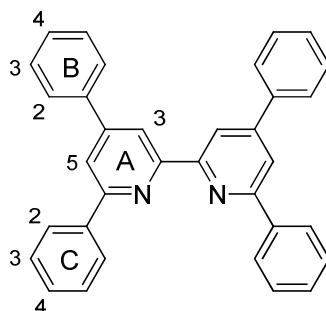
(1E,5E)-1,6-Diphenylhexa-1,5-diene-3,4-dione (0.60 g, 2.30 mmol), phenacylpyridinium bromide (1.28 g, 4.60 mmol) and ammonium acetate (1 g) were refluxed in ethanol (20 ml) for 18 h. After letting the solution cool down to room temperature, a white-beige solid was filtered and washed with ethanol (0.53 g, 1.16 mmol, 50 %). ^{1}H NMR spectrum agrees well with the values reported in the literature [192]. ^{13}C NMR spectrum has not been reported before.

^{1}H NMR (CDCl$_3$, 500 MHz): δ/ppm 8.88 (s, 2H; H^{3A}), 8.24 (d, J = 7.3 Hz, 4H; H^{2C}), 8.02 (s, 2H; H^{5A}), 7.86 (d, J = 7.2 Hz, 4H; H^{2B}), 7.56 (m, 8H; H^{3B}, H^{3C}), 7.49 (m, 4H; H^{4B}, H^{4C}).

^{13}C NMR (CDCl$_3$, 126 MHz): δ/ppm 157.23 (C^{6A}), 156.72 (C^{2A}), 150.43 (C^{4A}), 139.69 (C^{1C}), 139.27 (C^{1B}), 129.23 (C^{3B}/C^{3C}), 129.22 (C^{4B}/C^{4C}), 129.10 (C^{4B}/C^{4C}), 128.92 (C^{3B}/C^{3C}), 127.50 (C^{2B}), 127.30 (C^{2C}), 118.91 (C^{5A}), 118.22 (C^{3A}).

MS (EI): m/z 460.2 [M]$^+$ (calc. 460.2), 230.1 [M/2]$^+$ (calc. 230.1).

IR: υ/cm^{-1} 3056 (w), 3034 (w), 1591 (m), 1546 (m), 1492 (m), 1381 (m), 1078 (w), 1028 (w), 871 (m), 761 (s), 731 (m), 690 (s), 640 (m).

UV-VIS (CHCl$_3$): λ$_{max}$/nm (ε/M^{-1} cm^{-1}) 258 (65000), 319 (14000).

Anal. Calc. for C$_{34}$H$_{24}$N$_2$: C, 86.96; H, 5.37; N, 5.97; found: C, 87.03; H, 5.22; N, 6.12 %.

Dimethyl 4,4´-(6,6´-dimethyl-2,2´-bipyridine-4,4'-diyl)dibenzoate (L3)
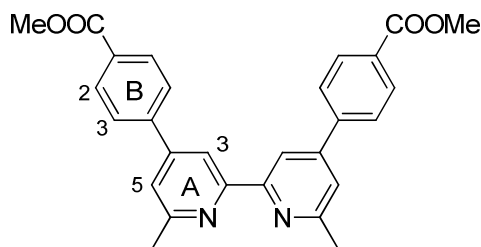
(1*E*,5*E*)-1,6-Bis[4-(methoxycarbonyl)phenyl]hexa-1,5-diene-3,4-dione (0.500 g, 1.32 mmol), 1-acetonylpyridinium chloride (0.463 g, 2.70 mmol) and ammonium acetate (1.00 g) were refluxed in ethanol (15 ml) for 18 h. After letting the solution cool down to room temperature, a beige solid was filtered and washed with ethanol. After column chromatography (SiO$_2$) using CH$_2$Cl$_2$ as eluant, followed by CH$_2$Cl$_2$:MeOH 98:2 and then CH$_2$Cl$_2$:MeOH 95:5, a white-beige solid was isolated after removal of solvent (CH$_2$Cl$_2$:MeOH 95:5, Rf = 0.28). Finally flash chromatography (Alox) yielded **L3** as a white solid after removal of solvent (0.313 g, 0.692 mmol, 52 %).

^{1}H NMR (CDCl$_3$, 500 MHz): δ/ppm 8.52 (d, *J* = 0.7 Hz, 2H; H^{3A}), 8.17 (d, *J* = 8.3 Hz, 4H; H^{2B}), 7.83 (d, *J* = 8.4 Hz, 4H; H^{3B}), 7.43 (d, *J* = 1.0 Hz, 2H; H^{5A}), 3.97 (s, 6H; H$^{COOC\underline{H}3}$), 2.73 (s, 6H; H$^{C\underline{H}3}$).

MS (EI): m/z 452.2 [M]$^+$ (calc. 452.2).

IR: υ/cm^{-1} 3006 (w), 2951 (w), 2924 (w), 1714 (s), 1593 (s), 1547 (m), 1427 (m), 1379 (m), 1277 (s), 1182 (m), 1107 (s), 1076 (m), 1014 (m), 964 (m), 889 (w), 879 (m), 848 (s), 824 (m), 767 (s), 747 (m), 735 (m), 700 (s), 664 (m), 597 (w), 579 (w), 556 (w), 514 (s), 471 (s), 447 (m), 434 (m), 418 (m).

UV-VIS (CHCl$_3$): λ$_{max}$/nm (ε/M^{-1} cm^{-1}) 263 (28000), 312 (9000).

Anal. Calc. for C$_{28}$H$_{24}$N$_2$O$_4$·0.4H$_2$O: C, 73.16; H, 5.44; N, 6.09; found: C, 73.13; H, 5.33; N, 5.80 %.

4,4´-(6,6´-Dimethyl-2,2´-bipyridine-4,4'-diyl)dibenzoic acid (H₂L4)
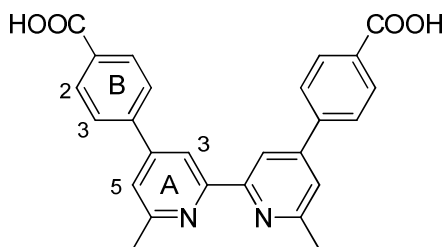
LiOH (52.9 mg, 2.210 mmol) dissolved in H_2O (0.7 ml) was added to a solution of **L3** (0.100 g, 0.221 mmol) in THF (5.3 ml). The resulting mixture was heated to reflux for 12 h. After letting the solution cool to room temperature, the pH was adjusted to 2 with 2M HCl. The resulting precipitate was filtered off and successively washed with H_2O and ether to afford pure **L4** as a white solid (0.426 g, 0.165 mmol, 75 %).

^{1}H NMR (TFA-d^1, 400 MHz): δ/ppm 8.78 (s, 2H; H^{3A}), 8.47 (d, J = 6.3 Hz, 4H; H^{2B}), 8.42 (s, 2H; H^{5A}), 8.08 (d, J = 6.9 Hz, 4H; H^{3B}), 3.14 (s, 6H; H$^{\underline{CH3}}$).

IR: υ/cm^{-1} 3391 (w), 2988 (w), 2879 (w), 2668 (w), 2540 (w), 1686 (s), 1596 (s), 1547 (m), 1424 (m), 1386 (m), 1320 (m), 1294 (m), 1241 (w), 1214 (w), 1181 (w), 1107 (w), 1072 (w), 1016 (w), 934 (w), 900 (w, 854 (s), 773 (m), 732 (m), 695 (m).

UV-VIS (DMSO): λ$_{max}$/nm (ε/M^{-1} cm^{-1}) 265 (24000), 316 (6600).

Anal. Calc. for $C_{26}H_{20}N_2O_4$·5LiOH: C, 57.38; H, 4.63; N, 5.15; found: C, 57.33; H, 4.46; N, 4.92 %.

Dimethyl 4,4´-(6,6´-diphenyl-2,2´-bipyridine-4,4´-diyl)dibenzoate (L5)
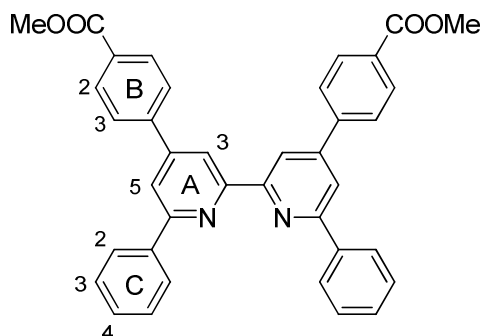
(1*E*,5*E*)-1,6-Bis[4-(methoxycarbonyl)phenyl]hexa-1,5-diene-3,4-dione (0.300 g, 0.793 mmol), phenacylpyridinium bromide (0.441 g, 1.587 mmol) and ammonium acetate (1.00 g) were refluxed in ethanol (10 ml) for 18 h. After letting the solution cool down to room temperature, a beige solid was filtered and washed with ethanol. After column chromatography (Alox) with CHCl$_2$ as eluant **L5** (Rf = 0.92) was obtained as a white solid after removal of solvent (0.148 g, 0.257 mmol, 32 %).

^{1}H NMR (CDCl$_3$, 500 MHz): δ/ppm 8.88 (d, *J* = 1.3 Hz, 2H; H^{3A}), 8.23 (d, *J* = 8.1 Hz, 8H; H^{2B}, H^{2C}), 8.03 (d, *J* = 1.3 Hz, 2H; H^{5A}), 7.92 (d, *J* = 8.3 Hz, 4H; H^{3B}), 7.56 (t, *J* = 7.5 Hz, 4H; H^{3C}), 7.49 (t, *J* = 7.3 Hz, 2H; H^{4C}), 3.99 (s, 6H; H$^{COOC\underline{H}3}$).

^{13}C NMR (CDCl$_3$, 126 MHz): δ/ppm 166.9 (C$^{\underline{C}OO}$), 157.6 (C^{6A}), 156.7 (C^{2A}), 149.4 (C^{1B}/C^{4A}), 143.6 (C^{4B}), 139.4 (C^{1C}), 130.5 (C^{2B}), 129.47 (C^{4C}), 129.01 (C^{3C}), 127.53 (C^{3B}), 127.30 (C^{2C}), 119.0 (C^{5A}), 118.2 (C^{3A}), 52.5 (C$^{COO\underline{C}H3}$). One carbon peak (C^{1B}/C^{4A}) is not observed.

MS (EI): m/z 576.2 [M]$^+$ (calc. 576.2), 288.1 [M/2]$^+$ (calc. 288.1).

IR: υ/cm^{-1} 3043 (w), 2953 (w), 1728 (m), 1716 (m), 1593 (m), 1544 (m), 1497 (w), 1438 (m), 1383 (m), 1321 (w), 1286 (m), 1272 (s), 1190 (m), 1109 (m), 1043 (w), 1025 (w), 1015 (m), 970 (w), 922 (w), 886 (w), 851 (m), 809 (w), 767 (s), 736 (m), 687 (s), 662 (m).

UV-VIS (CHCl$_3$): λ$_{max}$/nm (ε/M^{-1} cm^{-1}) 269 (60000), 324 (11000).

Anal. Calc. for $C_{38}H_{28}N_2O_4 \cdot 0.5H_2O$: C, 77.93; H, 4.99; N, 4.78; found: C, 78.08/77.67; H, 5.08/5.11; N, 4.58/4.55 %.

4,4´-(6,6´-Diphenyl-2,2´-bipyridine-4,4´-diyl)dibenzoic acid (H$_2$L6)
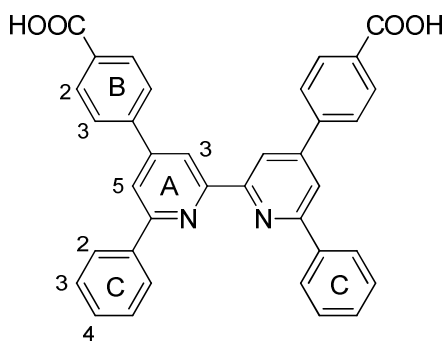
LiOH (36.8 mg, 1.536 mmol) dissolved in H$_2$O (0.5 ml) was added to a solution of **L5** (90.0 mg, 0.156 mmol) in THF (5 ml). The resulting mixture was heated to reflux for 6 h. After letting the solution cool to room temperature, the pH was adjusted to 2 with 2M HCl. The resulting precipitate was filtered off and successively washed with H$_2$O and ether to afford pure **L6** as a white solid (60.0 mg, 0.109 mmol, 71 %).

^{1}H NMR (TFA-d^1, 500 MHz): δ/ppm 8.82 (s, 2H; H^{3A}), 8.66 (s, 2H; H^{5A}), 8.40 (d, J = 7.3 Hz, 4H; H^{2B}), 8.07 (d, J = 7.3 Hz, 4H; H^{3B}), 7.94 (d, J = 7.0 Hz, 4H; H^{2C}), 7.77 (t, J = 7.0 Hz, 2H; H^{4C}), 7.67 (t, J = 7.0 Hz, 4H; H^{3C}).

MS (EI): m/z 548.2 [M]$^+$ (calc. 548.2), 503.2 [M-COOH]$^+$ (calc. 503.2), 274.1 [M/2]$^+$ (calc. 274.1).

IR: υ/cm^{-1} 3065.2 (w), 3035.1 (w), 2977.6 (w), 2851.2 (w), 2670.2 (w), 2549.7 (w), 1688.5 (s), 1591.7 (m), 1573.9 (m), 1543.4 (m), 1496.6 (w), 1424.8 (m), 1382.2 (m), 1320.5 (m), 1296.4 (s), 1189.4 (w), 1113.9 (w), 1080.7 (w), 1022.4 (w), 1014.4 (w), 933.1 (w), 888.5 (w), 851.0 (s), 797.1 (w), 767.5 (s), 730.7 (m), 689.3 (s).

UV-VIS (DMSO): λ$_{max}$/nm (ε/M^{-1} cm^{-1}) 271 (60000), 328 (11000).

Anal. Calc. for $C_{36}H_{24}N_2O_4 \cdot 0.9\ H_2O$: C, 76.56; H, 4.60; N, 4.96; found: C, 76.62; H, 4.46; N, 4.95 %.

Diethyl 6,6´-dimethyl-2,2´-bipyridine-5,5´-dicarboxylate (L7)
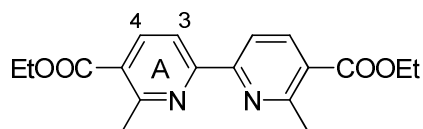
Ethyl-2-methylnicotinate (9.34 ml, 60.5 mmol) and Pd/C 5 % (1.35 g) were refluxed for 10 days under an inert atmosphere. After letting the mixture cool down, acetone (20 ml) was added and the Pd/C was filtered off. The filtrate was evaporated and the brown-black solid left in the fridge overnight. The day after, it was recrystallized from methanol to obtain white-beige needles (0.307 g, 0.93 mmol, 1.5 %).

^{1}H NMR (CDCl$_3$, 500 MHz): δ/ppm 8.41 (d, J = 8.2 Hz, 2H; H^{3A}), 8.33 (d, J = 8.2 Hz, 2H; H^{4A}), 4.41 (q, J = 7.1 Hz, 4H; H$^{C\underline{H}2CH3}$), 2.92 (s, 6H; H$^{C\underline{H}3}$), 1.43 (t, J = 7.1 Hz, 6H; H$^{CH2C\underline{H}3}$).

^{13}C NMR (CDCl$_3$, 126 MHz): δ/ppm 166.5 (C$^{\underline{C}OO}$), 159.5 (C^{6A}), 156.6 (C^{2A}), 139.5 (C^{4A}), 125.7 (C^{5A}), 118.8 (C^{3A}), 61.3 (C$^{\underline{C}H2CH3}$), 25.1 (C$^{\underline{C}H3}$), 14.3 (C$^{CH2\underline{C}H3}$).

MS (MALDI): m/z 330.1 [M+2H]$^+$ (calc. 330.4 for [M+2H]$^+$).

IR: υ/cm^{-1} 2976 (w), 2932 (w), 1716 (s), 1583 (s), 1547 (m), 1444 (m), 1428 (m), 1390 (m), 1353 (m), 1273 (s), 1249 (s), 1139 (m), 1114 (m), 1078 (s), 1020 (m), 986 (m), 850 (s), 773 (s), 723 (m).

Anal. Calc. for $C_{18}H_{20}N_2O_4$: C, 65.84; H, 6.14; N, 8.53; found: C, 65.89; H, 6.20; N, 8.54 %.

6,6´-Dimethyl-2,2´-bipyridine-5,5´-dicarboxylic acid (H$_2$L8)
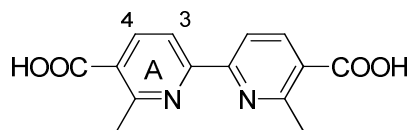
L7 (0.27 g, 0.82 mmol) was partially dissolved in a H$_2$O:EtOH 1:1 (20 ml) solution which contained KOH (0.46 g, 8.2 mmol). The mixture was refluxed for 12 h. After letting the solution cool down, it was partially evaporated under reduced pressure and the pH was adjusted to 2 with 1M HCl. A white precipitate was filtered off (0.2213 g, 0.8134 mmol, 99 %).

^{1}H NMR (DMSO-d^6, 500 MHz): δ/ppm 8.35 (m, 4H; H^{3A}, H^{4A}), 2.82 (s, 6H; H$^{\underline{CH3}}$).

^{13}C NMR (DMSO-d^6, 126 MHz): δ/ppm 167.6 (C^{COO}), 158.6 (C^{6A}), 155.5 (C^{2A}), 139.7 (C^{4A}), 126.4 (C^{5A}), 118.5 (C^{3A}), 24.7 (C$^{\underline{CH3}}$).

MS (EI): m/z 272.1 [M]$^+$ (calc. 272.1).

IR: υ/cm^{-1} 3000 (w), 2893 (w), 2795 (w), 2645 (w), 2526 (w), 1687 (s), 1582 (s), 1544 (s), 1435 (m), 1404 (s), 1379 (m), 1349 (w), 1284 (s), 1258 (s), 1219 (m), 1140 (m), 1118 (m), 1079 (m), 1033 (w), 986 (w), 926 (m), 851 (s), 774 (s), 666 (s), 641 (m), 621 (w).

UV-VIS (MeOH): λ$_{max}$/nm (ε/M^{-1} cm^{-1}) 212 (13000), 250 (13500), 305 (26000).

Anal. Calc. for C$_{14}$H$_{12}$N$_2$O$_4$·0.5H$_2$O: C, 59.78; H, 4.66; N, 9.96; found: C, 59.44/59.50; H, 4.61/4.58; N, 9.90/9.82 %.

4,4´-Di(furan-2-yl)-6,6´-dimethyl-2,2´-bipyridine (L9)
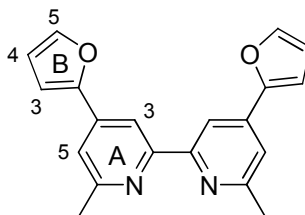
(1*E*,5*E*)-1,6-Di(furan-2-yl)hexa-1,5-diene-3,4-dione (0.5 g, 2.066mmol), 1-acetonylpyridinium chloride (0.708 g, 4.132 mmol) and ammonium acetate (1.00 g) were refluxed in methanol (20 ml) for 12 h. After letting the solution cool down to room temperature, a white-beige solid was filtered and washed with cold methanol (0.3607 g, 1.14 mmol, 55 %). The ^{1}H NMR spectrum measured was slightly different to the one reported in the literature [121]. ^{13}C NMR spectrum has not previously been reported.

^{1}H NMR (CDCl$_3$, 500 MHz): δ/ppm 8.61 (s, 2H; H^{3A}), 7.58 (dd, *J* = 1.7 Hz, *J* = 0.6 Hz, 2H; H^{5B}), 7.49 (d, *J* = 1.1 Hz, 2H; H^{5A}), 7.12 (d, *J* = 1.44 Hz, 2H; H^{3B}), 6.56 (dd, *J* = 1.7 Hz, *J* = 3.5 Hz, 2H; H^{4B}), 2.75 (s, 6H; H$^{\underline{CH3}}$).

^{13}C NMR (CDCl$_3$, 126 MHz): δ/ppm 158.3 (C^{6A}), 151.5 (C^{2B}), 143.9 (C^{5B}), 139.4 (C^{4A}), 117.6 (C^{5A}), 113.7 (C^{3A}), 112.3 (C^{4B}), 109.9 (C^{3B}), 24.3 (C$^{\underline{CH3}}$). C^{2A} was not observed.

MS (EI): m/z 316.1 [M]$^+$ (calc. 316.1), 158.0 [M/2]$^+$ (calc. 158.1).

IR: υ/cm^{-1} 3116 (w), 2370 (w), 1604 (m), 1574 (m), 1549 (s), 1485 (m), 1411 (m), 1374 (m), 1360 (m), 1218 (m), 1161 (m), 1016 (s), 985 (m), 930 (m), 866 (m), 848 (m), 814 (s), 744 (s), 700 (s), 669 (m), 595 (s).

Anal. Calc. for C$_{20}$H$_{16}$N$_2$O$_2$·0.3H$_2$O: C, 74.66; H, 5.20; N, 8.71; found: C, 74.52; H, 5.22; N, 8.60 %.

6,6´-Dimethyl-2,2´-bipyridine-4,4´-dicarboxylic acid (H₂L10)
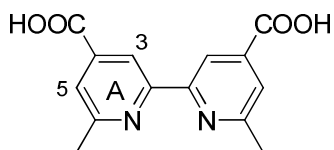
KMnO₄ (40.8 g, 258.13 mmol) was added to a warm mixture of **L9** (6.30 g, 19.93 mmol), *t*-BuOH (1150 ml) and H_2O (230 ml). After refluxing overnight, the mixture was filtered through *Celite*. The solution was evaporated to approx. 200 ml, the pH adjusted to 2 with 2M HCl, and the precipitated white product filtered (1.94 g, 7.13 mmol, 36%). The ^{1}H NMR spectrum agrees well with that given in the literature [121]. ^{13}C NMR spectrum has not previously been reported.

^{1}H NMR (DMSO-d[6], 500 MHz): δ/ppm 8.64 (s, 2H; H[3A]), 7.77 (s, 2H; H[5A]), 2.67 (s, 6H; H$^{\underline{CH3}}$).

^{13}C NMR (DMSO-d[6], 126 MHz): δ/ppm 166.3 (C[COO]), 159.3 (C[6A]), 155.1 (C[2A]), 139.4 (C[4A]), 122.8 (C[5A]), 116.8 (C[3A]), 24.2 (C$^{\underline{CH3}}$).

MS (EI): m/z 272.1 [M]⁺ (calc. 272.1).

IR: υ/cm⁻¹ 3093.6 (w), 2916.2 (w), 2854.5 (w), 2615.3 (w), 2545.9 (w), 1697.2 (s), 1566.1 (s), 1427.0 (s), 1396.4 (m), 1296.1 (s), 1218.9 (m), 1095.5 (w), 910.3 (m), 763.8 (m).

UV-VIS (MeOH): λ_{max}/nm (ε/M⁻¹ cm⁻¹) 218 (71200), 241 (39000), 306 (31900).

Anal. Calc. for $C_{14}H_{12}N_2O_4$: C, 61.76; H, 4.44; N, 10.29; found: C, 61.38/61.17; H, 5.03/4.90; N, 10.52/10.38 %.

Dimethyl 6,6´-dimethyl-2,2´-bipyridine-4,4´-dicarboxylate (L11)
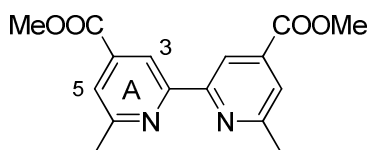
Conc. H_2SO_4 (2 ml) was added to a suspension of **L10** (1.00 g, 3.70 mmol) in MeOH (100ml). The solution was refluxed for 12 h. When the solution cooled down to room temperature, some of the solvent was evaporated under reduced pressure to approx. 60 ml and the pH was adjusted to 7 with 1M NaOH. The white solid that precipitated was filtered and washed with water and ether (0.77 g, 2.59 mmol, 70 %). The ^1H and ^{13}C NMR spectra agree well with those reported in the literature [193].

^1H NMR (CDCl$_3$, 500 MHz): δ/ppm 8.73 (s, 2H; H^{3A}), 7.75 (s, 2H; H^{5A}), 3.99 (s, 6H; H$^{COOC\underline{H}3}$), 2.72 (s, 6H; H$^{\underline{CH3}}$).

^{13}C NMR (CDCl$_3$, 126 MHz): δ/ppm 166.2 (C$^{\underline{COO}}$), 159.4 (C^{6A}), 156.4 (C^{2A}), 138.8 (C^{4A}), 122.8 (C^{5A}), 117.9 (C^{3A}), 52.8 (C$^{COO\underline{CH3}}$), 24.8(C$^{\underline{CH3}}$).

MS (EI): m/z 300.1 [M]$^+$ (calc. 300.1).

IR: υ/cm^{-1} 3076.3 (w), 2956.7 (w), 1728.1 (m), 1701.1 (m), 1564.2 (m), 1429.2 (m), 1390.6 (m), 1272.9 (s), 1249.8 (s), 1211.2 (s), 1139.9 (m), 1062.7 (m), 999.1 (s), 885.3 (w).

UV-VIS (CHCl$_3$): λ$_{max}$/nm (ε/M^{-1} cm^{-1}) 310 (22400), 321 (20000).

Anal. Calc. for $C_{16}H_{16}N_2O_4$: C, 63.99; H, 5.37; N, 9.33; found: C, 64.00; H, 5.32; N, 9.34 %.

4,4´-Bis(hydroxymethyl)-6,6´-dimethyl-2,2´-bipyridine (L12)
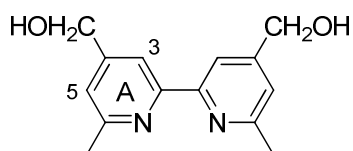
To a stirred suspension of **L11** (2 g, 6.66 mmol) in THF (125 ml) at -40°C, LiAlH$_4$ (1.7 ml, 6.69 mmol) was added. Within 1 h the temperature of the mixture was raised to -10°C, and more LiAlH$_4$ (1.7 ml, 6.69 mmol) was added. Stirring for 2 h at room temperature completed the

reaction. At 0°C H$_2$O (0.5 ml) was added dropwise very carefully followed by 1M NaOH (2 ml). After 15 min. the suspension was refluxed for 5 min and stirred at room temperature for 12 h. The white Al(OH)$_3$ precipitate was filtered off. Evaporation of the solvent yielded a yellow oil that was used without further purification (1.39 g, 5.72 mmol, 86 %). Both ^{1}H and ^{13}C NMR spectra agree well with the values reported in the literature [131]. However, not all ^{13}C signals were assigned; consequently, NMR data are reported in this thesis with full assignments.

^{1}H NMR (CDCl$_3$, 500 MHz): δ/ppm 8.02 (s, 2H; H^{3A}), 7.13 (s, 2H; H^{5A}), 4.70 (s, 4H; H^{CH2OH}), 2.59 (s, 6H; H^{CH3}).

^{13}C NMR (CDCl$_3$, 126 MHz): δ/ppm 158.2 (C^{6A}), 155.9 (C^{2A}), 151.3 (C^{4A}), 120.6 (C^{5A}), 116.1 (C^{3A}), 63.5 (C$^{\underline{CH2OH}}$), 24.5 (C$^{\underline{CH3}}$).

6,6´-Dimethyl-2,2´-bipyridine-4,4´-dicarbaldehyde (L13)
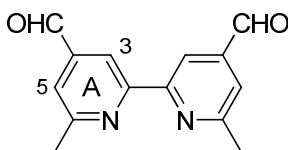
Oxalyl chloride (1.46 ml, 17 mmol) was added to dry CH$_2$Cl$_2$ (74 ml) at -60°C. DMSO (2.0 ml, 28.27 mmol) in CH$_2$Cl$_2$ (3.7 ml) was added dropwise over 5 min. under an inert atmosphere. After 10 min. a solution of **L12** (1.38 g, 5.65 mmol) in THF (74 ml) was added within 10 min. The temperature was kept under -40°C during this addition. After 45 min. at -50°C, Et$_3$N (7.4 ml, 50.5 mmol) was added dropwise over 5 min. The temperature was raised over a period of 1h to 0°C. Addition of CHCl$_3$ (100 ml) and a half-saturated aq. NH$_4$Cl solution (100 ml) gave two phases. The organic layer was separated and the aq. layer was washed twice with CHCl$_3$ (40 ml). Washing the combined organic layers with saturated aq. NaCl solution (100 ml) and water (100 ml) and drying over MgSO$_4$ yielded, after evaporation, a light brown solid which was used without further purification (1.21 g, 5.04 mmol, 89 %). The ^{1}H and ^{13}C NMR spectra agree well with the values reported in the literature [131], but they are reported in this thesis with full assignments.

^{1}H NMR (CDCl$_3$, 500 MHz): δ/ppm 10.17 (s, 2H; H$^{\underline{CHO}}$), 8.68 (s, 2H; H^{3A}), 4.61 (s, 2H; H^{5A}), 2.76 (s, 6H; H$^{\underline{CH3}}$).

^{13}C NMR (CDCl$_3$, 126 MHz): δ/ppm 192.1 (C$^{\underline{CHO}}$), 159.9 (C^{6A}), 156.6 (C^{2A}), 143.0 (C^{4A}), 121.3 (C^{5A}), 118.0 (C^{3A}), 24.6 (C$^{\underline{CH3}}$).

IR: υ/cm^{-1} 2922 (w), 2852 (w), 1707 (s), 1595 (m), 1568 (s), 1383 (s), 1259 (s), 1169 (s), 1103 (m), 1012 (w), 989 (m), 955 (w), 875 (s), 814 (w), 769 (w), 669 (s).

(2*E*,2´*E*)-Dimethyl 3,3´-(6,6´-dimethyl-2,2´-bipyridine-4,4´-diyl)diacrylate (L14)
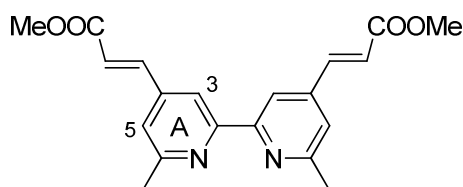
A mixture of **L13** (0.30 g, 1.24 mmol) and Ph$_3$P=CHCO$_2$Me (1.04 g, 3.10 mmol) in dry toluene (25 ml) was refluxed for 18h. After the solution cooled down to room temperature, the solvent was removed under reduced pressure and the brown residue was purified by column chromatography (Alox, CH$_2$Cl$_2$) to yield **L14** as a white solid after removal of solvent (0.322 g, 0.914 mmol, 74 %).

^{1}H NMR (CDCl$_3$, 500 MHz): δ/ppm 8.35 (s, 2H; H^{3A}), 7.68 (d, *J* = 16.1 Hz, 2H; H$^{\underline{CH}=CH\text{-}COO}$), 7.24 (s, 2H; H^{5A}), 6.71 (d, *J* = 16.1 Hz, 2H; H$^{CH=\underline{CH}\text{-}COO}$), 3.84 (s, 6H; H$^{COOC\underline{H3}}$), 2.67 (s, 6H; H$^{\underline{CH3}}$).

^{13}C NMR (CDCl$_3$, 126 MHz): δ/ppm 166.9 (C$^{\underline{COO}}$), 159.1 (C^{6A}), 156.3 (C^{2A}), 142.89 (C^{4A}), 142.74 (C$^{\underline{CH}=CH\text{-}COO}$), 122.23 (C$^{CH=\underline{CH}\text{-}COO}$), 121.9 (C^{5A}), 116.6 (C^{3A}), 52.1 (C$^{COO\underline{CH3}}$), 24.8 (C$^{\underline{CH3}}$).

MS (EI): m/z 352.1 [M]$^+$ (calc. 352.1).

IR: υ/cm^{-1} 3034 (w), 2953 (w), 2922 (w), 2849 (w), 1714 (s), 1641 (m), 1592 (m), 1551 (s), 1435 (s), 1398 (m), 1311 (s), 1261 (m), 1230 (m), 1182 (s), 1169 (s), 993 (s), 922 (m), 872 (m), 850 (s), 729 (m), 710 (m).

UV-VIS (CHCl$_3$): λ_{max}/nm (ε/M^{-1} cm^{-1}) 256 (84000), 321 (19000).

Anal. Calc. for C$_{20}$H$_{20}$N$_2$O$_4$: C, 68.17; H, 5.72; N, 7.95; found: C, 68.41/68.38; H, 6.04/6.07; N, 7.10/6.99 %.

(2*E*,2´*E*)-3,3´-(6,6´-Dimethyl-2,2´-bipyridine-4,4´-diyl)diacrylic acid (H$_2$L15)
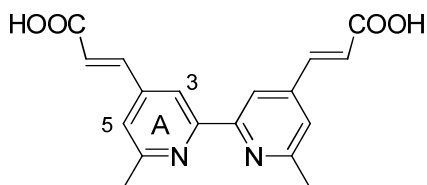
LiOH (68.0 mg) dissolved in H$_2$O (1.0 ml) was added to a solution of **L14** (0.100 g, 0.284 mmol) in THF (9.5 ml). The resulting mixture was heated to reflux for 5h. After being cooled to room temperature, the pH was adjusted to 2 with 2M HCl. The resulting precipitate was filtered and successively washed with H$_2$O, acetone and Et$_2$O to afford **L15** as a white solid (84.7 mg, 0.261 mmol, 92 %).

^{1}H NMR (TFA-d^1, 500 MHz): δ/ppm 8.60 (s, 2H; H^{3A}), 8.24 (s, 2H; H^{5A}), 8.00 (d, *J* = 16 Hz, 2H; H$^{C\underline{H}=CH-COO}$), 7.15 (d, *J* = 16 Hz, 2H; H$^{CH=C\underline{H}-COO}$), 3.06 (s, 6H; H$^{C\underline{H}3}$).

^{13}C NMR (TFA-d^1, 126 MHz): δ/ppm 171.9 (C$^{\underline{C}OO}$), 161.3 (C^{6A}), 155.4 (C^{4A}), 144.1 (C^{2A}), 141.5 (C$^{\underline{C}H=CH-COO}$), 131.8 (C$^{CH=\underline{C}H-COO}$), 130.9 (C^{5A}), 126.3 (C^{3A}), 21.3 (C^{CH3}).

MS (ES): m/z 325.2 [M+H$^+$]$^+$ (calc. 325.1).

IR: υ/cm^{-1} 2916.2 (w), 2854.5 (w), 2515.0 (w), 1705.0 (s), 1634.2 (m), 1596.9 (s), 1550.7 (s), 1373.2 (w), 1257.5 (s), 1164.9 (s), 972.1 (m), 848.6 (s), 686.6 (m).

UV-VIS (DMSO): λ_{max}/nm (ε/M^{-1} cm^{-1}) 319 (10000).

Anal. Calc. for $C_{18}H_{16}N_2O_4 \cdot 2H_2O$: C, 59.99; H, 5.59; N, 7.77; found, C, 60.65; H, 5.60; N, 7.20 %.

4,4´-Di(furan-2-yl)-6,6´-diphenyl-2,2´-bipyridine (L16)
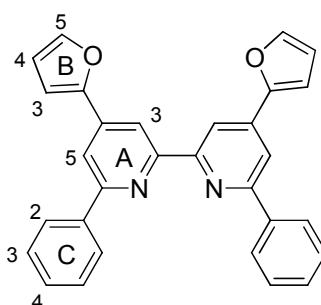
1,6-Di(furan-2-yl)hexa-1,5-diene-3,4-dione (0.5 g, 2.1 mmol), phenacylpyridinium bromide (1.149 g, 4.132 mmol) and ammonium acetate (1.00 g) were refluxed in ethanol (20 ml) for 12 h. After letting the solution cool down to room temperature, a white-beige solid was filtered and washed with cold ethanol (0.464 g, 1.05 mmol, 51 %).

^{1}H NMR (CDCl$_3$, 500 MHz): δ/ppm 8.82 (d, $J = 1.3$ Hz, 2H; H^{3A}), 8.23 (d, $J = 7.4$ Hz, 4H; H^{2C}), 8.07 (d, $J = 1.4$ Hz, 2H; H^{5A}), 7.63 (d, $J = 1.6$ Hz, 2H; H^{5B}), 7.57 (dt, $J = 1.5$ Hz, $J = 7.8$ Hz, 4H; H^{3C}), 7.49 (tt, $J = 1.5$ Hz, $J = 7.3$ Hz, 2H; H^{4C}), 7.11 (d, $J = 3.3$Hz, 2H; H^{3B}), 6.60 (dd, $J = 3.4$ Hz, $J = 1.7$ Hz, 2H; H^{4B}).

^{13}C NMR (CDCl$_3$, 126 MHz): δ/ppm 157.1 (C^{6A}), 156.1 (C^{2A}), 151.9 (C^{2B}), 143.8 (C^{5B}), 139.38 (C^{1C}), 139.23 (C^{4A}), 129.2 (C^{4C}), 128.8 (C^{3C}), 127.1 (C^{2C}), 114.80 (C^{5A}), 114.24 (C^{3A}), 112.2 (C^{4B}), 109.1 (C^{3B}).

MS (EI): m/z 440.2 [M]$^+$ (calc. 440.2), 220.1 [M/2]$^+$ (calc. 220.1).

IR: υ/cm^{-1} 3039 (w), 1601 (m), 1570 (w), 1543 (m), 1489 (w), 1404 (w), 1365 (w), 1215 (w), 1153 (w), 1009 (m), 918 (w), 868 (m), 814 (w), 771 (m), 729 (m), 686 (s), 590 (s), 513 (s), 486 (s), 455 (s), 409 (s).

UV-VIS (CHCl$_3$): λ_{max}/nm (ε/M^{-1} cm^{-1}) 275 (48000), 305 (37000), 338 (12000).

Anal. Calc. for C$_{30}$H$_{20}$N$_2$O$_2$·H$_2$O: C, 78.59; H, 4.84; N, 6.11; found: C, 78.87; H, 4.42; N, 6.02 %.

6,6´-Diphenyl-2,2´-bipyridine-4,4´-dicarboxylic acid (H$_2$L17)
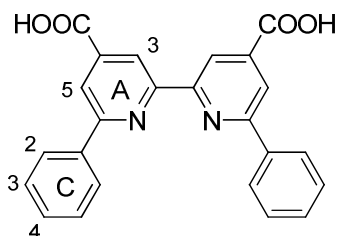
KMnO$_4$ (4.95 g, 31.34 mmol) was added to a warm mixture (approx. temperature 40°C) of **L16** (1.06 g, 2.42 mmol), *t*-BuOH (145 ml) and H$_2$O (30 ml). After refluxing overnight, the mixture was filtered through *Celite*. The solution was evaporated to approx. 50 ml, the pH adjusted to 2 with 2M HCl, and the precipitated white product filtered (0.62 g, 1.55 mmol, 64 %).

^{1}H NMR (TFA-d^1, 400 MHz): δ/ppm 9.22 (s, 2H; H^{3A}), 9.00 (s, 2H; H^{5A}), 8.19 (d, J = 7.2 Hz, 4H; H^{2C}), 7.82 (m, 2H; H^{4C}), 7.78 (m, 4H; H^{3C}).

^{13}C NMR (TFA-d^1, 101 MHz): δ/ppm 168.7 (C^{COO}), 159.9 (C^{6A}), 147.8 (C^{2A}), 146.0 (C^{4A}), 135.1 (C^{4C}), 133.6 (C^{1C}), 131.8 (C^{3C}), 128.9 (C^{2C}), 127.7 (C^{5A}), 123.0 (C^{3A}).

MS (ES): m/z 397.2 [M+H]$^+$ (calc. 397.1).

IR: υ/cm^{-1} 2978 (w), 2831 (w), 2561 (w), 2361 (w), 1689 (s), 1551 (s), 1427 (m), 1389 (s), 1296 (m), 1250 (s), 1142 (m), 895 (m), 756 (s), 679 (s).

UV-VIS (DMSO): λ_{max}/nm (ε/M^{-1} cm^{-1}) 264 (15000), 330 (8400).

Satisfactory elemental analysis could not be obtained.

Dimethyl 6,6´-diphenyl-2,2´-bipyridine-4,4´-dicarboxylate (L18)
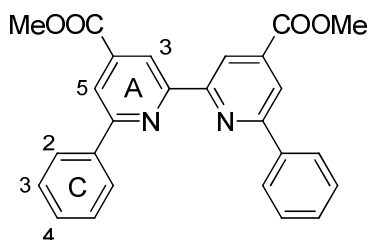
Conc. H_2SO_4 (2 ml) was added to a suspension of **L17** (0.90 g, 2.27 mmol) in MeOH (100ml). The solution was refluxed for 12 h. When the solution cooled down to room temperature, some of the solvent was evaporated under reduced pressure to approx. 60 ml and the pH was adjusted to 7 with 1M NaOH. The white solid that precipitated was filtered and washed with water and ether (0.78 g, 1.83 mmol, 80 %).

^{1}H NMR (CDCl$_3$, 500 MHz): δ/ppm 9.08 (s, J = 1.2 Hz, 2H; H^{3A}), 8.39 (s, J = 1.2 Hz, 2H; H^{5A}), 8.25 (d, J = 7.2 Hz, 4H; H^{2C}), 7.57 (t, J = 7.5 Hz, 4H; H^{3C}), 7.50 (t, J = 7.3 Hz, 2H; H^{4C}), 4.06 (s, 6H; H$^{COOC\underline{H}3}$).

^{13}C NMR (CDCl$_3$, 126 MHz): δ/ppm 166.2 (C^{COO}), 157.8 (C^{6A}), 156.6 (C^{2A}), 139.6 (C^{4A}), 138.5 (C^{1C}), 129.78 (C^{4C}), 129.06 (C^{3C}), 127.3 (C^{2C}), 120.1 (C^{5A}), 119.2 (C^{3A}), 53.0 (C$^{COO\underline{C}H3}$).

MS (EI): m/z 424.1 [M]$^+$ (calc. 424.1).

IR: υ/cm^{-1} 3079 (w), 3033 (w), 2955 (w), 1728 (s), 1558 (m), 1435 (m), 1389 (m), 1296 (m), 1250 (s), 1134 (w), 1057 (w), 964 (m), 902 (w), 856 (w), 756 (s), 725 (m), 686 (s).

UV-VIS (CH$_2$Cl$_2$): λ_{max}/nm (ε/M^{-1} cm^{-1}) 235 (39000), 266 (20000), 332 (14000).

Anal. Calc. for $C_{26}H_{20}N_2O_4 \cdot 0.5H_2O$: C, 72.04; H, 4.88; N, 6.46; found: C, 72.03/71.99; H, 4.70/4.85; N, 6.35/6.51 %.

4,4´-Bis(hydroxymethyl)-6,6´-diphenyl-2,2´-bipyridine (L19)
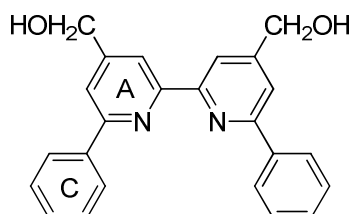
This ligand was synthesized by a modification of a reported procedure [131]. To a stirring suspension of **L18** (1 g, 2.35 mmol) in THF (44 ml) at -40°C, LiAlH$_4$ (0.58 ml, 2.35 mmol) was added. Within 1 h the temperature of the mixture was raised to -10°C, and more LiAlH$_4$ (0.58 ml, 2.35 mmol) was added. Stirring for 2 h at room temperature completed the reaction. At 0°C H$_2$O (0.25 ml) was added dropwise very carefully followed by 1M NaOH (1 ml). After 15 min. the suspension was refluxed for 5 min and stirred at room temperature for 12 h. The white Al(OH)$_3$ precipitate was filtered. Evaporation of the solvent yielded a yellow oil that was used without further purification (0.77 g, 2.09 mmol, 89 %).

6,6´-Diphenyl-2,2´-bipyridine-4,4´-dicarbaldehyde (L20)
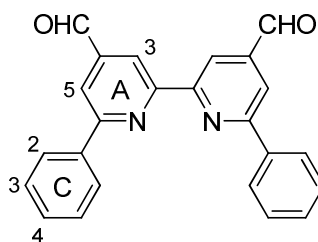
L19 (0.5 g, 1.17 mmol) dissolved in CH$_2$Cl$_2$ (60 ml) was stirred at room temperature with MnO$_2$ (2.0 g, 23.40 mmol) for 12 h. Then the solution was filtered over Celite and the solvent evaporated under reduced pressure. Because not all the alcohol was converted to the aldehyde, the same procedure was repeated, this time yielding the aldehyde as a yellow solid that was used without further purification (0.341 g, 0.94 mmol, 80 %).

^{1}H NMR (CDCl$_3$, 500 MHz): δ/ppm 10.31 (s, 2H; H$^{\underline{CH}O}$), 8.99 (d, J = 1.2 Hz, 2H; H^{3A}), 8.25 (m, 6H; H^{5A}, H^{2C}), 7.59 (m, 4H; H^{3C}), 7.53 (tt, J = J = , 2H; H^{4C}).

^{13}C NMR (CDCl$_3$, 126 MHz): δ/ppm 191.8 (C$^{\underline{C}HO}$), 158.3 (C^{6A}), 156.8 (C^{2A}), 143.8 (C^{4A}), 138.0 (C^{1C}), 130.0 (C^{4C}), 129.0 (C^{3C}), 127.1 (C^{2C}), 119.3 (C^{3A}), 118.6 (C^{5A}).

MS (EI): m/z 364.1 [M]$^+$ (calc. 364.1).

(2E,2´E)-Dimethyl 3,3´-(6,6´-diphenyl-2,2´-bipyridine-4,4´-diyl)diacrylate (L21)
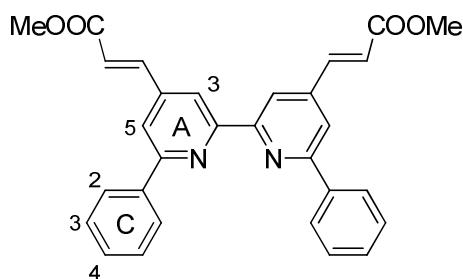
A mixture of **L20** (0.426 g, 1.17 mmol) and Ph$_3$P=CHCO$_2$Me (0.913 g, 2.73 mmol) in dry toluene (25 ml) was refluxed for 18h. After the solution cooled down to room temperature, the solvent was removed under reduced pressure and the remained brown solid cleaned by column chromatography (Alox, CH$_2$Cl$_2$) to yield **L21** as a white solid (0.228 g, 0.478 mmol, 41 %).

^{1}H NMR (CDCl$_3$, 500 MHz): δ/ppm 8.68 (s, 2H; H^{3A}), 8.18 (d, J = 7.2 Hz, 4H; H^{2C}), 7.86 (s, 2H; H^{5A}), 7.83 (d, J = 16.1 Hz, 2H; H$^{\underline{CH}=CH\text{-}COO}$), 7.56 (m, 4H; H^{3C}), 7.49 (m, 2H; H^{4C}), 6.81 (d, J = 16.0 Hz, 2H; H$^{CH=\underline{CH}\text{-}COO}$), 3.88 (s, 6H; H$^{COO\underline{CH3}}$).

^{13}C NMR (CDCl$_3$, 126 MHz): δ/ppm 166.9 (C^{COO}), 157.7 (C^{6A}), 156.5 (C^{2A}), 143.6 (C^{4A}), 142.9 (C$^{\underline{C}H=CH\text{-}COO}$), 138.9 (C^{1C}), 129.6 (C^{4C}), 129.1 (C^{3C}), 127.2 (C^{2C}), 122.5 (C$^{CH=\underline{C}H\text{-}COO}$), 119.1 (C^{5A}), 118.0 (C^{3A}), 52.2 (C$^{COO\underline{C}H3}$).

MS (EI): m/z 476.2 [M]$^+$ (calc. 476.2), 238.1 [M/2]$^+$ (calc. 238.1).

IR: υ/cm^{-1} 3040 (w), 2924 (w), 2854 (w), 2361 (w), 1713 (s), 1643 (w), 1589 (m), 1551(s), 1497 (w), 1435 (m), 1404 (m), 1288 (m), 1250 (m), 1165 (s), 1072 (w), 1026 (w), 987 (m), 856 (m), 771 (m), 740 (w), 694 (s), 632 (w).

UV-VIS (CH_2Cl_2): λ_{max}/nm ($\varepsilon/M^{-1}\ cm^{-1}$) 257 (60000), 338 (10000).

Anal. Calc. for $C_{30}H_{24}N_2O_4$: C, 75.62; H, 5.08; N, 5.88; found: C, 73.07; H, 6.68; N, 4.18 %.

(2*E*,2´*E*)-3,3´-(6,6´-Diphenyl-2,2´-bipyridine-4,4´-diyl)diacrylic acid (H$_2$L22)
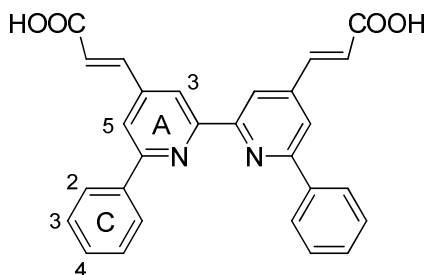
LiOH (50.0 mg) dissolved in H_2O (0.7 ml) was added to a solution of **L21** (0.100 g, 0.209 mmol) in THF (7.0 ml). The resulting mixture was heated to reflux for 5h. After being cooled to room temperature, the pH was adjusted to 2 with 2M HCl. The resulting precipitate was filtered and successively washed with H_2O, acetone and Et_2O to afford **L22** as a white solid (72.0 mg, 0.161 mmol, 77 %).

^{1}H NMR (TFA-d^1, 500 MHz): δ/ppm 8.71 (s, 2H; H^{3A}), 8.54 (s, 2H; H^{5A}), 8.12 (d, J = 16.0 Hz, 2H; H$^{\underline{CH}=CH\text{-}COO}$), 8.01 (d, J = 7.1 Hz, 4H; H^{2C}), 7.80 (t, J = 6.6 Hz, 4H; H^{4C}), 7.72 (t, J = 6.6 Hz, 4H; H^{3C}), 7.24 (d, J = 15.9 Hz, 2H; H$^{CH=\underline{CH}\text{-}COO}$).

MS (ES): m/z 449.2 [M+H]$^+$ (calc. 449.2).

IR: υ/cm^{-1} 2924 (w), 2847 (w), 2669 (w), 2553 (w), 2507 (w), 1689 (s), 1643 (m), 1589 (m), 1551 (s), 1419 (m), 1396 (m), 1288 (s), 1203 (m), 1072 (w), 1026 (w), 941 (m), 856 (s), 771 (s), 686 (s).

UV-VIS (DMSO): λ_{max}/nm (ε/M^{-1} cm^{-1}) 260 (56000), 340 (10000).

Anal. Calc. for $C_{28}H_{20}N_2O_4 \cdot 0.7H_2O$: C, 72.94; H, 4.68; N, 6.08; found: C, 73.04; H, 5.04; N, 5.45 %.

Tetraethyl 6,6´-dimethyl-2,2´-bipyridine-4,4´-diyldiphosphonate (L23)
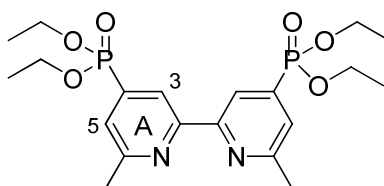
This ligand was synthesized after modification of a reported procedure [135]. 4,4´-Dibromo-6,6´-dimethyl bipyridine (0.200 g, 0.588 mmol), diethyl phosphate (0.185 g, 1.310 mmol), freshly made Pd(PPh$_3$)$_4$ [194] (0.0678 g, 0.059 mmol), triphenylphosphine (1.541 g, 5.880 mmol), triethylamine (0.185 ml) and toluene (6 ml) were heated at 110°C under nitrogen for 6 h. After the yellow reaction mixture cooled down to room temperature, it was washed with ammonium hydroxide solution, then with water and dried over MgSO$_4$. Then the solvent was removed in vacuo and the crude product was flash cromatographed (SiO$_2$) eluting with CH$_2$Cl$_2$ to give pure PPh$_3$. After an elution with CH$_2$Cl$_2$/CH$_3$OH: 99/1, a white solid was obtained that was further purified by recrystallisation from hexane to give white crystals (0.150 g, 0.328 mmol, 56 %).

^{1}H NMR (CDCl$_3$, 500 MHz): δ/ppm 8.57 (s, J = 13.9 Hz, 2H; H^{3A}), 7.55 (s, J = 13.5 Hz, 2H; H^{5A}), 4.18 (m, 4H; H^{CH2CH3}), 2.68 (s, 6H; H^{CH3}), 1.36 (m, 6H; H^{CH2CH3}).

^{13}C NMR (CDCl$_3$, 126 MHz): δ/ppm 158.9 (d, J = 13.4 Hz, C^{6A}), 155.5 (s; C^{2A}), 138.5 (d, J = 186.4 Hz; C^{4A}), 125.2 (d, J = 9.4 Hz; C^{5A}), 120.0 (d, J = 9.7 Hz; C^{3A}), 62.8 (d, J = 5.6 Hz; C^{CH2CH3}), 24.8 (s; C^{CH3}), 16.5 (d, J = 6.3 Hz; C^{CH2CH3}).

^{31}P NMR (CDCl$_3$, 162 MHz): δ/ppm 16.39 (85 % H$_3$PO$_4$ at δ 0 ppm).

MS (EI): m/z 456.3 [M]$^+$ (calc. 456.2).

IR: υ/cm^{-1} 2980 (w), 2932 (w), 2912 (w), 1584 (w), 1547 (m), 1456 (w), 1436 (w), 1386 (w), 1363 (m), 1254 (m), 1230 (m), 1160 (w), 1111 (w), 1097 (w), 1041 (s), 1011 (s), 952 (s), 882 (m), 791 (m), 749 (m), 566 (s), 553 (s), 513 (s), 492 (m), 481 (s), 470 (s), 441 (m).

Anal. Calc. for $C_{20}H_{30}N_2O_6P_2\cdot0.1C_{18}H_{15}OP$: C, 54.07; H, 6.56; N, 5.79; found: C, 53.95/53.76; H, 6.27/6.43; N, 5.50/5.70 %.

6,6′-Dimethyl-2,2′-bipyridine-4,4′-diyl diphosphonic acid (H₄L24)
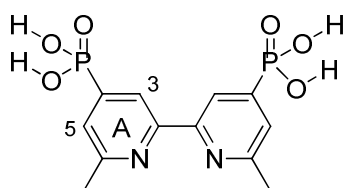
This ligand was synthesized by a modification of a reported procedure [135]. **L23** (78.2 mg, 0.171 mmol) and bromotrimethylsilane (0.23 ml, 1.71 mmol) were stirred in dry CH_2Cl_2 (5 ml) for 24 h. Then all the solvent was removed under reduced pressure and the yellow residue was dissolved and stirred in MeOH (7 ml). After 4 h a white precipitate appeared; the reaction mixture was stirred for 24 h. After this time the white precipitate, **L24**, was filtered and washed with MeOH (35.2 mg, 0.102 mmol, 60 %).

^{1}H NMR (TFA-d^1, 400 MHz): δ/ppm 9.43 (d, J = 12.6 Hz, 2H; H^{3A}), 8.59 (d, J = 12.2 Hz, 2H; H^{5A}), 3.10 (s, 6H; H$^{\underline{CH3}}$).

^{13}C NMR (TFA-d^1, 101 MHz): δ/ppm 161.7 (d, J = 12.6 Hz, C^{6A}), 158.1 (d, J = 176.3 Hz, C^{4A}), 142.6 (d, J = 13.5 Hz, C^{2A}), 134.5 (d, J = 8.4 Hz, C^{5A}), 129.6 (d, J = 10.5 Hz, C^{3A}), 21.4 (s, C^{CH3}).

^{31}P NMR (TFA-d^1, 162 MHz): δ/ppm 6.52 (85 % H$_3$PO$_4$ at δ 0 ppm).

MS (MALDI): m/z 345.0 [M+H]$^+$ (calc. 345.0).

IR: υ/cm^{-1} 3152 (w), 3097 (w), 3072 (w), 2922 (w), 1611 (m), 1593 (m), 1550 (m), 1433 (m), 1393 (m), 1344 (w), 1269 (w), 992 (s), 958 (s), 940 (s), 914 (s), 870 (s), 721(s).

UV-VIS (DMSO): λ_{max}/nm 301 (6100).

Anal. Calc. for $C_{12}H_{14}N_2O_6P_2$: C, 41.87; H, 4.10; N, 8.14; found: C, 41.25/41.10; H, 3.97/4.00; N, 7.77/7.81 %.

Dimethyl 2,2´-biquinoline-4,4´-dicarboxylate (L26)
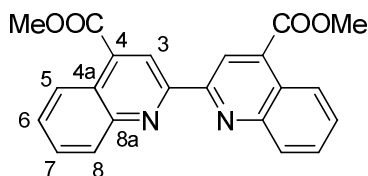
Conc. H_2SO_4 (3.0 ml) was added to a suspension of **L25** (2.00 g, 5.80 mmol) in MeOH (100ml). The solution was refluxed for 12 h. When the solution cooled down to room temperature, some of the solvent was evaporated under reduced pressure to approx. 60 ml and the pH was adjusted to 7 with 1M NaOH. The white solid that precipitated was filtered and washed with water and ether (1.20 g, 3.23 mmol, 56 %).

^{1}H NMR (CDCl$_3$, 500 MHz): δ/ppm 9.33 (s, 2H; H^3), 8.82 (d, J = 8.5 Hz, 2H; H^8), 8.33 (d, J = 8.4 Hz, 2H; H^5), 7.83 (t, J = 7.5 Hz, 2H; H^6), 7.71 (t, J = 7.6 Hz, 2H; H^7), 4.13 (s, 6H; H$^{COOC\underline{H}3}$).

^{13}C NMR (CDCl$_3$, 126 MHz): δ/ppm 167.0 (C$^{\underline{C}OO}$), 155.1 (C^2), 149.0 (C^{8a}), 136.0 (C^4), 130.7 (C^5), 130.1 (C^6), 128.9 (C^7), 125.78 (C^8), 125.47 (C^{4a}), 120.6 (C^3), 53.0 (C$^{COO\underline{C}H3}$).

MS (EI): m/z 372.1 [M]$^+$ (calc. 372.1).

IR: υ/cm^{-1} 2958 (w), 1724 (s), 1588 (m), 1548 (w), 1502 (m), 1434 (m), 1365 (w), 1271 (m), 1236 (m), 1197 (m), 1140 (m), 1084 (m), 1019 (m), 946 (m), 915 (w), 864 (w), 794 (m), 771 (s), 741 (m), 668 (m), 615 (w).

Anal. Calc. for $C_{22}H_{16}N_2O_4 \cdot 0.3H_2O$: C, 69.94; H, 4.43; N, 7.42; found: C, 70.04; H, 4.04; N, 7.05 %.

Dimethyl 4,4´-(6,6´´-dimethyl-2,2´:6´,2´´-terpyridine-4,4´´-diyl)dibenzoate (L27)
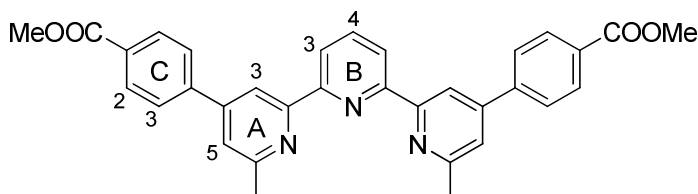
Dimethyl 4,4´-(1*E*,1´*E*)-3,3´-(pyridine-2,6-diyl)bis(3-oxoprop-1-ene-3,1-diyl)dibenzoate (0.40 g, 0.88 mmol), 1-acetonylpyridinium chloride (0.33 g, 1.93 mmol), and ammonium acetate (2.00 g) were refluxed in methanol (10 ml) with 10 drops of acetic acid for 12 h. After letting the solution cool down to room temperature, a beige solid was filtered. This solid was purified by column chromatography (Alox, CH_2Cl_2, Rf = 0.4) to yield the product as a white solid (0.19 g, 0.36 mmol, 41 %).

^{1}H NMR (CDCl$_3$, 500 MHz): δ/ppm 8.62 (s, 2H; H^{3A}), 8.52 (d, *J* = 7.8 Hz, 2H; H^{3B}), 8.17 (d, *J* = 7.8 Hz, 4H; H^{2C}), 7.99 (d, *J* = 7.8 Hz, 1H; H^{4B}), 7.81 (d, *J* = 8.0 Hz, 4H; H^{3C}), 7.44 (s, 2H; H^{5A}), 3.97 (s, 6H; H$^{COOC\underline{H}3}$), 2.74 (s, 6H; H$^{\underline{CH}3}$).

^{13}C NMR (CDCl$_3$, 126 MHz): δ/ppm 166.9 (C$^{\underline{COO}}$), 158.8 (C^{6A}), 156.7 (C^{2B}), 155.7 (C^{2A}), 148.5 (C^{4A}/C^{1C}), 143.5 (C^{4C}), 138.1 (C^{4B}), 130.6 (C^{4A}/C^{1C}), 130.4 (C^{2C}), 127.3 (C^{3C}), 121.6 (C^{3B}), 121.54 (C^{5A}), 116.7 (C^{3A}), 52.44 (C$^{COO\underline{C}H3}$), 24.9 (C$^{\underline{CH}3}$).

MS (EI): m/z 529.2 [M]$^+$ (calc. 529.2).

IR: υ/cm^{-1} 3139.9 (w), 3047.3 (w), 2954.7 (w), 1712.7 (s), 1604.7 (w), 1573.8 (m), 1550.7 (m), 1388.7 (m), 1272.9 (s), 1188.1 (m), 1103.2 (s), 964.3 (w), 848.6 (w), 817.8 (m), 771.5 (m), 702.0 (m).

UV-VIS (CHCl$_3$): λ_{max}/nm (ε/M^{-1} cm^{-1}) 259 (28000), 314 (9000), 345 (2000).

4,4´-(6,6´´-Dimethyl-2,2´:6´,2´´-terpyridine-4,4´´-diyl) dibenzoic acid (H$_2$L28)
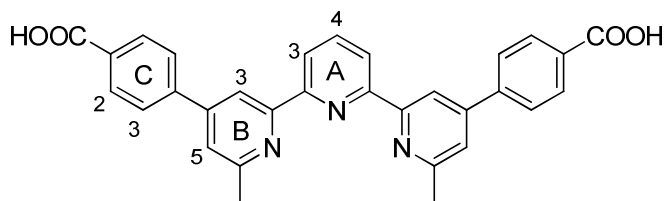
LiOH (31.6 mg) dissolved in H$_2$O (0.5 ml) was added to a solution of **L27** (70.0 g, 0.132 mmol) in THF (5 ml). The resulting mixture was heated to reflux for 12h. After being cooled to room temperature, the pH was adjusted to 2 with 2M HCl. The resulting precipitate was filtered and successively washed with H$_2$O, acetone and Et$_2$O to afford **L28** as a white solid (43.1 mg, 0.086 mmol, 65 %).

^{1}H NMR (TFA-d^1, 250 MHz): δ/ppm 8.84 (s, 2H; H^{3A}), 8.73 (d, J = 7.6 Hz, 2H; H^{3B}), 8.57 (m, 1H; H^{4B}), 8.57 (d, J = 7.6 Hz, 4H; H^{2C}), 8.32 (s, 2H; H^{5A}), 8.17 (d, J = 8.0 Hz, 4H; H^{3C}), 3.33 (s, 6H; H$^{C\underline{H}3}$).

MS (MALDI): m/z 501.1 [M]$^+$ (calc. 501.2).

IR: υ/cm^{-1} 2916 (w), 1697 (s), 1605 (s), 1389 (m), 1226 (s), 1180 (m), 1111 (m), 987 (w), 848 (m), 771 (s), 694 (m).

UV-VIS (DMSO): λ_{max}/nm (ε/M^{-1} cm^{-1}) 260 (11000), 318 (3400).

Anal. Calc. for C$_{31}$H$_{23}$N$_3$O$_4$·6H$_2$O: C, 61.08; H, 5.79; N, 6.89; found: C, 61.22; H, 5.00; N, 6.73 %.

Dimethyl 4,4´-(6,6´´-diphenyl-2,2´:6´,2´´-terpyridine-4,4´´-diyl)dibenzoate (L29)
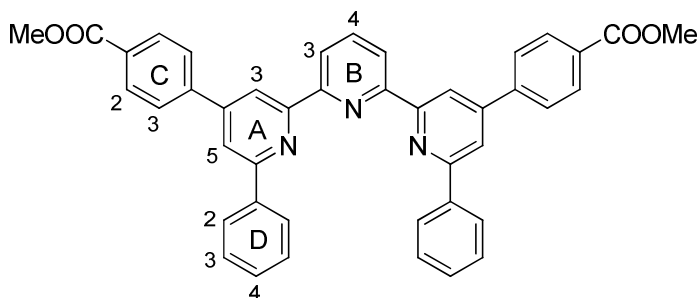
Dimethyl 4,4´-(1*E*,1´*E*)-3,3´-(pyridine-2,6-diyl)bis(3-oxoprop-1-ene-3,1-diyl)dibenzoate (0.50 g, 1.10 mmol), phenacylpyridinium bromide (0.67 g, 2.41 mmol), and ammonium acetate (2.00 g) were refluxed in methanol (10 ml) with 10 drops of acetic acid for 12 h. After letting the solution cool down to room temperature, a beige solid was filtered. This solid was purified by column chromatography (Alox, CH_2Cl_2) to yield the product as a white solid (0.37 g, 0.57 mmol, 52 %).

^{1}H NMR (CDCl$_3$, 400 MHz): δ/ppm 8.82 (d, *J* = 1.5 Hz, 2H; H^{3A}), 8.76 (d, *J* = 7.8 Hz, 2H; H^{3B}), 8.24 (m 8H; H^{2C}, H^{2D}), 8.07 (t, *J* = 7.8 Hz, 1H; H^{4B}), 8.02 (d, *J* = 1.5 Hz, 2H; H^{5A}), 7.91 (d, *J* = 8.5 Hz, 4H; H^{3C}), 7.56 (m, 4H; H^{3D}), 7.49 (m, 2H; H^{2D}), 4.00 (s, 6H; H$^{COOC\underline{H}3}$).

MS (EI): m/z 653.0 [M]$^+$ (calc. 653.2).

IR: υ/cm^{-1} 3040 (w), 2955 (w), 1713 (s), 1605 (m), 1574 (m), 1543 (m), 1435 (w), 1381 (m), 1273 (s), 1188 (w), 1103 (s), 1018 (w), 972 (w), 887 (w), 848 (m), 818 (m), 764 (s), 686 (s), 640 (m), 586 (s).

UV-VIS (CHCl$_3$): λ$_{max}$/nm (ε/M^{-1} cm^{-1}) 265 (87000), 320 (20500).

Anal. Calc. for $C_{43}H_{31}N_3O_4·H_2O$: C, 76.88; H, 4.95; N, 6.26; found: C, 76.29; H, 5.04; N, 5.94 %.

[Cu(L1)₂][PF₆]

[Cu(CH₃CN)₄][PF₆] (18.6 mg, 0.05 mmol) dissolved in CH₃CN (2 ml) was added to a solution of **L1** (33.6 mg, 0.10 mmol) in CHCl₃ (5 ml), and the colourless solution turned red. A red solid precipitated upon addition of ether to the solution. It was filtered and washed with water and ether (38.1 mg, 0.04 mmol, 86 %).

^{1}H NMR (CDCl₃, 500 MHz): δ/ppm 8.39 (s, 4H; H^{3A}), 7.81 (d, J = 7.4 Hz, 8H; H^{2B}), 7.70 (s, 4H; H^{5A}), 7.59 (t, J = 7.3 Hz, 8H; H^{3B}), 7.54 (t, J = 7.2 Hz, 8H; H^{4B}), 2.40 (s, 12H; H^{CH3}).

^{13}C NMR (CDCl₃, 126 MHz): δ/ppm 157.8 (C^{6A}), 152.3 (C^{2A}), 151.0 (C^{4A}), 137.3 (C^{1B}), 130.1 (C^{4B}), 129.6 (C^{3B}), 127.4 (C^{2B}), 124.2 (C^{5A}), 117.6 (C^{3A}), 25.6 (C$^{\underline{C}H3}$).

MS (ES): m/z 735.1 [M-PF₆]$^+$ (calc.735.3).

IR: υ/cm^{-1} 3059 (w), 2959 (w), 2919 (w), 1771 (w), 1710 (m), 1608 (m), 1545 (m), 1497 (w), 1451 (w), 1432 (w), 1418 (w), 1398 (w), 1386 (w), 1354 (w), 1259 (w), 1242 (w), 1225 (w), 1184 (w), 1028 (w), 1008 (w), 880 (w), 835 (s), 825 (s), 762 (s), 741 (m), 690 (s), 641 (m), 627 (m).

UV-VIS (CHCl₃): λ$_{max}$/nm (ε/M^{-1} cm^{-1}) 274 (1000), 310 (500), 352 (120), 481 (150).

E° Cu^{II}/Cu^I (CH₂Cl₂)/V vs. Fc: +0.065 (reversible).

Anal. Calc. for C₄₈H₄₀CuF₆N₄P·3.5H₂O·CH₃CN: C, 60.94; H, 5.11; N, 7.11; found: C, 60.55; H, 4.44; N, 6.84 %.

[Cu(L2)₂][PF₆]

[Cu(CH₃CN)₄][PF₆] (18.6 mg, 0.05 mmol) dissolved in CH₃CN (2 ml) was added to a solution of **L2** (46.0 mg, 0.10 mmol) in CHCl₃ (5 ml), and the colourless solution turned dark red. A red-

brown solid precipitated upon addition of hexane to the solution. It was filtered and washed with hexane (31.1 mg, 0.027 mmol, 55 %). This complex has recently been reported [192].

^{1}H NMR (CDCl$_3$, 400 MHz): δ/ppm 8.13 (d, J = 1.2 Hz, 4H; H^{3A}), 7.81 (d, J = 7.8 Hz, 8H; H^{2B}/H^{2C}), 7.72 (d, J = 0.8 Hz, 4H; H^{5A}), 7.62 (m, 20H; H^{2B}/H^{2C}, H^{3B}/H^{3C}, H^{4B}/H^{4C}), 7.07 (t, J = 7.3 Hz, 4H; H^{4B}/H^{4C}), 6.96 (t, J = 7.5 Hz, 8H; H^{3B}/H^{3C}).

MS (ES): m/z 984.0 [M-PF$_6$]$^+$ (calc. 983.3).

IR: υ/cm^{-1} 3057 (w), 3034 (w), 2922 (w), 2853 (w), 1674 (w), 1604 (m), 1536 (m), 1495 (w), 1448 (w), 1434 (w), 1416 (w), 1389 (m), 1230 (w), 1183 (w), 1158 (w), 1108 (w), 1077 (w), 1027 (w), 1000 (w), 877 (w), 827 (s), 762 (s), 740 (m), 691 (s), 643 (m), 625 (m).

UV-VIS (CHCl$_3$): λ$_{max}$/nm (ε/M^{-1} cm^{-1}) 261 (48000), 289 (35000), 332 (16000), 421 (3300), 572 (2200).

E° Cu^{II}/Cu^{I} (CH$_2$Cl$_2$) /V vs. Fc: +0.363 (reversible).

[Cu(L3)$_2$][PF$_6$]

[Cu(CH$_3$CN)$_4$][PF$_6$] (10.22 mg, 0.055 mmol) dissolved in CH$_3$CN (2 ml) was added to a solution of **L3** (24.8 mg, 0.055 mmol) in CHCl$_3$ (4 ml), and the colorless solution turned red. A red solid precipitated upon addition of ether to the solution. It was filtered and washed with water and ether (59.1 mg, 0.053 mmol, 96 %).

^{1}H NMR (CDCl$_3$, 500 MHz): δ/ppm 8.44 (s, 4H; H^{3A}), 8.24 (d, J = 7.5 Hz, 8H; H^{2B}), 7.90 (d, J = 7.7 Hz, 8H; H^{3B}), 7.74 (s, 4H; H^{5A}), 3.98 (s, 12H; H$^{COOC\underline{H}3}$), 2.41 (s, 12H; H$^{C\underline{H}3}$).

MS (ES): m/z 967.2 [M-PF$_6$]$^+$ (calc. 967.3).

IR: υ/cm^{-1} 2961 (w), 1713 (s), 1606 (m), 1578 (w), 1541 (m), 1429 (m), 1387 (w), 1275 (s), 1188 (w), 1107 (m), 1017 (m), 964 (w), 831 (s), 771 (s), 747 (m), 701 (m), 668 (w).

UV-VIS (CHCl$_3$): λ_{max}/nm (ε/M^{-1} cm^{-1}) 271 (50000), 323 (25000), 488 (4300).

E° Cu^{II}/Cu^{I} (CH$_2$Cl$_2$)/V vs. Fc: +0.450 (reversible).

Anal. Calc. for C$_{56}$H$_{48}$CuF$_6$N$_4$O$_8$P·4H$_2$O: C, 55.88; H, 4.86; N, 4.65; found: C, 55.77; H, 4.14; N, 4.45 %.

[Cu(H$_2$L4)$_2$]Cl

L4 (0.140 g, 0.33 mmol) in water (2 ml) was warmed to 70 °C, and then 15 drops of 1M NaOH solution were added. To this solution, copper(II) sulfate [CuSO$_4$·5H$_2$O, 0.042 g, 0.17 mmol] in water (2 ml) was added, followed by further addition of 20 drops of 1M NaOH solution. Ascorbic acid (0.0440 g, 0.25 mmol) in water (0.3 ml) was added to this solution and the solution turned dark red. The solution pH was adjusted to 2 by addition of 1M HCl to afford a dark red precipitate (0.142 g, 0.15 mmol, 48 %).

MS (ES): m/z 911.6 [M-PF$_6$]$^+$ (calc. 911.2).

E° Cu^{II}/Cu^{I} (DMSO)/V vs. Fc: -0.144 V (reversible).

[Cu(L5)$_2$][PF$_6$]

[Cu(CH$_3$CN)$_4$][PF$_6$] (27.90 mg, 0.075 mmol) dissolved in CH$_3$CN (1 ml) was added to a solution of **L5** (86.4 mg, 0.15 mmol) in CHCl$_3$ (2 ml), and the colourless solution turned dark green. A dark green solid precipitated upon addition of ether to the solution. It was filtered and washed with water and ether (82.8 mg, 0.061 mmol, 81 %).

^{1}H NMR (CDCl$_3$, 500 MHz): δ/ppm 8.29 (d, J = 8.3 Hz, 8H; H^{2B}), 8.22 (s, 4H; H^{3A}), 7.90 (d, J = 8.3 Hz, 8H; H^{3B}), 7.60 (d, J = 7.5 Hz, 8H; H^{2C}), 7.59 (s, 4H; H^{5A}), 6.99 (t, J = 7.3 Hz, 4H; H^{4C}), 6.90 (t, J = 7.5 Hz, 8H; H^{3C}), 4.00 (s, 12H; H^{COOCH3}).

^{13}C NMR (CDCl$_3$, 126 MHz): δ/ppm 166.8 (C^{COO}), 157.1 (C^{6A}), 153.4 (C^{2A}), 149.8 (C$^{1(B)}$/C$^{4(A)}$), 141.3 (C^{4B}), 137.9 (C^{1C}), 131.6 (C$^{1(B)}$/C$^{4(A)}$), 130.9 (C^{2B}), 129.7 (C^{4C}), 127.77 (C^{3C}), 127.74 (C^{2C}), 127.58 (C^{3B}), 123.1 (C^{5A}), 119.9 (C^{3A}), 52.6 (C^{COOCH3}).

MS (ES): m/z 1215.1 [M-PF$_6$]$^+$ (calc. 1215.3).

IR: υ/cm^{-1} 3055 (w), 2948 (w), 1712 (m), 1605 (m), 1574 (w), 1537 (m), 1435 (m), 1386 (w), 1276 (s), 1185 (m), 1106 (m), 1015 (m), 828 (s), 768 (s), 734 (m), 695 (s), 553(m).

UV-VIS (CHCl$_3$): λ$_{max}$/nm (ε/M^{-1} cm^{-1}) 271 (100000), 337 (27000), 434 (6000), 589 (4300).

E° Cu^{II}/Cu^{I} (CH$_2$Cl$_2$)/V vs. Fc: +0.40 V (reversible).

Anal. Calc. for C$_{76}$H$_{56}$CuF$_6$N$_4$O$_8$P·3H$_2$O: C, 64.47; H, 4.41; N, 3.96; found: C, 64.12; H, 3.89; N, 3.81 %.

[Cu(H$_2$L6)$_2$]Cl

L6 (0.181 g, 0.33 mmol) in water (2 ml) was warmed to 70 °C, and then 15 drops of 1M NaOH solution were added. To this solution, copper(II) sulfate [CuSO$_4$·5H$_2$O, 0.042 g, 0.17 mmol] in water (2 ml) was added, followed by further addition of 20 drops of 1M NaOH solution. Ascorbic acid (0.0440 g, 0.25 mmol) in water (0.3 ml) was added to this solution and the solution turned dark green. The solution pH was adjusted to 2 by addition of 1M HCl to afford a dark green precipitate (0.179 g, 0.15 mmol, 45 %).

^{1}H NMR: no good ^{1}H NMR could be obtained due to instability of the complex in DMSO, the only solvent in which it is soluble.

MS (ES): m/z 1159.5 [M-Cl]$^+$ (calc. 1159.3).

IR: υ/cm^{-1} 3037 (w), 2921 (w), 2851 (w), 1689 (m), 1601 (m), 1573 (w), 1538 (m), 1381 (w), 1225 (m), 1177 (m), 1102 (m), 1015 (w), 852 (s), 767 (s), 740 (w), 722 (m), 692 (s).

UV-VIS (DMSO): λ_{max}/nm (ε/M^{-1} cm^{-1}) 271 (192000), 325 (37000), 435 (1500), 590 (900).

E° Cu^{II}/Cu^{I} (DMSO)/V vs. Fc: -0.050 V (reversible).

Anal. Calc. for C$_{72}$H$_{48}$ClCuN$_4$O$_8$·5H$_2$O: C, 67.23; H, 4.55; N, 4.36; found: C, 67.33; H, 4.27; N, 4.10 %.

[Cu(H$_2$L8)$_2$]Cl

L8 (0.0897 g, 0.33 mmol) in water (2 ml) was warmed to 70°C, and then 15 drops of 1M NaOH solution were added. To this solution, copper(II) sulfate [CuSO$_4$·5H$_2$O, 0.042 g, 0.17 mmol] in water (2 ml) was added, followed by further addition of 20 drops of 1M NaOH solution. Ascorbic acid (0.0440 g, 0.25 mmol) in water (0.3 ml) was added to this solution and the solution turned dark red. The solution pH was adjusted to 2 by addition of 1M HCl to afford a red precipitate (0.0702 g, 0.11 mmol, 33 %).

^{1}H NMR (methanol-d^4, 500 MHz): δ/ppm 8.54 (s, 8H; H^{3A}, H^{4A}), 2.57 (s, 12H; H$^{\underline{CH}3}$).

MS (ES): m/z 605.1 [M-Cl-2H]$^-$ (calc. 605.1).

IR: υ/cm^{-1} 3525 (w), 2916 (w), 1712 (m), 1581 (m), 1404 (w), 1381 (w), 1265 (m), 1157 (s), 1095 (w), 980 (w), 956 (w), 926 (w), 848 (m), 771 (s), 663 (w), 578 (m), 501 (m), 463 (s), 447 (s).

UV-VIS (MeOH): λ_{max}/nm (ε/M^{-1} cm^{-1}) 214 (74400), 274 (47000), 314 (60000), 482 (8000).

E° Cu^{II}/Cu^{I} (MeOH)/V vs. Fc: +0.53 (quasireversible).

Anal. Calc. for C$_{28}$H$_{24}$ClCuN$_4$O$_8$: C, 52.26; H, 3.76; N, 8.71; found: C, 52.94; H, 4.25; N, 8.62 %.

[Cu(L9)$_2$][PF$_6$]

[Cu(CH$_3$CN)$_4$][PF$_6$] (18.6 mg, 0.050 mmol) dissolved in CH$_3$CN (2 ml) was added to a solution of **L9** (31.6 mg, 0.100 mmol) in CHCl$_3$ (5 ml), and the colourless solution turned red. Upon addition of ether to the solution a red solid precipitated and it was filtered (38.8 mg, 0.046 mmol, 46 %).

^{1}H NMR (CDCl$_3$, 500 MHz): δ/ppm 8.42 (s, 4H; H^{3A}), 7.68 (s, 8H; H^{5A}, H^{5B}), 7.26 (m, 4H; H^{3B}), 6.66 (d, J = 1.4 Hz, 4H; H^{4B}), 2.29 (s, 12H; H^{CH3}).

MS (ES): m/z 695.8 [M-PF$_6$]$^+$ (calc. 695.2).

IR: υ/cm^{-1} 3115 (w), 2949 (w), 2912 (w), 2361 (w), 2334 (w), 1610 (m), 1547 (m), 1489 (m), 1441 (w), 1371 (w), 1250 (w), 1221 (w), 1159 (w), 1078 (w), 1020 (m), 937 (w), 931 (w), 885 (w), 871 (w), 835 (s), 738 (s), 704 (m), 673 (w).

UV-VIS (CH$_3$CN): λ$_{max}$/nm (ε/M^{-1} cm^{-1}) 274 (67000), 289 (71000), 493 (4100).

E° Cu^{II}/Cu^{I} (CH$_3$CN)/V vs. Fc: +0.294 (reversible).

Anal. Calc. for C$_{40}$H$_{32}$CuF$_6$N$_4$O$_4$P·1H$_2$O: C, 55.91; H, 3.99; N, 6.52; found: C, 55.83; H, 3.77; N, 6.36 %.

[Cu(H$_2$L10)$_2$]Cl

L10 (89.7 mg, 0.33 mmol) in water (2 ml) was warmed to 70°C, and then 15 drops of 1M NaOH solution were added. To this solution, copper(II) sulfate [CuSO$_4$·5H$_2$O, 42.0 mg, 0.17 mmol] in

water (2.0 ml) was added, followed by further addition of 20 drops of 1M NaOH solution. Ascorbic acid (44.0 mg, 0.25 mmol) in water (0.3 ml) was added to this solution and it turned dark red. The solution pH was adjusted to 2 by addition of 1M HCl to afford a red precipitate (58.3 mg, 0.09 mmol, 27 %).

^{1}H NMR (methanol-d^4, 500 MHz): δ/ppm 8.91 (s, 4H; H^{3A}), 8.12 (s, 4H; H^{5A}), 2.32 (s, 12H; H$^{C\underline{H}3}$).

MS (ES): m/z 607.2 [M-Cl]$^+$ (calc. 607.1).

IR: υ/cm^{-1} 3180 (w), 1712 (s), 1558 (s), 1434 (m), 1388 (m), 1265 (m), 1218 (m) 894 (m), 763 (s), 671 (m).

UV-VIS (MeOH): λ$_{max}$/nm (ε/M^{-1} cm^{-1}) 202 (34300), 252 (27200), 268 (25000), 319 (35400), 483 (9900).

E° Cu^{II}/Cu^{I} (MeOH)/V vs. Fc: +0.417 V (quasireversible).

Anal. Calc. for: C$_{28}$H$_{24}$ClCuN$_4$O$_8$·4H$_2$O: C, 47.00; H, 4.51; N, 7.83; found: C, 47.46; H, 3.99; N, 7.90 %.

[Cu(L11)$_2$][PF$_6$]

[Cu(CH$_3$CN)$_4$][PF$_6$] (18.6 mg, 0.050 mmol) dissolved in CH$_3$CN (2 ml) was added to a solution of **L11** (30.0 mg, 0.100 mmol) in CHCl$_3$ (5 ml), and the colorless solution turned red. Upon addition of ether to the solution a red solid precipitated and it was filtered (26.7 mg, 0.033 mmol, 65 %).

^{1}H NMR (CDCl$_3$, 500 MHz): δ/ppm 8.78 (s, 4H; H^{3A}), 8.08 (s, 4H; H^{5A}), 4.08 (s, 12H; H$^{COOC\underline{H}3}$), 2.30 (s, 12H; H$^{C\underline{H}3}$).

MS (ES): m/z 663.1 [M-PF$_6$]$^+$ (calc. 663.2).

IR: υ/cm^{-1} 2924 (w), 2849 (w, 1956 (w), 1734 (m), 1724 (m), 1560 (w), 1439 (w), 1389 (w), 1354 (w), 1294 (w), 1230 (m), 1163 (w), 993 (w), 985 (w), 839 (s).

UV-VIS (CH$_3$CN): λ_{max}/nm (ε/M^{-1} cm^{-1}) 204 (90000), 241 (23000), 308 (27000), 317 (25000), 495 (500).

E° Cu^{II}/Cu^{I} (CH$_2$Cl$_2$)/V vs. Fc: +0.588 V (quasireversible).

Anal. Calc. for C$_{32}$H$_{32}$CuF$_6$N$_4$O$_8$P·1.5H$_2$O: C, 45.97; H, 4.22; N, 6.70; found: C, 45.82, H, 3.68; N, 6.74 %.

[Cu(L14)$_2$][PF$_6$]

[Cu(CH$_3$CN)$_4$][PF$_6$] (18.6 mg, 0.050 mmol) dissolved in CH$_3$CN (2 ml) was added to a solution of **L14** (35.2 mg, 0.100 mmol) in CHCl$_3$ (5 ml), and the colourless solution turned red. Upon addition of ether to the solution a red solid precipitated and it was filtered (41.0 mg, 0.045 mmol, 45 %).

^{1}H NMR (CDCl$_3$, 500 MHz): δ/ppm 8.26 (s, 4H; H^{3A}), 7.74 (d, J = 15.8 Hz, 4H; H$^{C\underline{H}=CH-COO}$), 7.56 (s, 4H; H^{5A}), 6.83 (d, J = 16.0 Hz, 4H; H$^{CH=C\underline{H}-COO}$), 3.87 (s, 12H; H$^{COOC\underline{H}3}$), 2.26 (s, 12H; H$^{C\underline{H}3}$).

MS (ES): m/z 767.5 [M-PF$_6$]$^+$ (calc. 767.2).

IR: υ/cm^{-1} 3078 (w), 2993 (w), 2955 (w), 1705 (m), 1643 (m), 1612 (m), 1551 (m), 1435 (m), 1281 (m), 1180 (m), 1034 (w), 980 (m), 833 (s), 710 (w), 648 (w).

UV-VIS (CH$_3$CN): λ_{max}/nm (ε/M^{-1} cm^{-1}) 255 (94000), 324 (24000), 508 (4000).

$E°$ Cu^{II}/Cu^{I} (CH_3CN)/V vs. Fc: +0.331 (reversible).

Anal. Calc. for $C_{40}H_{40}CuF_6N_4O_8P·3H_2O$: C, 49.67; H, 4.79; N, 5.79; found: C, 49.29; H, 4.15; N, 5.71 %.

[Cu(H₂L15)₂]Cl

L15 (113.9 mg, 0.35 mmol) in water (2.1 ml) was warmed to 70°C, and then 16 drops of 1M NaOH solution were added. To this solution, copper(II) sulfate [$CuSO_4·5H_2O$, 44.7 mg, 0.18 mmol] in water (2.1 ml) was added, followed by further addition of 21 drops of 1M NaOH solution. Ascorbic acid (45.7 mg, 0.26 mmol) in water (0.3 ml) was added to this solution and it turned dark red. The solution pH was adjusted to 2 by addition of 1M HCl to afford a red precipitate (58.6 mg, 0.08 mmol, 23 %).

^{1}H NMR (DMSO-d^6, 500 MHz): δ/ppm 12.89 (s, 4H; H^{COOH}), 8.95 (s, 4H; H^{3A}), 7.93 (s, 4H; H^{5A}), 7.67 (d, J = 15.6 Hz, 4H; H$^{CH=CH-COOH}$), 7.13 (d, J = 14.9 Hz, 4H; H$^{CH=CH-COOH}$), 2.18 (s, 12H; ^{CH3}).

MS (ES): m/z 711.5 [M-Cl]$^+$ (calc. 711.2).

IR: υ/cm^{-1} 2925 (w), 2867 (w), 1705 (s), 1699 (s), 1633 (m), 1606 (s), 1549 (s), 1429 (m), 1385 (m), 1263 (m), 1180 (s), 1032 (w), 976 (s), 856 (s), 686 (s).

UV-VIS (DMSO): $λ_{max}$/nm (ε/M^{-1} cm^{-1}) 260 (75000), 331 (24000), 515 (7000).

$E°$ Cu^{II}/Cu^{I} (DMSO)/V vs. Fc: -0.122 V (reversible).

Anal. Calc. for $C_{36}H_{32}ClCuN_4O_8·2.5H_2O·2NaCl$: C, 47.54; H, 4.10; N, 6.16; found: C, 47.18; H, 3.82; N, 6.08 %.

[Cu(L16)$_2$][PF$_6$]

[Cu(CH$_3$CN)$_4$][PF$_6$] (84.6 mg, 0.227 mmol) dissolved in CH$_3$CN (3 ml) was added to a solution of **L16** (200.0 mg, 0.455 mmol) in CHCl$_3$ (7ml), and the colorless solution turned dark green. Upon addition of ether to the solution a dark green solid precipitated and it was filtered (336.0 mg, 0.309 mmol, 68 %).

^{1}H NMR (CD$_2$Cl$_2$ with added K$_2$CO$_3$, 600 MHz): δ/ppm 8.13 (s, 4H; H^{3A}), 7.77 (d, J = 1.1 Hz, 4H; H^{5B}), 7.75 (s, 4H; H^{5A}), 7.58 (d, J = 7.4 Hz, 8H; H^{2C}), 7.21 (d, J = 3.4 Hz, 4H; H^{3B}), 7.06 (t, J = 7.4 Hz, 4H; H^{4C}), 6.91 (t, J = 7.6 Hz, 8H; H^{3C}), 6.73 (dd, J = 3.3 Hz, J = 1.7 Hz, 4H; H^{4B}).

^{13}C NMR (CD$_2$Cl$_2$ with added K$_2$CO$_3$, 151 MHz): δ/ppm 157.8 (C^{6A}), 153.9 (C^{2A}), 150.9 (C^{2B}), 145.7 (C^{5B}), 139.7 (C^{4A}), 138.8 (C^{1C}), 129.9 (C^{4C}), 128.1 (C^{2C}, C^{3C}), 119.2 (C^{5A}), 115.5 (C^{3A}), 113.5 (C^{4B}), 111.5 (C^{3B}).

MS (ES): m/z 943 [M-PF$_6$]$^+$ (calc. 943.2).

IR: υ/cm^{-1} 3122 (w), 3058 (w), 1735 (w), 1608 (s), 1539 (m), 1486 (m), 1453 (w), 1440 (w), 1429 (w), 1407 (w), 1371 (w), 1308 (w), 1244 (w), 1222 (m), 1157 (w), 1076 (w), 1016 (m), 936 (w), 920 (w), 884 (m), 833 (s), 769 (s), 738 (s), 692 (s), 642 (m), 590 (m), 554 (s).

UV-VIS (CHCl$_3$): λ$_{max}$/nm (ε/M^{-1} cm^{-1}) 244 (35000), 282 (36000), 313 (48000), 432 (4000), 587 (2400).

E° Cu^{II}/Cu^I (CH$_3$CN)/V vs. Fc: +0.271 (reversible).

Anal. Calc. for C$_{60}$H$_{40}$CuF$_6$N$_4$O$_4$P·2.4H$_2$O: C, 63.62; H, 3.99; N, 4.95; found: C, 63.89/63.63; H, 3.52/3.72; N, 4.92/4.79 %.

[Cu(H₂L17)₂]Cl

L17 (39.6 mg, 0.10 mmol) in water (0.6 ml) was warmed to 70°C, and then 5 drops of 1M NaOH solution were added. To this solution, copper(II) sulfate [CuSO₄·5H₂O, 12.5 mg, 0.05 mmol] in water (0.6 ml) was added, followed by further addition of 6 drops of 1M NaOH solution. Ascorbic acid (13.2 mg, 0.075 mmol) in water (0.1 ml) was added to this solution and it turned dark green. The solution pH was adjusted to 2 by addition of 1M HCl to afford a dark green precipitate (31.1 mg, 0.035 mmol, 35 %).

^{1}H NMR (D₂O, 600 MHz): δ/ppm 8.08 (s, 4H; H^{3A}), 6.99 (m, 12H; H^{5A}, H^{2C}), 6.49 (m, 4H; H^{4C}), 6.40 (m, 8H; H^{3C}).

IR: υ/cm^{-1} 3059 (w), 2356 (w), 1716 (s), 1608 (w), 1552 (s), 1456 (m), 1437 (m), 1377 (m), 1296 (w), 1217 (s), 1026 (w), 999 (w), 901 (m), 841 (m), 764 (s), 737 (m), 692 (s), 640 (m).

UV-VIS (H₂O): λ$_{max}$/nm (ε/M^{-1} cm^{-1}) 296 (10000), 343 (11000), 437 (2000), 608 (1170).

E° Cu^{II}/Cu^{I} (H₂O)/V vs. Fc: 0.0 V (reversible).

Anal. Calc. for C₄₈H₃₁ClCuN₄O₈·1.7H₂O: C, 62.57; H, 3.76; N, 6.08; found: C, 62.82; H, 3.86; N, 6.05 %.

[Cu(L18)₂][PF₆]

[Cu(CH₃CN)₄][PF₆] (18.6 mg, 0.050 mmol) dissolved in CH₃CN (2.0 ml) was added to a solution of **L18** (42.4 mg, 0.100 mmol) in CHCl₃ (5.0 ml), and the colourless solution turned dark green. A dark green solid precipitated upon addition of ether to the solution. It was filtered and washed with water and ether (43.3 mg, 0.041 mmol, 82 %).

^{1}H NMR (CDCl₃, 400 MHz): δ/ppm 8.52 (s, 4H; H^{3A}), 8.11 (s, 4H; H^{5A}), 7.49 (d, J = 7.9 Hz, 8H; H^{2C}), 7.10 (t, J = 7.5 Hz, 4H; H^{4C}), 6.90 (t, J = 7.7 Hz, 8H; H^{3C}), 4.14 (s, 12H; H$^{COOC\underline{H}3}$).

MS (ES): m/z 911.9 [M-PF$_6$]$^+$ (calc. 911.2).

IR: υ/cm^{-1} 3063 (w), 2955 (w), 1728 (m), 1612 (w), 1558 (w), 1443 (w), 1373 (w), 1257 (s), 1226 (s), 1134 (w), 1072 (w), 995 (m), 910 (w), 833 (s), 764 (m), 694 (m), 640 (w).

UV-VIS (CH$_2$Cl$_2$): λ_{max}/nm (ε/M^{-1} cm^{-1}) 300 (12000), 350 (16000), 441 (3000), 610 (2000).

E$^\circ$ Cu^{II}/Cu^{I} (CH$_2$Cl$_2$)/V vs. Fc: +0.589 V (reversible).

Anal. Calc. for C$_{52}$H$_{40}$CuF$_6$N$_4$O$_8$P·5H$_2$O·4.5CHCl$_3$: C, 40.28; H, 3.26; N, 3.33; found: C, 40.09; H, 3.49; N, 3.48 %.

[Cu(L21)$_2$][PF$_6$]

[Cu(CH$_3$CN)$_4$][PF$_6$] (18.6 mg, 0.050 mmol) dissolved in CH$_3$CN (2.0 ml) was added to a solution of **L21** (47.6 mg, 0.100 mmol) in CHCl$_3$ (5.0 ml), and the colourless solution turned dark green. A dark green solid precipitated upon addition of ether to the solution. It was filtered and washed with water and ether (43.5 mg, 0.037 mmol, 75 %).

^{1}H NMR (CDCl$_3$, 400 MHz): δ/ppm 8.10 (s, 4H; H^{3A}), 7.78 (d, J = 16.2 Hz, 4H; H$^{C\underline{H}=CH-COO}$), 7.53 (m, 12H; H^{5A}, H^{2C}), 7.11 (bs, 4H; H^{4C}), 6.92 (m, 12H; H$^{CH=C\underline{H}-COO}$, H^{3C}), 3.94 (s, 12H; H$^{COOC\underline{H}3}$).

MS (ES): m/z 1015.0 [M-PF$_6$]$^+$ (calc. 1015.3).

IR: υ/cm^{-1} 2949 (w), 2924 (w), 2850 (w), 1714 (m), 1645 (w), 1608 (w), 1593 (w), 1580 (w), 1545 (m), 1497 (w), 1433 (m), 1402 (w), 1315 (w), 1281 (m), 1167 (m), 1115 (w), 1074 (w), 1026 (w), 983 (w), 943 (w), 831 (s), 773 (m), 740 (m), 694 (m), 634 (w).

UV-VIS (CH$_2$Cl$_2$): λ_{max}/nm (ε/M^{-1} cm^{-1}) 244 (88000), 348 (23000), 420 (10000), 615 (4000).

E° Cu^{II}/Cu^{I} (CH$_2$Cl$_2$)/V vs. Fc: +0.443 V (reversible).

Anal. Calc. for C$_{60}$H$_{48}$CuF$_6$N$_4$O$_8$P·7.5H$_2$O·CH$_3$CN: C, 55.67; H, 4.97; N, 5.24; found: C, 55.23; H, 4.35; N, 5.08 %.

[Cu(H$_2$L22)$_2$]Cl

L22 (44.8 mg, 0.10 mmol) in water (0.6 ml) was warmed to 70°C, and then 5 drops of 1M NaOH solution were added. To this solution, copper(II) sulfate [CuSO$_4$·5H$_2$O, 12.5 mg, 0.05 mmol] in water (0.6 ml) was added, followed by further addition of 6 drops of 1M NaOH solution. Ascorbic acid (13.2 mg, 0.075 mmol) in water (0.1 ml) was added to this solution and it turned dark green. The solution pH was adjusted to 2 by addition of 1M HCl to afford a dark green precipitate that was washed with water (20.8 mg, 0.021 mmol, 31 %).

^{1}H NMR: no good ^{1}H NMR could be obtained due to instability of the complex in DMSO, the only solvent in which it is soluble.

IR: υ/cm^{-1} 3053.1 (w), 2922.0 (w), 2850.6 (w), 1699.2 (s), 1639.4 (m), 1606.6 (m), 1597.0 (m), 1541.0 (s), 1456.2 (w), 1433.0 (w), 1398.3 (s), 1276.8 (w), 1168.8 (m), 1074.3 (w), 1026.1 (w), 974.0 (m), 858.3 (m), 771.5 (s), 744.5 (m), 692.4 (s).

UV-VIS (DMSO): λ$_{max}$/nm (ε/M^{-1} cm^{-1}) 261 (100000), 339 (20000), 462 (1700), 630 (1000).

E° Cu^{II}/Cu^{I} (DMSO)/V vs. Fc: -0.098 (quasireversible).

Anal. Calc. for C$_{56}$H$_{40}$ClCuN$_4$O$_8$·H$_2$O: C, 66.33; H, 4.18, N, 5.53; found: C, 66.65; H, 4.92; N, 5.12 %.

[Cu(L23)$_2$][PF$_6$]

[Cu(CH$_3$CN)$_4$][PF$_6$] (8.16 mg, 0.022 mmol) dissolved in CH$_3$CN (0.5 ml) was added to a solution of **L23** (20.0 mg, 0.044 mmol) in CHCl$_3$ (2.0 ml), and the colourless solution turned red.

A red solid precipitated upon addition of hexane to the solution. It was filtered and washed with ether (23.9 mg, 0.021 mmol, 98 %).

^{1}H NMR (CDCl$_3$, 400 MHz): δ/ppm 8.54 (d, J = 7.3 Hz, 4H; H^{3A}), 7.84 (d, J = 8.5 Hz, 4H; H^{5A}), 4.27 (s, 16H; H$^{C\underline{H2}CH3}$), 2.30 (s, 12H; H$^{C\underline{H3}}$), 1.42 (t, J = 6.6 Hz, 24H; H$^{CH2C\underline{H3}}$).

MS (ES): m/z 975.7 [M-PF$_6$]$^+$ (calc. 975.3).

UV-VIS (CHCl$_3$): λ$_{max}$/nm (ε/M^{-1} cm^{-1}) 254 (16000), 273 (16000), 317 (30000), 490 (5700).

[Cu(H$_4$L24)$_2$]Cl

L24 (80.0 mg, 0.233 mmol) in water (1.4 ml) was warmed to 70°C, and then 11 drops of 1M NaOH solution were added. To this solution, copper(II) sulfate [CuSO$_4$·5H$_2$O, 29.0 mg, 0.116 mmol] in water (1.4 ml) was added, turning the solution blue. This was followed by further addition of 14 drops of 1M NaOH solution. Ascorbic acid (31.0 mg, 0.176 mmol) in water (0.2 ml) was added to this solution and it turned red. The solution pH was adjusted to 2 by addition of 1M HCl, however, no precipitate appeared. Upon addition of ethanol an orange-red solid precipitates (91.3 mg, 0.116 mmol, 50 %).

^{1}H NMR (D$_2$O, 500 MHz): δ/ppm 8.52 (d, J = 12.4 Hz, 4H; H^{3A}), 7.73 (d, J = 12.0 Hz, 4H; H^{5A}), 2.23 (s, 12H; H$^{C\underline{H3}}$).

^{13}C NMR (D$_2$O, 126 MHz): δ/ppm 158.3 (d, J = 12.0 Hz; C^{6A}), 152.1 (s; C^{2A}), 146.8 (d, J = 170.4 Hz; C^{4A}), 127.0 (d, J = 6.1 Hz; C^{5A}), 120.6 (d, J = 8.3 Hz; C^{3A}), 24.9 (s; C$^{\underline{CH3}}$).

^{31}P NMR (D$_2$O, 162 MHz): δ/ppm 9.41 (ref. to 85 % H$_3$PO$_4$ at δ 0 ppm).

IR: υ/cm^{-1} 3304 (bs), 2967 (w), 1633 (w), 1602 (w), 1541 (w), 1431 (w), 1383 (w), 1331 (w), 1134 (m), 1050 (m), 912 (m), 876 (m), 736 (w), 726 (w), 620 (w), 575 (s), 560(s).

UV-VIS (DMSO): λ_{max}/nm (ε/M^{-1} cm^{-1}) 271 (1800), 313 (2100), 324 (2000), 478 (800).

Anal. Calc. for $C_{24}H_{28}ClCuN_4O_{12}P_4 \cdot 6NaOH \cdot EtOH$: C, 29.09; H, 3.76; N, 5.22; found: C, 28.84/ 28.51; H, 3.28/3.25; N, 4.45/4.50 %.

[Cu(H$_2$L25)$_2$]Cl

L25 (113.6 mg, 0.33 mmol) in water (2.0 ml) was warmed to 70°C, and then 15 drops of 1N NaOH solution were added. To this solution, copper sulfate [$CuSO_4 \cdot 5H_2O$, 42.4 mg, 0.17 mmol] in water (2.0 ml) was added, followed by further addition of 18 drops of 1N NaOH solution. Ascorbic acid (44.0 mg, 0.25 mmol) in water (0.3 ml) was added to this solution and it turned dark purple. The solution pH was adjusted to 2 by addition of 1N HCl to afford a dark purple precipitate (34.7 mg, 0.044 mmol, 26 %). This complexation was done according to a procedure mentioned in literature. [61]

^{1}H NMR: it was not possible to obtain a well resolved ^{1}H NMR spectrum.

MS (ES): m/z 749.3 [M-Cl-2H]$^-$ (calc. 749.1).

IR: υ/cm^{-1} 3066 (w), 2359 (w), 2334 (w, 1699 (m), 1583 (w), 1558 (w), 1508 (m), 1454 (w), 1394 (w), 1358 (m), 1200 (m), 1151 (m), 1103 (w), 958 (w), 895 (w), 874 (w), 798 (w), 771 (m), 681 (w), 600 (m), 580 (m), 503 (m), 469(s), 413(s).

UV-VIS (MeOH:DMSO 9:1): λ_{max}/nm (ε/M^{-1} cm^{-1}) 268 (57000), 344 (24000), 358 (22000), 553 (4000).

E° Cu^{II}/Cu^{I} (DMSO)/V vs. Fc: -0.178 V (reversible)

Anal. Calc. for $C_{40}H_{24}ClCuN_4O_8 \cdot 1.3H_2O$: C, 59.23; H, 3.31; N, 6.91; found: C, 59.26; H, 3.32; N, 6.78 %.

[Cu(L26)$_2$][PF$_6$]

[Cu(CH$_3$CN)$_4$][PF$_6$] (11.4 mg, 0.031 mmol) dissolved in CH$_3$CN (1.0 ml) was added to a solution of **L26** (23.0 mg, 0.062 mmol) in CHCl$_3$ (2.0 ml), and the colourless solution turned dark purple. A dark purple solid precipitated upon addition of ether to the solution. It was filtered and washed with CHCl$_3$ and ether (12.0 mg, 0.013 mmol, 41 %).

^{1}H NMR (DMSO-d^6, 500 MHz): δ/ppm 9.51 (s, 4H; H^3), 8.59 (d, J = 8.1 Hz, 4H; H^8), 7.84 (bs, 4H; H^5), 7.74 (m, 4H; H^7), 7.54 (bs, 4H; H^6), 4.16 (s, 6H; H$^{COOOC\underline{H}3}$).

MS (ES): m/z 807.7 [M-PF$_6$]$^+$ (calc. 807.2).

IR: υ/cm^{-1} 2954 (w), 1732 (m), 1709 (m), 1586 (w), 1567 (w), 1512 (w), 1442 (w), 1360 (m), 1270 (m), 1236 (w), 1218 (w), 1156 (w), 1108 (m), 1023 (w), 983 (w), 952 (w), 875 (w), 834 (s), 796 (m), 773 (m), 637 (w), 619 (w).

UV-VIS (DMSO): λ$_{max}$/nm (ε/M^{-1} cm^{-1}) 272 (50000), 343 (26000), 581 (1100).

E° Cu^{II}/Cu^{I} (DMSO)/V vs. Fc: -0.384 V (reversible).

Anal. Calc. for C$_{44}$H$_{32}$CuF$_6$N$_4$O$_8$P·H$_2$O·CHCl$_3$: C, 49.56; H, 3.23; N, 5.14; found: C, 49.40; H, 3.19; N, 5.39 %.

VII   Crystallographic data

(1*E*,5*E*)-1,6-Diphenylhexa-1,5-diene-3,4-dione

Crystal data and structure refinement for (1*E*,5*E*)-1,6-diphenylhexa-1,5-diene-3,4-dione.

Formula	$C_{18} H_{14} O_2$
Formula weight	262.31
Temperature [K]	173
Wavelength [Å]	0.71073
Crystal system	Orthorhombic
Space group	*Pcab*
a, *b*, *c*, [Å]	7.13530(10), 10.0052(2), 18.7210(5)
α, *β*, *γ*, [°]	90, 90, 90
Volume [Å^3]	1336.49(5)
Z	4
Density (calc.) [g cm^{-3}]	1.304
Absorption coefficient [mm^{-1}]	0.084
F(000)	552
Crystal size	0.26 x 0.22 x 0.01
Theta range for data collection [°]	2.176 to 30.007
Index ranges: h, k, l	-9 to 9, -14 to 14, -26 to 25
Reflections collected	12637
Independent reflections	1944 [R(int) = 0.146]
Completeness to theta = 30.007°	99.8 %
Absorption correction	Semi-empirical from equivalents
Max. and min. transmission	1.00 and 0.98
Refinement method	Full-matrix least-squares on F^2
Data / restraints / parameters	1132 / 0 / 91
Goodness-of-fit on F^2	1.1079

Final R indices [I>2sigma(I)]	R1 = 0.0320, wR2 = 0.0397
R indices (all data)	R1 = 0.0558, wR2 = 0.0583
Largest diff. peak and hole [e Å^{-3}]	0.25 and -0.13

(1*E*,5*E*)-1,6-Di(furan-2-yl)hexa-1,5-diene-3,4-dione

Crystal data and structure refinement for (1*E*,5*E*)-1,6-di(furan-2-yl)hexa-1,5-diene-3,4-dione.

Formula	$C_{14} H_{10} O_4$
Formula weight	242.23
Temperature [K]	173
Wavelength [Å]	0.71073
Crystal system	Monoclinic
Space group	*C*2/*c*
a, *b*, *c*, [Å]	37.4261(14), 3.7745(2), 18.0118(7)
α, *β*, *γ*, [°]	90, 118.174(2), 90
Volume [Å^3]	2242.96(18)
Z	8
Density (calc.) [g cm^{-3}]	1.435
Absorption coefficient [mm^{-1}]	0.106
F(000)	1008
Crystal size	0.38 x 0.10 x 0.07
Theta range for data collection [°]	3.332 to 27.480
Index ranges: h, k, l	-48 to 47, -4 to 4, -23 to 23
Reflections collected	9272
Independent reflections	2556 [R(int) = 0.026]
Completeness to theta = 27.480°	99.7 %
Absorption correction	Semi-empirical from equivalents
Max. and min. transmission	0.99 and 0.99
Refinement method	Full-matrix least-squares on F^2

Data / restraints / parameters	1651 / 0 / 164
Goodness-of-fit on F^2	1.1377
Final R indices [I>2sigma(I)]	R1 = 0.0470, wR2 = 0.0519
R indices (all data)	R1 = 0.0717, wR2 = 0.0648
Largest diff. peak and hole [e Å^{-3}]	0.16 and -0.20

6,6´-Dimethyl-4,4´-diphenyl-2,2´-bipyridine (L1)

Crystal data and structure refinement for 6,6´-dimethyl-4,4´-diphenyl-2,2´-bipyridine (**L1**).

Formula	$C_{24} H_{20} N_2$
Formula weight	336.42
Temperature [K]	223(2)
Wavelength [Å]	0.71073
Crystal system	Monoclinic
Space group	$P2_1/c$
a, b, c, [Å]	11.100(2), 7.4744(15), 11.986(2)
α, β, γ, [°]	90, 117.27(3), 90
Volume [Å^3]	883.9(4)
Z	2
Density (calc.) [g cm^{-3}]	1.264
Absorption coefficient [mm^{-1}]	0.074
F(000)	356
Crystal size	0.35 x 0.25 x 0.10
Theta range for data collection [°]	3.33 to 29.99
Index ranges: h, k, l	-14 to 15, -10 to 10, -16 to 16
Reflections collected	17340
Independent reflections	2520 [R(int) = 0.0392]
Completeness to theta = 29.99°	97.8 %

Absorption correction	None
Refinement method	Full-matrix least-squares on F^2
Data / restraints / parameters	2520 / 0 / 119
Goodness-of-fit on F^2	1.078
Final R indices [I>2sigma(I)]	R1 = 0.0474, wR2 = 0.1338
R indices (all data)	R1 = 0.0492, wR2 = 0.1354
Largest diff. peak and hole [e Å^{-3}]	0.318 and -0.153

4,4´,6,6´-Tetraphenyl-2,2´-bipyridine (L2)

Crystal data and structure refinement for 4,4´,6,6´-tetraphenyl-2,2´-bipyridine (**L2**).

Formula	$C_{34} H_{24} N_2$
Formula weight	460.55
Temperature [K]	200(2)
Wavelength [Å]	0.71073
Crystal system	Triclinic
Space group	*P*-1
a, *b*, *c*, [Å]	10.444(2), 10.573(2), 12.728(3)
α, *β*, *γ*, [°]	95.43(3), 102.65(3), 113.15(3)
Volume [Å^3]	1235.1(6)
Z	2
Density (calc.) [g cm^{-3}]	1.238
Absorption coefficient [mm^{-1}]	0.072
F(000)	484
Crystal size	0.38 x 0.15 x 0.10
Theta range for data collection [°]	2.97 to 25.05
Index ranges: h, k, l	-12 to 12, -12 to 12, -15 to 15
Reflections collected	14903

Independent reflections	4343 [R(int) = 0.0847]
Completeness to theta = 25.05°	99.1 %
Absorption correction	None
Refinement method	Full-matrix least-squares on F^2
Data / restraints / parameters	4343 / 0 / 326
Goodness-of-fit on F^2	1.159
Final R indices [I>2sigma(I)]	R1 = 0.0663, wR2 = 0.1471
R indices (all data)	R1 = 0.0848, wR2 = 0.1573
Largest diff. peak and hole [e Å^{-3}]	0.176 and -0.167

Dimethyl 4,4´-(6,6´-dimethyl-2,2´-bipyridine-4,4'-diyl)dibenzoate (L3)

Crystal data and structure refinement for dimethyl 4,4´-(6,6´-dimethyl-2,2´-bipyridine-4,4´-diyl)-dibenzoate (**L3**).

Formula	$C_{28} H_{24} N_2 O_4$
Formula weight	452.5
Temperature [K]	173
Wavelength [Å]	0.71073
Crystal system	Triclinic
Space group	P-1
a, b, c, [Å]	3.8467(4), 11.1122(10), 13.3242(12)
α, β, γ, [°]	107.904(6), 95.813(6), 94.638(6)
Volume [Å^3]	535.39(9)
Z	1
Density (calc.) [g cm^{-3}]	1.403
Absorption coefficient [mm^{-1}]	0.095
F(000)	238
Crystal size	0.20 x 0.03 x 0.01

Theta range for data collection [°]	1.620 to 31.727
Index ranges: h, k, l	-5 to 5, -16 to 15, -19 to 19
Reflections collected	7553
Independent reflections	3452 [R(int) = 0.049]
Completeness to theta = 25.064°	99.0 %
Absorption correction	Semi-empirical from equivalents
Max. and min. transmission	1.00 and 1.00
Refinement method	Full-matrix least-squares on F^2
Data / restraints / parameters	1572 / 0 / 154
Goodness-of-fit on F^2	1.1233
Final R indices [I>2sigma(I)]	R1 = 0.0531, wR2 = 0.0468
R indices (all data)	R1 = 0.1423, wR2 = 0.118
Largest diff. peak and hole [e Å^{-3}]	0.39 and -0.26

4,4´-Di(furan-2-yl)-6,6´-dimethyl-2,2´-bipyridine (L9)

Crystal data and structure refinement for 4,4´-di(furan-2-yl)-6,6´-dimethyl-2,2´-bipyridine (**L9**).

Formula	$C_{20} H_{16} N_2 O_2$
Formula weight	316.36
Temperature [K]	173
Wavelength [Å]	0.71073
Crystal system	Orthorhombic
Space group	*Pcab*
a, *b*, *c*, [Å]	6.51940(10), 12.1847(2), 19.5707(3)
α, *β*, *γ*, [°]	90, 90, 90
Volume [Å^3]	1554.64(4)
Z	4
Density (calc.) [g cm^{-3}]	1.352
Absorption coefficient [mm^{-1}]	0.089

F(000)	664
Crystal size	0.21 x 0.16 x 0.04
Theta range for data collection [°]	2.081 to 27.868
Index ranges: h, k, l	-8 to 8, -16 to 16, -25 to 25
Reflections collected	13630
Independent reflections	1855 [R(int) = 0.071]
Completeness to theta = 27.868°	100.0 %
Absorption correction	Semi-empirical from equivalents
Max. and min. transmission	1.00 and 0.99
Refinement method	Full-matrix least-squares on F^2
Data / restraints / parameters	1101 / 0 / 109
Goodness-of-fit on F^2	1.1205
Final R indices [I>2sigma(I)]	R1 = 0.0408, wR2 = 0.0349
R indices (all data)	R1 = 0.0641, wR2 = 0.0416
Largest diff. peak and hole [e Å^{-3}]	0.24 and -0.21

6,6´-Dimethyl-2,2´-bipyridine-4,4´-dicarboxylic acid (H$_2$L10)

Crystal data and structure refinement for 6,6´-dimethyl-2,2´-bipyridine-4,4´-dicarboxylic acid (H$_2$**L10**).

Formula	$C_{14} H_{12} N_2 O_4$
Formula weight	272.26
Temperature [K]	173
Wavelength [Å]	0.71073
Crystal system	Triclinic
Space group	*P*-1
a, *b*, *c*, [Å]	3.8591(6), 8.1105(11), 10.6066(16)
α, *β*, *γ*, [°]	73.344(9), 84.983(7), 77.881(10)
Volume [Å^3]	310.83(8)

Z	1
Density (calc.) [g cm^{-3}]	1.454
Absorption coefficient [mm^{-1}]	0.109
F(000)	142
Crystal size	0.41 x 0.17 x 0.02
Theta range for data collection [°]	2.005 to 27.893
Index ranges: h, k, l	-5 to 5, -10 to 10, -13 to 13
Reflections collected	2789
Independent reflections	1468 [R(int) = 0.030]
Completeness to theta = 27.335°	99.7 %
Absorption correction	Semi-empirical from equivalents
Max. and min. transmission	1.00 and 0.98
Refinement method	Full-matrix least-squares on F^2
Data / restraints / parameters	1461 / 0 / 91
Goodness-of-fit on F^2	1.0397
Final R indices [I>2sigma(I)]	R1 = 0.0513, wR2 = 0.0870
R indices (all data)	R1 = 0.0834, wR2 = 0.1174
Largest diff. peak and hole [e Å^{-3}]	0.46 and -0.34

Dimethyl 6,6´-dimethyl-2,2´-bipyridine-4,4´-dicarboxylate (L11)

Crystal data and structure refinement for dimethyl 6,6´-dimethyl-2,2´-bipyridine-4,4´-dicarboxylate (**L11**).

Formula	$C_8 H_8 N O_2$
Formula weight	150.15
Temperature [K]	200(2)
Wavelength [Å]	0.71073
Crystal system	Triclinic
Space group	*P*-1

a, b, c, [Å]	3.9139(8), 9.1945(18), 11.050(2)
α, β, γ, [°]	113.18(3), 92.60(3), 96.02(3)
Volume [Å^3]	361.90(13)
Z	2
Density (calc.) [g cm^{-3}]	1.378
Absorption coefficient [mm^{-1}]	0.100
F(000)	158
Crystal size	0.65 x 0.38 x 0.05
Theta range for data collection [°]	3.73 to 27.49
Index ranges: h, k, l	-5 to 5, -11 to 11, -14 to 14
Reflections collected	11231
Independent reflections	1634 [R(int) = 0.1384]
Completeness to theta = 27.49°	98.5 %
Absorption correction	None
Refinement method	Full-matrix least-squares on F^2
Data / restraints / parameters	1634 / 0 / 102
Goodness-of-fit on F^2	1.104
Final R indices [I>2sigma(I)]	R1 = 0.0613, wR2 = 0.1680
R indices (all data)	R1 = 0.0650, wR2 = 0.1721
Largest diff. peak and hole [e Å^{-3}]	0.400 and -0.254

4,4´-Di(furan-2-yl)-6,6´-diphenyl-2,2´-bipyridine (L16)

Crystal data and structure refinement for 4,4´-di(furan-2-yl)-6,6´-diphenyl-2,2´-bipyridine (**L16**).

Formula	$C_{30} H_{20} N_2 O_2$
Formula weight	440.50
Temperature [K]	200(2)
Wavelength [Å]	0.71073

Crystal system	Trigonal
Space group	*R*-3
a, *b*, *c*, [Å]	33.495(2), 33.495(2), 5.1499(3)
α, *β*, *γ*, [°]	90, 90, 120
Volume [Å^3]	5003.7(5)
Z	9
Density (calc.) [g cm^{-3}]	1.316
Absorption coefficient [mm^{-1}]	0.083
F(000)	2070
Crystal size	0.07 x 0.08 x 0.40
Theta range for data collection [°]	2.432 to 26.060
Index ranges: h, k, l	-37 to 41, -40 to 41, -6 to 5
Reflections collected	21185
Independent reflections	2084 [R(int) = 0.050]
Completeness to theta = 25.017°	94.9%
Absorption correction	Semi-empirical from equivalents
Max. and min. transmission	0.99 and 0.99
Refinement method	Full-matrix least-squares on F^2
Data / restraints / parameters	2064/0/155
Goodness-of-fit on F^2	1.0180
Final R indices [I>2sigma(I)]	R1 = 0.0375, wR2 = 0.0554
R indices (all data)	R1 = 0.0773, wR2 = 0.0800
Largest diff. peak and hole [e Å^{-3}]	0.33 and -0.30

6,6´-Diphenyl-2,2´-bipyridine-4,4´-dicarboxylic acid (H$_3$L17)

Crystal data and structure refinement for 6,6´-diphenyl-2,2´-bipyridine-4,4´-dicarboxylic acid (H$_3$**L17**).

Formula	C$_{30}$ H$_{19}$ F$_9$ N$_2$ O$_{10}$

Formula weight	738.47
Temperature [K]	173
Wavelength [Å]	0.71073
Crystal system	Triclinic
Space group	*P*-1
a, *b*, *c*, [Å]	9.0489(7), 9.8221(8), 17.5416(13)
α, *β*, *γ*, [°]	93.451(5), 98.501(5), 95.971(5)
Volume [Å^3]	1529.1(2)
Z	2
Density (calc.) [g cm^{-3}]	1.604
Absorption coefficient [mm^{-1}]	0.155
F(000)	748
Crystal size	0.31 x 0.03 x 0.01
Theta range for data collection [°]	2.291 to 31.013
Index ranges: h, k, l	-13 to 13, -14 to 14, -25 to 25
Reflections collected	33221
Independent reflections	9445 [R(int) = 0.075]
Completeness to theta = 25.121°	99.4 %
Absorption correction	Semi-empirical from equivalents
Max. and min. transmission	1.00 and 1.00
Refinement method	Full-matrix least-squares on F^2
Data / restraints / parameters	4614 / 192 / 505
Goodness-of-fit on F^2	1.2854
Final R indices [I>2sigma(I)]	R1 = 0.0833, wR2 = 0.0638
R indices (all data)	R1 = 0.1798, wR2 = 0.0966
Largest diff. peak and hole [e Å^{-3}]	0.62 and -0.62

Dimethyl 6,6´-diphenyl-2,2´-bipyridine-4,4´-dicarboxylate (L18)

Crystal data and structure refinement for dimethyl 6,6´-diphenyl-2,2´-bipyridine-4,4´-dicarboxylate (**L18**).

Formula	$C_{26} H_{20} N_2 O_4$
Formula weight	424.44
Temperature [K]	173(2)
Wavelength [Å]	0.71073
Crystal system	Monoclinic
Space group	$P2(1)/n$
a, b, c, [Å]	8.2099(16), 5.8537(12) , 21.526(4)
α, β, γ, [°]	90, 91.77(3), 90
Volume [Å^3]	1034.0(4)
Z	2
Density (calc.) [g cm^{-3}]	1.363
Absorption coefficient [mm^{-1}]	0.093
F(000)	444
Crystal size	0.65 x 0.30 x 0.03
Theta range for data collection [°]	2.63 to 25.05
Index ranges: h, k, l	-9 to 9, -6 to 6, -25 to 25
Reflections collected	27377
Independent reflections	1806 [R(int) = 0.2309]
Completeness to theta = 25.05°	99.6 %
Absorption correction	None
Refinement method	Full-matrix least-squares on F^2
Data / restraints / parameters	1806 / 0 / 145
Goodness-of-fit on F^2	1.199
Final R indices [I>2sigma(I)]	R1 = 0.0747, wR2 = 0.1870
R indices (all data)	R1 = 0.0811, wR2 = 0.1935
Largest diff. peak and hole [e Å^{-3}]	0.308 and -0.227

Tetraethyl 6,6´-dimethyl-2,2´-bipyridine-4,4´-diyldiphosphonate (L23)

Crystal data and structure refinement for tetraethyl 6,6´-dimethyl-2,2´-bipyridine-4,4´-diyldiphosphonate (**L23**).

Formula	$C_{10} H_{15} N O_3 P$
Formula weight	228.20
Temperature [K]	223(2)
Wavelength [Å]	0.71073
Crystal system	Monoclinic
Space group	$P2_1/n$
a, b, c, [Å]	8.3712(17), 14.754(3), 9.992(2)
α, β, γ, [°]	90, 101.38(3), 90
Volume [Å^3]	1209.9(4)
Z	4
Density (calc.) [g cm^{-3}]	1.253
Absorption coefficient [mm^{-1}]	0.215
F(000)	484
Crystal size	0.25 x 0.25 x 0.03
Theta range for data collection [°]	2.50 to 25.05
Index ranges: h, k, l	-9 to 9, -17 to 17, -11 to 11
Reflections collected	11795
Independent reflections	2114 [R(int) = 0.0720
Completeness to theta = 25.05°	98.9 %
Absorption correction	None
Max. and min. transmission	0.9936 and 0.9481
Refinement method	Full-matrix least-squares on F^2
Data / restraints / parameters	2114 / 0 / 139
Goodness-of-fit on F^2	1.106
Final R indices [I>2sigma(I)]	R1 = 0.0773, wR2 = 0.2049
R indices (all data)	R1 = 0.0851, wR2 = 0.2121

Largest diff. peak and hole [e Å^{-3}]	0.576 and -0.263

[Cu(L1)$_2$][PF$_6$]·2CHCl$_3$

Crystal data and structure refinement for [Cu(**L1**)$_2$][PF$_6$]·2CHCl$_3$.

Formula	C$_{49}$ H$_{41}$ Cl$_3$ Cu F$_6$ N$_4$ P
Formula weight	1000.76
Temperature [K]	173
Wavelength [Å]	0.71073
Crystal system	Monoclinic
Space group	*C2/c*
a, *b*, *c*, [Å]	38.2782(6), 11.3237(2), 23.1019(4)
α, *β*, *γ*, [°]	90, 111.0190(9), 90
Volume [Å^3]	9347.3(3)
Z	8
Density (calc.) [g cm^{-3}]	1.422
Absorption coefficient [mm^{-1}]	0.736
F(000)	4096
Crystal size	0.50 x 0.34 x 0.04
Theta range for data collection [°]	3.213 to 28.029
Index ranges: h, k, l	-50 to 50, -14 to 14, -30 to 30
Reflections collected	74125
Independent reflections	11270 [R(int) = 0.102]
Completeness to theta = 28.029°	99.6 %
Absorption correction	Semi-empirical from equivalents
Max. and min. transmission	0.97 and 0.78
Refinement method	Full-matrix least-squares on F^2
Data / restraints / parameters	7422 / 220 / 618

Goodness-of-fit on F^2	1.2358
Final R indices [I>2sigma(I)]	R1 = 0.0588, wR2 = 0.0562
R indices (all data)	R1 = 0.0921, wR2 = 0.0710
Largest diff. peak and hole [e Å^{-3}]	1.18 and -0.74

2{[Cu(L2)$_2$][PF$_6$]}·Et$_2$O

Crystal data and structure refinement for 2{[Cu(**L2**)$_2$][PF$_6$]}·Et$_2$O.

Formula	C$_{140}$ H$_{106}$ Cu$_2$ F$_{12}$ N$_8$ O P$_2$
Formula weight	2333.45
Temperature [K]	173
Wavelength [Å]	0.71073
Crystal system	Triclinic
Space group	*P*-1
a, *b*, *c*, [Å]	14.5978(3), 15.4344(3), 16.5702(3)
α, *β*, *γ*, [°]	72.8454(9), 66.0782(8), 65.5164(11)
Volume [Å^3]	3069.48(10)
Z	1
Density (calc.) [g cm^{-3}]	1.262
Absorption coefficient [mm^{-1}]	0.445
F(000)	1206
Crystal size	0.14 x 0.10 x 0.06
Theta range for data collection [°]	1.726 to 27.469
Index ranges	-18 to 18, -20 to 20, -21 to 21
Reflections collected	26435
Independent reflections	14029 [R(int) = 0.019]
Completeness to theta = 27.469°	99.8 %
Absorption correction	Semi-empirical from equivalents

Max. and min. transmission	0.97 and 0.96
Refinement method	Full-matrix least-squares on F^2
Data / restraints / parameters	8926 / 1373 / 889
Goodness-of-fit on F^2	0.9952
Final R indices [I>2sigma(I)]	R1 = 0.0607, wR2 = 0.0678
R indices (all data)	R1 = 0.0955, wR2 = 0.0952
Largest diff. peak and hole [e Å^{-3}]	1.21 and -0.45

2{[Cu(L5)$_2$][PF$_6$]}·2Et$_2$O·CHCl$_3$
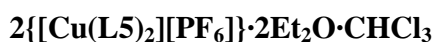
Crystal data and structure refinement for 2{[Cu(**L5**)$_2$][PF$_6$]}·2Et$_2$O·CHCl$_3$.

Formula	C$_{161}$ H$_{134}$ Cl$_2$ Cu$_2$ F$_{12}$ N$_8$ O$_{18}$ P$_2$
Formula weight	2956.80
Temperature [K]	173
Wavelength [Å]	0.71073
Crystal system	Triclinic
Space group	*P*-1
a, b, c, [Å]	16.94240(10), 17.19080(10), 25.3573(2)
α, β, γ, [°]	94.1593(4), 95.4456(4), 97.4474(4)
Volume [Å^3]	7263.08(8)
Z	2
Density (calc.) [g cm^{-3}]	1.352
Absorption coefficient [mm^{-1}]	0.436
F(000)	3060
Crystal size	0.43 x 0.08 x 0.06
Theta range for data collection [°]	1.771 to 27.472
Index ranges: h, k, l	-21 to 21, -22 to 22, -32 to 32
Reflections collected	65037

Independent reflections	33247 [R(int) = 0.018]
Completeness to theta = 27.472°	99.9 %
Absorption correction	Semi-empirical from equivalents
Max. and min. transmission	0.97 and 0.97
Refinement method	Full-matrix least-squares on F^2
Data / restraints / parameters	21034 / 112 / 1942
Goodness-of-fit on F^2	1.1298
Final R indices [I>2sigma(I)]	R1 = 0.0488, wR2 = 0.0378
R indices (all data)	R1 = 0.0772, wR2 = 0.0496
Largest diff. peak and hole [e Å^{-3}]	1.44 and -0.72

4[Cu(H$_2$L8)(HL8)]·3H$_2$O

Crystal data and structure refinement for 4[Cu(H$_2$**L8**)(H**L8**)]·3H$_2$O.

Formula	$C_{112} H_{92} Cu_4 N_{16} O_{35}$
Formula weight	2476.23
Temperature [K]	173
Wavelength [Å]	0.71073
Crystal system	Monoclinic
Space group	*C2/c*
a, *b*, *c*, [Å]	19.3405(4), 19.6142(4), 15.5801(3)
α, *β*, *γ*, [°]	90, 114.0211(9), 90
Volume [Å^3]	5398.43(19)
Z	2
Density (calc.) [g cm^{-3}]	1.523
Absorption coefficient [mm^{-1}]	0.871
F(000)	2544
Crystal size	0.37 x 0.17 x 0.09

|	
Theta range for data collection [°]	1.764 to 27.479
Index ranges: h, k, l	-25 to 25, -25 to 25, -20 to 20
Reflections collected	45813
Independent reflections	6190 [R(int) = 0.033]
Completeness to theta = 27.479°	99.9 %
Absorption correction	Semi-empirical from equivalents
Max. and min. transmission	0.92 and 0.81
Refinement method	Full-matrix least-squares on F^2
Data / restraints / parameters	6126 / 38 / 411
Goodness-of-fit on F^2	1.0816
Final R indices [I>2sigma(I)]	R1 = 0.0439, wR2 = 0.0754
R indices (all data)	R1 = 0.0548, wR2 = 0.0824
Largest diff. peak and hole [e Å^{-3}]	0.82 and -0.99

[Cu(L9)$_2$][PF$_6$]

Crystal data and structure refinement for [Cu(**L9**)$_2$][PF$_6$].

Formula	C$_{40}$ H$_{32}$ Cu F$_6$ N$_4$ O$_4$ P
Formula weight	841.23
Temperature [K]	173
Wavelength [Å]	0.71073
Crystal system	Triclinic
Space group	*P*-1
a, *b*, *c*, [Å]	8.9016(2), 10.9570(3), 19.0865(4)
α, *β*, *γ*, [°]	81.7240(10), 81.0490(10), 88.7430(10)
Volume [Å^3]	1819.78(8)
Z	2
Density (calc.) [g cm^{-3}]	1.535

Absorption coefficient [mm^{-1}]	0.724
F(000)	860
Crystal size	0.26 x 0.11 x 0.03
Theta range for data collection [°]	2.034 to 32.510
Index ranges: h, k, l	-13 to 13, -16 to 16, -28 to 28
Reflections collected	61611
Independent reflections	13054 [R(int) = 0.051]
Completeness to theta = 31.535°	99.5 %
Absorption correction	Semi-empirical from equivalents
Max. and min. transmission	0.98 and 0.92
Refinement method	Full-matrix least-squares on F^2
Data / restraints / parameters	7298 / 35 / 505
Goodness-of-fit on F^2	1.1057
Final R indices [I>2sigma(I)]	R1 = 0.0378, wR2 = 0.0408
R indices (all data)	R1 = 0.0715, wR2 = 0.0594
Largest diff. peak and hole [e Å^{-3}]	0.43 and -0.43

[Cu(L11)$_2$][PF$_6$]

Crystal data and structure refinement for [Cu(**L11**)$_2$][PF$_6$].

Formula	C$_{32}$ H$_{32}$ Cu F$_6$ N$_4$ O$_8$ P
Formula weight	809.14
Temperature [K]	173
Wavelength [Å]	0.71073
Crystal system	Monoclinic
Space group	$P2_1/c$
a, b, c, [Å]	10.8110(2), 20.0824(4), 16.3507(3)
α, β, γ, [°]	90, 98.6805(10), 90

Volume [Å^3]	3509.25(12)
Z	4
Density (calc.) [g cm^{-3}]	1.531
Absorption coefficient [mm^{-1}]	0.755
F(000)	1656
Crystal size	0.49 x 0.07 x 0.02
Theta range for data collection [°]	1.906 to 27.084
Index ranges: h, k, l	-13 to 13, -25 to 23, -20 to 20
Reflections collected	24693
Independent reflections	7729 [R(int) = 0.044]
Completeness to theta = 27. 084°	100.0 %
Absorption correction	Semi-empirical from equivalents
Max. and min. transmission	0.99 and 0.95
Refinement method	Full-matrix least-squares on F^2
Data / restraints / parameters	4831 / 676 / 469
Goodness-of-fit on F^2	1.1628
Final R indices [I>2sigma(I)]	R1 = 0.0505, wR2 = 0.0564
R indices (all data)	R1 = 0.0890, wR2 = 0.0779
Largest diff. peak and hole [e Å^{-3}]	0.80 and -0.58

Na$_3$[Cu(L17)$_2$]

Crystal data and structure refinement for Na$_3$[Cu(**L17**)$_2$].

Formula	$C_{48.50} H_{29.50} Cu N_4 Na_3 O_{10.25}$
Formula weight	964.80
Temperature [K]	173
Wavelength [Å]	0.71073
Crystal system	Triclinic

Space group	*P*-1
a, *b*, *c*, [Å]	13.1609(7), 14.4017(9), 14.6202(8)
α, *β*, *γ*, [°]	84.622(3), 69.111(3), 72.106(3)
Volume [Å^3]	2463.3(3)
Z	2
Density (calc.) [g cm^{-3}]	1.301
Absorption coefficient [mm^{-1}]	0.529
F(000)	985.000
Crystal size	0.50 x 0.14 x 0.02
Theta range for data collection [°]	1.491 to 27.825
Index ranges: h, k, l	-17 to 17, -18 to 18, -19 to 19
Reflections collected	21446
Independent reflections	11594 [R(int) = 0.052]
Completeness to theta = 27. 825°	99.5 %
Absorption correction	Semi-empirical from equivalents
Max. and min. transmission	0.99 and 0.93
Refinement method	Full-matrix least-squares on F^2
Data / restraints / parameters	6862 / 1076 / 721
Goodness-of-fit on F^2	1.0093
Final R indices [I>2sigma(I)]	R1 = 0.0614, wR2 = 0.0680
R indices (all data)	R1 = 0.1090, wR2 = 0.0991
Largest diff. peak and hole [e Å^{-3}]	0.74 and -0.52

[Cu(L18)$_2$][PF$_6$]

Crystal data and structure refinement for [Cu(**L18**)$_2$][PF$_6$].

Formula	C$_{52}$ H$_{40}$ Cu F$_6$ N$_4$ O$_8$ P
Formula weight	1057.42

Temperature [K]	173
Wavelength [Å]	0.71073
Crystal system	Monoclinic
Space group	$P2_1$
a, b, c, [Å]	12.2744(17), 15.957(2), 12.816(2)
α, β, γ, [°]	90, 112.687(7), 90
Volume [Å^3]	2315.9(6)
Z	2
Density (calc.) [g cm^{-3}]	1.516
Absorption coefficient [mm^{-1}]	0.592
F(000)	1084
Crystal size	0.37 x 0.12 x 0.08
Theta range for data collection [°]	1.798 to 30.386
Index ranges: h, k, l	-12 to 17, -22 to 22, -18 to 18
Reflections collected	38661
Independent reflections	13741 [R(int) = 0.072]
Completeness to theta = 29.778°	99.8 %
Absorption correction	Semi-empirical from equivalents
Max. and min. transmission	0.95 and 0.93
Refinement method	Full-matrix least-squares on F^2
Data / restraints / parameters	7416 / 294 / 686
Goodness-of-fit on F^2	1.2975
Final R indices [I>2sigma(I)]	R1 = 0.0434, wR2 = 0.0492
R indices (all data)	R1 = 0.0836, wR2 = 0.0716
Largest diff. peak and hole [e Å^{-3}]	0.53 and -0.70

Na$_3$[Cu(H$_2$L24)$_2$]·15O

Crystal data and structure refinement for Na$_3$[Cu(H$_2$**L24**)$_2$]·15O.

Formula	$C_{25} H_{22.50} Cu N_4 Na_3 O_{27} P_4$
Formula weight	1067.36
Temperature [K]	173(2)
Wavelength [Å]	0.71073
Crystal system	Monoclinic
Space group	$P2_1/c$
a, b, c, [Å]	18.421(4), 22.244(4), 12.080(2)
α, β, γ, [°]	90, 105.96(3), 90
Volume [Å^3]	4759.4(16)
Z	4
Density (calc.) [g cm^{-3}]	1.490
Absorption coefficient [mm^{-1}]	0.708
F(000)	2154
Crystal size	0.35 x 0.20 x 0.03
Theta range for data collection [°]	2.48 to 27.50
Index ranges: h, k, l	-23 to 23, -28 to 28, -15 to 15
Reflections collected	53626
Independent reflections	10909 [R(int) = 0.1945]
Completeness to theta = 27.50°	99.9 %
Absorption correction	None
Refinement method	Full-matrix least-squares on F^2
Data / restraints / parameters	10909 / 14 / 636
Goodness-of-fit on F^2	1.158
Final R indices [I>2sigma(I)]	R1 = 0.0689, wR2 = 0.1849
R indices (all data)	R1 = 0.0773, wR2 = 0.1912
Largest diff. peak and hole [e Å^{-3}]	1.449 and -1.593

VIII   Bibliography

1.   International Energy Outlook 2008. Energy Information Administration, http://www.eia.doe.gov/oiaf/ieo/index.html.
2.   M. K. Nazeeruddin, *Coord. Chem. Rev.*, 2004, **248**, 1161-1164.
3.   W. Hoffmann, *Sol. Energy Mater. Sol. Cells*, 2006, **90**, 3285-3311.
4.   D. M. Chapin, C. S. Fuller and G. L. Pearson, *J. Appl. Phys.*, 1954, **25**, 676.
5.   A. Goetzberger, J. Luther and G. Willeke, *Sol. Energy Mater. Sol. Cells*, 2002, **74**, 1-11.
6.   B. O'Regan and M. Graetzel, *Nature (London)*, 1991, **353**, 737-740.
7.   A. Hagfeldt and M. Graetzel, *Acc. Chem. Res.*, 2000, **33**, 269-277.
8.   J. J. Lagref, M. K. Nazeeruddin and M. Graetzel, *Inorg. Chim. Acta*, 2008, **361**, 735-745.
9.   W. West, *Photogr. Sci. Eng.*, 1974, **18**, 35-48.
10.   H. Tsubomura, M. Matsumura, Y. Nomura and T. Amamiya, *Nature (London)*, 1976, **261**, 402-403.
11.   M. P. Dare-Edwards, J. B. Goodenough, A. Hamnett, K. R. Seddon and R. D. Wright, *Faraday Discuss. Chem. Soc.*, 1981, **70**, 285-298.
12.   J.-H. Yum, S.-R. Jang, P. Walter, T. Geiger, F. Nueesch, S. Kim, J. Ko, M. Graetzel and M. K. Nazeeruddin, *Chem. Commun.*, 2007, 4680-4682.
13.   C. A. Kelly and G. J. Meyer, *Coord. Chem. Rev.*, 2001, **211**, 295-315.
14.   N. Vlachopoulos, P. Liska, J. Augustynski and M. Graetzel, *J. Am. Chem. Soc.*, 1988, **110**, 1216-1220.
15.   M. Gratzel, *J. Photochem. Photobiol., A*, 2004, **164**, 3-14.
16.   K. Tennakone, G. R. R. A. Kumara, I. R. M. Kottegoda and V. P. S. Perera, *Chem. Commun.*, 1999, 15-16.
17.   K. Sayama, H. Sugihara and H. Arakawa, *Chem. Mater.*, 1998, **10**, 3825-3832.
18.   K. Kalyanasundaram and M. Gratzel, *Coord. Chem. Rev.*, 1998, **177**, 347-414.
19.   N. G. Park, J. van de Lagemaat and A. J. Frank, *J. Phys. Chem. B*, 2000, **104**, 8989-8994.
20.   R. J. Ellingson, J. B. Asbury, S. Ferrere, H. N. Ghosh, J. R. Sprague, T. Lian and A. J. Nozik, *J. Phys. Chem. B*, 1998, **102**, 6455-6458.
21.   M. Gratzel, *J. Photochem. Photobiol., C*, 2003, **4**, 145-153.
22.   J. N. Hart, D. Menzies, Y.-B. Cheng, G. P. Simon and L. Spiccia, *C. R. Chim.*, 2006, **9**, 622-626.
23.   S. Ito, K. Ishikawa, C.-J. Wen, S. Yoshida and T. Watanabe, *Bull. Chem. Soc. Jpn.*, 2000, **73**, 2609-2614.
24.   Z.-S. Wang, H. Kawauchi, T. Kashima and H. Arakawa, *Coord. Chem. Rev.*, 2004, **248**, 1381-1389.
25.   G. K. Mor, K. Shankar, M. Paulose, O. K. Varghese and C. A. Grimes, *Nano Lett.*, 2006, **6**, 215-218.
26.   M. Adachi, Y. Murata, J. Takao, J. Jiu, M. Sakamoto and F. Wang, *J. Am. Chem. Soc.*, 2004, **126**, 14943-14949.
27.   J. Jiu, S. Isoda, F. Wang and M. Adachi, *J. Phys. Chem. B*, 2006, **110**, 2087-2092.
28.   K. Murakoshi, G. Kano, Y. Wada, S. Yanagida, H. Miyazaki, M. Matsumoto and S. Murasawa, *J. Electroanal. Chem.*, 1995, **396**, 27-34.

29. M. K. Nazeeruddin, C. Klein, P. Liska and M. Graetzel, *Coord. Chem. Rev.*, 2005, **249**, 1460-1467.
30. I. Gillaizeau-Gauthier, F. Odobel, M. Alebbi, R. Argazzi, E. Costa, C. A. Bignozzi, P. Qu and G. J. Meyer, *Inorg. Chem.*, 2001, **40**, 6073-6079.
31. H. Zabri, I. Gillaizeau, C. A. Bignozzi, S. Caramori, M.-F. Charlot, J. Cano-Boquera and F. Odobel, *Inorg. Chem.*, 2003, **42**, 6655-6666.
32. S. Altobello, C. A. Bignozzi, S. Caramori, G. Larramona, S. Quici, G. Marzanni and R. Lakhmiri, *J. Photochem. Photobiol., A*, 2004, **166**, 91-98.
33. W. E. Ford and M. A. J. Rodgers, *J. Phys. Chem.*, 1994, **98**, 3822-3831.
34. M. A. Fox, F. J. Nobs and T. A. Voynick, *J. Am. Chem. Soc.*, 1980, **102**, 4036-4039.
35. C. Zou and M. S. Wrighton, *J. Am. Chem. Soc.*, 1990, **112**, 7578-7584.
36. A. S. Polo, M. K. Itokazu and N. Y. Murakami Iha, *Coord. Chem. Rev.*, 2004, **248**, 1343-1361.
37. A. Islam, H. Sugihara and H. Arakawa, *J. Photochem. Photobiol., A*, 2003, **158**, 131-138.
38. M. K. Nazeeruddin, A. Kay, I. Rodicio, R. Humphry-Baker, E. Mueller, P. Liska, N. Vlachopoulos and M. Graetzel, *J. Am. Chem. Soc.*, 1993, **115**, 6382-6390.
39. M. K. Nazeeruddin, P. Pechy and M. Graetzel, *Chem. Commun.*, 1997, 1705-1706.
40. M. K. Nazeeruddin, P. Pechy, T. Renouard, S. M. Zakeeruddin, R. Humphry-Baker, P. Comte, P. Liska, L. Cevey, E. Costa, V. Shklover, L. Spiccia, G. B. Deacon, C. A. Bignozzi and M. Graetzel, *J. Am. Chem. Soc.*, 2001, **123**, 1613-1624.
41. R. Argazzi, C. A. Bignozzi, G. M. Hasselmann and G. J. Meyer, *Inorg. Chem.*, 1998, **37**, 4533-4537.
42. S. Campagna, F. Puntoriero, F. Nastasi, G. Bergamini and V. Balzani, *Top. Curr. Chem.*, 2007, **280**, 117-214.
43. M. K. Nazeeruddin and M. Gratzel, *Struct. Bonding*, 2007, **123**, 113-175.
44. S. Pelet, J.-E. Moser and M. Graetzel, *J. Phys. Chem. B*, 2000, **104**, 1791-1795.
45. M. K. Nazeeruddin, P. Liska, J. Moser, N. Vlachopoulos and M. Graetzel, *Helv. Chim. Acta*, 1990, **73**, 1788-1803.
46. S. M. Zakeeruddin, M. K. Nazeeruddin, R. Humphry-Baker, P. Pechy, P. Quagliotto, C. Barolo, G. Viscardi and M. Graetzel, *Langmuir*, 2002, **18**, 952-954.
47. T. Renouard, R. A. Fallahpour, M. K. Nazeeruddin, R. Humphry-Baker, S. I. Gorelsky, A. B. P. Lever and M. Graetzel, *Inorg. Chem.*, 2002, **41**, 367-378.
48. J. M. Kroon, N. J. Bakker, H. J. P. Smit, P. Liska, K. R. Thampi, P. Wang, S. M. Zakeeruddin, M. Gratzel, A. Hinsch, S. Hore, U. Wuerfel, R. Sastrawan, J. R. Durrant, E. Palomares, H. Pettersson, T. Gruszecki, J. Walter, K. Skupien and G. E. Tulloch, *Prog. Photovoltaics*, 2007, **15**, 1-18.
49. F. Gao, Y. Wang, J. Zhang, D. Shi, M. Wang, R. Humphry-Baker, P. Wang, S. M. Zakeeruddin and M. Gratzel, *Chem. Commun.*, 2008, 2635-2637.
50. R. Argazzi, C. A. Bignozzi, T. A. Heimer and G. J. Meyer, *Inorg. Chem.*, 1997, **36**, 2-3.
51. G. Sauve, M. E. Cass, G. Coia, S. J. Doig, I. Lauermann, K. E. Pomykal and N. S. Lewis, *J. Phys. Chem. B*, 2000, **104**, 6821-6836.
52. D. Kuciauskas, J. E. Monat, R. Villahermosa, H. B. Gray, N. S. Lewis and J. K. McCusker, *J. Phys. Chem. B*, 2002, **106**, 9347-9358.
53. S. Ferrere and B. A. Gregg, *J. Am. Chem. Soc.*, 1998, **120**, 843-844.
54. S. Ferrere, *Chem. Mater.*, 2000, **12**, 1083-1089.
55. G. M. Hasselmann and G. J. Meyer, *Z. Phys. Chem.*, 1999, **212**, 39-44.

56. N. Alonso-Vante, J.-F. Nierengarten and J.-P. Sauvage, *J. Chem. Soc., Dalton Trans.*, 1994, 1649-1654.

57. T. Bessho, E. C. Constable, M. Graetzel, A. Hernandez Redondo, C. E. Housecroft, W. Kylberg, M. K. Nazeeruddin, M. Neuburger and S. Schaffner, *Chem. Commun.*, 2008, 3717-3719.

58. A. Islam, H. Sugihara, K. Hara, L. Pratap Singh, R. Katoh, M. Yanagida, Y. Takahashi, S. Murata and H. Arakawa, *New J. Chem.*, 2000, **24**, 343-345.

59. A. Islam, H. Sugihara, K. Hara, L. P. Singh, R. Katoh, M. Yanagida, Y. Takahashi, S. Murata, H. Arakawa and G. Fujihashi, *Inorg. Chem.*, 2001, **40**, 5371-5380.

60. J. A. Bailey, M. G. Hill, R. E. Marsh, V. M. Miskowski, W. P. Schaefer and H. B. Gray, *Inorg. Chem.*, 1995, **34**, 4591-4599.

61. S. Sakaki, T. Kuroki and T. Hamada, *J. Chem. Soc., Dalton Trans.*, 2002, 840-842.

62. F.-T. Kong, S.-Y. Dai and K.-J. Wang, *Adv. OptoElectron.*, 2007, 75384/75381-75384/75313.

63. L. Schmidt-Mende, U. Bach, R. Humphry-Baker, T. Horiuchi, H. Miura, S. Ito, S. Uchida and M. Graetzel, *Adv. Mater. (Weinheim, Ger.)*, 2005, **17**, 813-815.

64. H. Tokuhisa and P. T. Hammond, *Adv. Funct. Mater.*, 2003, **13**, 831-839.

65. L. Giribabu, C. V. Kumar, V. G. Reddy, P. Y. Reddy, C. S. Rao, S.-R. Jang, J.-H. Yum, M. K. Nazeeruddin and M. Graetzel, *Sol. Energy Mater. Sol. Cells*, 2007, **91**, 1611-1617.

66. K. Hara, K. Sayama, H. Arakawa, Y. Ohga, A. Shinpo and S. Suga, *Chem. Commun.*, 2001, 569-570.

67. K. Hara, M. Kurashige, Y. Dan-oh, C. Kasada, A. Shinpo, S. Suga, K. Sayama and H. Arakawa, *New J. Chem.*, 2003, **27**, 783-785.

68. K. Sayama, S. Tsukagoshi, T. Mori, K. Hara, Y. Ohga, A. Shinpou, Y. Abe, S. Suga and H. Arakawa, *Sol. Energy Mater. Sol. Cells*, 2003, **80**, 47-71.

69. J. N. Clifford, E. Palomares, M. K. Nazeeruddin, R. Thampi, M. Graetzel and J. R. Durrant, *J. Am. Chem. Soc.*, 2004, **126**, 5670-5671.

70. J. Fang, L. Su, J. Wu, Y. Shen and Z. Lu, *New J. Chem.*, 1997, **21**, 839-840.

71. R. Plass, S. Pelet, J. Krueger, M. Graetzel and U. Bach, *J. Phys. Chem. B*, 2002, **106**, 7578-7580.

72. H. Tributsch, *Coord. Chem. Rev.*, 2004, **248**, 1511-1530.

73. E. Figgemeier and A. Hagfeldt, *Int. J. Photoenergy*, 2004, **6**, 127-140.

74. T. W. Hamann, R. A. Jensen, A. B. F. Martinson, H. Van Ryswyk and J. T. Hupp, *Energy Environ. Sci.*, 2008, **1**, 66-78.

75. R. Argazzi, C. A. Bignozzi, T. A. Heimer, F. N. Castellano and G. J. Meyer, *J. Phys. Chem. B*, 1997, **101**, 2591-2597.

76. G. Oskam, B. V. Bergeron, G. J. Meyer and P. C. Searson, *J. Phys. Chem. B*, 2001, **105**, 6867-6873.

77. Z.-S. Wang, K. Sayama and H. Sugihara, *J. Phys. Chem. B*, 2005, **109**, 22449-22455.

78. H. Nusbaumer, S. M. Zakeeruddin, J.-E. Moser and M. Graetzel, *Chem. Eur. J.*, 2003, **9**, 3756-3763.

79. P. J. Cameron, L. M. Peter, S. M. Zakeeruddin and M. Gratzel, *Coord. Chem. Rev.*, 2004, **248**, 1447-1453.

80. T. Ma, X. Fang, M. Akiyama, K. Inoue, H. Noma and E. Abe, *J. Electroanal. Chem.*, 2004, **574**, 77-83.

81. A. Kay and M. Graetzel, *Sol. Energy Mater. Sol. Cells*, 1996, **44**, 99-117.

82. Y. Saito, W. Kubo, T. Kitamura, Y. Wada and S. Yanagida, *J. Photochem. Photobiol., A*, 2004, **164**, 153-157.

83. N. Papageorgiou, Y. Athanassov, M. Armand, P. Bonhote, H. Pettersson, A. Azam and M. Graetzel, *J. Electrochem. Soc.*, 1996, **143**, 3099-3108.

84. S. Murai, S. Mikoshiba, H. Sumino, T. Kato and S. Hayase, *Chem. Commun.*, 2003, 1534-1535.

85. P. Wang, S. M. Zakeeruddin, J.-E. Moser and M. Graetzel, *J. Phys. Chem. B*, 2003, **107**, 13280-13285.

86. H. Matsumoto, T. Matsuda, T. Tsuda, R. Hagiwara, Y. Ito and Y. Miyazaki, *Chem. Lett.*, 2001, 26-27.

87. P. Wang, S. M. Zakeeruddin, P. Comte, I. Exnar and M. Graetzel, *J. Am. Chem. Soc.*, 2003, **125**, 1166-1167.

88. W. Kubo, T. Kitamura, K. Hanabusa, Y. Wada and S. Yanagida, *Chem. Commun.*, 2002, 374-375.

89. U. Bach, D. Lupo, P. Comte, J. E. Moser, F. Weissortel, J. Salbeck, H. Spreitzer and M. Gratzel, *Nature (London)*, 1998, **395**, 583-585.

90. A. Burke, L. Schmidt-Mende, S. Ito and M. Graetzel, *Chem. Commun.*, 2007, 234-236.

91. J.-H. Yum, S.-r. Jang, R. Humphry-Baker, M. Graetzel, J.-J. Cid, T. Torres and M. K. Nazeeruddin, *Langmuir*, 2008, **24**, 5636-5640.

92. E. Olsen, G. Hagen and S. E. Lindquist, *Sol. Energy Mater. Sol. Cells*, 2000, **63**, 267-273.

93. T. Kitamura, M. Maitani, M. Matsuda, Y. Wada and S. Yanagida, *Chem. Lett.*, 2001, 1054-1055.

94. S. A. Sapp, C. M. Elliott, C. Contado, S. Caramori and C. A. Bignozzi, *J. Am. Chem. Soc.*, 2002, **124**, 11215-11222.

95. C. J. Barbe, F. Arendse, P. Comte, M. Jirousek, F. Lenzmann, V. Shklover and M. Gratzel, *J. Am. Ceram. Soc.*, 1997, **80**, 3157-3171.

96. K. Kalyanasundaram, *Coord. Chem. Rev.*, 1982, **46**, 159-244.

97. N. Armaroli, *Chem. Soc. Rev.*, 2001, **30**, 113-124.

98. C. C. Phifer and D. R. McMillin, *Inorg. Chem.*, 1986, **25**, 1329-1333.

99. M. Ruthkosky, C. A. Kelly, F. N. Castellano and G. J. Meyer, *Coord. Chem. Rev.*, 1998, **171**, 309-322.

100. E. C. Constable, C. E. Housecroft, M. Neuburger, I. Poleschak and M. Zehnder, *Polyhedron*, 2003, **22**, 93-108.

101. S. Welter, K. Brunner, J. W. Hofstraat and L. De Cola, *Nature (London)*, 2003, **421**, 54-57.

102. F. Blau, *B. D. D. Chem. Gesell.*, **21**, 1077-1078.

103. F. Blau, *Monatshefte fuer Chemie*, **10**, 375-388.

104. E. C. Constable, *Adv. Inorg. Chem.*, 1989, **34**, 1-63.

105. G. R. Newkome, A. K. Patri, E. Holder and U. S. Schubert, *Eur. J. Org. Chem.*, 2004, 235-254.

106. J. M. Lehn, *Prix Nobel*, 1988, 129-176.

107. N. C. Fletcher, *J. Chem. Soc., Perkin Trans.*, 2002, 1831-1842.

108. J. M. Lehn, A. Rigault, J. Siegel, J. Harrowfield, B. Chevrier and D. Moras, *PNAS*, 1987, **84**, 2565-2569.

109. V. Marvaud and D. Astruc, *Chem. Commun.*, 1997, 773-774.

110. R. Ballardini, V. Balzani, A. Credi, M. T. Gandolfi and M. Venturi, *Int. J. Photoenergy*, 2001, **3**, 63-77.
111. H. Korpi, V. Sippola, I. Filpponen, J. Sipilae, O. Krause, M. Leskelae and T. Repo, *App. Catalysis, A: Gen.*, 2006, **302**, 250-256.
112. W. D. McFarlane, *Ind. Eng. Chem., Anal. Ed.*, 1936, **8**, 124-126.
113. A. H. Malkawi, A. M. Al-Ghananeem, S. Nasim, J. De Leon and P. A. Crooks, *J. Pharm. Biomed. Anal.*, 2007, **45**, 120-124.
114. N. Teshima and T. Kawashima, *Bull. Chem. Soc. Jpn.*, 1996, **69**, 1975-1979.
115. K. T. Potts, K. A. G. Raiford and M. Keshavarz-K, *J. Am. Chem. Soc.*, 1993, **115**, 2793-2807.
116. B. R. James and R. J. P. Williams, *J. Chem. Soc.*, 1961, 2007-2019.
117. C. O. Dietrich-Buchecker, P. A. Marnot, J. P. Sauvage, J. P. Kintzinger and P. Maltese, *New J. Chem.*, 1984, **8**, 573-582.
118. C. O. Dietrich-Buchecker, P. A. Marnot and J. P. Sauvage, *Tetrahedron Lett.*, 1982, **23**, 5291-5294.
119. N. A. Vante, V. Ern, P. Chartier, C. O. Dietrich-Buchecker, D. R. McMillin, P. A. Marnot and J. P. Sauvage, *New J. Chem.*, 1983, **7**, 3-5.
120. F. Kroehnke, *Synth.*, 1976, 1-24.
121. V. M. Mukkala and J. J. Kankare, *Helv. Chim. Acta*, 1992, **75**, 1578-1592.
122. E. C. Constable, P. Harverson, D. R. Smith and L. A. Whall, *Tetrahedron*, 1994, **50**, 7799-7806.
123. E. C. Constable, G. Baum, E. Bill, R. Dyson, R. Van Eldik, D. Fenske, S. Kaderli, D. Morris, A. Neubrand, M. Neuburger, D. R. Smith, K. Wieghardt, M. Zehnder and A. D. Zuberbuhler, *Chem.--Eur. J.*, 1999, **5**, 498-508.
124. T. Renouard and M. Gratzel, *Tetrahedron*, 2001, **57**, 8145-8150.
125. E. C. Constable, M. J. Hannon and D. R. Smith, *Tetrahedron Lett.*, 1994, **35**, 6657-6660.
126. N. A. Sorensen, E. Samuelsen and F. Oxaal, *Acta. Chem. Scand.*, 1947, **1**, 458-460.
127. P. Karrer, C. Cochand and N. Neuss, *Helv. Chim. Acta*, 1946, **29**, 1836-1841.
128. K. Wimalasena and D. C. Haines, *J. Org. Chem.*, 1994, **59**, 6472-6475.
129. C. Klein, M. K. Nazeeruddin, P. Liska, D. Di Censo, N. Hirata, E. Palomares, J. R. Durrant and M. Graetzel, *Inorg. Chem.*, 2005, **44**, 178-180.
130. S. Sakaki, H. Ishikura, K.-I. Kuraki, K.-J. Tanaka, T. Satoh, T. Arai and T. Hamada, *J. Chem. Soc., Dalton Trans.*, 1997, 1815-1820.
131. M. M. Harding, U. Koert, J. M. Lehn, A. Marquis-Rigault, C. Piguet and J. Siegel, *Helv. Chim. Acta*, 1991, **74**, 594-610.
132. R. Bruckner, *Advanced Organic Chemistry: Reaction Mechanisms*, 2002.
133. M. Shaul and Y. Cohen, *J. Org. Chem.*, 1999, **64**, 9358-9364.
134. R. A. Jones, B. D. Roney, W. H. F. Sasse and K. O. Wade, *J. Chem. Soc. B*, 1967, 106-111.
135. V. Penicaud, F. Odobel and B. Bujoli, *Tetrahedron Lett.*, 1998, **39**, 3689-3692.
136. C. E. McKenna, M. T. Higa, N. H. Cheung and M. C. McKenna, *Tetrahedron Lett.*, 1977, 155-158.
137. J. Guerrero, L. Farias, L. Lemus, A. Quintanilla, A. Mena, L. Cortez, R. F. Baggio and M. T. Garland, *Polyhedron*, 2006, **25**, 9-16.
138. J. R. Allan, B. R. Carson and S. Levey, *Eur- Polymer J.*, 1995, **31**, 445-448.

139. C. Klein, E. Graf, M. Wais Hosseini, G. Mislin and A. De Cian, *Tetrahedron Lett.*, 2000, **41**, 9043-9047.
140. E. C. Constable and A. M. W. Cargill Thompson, *Inorg. Chim. Acta*, 1994, **223**, 177-179.
141. H. S. Chow, E. C. Constable, C. E. Housecroft, M. Neuburger and S. Schaffner, *Polyhedron*, 2006, **25**, 1831-1843.
142. J. E. Beves, E. C. Constable, C. E. Housecroft, C. J. Kepert, M. Neuburger, D. J. Price, S. Schaffner and J. A. Zampese, *Dalton Trans.*, 2008, 6742-6751.
143. G. Baum, E. C. Constable, D. Fenske, C. E. Housecroft, T. Kulke, M. Neuburger and M. Zehnder, *Dalton*, 2000, 945-959.
144. G. T. Morgan and F. H. Burstall, *J. Chem. Soc.*, 1932, 20-30.
145. G. Morgan and F. H. Burstall, *J. Chem. Soc.*, 1937, 1649-1655.
146. E. C. Constable, *Macromolecular Symposia*, 1995, **98**, 503-524.
147. W. R. McWhinnie and J. D. Miller, *Adv. Inorg. Chem. Radiochem.*, 1969, **12**, 135-215.
148. H. Inoue, T. Furukawa, M. Shimizu, T. Tamura, M. Matsui and E. Ohtsuka, *Chem. Commun. (Cambridge)*, 1999, 45-46.
149. M. Kimura, T. Shiba, T. Muto, K. Hanabusa and H. Shirai, *Chem. Commun. (Cambridge)*, 2000, 11-12.
150. C. Mikel and P. G. Potvin, *Inorg. Chim. Acta*, 2001, **325**, 1-8.
151. E. C. Constable, A. J. Edwards, M. J. Hannon and P. R. Raithby, *J. Chem. Soc., Chem. Comm.*, 1994, 1991-1992.
152. K. T. Potts, M. Keshavarz-K, F. S. Tham, H. D. Abruna and C. R. Arana, *Inorg. Chem.*, 1993, **32**, 4422-4435.
153. E. C. Constable, E. Figgemeier, I. A. Hougen, C. E. Housecroft, M. Neuburger, S. Schaffner and L. A. Whall, *Dalton Trans.*, 2005, 1168-1175.
154. P. J. Burke, D. R. McMillin and W. R. Robinson, *Inorg. Chem.*, 1980, **19**, 1211-1214.
155. D. A. Bardwell, A. M. W. C. Thompson, J. C. Jeffery, E. E. M. Tilley and M. D. Ward, *J. Chem. Soc., Dalton Trans.*, 1995, 835-841.
156. D. A. Bardwell, J. C. Jeffery, C. A. Otter and M. D. Ward, *Polyhedron*, 1996, **15**, 191-194.
157. V. Chaurin, E. C. Constable and C. E. Housecroft, *New J. Chem.*, 2006, **30**, 1740-1744.
158. S. Goldstein and G. Czapski, *Inorg. Chem.*, 1985, **24**, 1087-1092.
159. D. V. Scaltrito, C. A. Kelly, M. Ruthkosky, M. C. Zaros and G. J. Meyer, *Inorg. Chem.*, 2000, **39**, 3765-3770.
160. D. V. Scaltrito, D. W. Thompson, J. A. O'Callaghan and G. J. Meyer, *Coord. Chem. Rev.*, 2000, **208**, 243-266.
161. M. T. Miller, P. K. Gantzel and T. B. Karpishin, *Inorg. Chem.*, 1998, **37**, 2285-2290.
162. R. M. Everly and D. R. McMillin, *Photochem. Photobiol.*, 1989, **50**, 711-716.
163. P. Chen and T. J. Meyer, *Chem. Rev.*, 1998, **98**, 1439-1477.
164. A. Juris, V. Balzani, F. Barigelletti, S. Campagna, P. Belser and A. Von Zelewsky, *Coord. Chem. Rev.*, 1988, **84**, 85-277.
165. R. M. Everly and D. R. McMillin, *J. Phys. Chem.*, 1991, **95**, 9071-9075.
166. W. L. Parker and G. A. Crosby, *J. Phys. Chem.*, 1989, **93**, 5692-5696.
167. H. M. Irving and R. J. P. Williams, *J. Chem. Soc.*, 1953, 3192-3210.
168. A. K. Ichinaga, J. R. Kirchhoff, D. R. McMillin, C. O. Dietrich-Buchecker, P. A. Marnot and J. P. Sauvage, *Inorg. Chem.*, 1987, **26**, 4290-4292.

169. Y. Jahng, J. Hazelrigg, D. Kimball, E. Riesgo, R. Wu and R. P. Thummel, *Inorg. Chem.*, 1997, **36**, 5390-5395.

170. M. T. Miller, P. K. Gantzel and T. B. Karpishin, *J. Am. Chem. Soc.*, 1999, **121**, 4292-4293.

171. M. Geoffroy, M. Wermeille, C. O. Buchecker, J. P. Sauvage and G. Bernardinelli, *Inorg. Chim. Acta*, 1990, **167**, 157-164.

172. R. Hamalainen, M. Ahlgren, U. Turpeinen and T. Raikas, *Cryst. Struct. Commun.*, 1979, **8**, 75-80.

173. F. K. Klemens, C. E. A. Palmer, S. M. Rolland, P. E. Fanwick, D. R. McMillin and J. P. Sauvage, *New J. Chem.*, 1990, **14**, 129-133.

174. P. J. Burke, K. Henrick and D. R. McMillin, *Inorg. Chem.*, 1982, **21**, 1881-1886.

175. R. M. Williams, L. De Cola, F. Hartl, J.-J. Lagref, J.-M. Planeix, A. De Cian and M. W. Hosseini, *Coord. Chem. Rev.*, 2002, **230**, 253-261.

176. D. R. McMillin, M. T. Buckner and B. T. Ahn, *Inorg. Chem.*, 1977, **16**, 943-945.

177. C. J. Hawkins and D. D. Perrin, *J. Chem. Soc.*, 1963, 2996-3002.

178. P. Federlin, J. M. Kern, A. Rastegar, C. Dietrich-Buchecker, P. A. Marnot and J. P. Sauvage, *New J. Chem.*, 1990, **14**, 9-12.

179. J. Nelson and Editor, *The Physics of Solar Cells: Photons In, Electrons Out*, 2003.

180. S. Ito, T. N. Murakami, P. Comte, P. Liska, C. Gratzel, M. K. Nazeeruddin and M. Gratzel, *Thin Solid Films*, 2008, **516**, 4613-4619.

181. M. K. Nazeeruddin, F. De Angelis, S. Fantacci, A. Selloni, G. Viscardi, P. Liska, S. Ito, B. Takeru and M. Graetzel, *J. Am. Chem. Soc.*, 2005, **127**, 16835-16847.

182. S. Ito, P. Chen, P. Comte, M. K. Nazeeruddin, P. Liska, P. Pechy and M. Graetzel, *Prog. Photovoltaics*, 2007, **15**, 603-612.

183. R. Argazzi, C. A. Bignozzi, T. A. Heimer, F. N. Castellano and G. J. Meyer, *Inorg. Chem.*, 1994, **33**, 5741-5749.

184. S. M. Zakeeruddin, M. K. Nazeeruddin, P. Pechy, F. P. Rotzinger, R. Humphry-Baker, K. Kalyanasundaram, M. Graetzel, V. Shklover and T. Haibach, *Inorg. Chem.*, 1997, **36**, 5937-5946.

185. C. Houarner-Rassin, F. Chaignon, C. She, D. Stockwell, E. Blart, P. Buvat, T. Lian and F. Odobel, *J. Photochem. Photobiol., A*, 2007, **192**, 56-65.

186. K. S. Finnie, J. R. Bartlett and J. L. Woolfrey, *Langmuir*, 1998, **14**, 2744-2749.

187. K. Kils, E. I. Mayo, B. S. Brunschwig, H. B. Gray, N. S. Lewis and J. R. Winkler, *J. Phys. Chem. B*, 2004, **108**, 15640-15651.

188. A. Fillinger and B. A. Parkinson, *J. Electrochem. Soc.*, 1999, **146**, 4559-4564.

189. P. Wang, S. M. Zakeeruddin, J. E. Moser, M. K. Nazeeruddin, T. Sekiguchi and M. Graetzel, *Nat. Mater.*, 2003, **2**, 402-407.

190. E. C. Constable, M. J. Hannon, P. Harverson, M. Neuburger, D. R. Smith, V. F. Wanner, L. A. Whall and M. Zehnder, *Polyhedron*, 2000, **19**, 23-34.

191. e. C. Constable, M. A. M. Daniels, M. G. B. Drew, D. A. Tocher, J. V. Walker and P. D. Wood, *J. Chem. Soc., Dalton Trans.*, 1993, 1947-1958.

192. F. Fabrizi de Biani, E. Grigiotti, F. Laschi, P. Zanello, A. Juris, L. Prodi, K. S. Chichak and N. R. Branda, *Inorg. Chem.*, 2008, **47**, 5425-5440.

193. B. Alpha, E. Anklam, R. Deschenaux, J. M. Lehn and M. Pietraskiewicz, *Helv. Chim. Acta*, 1988, **71**, 1042-1052.

194. D. R. Coulson, *Inorg. Syn.*, 1971, **13**, 121-124.

IX   Curriculum Vitae

Ana Hernández Redondo
Landoltstrasse 64
3007 Bern

Phone: (+41) 031 371 34 82
Phone (mobile): (+41) 078 737 56 26
e-mail: ana.hernandez@stud.unibas.ch

Date of birth: 31/10/1982
Nationality: Spain

PROFILE

PhD student in chemistry with extensive experience in physical methods of characterisation. Additional inorganic and organic synthetic experience. Accomplished in all areas related to project and time management, research and analysis.
I am a highly motivated individual with an intuitive mind and practical nature. Able to work well in teams, I am a confident and easy-going person who enjoys challenges and learning new skills.

EDUCATION

09/2005 – present
PhD studies
University of Basel, Switzerland.
Area of research: Synthesis of transition metal polypyridine complexes for solar cell sensitization.

09/2000 – 07/2005
Master in chemistry
University of the Basque Country, San Sebastian, Spain (2000-2004).
Ruprecht-Karls University of Heidelberg, Germany (Erasmus exchange program 2004-2005).

1996 – 2000
High School Studies
Instituto Rodrigo Mercado de Zuazola, Oñati, Spain.

EXPERIENCE

09/2005 – present
Laboratory teaching assistant, University of Basel
Involved supervising, correcting reports and having responsibility for the safety of students within the inorganic chemistry laboratory.

07/2004 – 09/2004
Laboratory Training
Inorganic Department of Chemistry, University of Chemnitz, Germany.
Synthesis of polynuclear transition metal complexes.

SKILLS

Language: Spanish (mother language), Basque (mother language), English (fluent), German (fluent), French (working knowledge).

I have highly developed oral presentation and scientific writing skills. Consequently, I have presented my research in a number of international conferences both as poster and oral presentations.

AWARDS

- Premio Fin de Carrera. Prize for the best student in chemistry at the University of the Basque Country (2004-2005).
- Prize for the best poster in the Swiss Chemical Society Fall Meeting 2008.

INTERESTS

I have a general interest in sport, particularly fitness and swimming. I also enjoy reading in my spare time.

PUBLICATION LIST

- An element of surprise – efficient copper-functionalized dye-sensitized solar cells.

  Takeru Bessho, Edwin C. Constable, Michael Graetzel, Ana Hernandez Redondo, Catherine E. Housecroft, William Kylberg, Md. K. Nazeeruddin, Markus Neuburger and Silvia Schaffner. *Chem. Commun.*, 2008, 3717-3719.

- Towards sustainable dyes for dye-sensitized solar cells.

  Ana Hernandez Redondo, Edwin C. Constable and Catherine E. Housecroft. *Chimia* 2009, 63, No. 4.

- Copper(I) complexes of 6,6´-disubstituted 2,2´-bipyridine dicarboxylic acids: new complexes for incorporation into copper-based dye sensitised solar cells (DSCs).

  Edwin C. Constable, Ana Hernandez Redondo, Catherine E. Housecroft, Markus Neuburger and Silvia Schaffner. Accepted in *Dalton Transactions*.

REFERENCES

Prof. Dr. Edwin C. Constable
University of Basel
Departement of Chemistry
CH-4056 Basel, Switzerland
Phone: +41 (0) 61 267 1001
e-mail: edwin.constable@unibas.ch

Prof. Dr. Catherine E. Housecroft
University of Basel
Departement of Chemistry
CH-4056 Basel, Switzerland
Phone: +41 (0) 61 267 1008
e-mail: catherine.housecroft@unibas.ch